Interplay of the impaired tight junction and subjacent immune cells in inflammatory bowel disease

Inaugural-Dissertation
to obtain the academic degree
Doctor rerum naturalium (Dr. rer. nat.)

submitted to the Department of Biology, Chemistry, Pharmacy
of Freie Universität Berlin

by

Franziska Weiß

2023

This dissertation was carried out from February 1st, 2019 to July 25th, 2023 under the supervision of PD Dr. Susanne M. Krug in the Clinical Physiology / Nutritional Medicine, Department of Gastroenterology, Infectious Diseases and Rheumatology, Charité – Universitätsmedizin Berlin, Berlin, Germany.

1st Reviewer: PD Dr. Susanne M. Krug
Clinical Physiology / Nutritional Medicine
Charité – Universitätsmedizin Berlin, Campus Benjamin Franklin

2nd Reviewer: Univ.-Prof. Dr. med. Andreas Diefenbach
Institute of Microbiology, Infectious Diseases and Immunology
Charité – Universitätsmedizin Berlin, Campus Benjamin Franklin

Date of defense: 11.01.2024

Acknowledgment

First and foremost, I want to thank my supervisor PD Dr. Susanne Krug for letting me conduct my doctoral thesis in her group and the chance to work on this fascinating topic. Thank you for always being available and the helpful advises and discussions when I struggled, without your support this thesis would not have become reality. I appreciated the freedom you gave me, knowing that you would steer me in the right direction if needed.

I would also like to thank my supervisor of the Freie Universität Prof. Dr. Andreas Diefenbach for his fruitful input as a member of my thesis advisor committee.

I extend my gratitude to my other thesis advisor committee members Prof. Dr. Jörg-Dieter Schulzke for his help and for sharing his knowledge as well as his resources and Prof. Dr. Christoph Becker for his valuable suggestions at the thesis advisor committee meetings.
I would also like to thank Prof. Dr. Michael Fromm for his stimulating ideas, the review of publications as well as this work and PD Dr. Rita Rosenthal for meaningful discussions and support during the last years.

Great thanks to all technicians of the clinical physiology. Special thanks to Anja Fromm, without you we all would be lost and In-Fah Lee without your immense help, I would still be sitting in the lab isolating immune cells.
Thanks to Nadine Sommer for organising all these important patient samples, to Roodline Cineus for performing the qPCR for this project and a big thank you to Marilena Letizia and Fabian Guendel for helping me with my flow cytometry experiments. I want to thank the AG Klotz for supporting me with their knowledge about organoid culture especially David Holthaus.

I thank all the doctoral students and colleagues in the clinical physiology for providing a friendly working atmosphere. Thank you, Martina and Lena, for all the fun moments and Jakob for sharing all the good and bad moments during this journey since day one.

I would like to thank my friends for always standing by me. A special thanks to my family for always supporting me in every way and their love. I would like to thank Jens for always being by my side, celebrating successes with me and supporting me in difficult times.

Declaration of Independence

Herewith I certify that I have prepared and written my thesis independently and that I have not used any sources and aids other than those indicated by me.

I also declare that I have not submitted the dissertation in this or any other form to any other institution as a dissertation.

July 2023, Berlin, Germany

Franziska Weiß

Table of Content

Summary

In inflammatory bowel disease (IBD), the homeostasis between intestinal immunity, the epithelial layer and the microbiota is disturbed, resulting in an overreaction of the immune system, barrier damage and inflammation. The two major forms of IBD are Crohn's disease (CD) and ulcerative colitis (UC). The tight junction (TJ) regulates the passage of solutes between the spaces of adjacent cells. In UC patients the expression of tetra-span TJ-associated Marvel Proteins (TAMPs) including marvelD3 (MD3), occludin (Ocln) and tricellulin (Tric) are altered and thus TAMPs might play a role in the pathogenies of IBD. MD3 and Ocln are known to have more regulatory functions, whereas Tric and the tricellular TJ (tTJ) were found to be directly involved in paracellular macromolecule passage and presumably in immune cell migration. Hence, TAMPs might have immune regulatory functions.

To investigate this, mice with intestinal epithelial specific overexpression of either MD3, Ocln or Tric were subjected to dextran sulfate sodium (DSS) induced colitis, which initially targets the epithelium. Intestinal immune cells from the large intestine were isolated and analysed by flow cytometry to ascertain changes in immune cell subtypes due to TAMP overexpression (OE) under control and DSS conditions. Furthermore, RNA was isolated from colon tissue and expression of different pro- and anti-inflammatory cytokines was determined. Results showed that TAMP-OE caused alterations in the composition of subjacent immune cells. MD3-OE showed an increase in the occurrence of $CD19^+$ B-cells, Tric-OE appeared to depress $CD103^+$ subpopulations of both intraepithelial lymphocytes (IEL) and dendritic cells (DC), whereas Ocln-OE supported $CD103^+$ IELs and DCs and additionally facilitated the maintenance of resident, particularly $CD4^+$ resident macrophages in DSS-induced colitis.

As another project, organoid derived monolayers (ODM) were established and validated for their ability to mimic *in vivo* barrier properties. Organoids can fill the gap between traditional cell culture and animal experiments due to the greater complexity compared to cell lines and the better accessibility compared to animals. Moreover, organoids retain donor properties, which makes them a great tool for personalised medicine and many other research topics. Initial studies were performed comparing colon ODMs of healthy controls with those of UC patients. Comparison of duodenum ODMs to Caco-2 cells and duodenal tissue, demonstrated that ODMs reflected well both the para- and the transcellular properties of human duodenum tissue and therefore can be considered as a suitable and good model for barrier research. Initial analysis of colon ODMs from healthy controls and UC patients showed changes in transepithelial resistance (TER) and donor specific TJ-protein expression.

In conclusion, the results of the first part could further strengthen the hypothesis that TAMPs not only play a role within in the TJ but also influence neighbouring cells and compartments, as demonstrated here for immune cells. However, further studies need to clarify the outcomes of the changed immune cell composition in more detail and the regulatory mechanisms beyond. In the second project, the ODM model was successfully established in our laboratory and evaluated considering barrier properties indicating that this model reflects well the tissue properties and complexity. ODMs can therefore be used as a more realistic model than conventional epithelial cell lines to elucidate further mechanisms and drug targets for IBD.

Zusammenfassung

In chronisch-entzündlichen Darmerkrankungen (CED; inflammatory bowel disease / IBD) ist die Homöostase zwischen dem intestinalen Immunsystem, dem Epithel und der Mikrobiota gestört, dies führt zu einer Überreaktion des Immunsystems, einer beschädigten Barriere und Entzündungen. IBD manifestiert sich in den zwei Hauptformen Morbus Crohn (MC; Crohn's Disease / CD) und Colitis ulzerosa (CU; ulcerative colitis / UC). Der Durchtritt von Substanzen zwischen zwei benachbarten Zellen wird von der Tight Junction (TJ / Schlüsselleiste) reguliert. In UC-Patienten ist die Expression von TAMPs (TJ-associated Marvel Proteins) welche MarvelD3 (MD3), Occludin (Ocln) und Tricellulin (Tric) einschließen verändert. Es ist bekannt, dass MD3 und Ocln eher regulatorische Funktionen haben, während Tric und die trizelluläre TJ direkt am parazellulären Durchtritt von Makromolekülen und wahrscheinlich auch bei der Migration von Immunzellen beteiligt sind. Aufgrund der Expressionsveränderungen bei CED-Patienten und dieser Funktionen ergibt sich die Hypothese, dass TAMPs eine Rolle bei der Pathogenese von CED spielen und hierbei auch immunregulatorische Funktionen besitzen.

Um dies zu untersuchen, wurden Mäuse mit einer intestinalen epithelialen spezifischen Überexpression von entweder MD3, Ocln oder Tric mit Dextransulfat-Natrium behandelt (dextran sulfate sodium / DSS) um eine chemisch-induzierte Kolitis hervorzurufen, welche zunächst das Epithel angreift. Um Veränderungen in Immunzellsubtypen durch die TAMP Überexpression unter Kontroll- und DSS-Bedingungen feststellen zu können, wurden Immunzellen des Dickdarms isoliert und mittels Durchflusszytometrie analysiert. Zusätzlich wurde die Expression von pro- und anti- entzündlichen Zytokinen bestimmt, indem mRNA von Dickdarmgewebe isoliert wurde. Die Ergebnisse zeigten, dass eine TAMP-Überexpression zu Veränderungen in der Immunzellzusammensetzung führte. Bei einer MD3-Überexpression war das Vorkommen von $CD19^+$ B-Zellen erhöht, eine Tric-Überexpression verringerte die $CD103^+$-Unterpopulation von intraepithelialen Lymphozyten (IEL) als auch von dendritischen Zellen (DC), wohingegen eine Ocln-Überexpression zum vermehrten Vorkommen von $CD103^+$ IELs und DCs führte. Zusätzlich unterstützte eine Ocln-Überexpression die Erhaltung von residenten Makrophagen, im speziellen von $CD4^+$ residenten Makrophagen in DSS-induzierter Kolitis.

In einem weiteren Projekt wurden intestinale Organoide generiert, daraus erhaltene Einzelzellschichten (organoid derived Monolayers / ODM) in ihrer Verwendung als Modell der epithelialen Barriere etabliert und validiert. Organoide können die Lücke zwischen traditioneller Zellkultur und Tierexperimenten schließen, da sie komplexer als Zelllinien und gleichzeitig leichter verfügbar als Tiermodelle sind. Zusätzlich behalten Organoide spenderspezifische

Eigenschaften, was sie zu einem guten Modell in personalisierter Medizin und vielen weiteren Forschungsthemen macht. Ein Vergleich zwischen duodenalen ODMs, Caco-2-Zellen und Duodenumgewebe zeigte, dass ODMs die para- und transzellulären Eigenschaften von humanem Duodenum gut darstellen konnten und daher als ein nützliches und gutes Modell für die Barriereforschung betrachtet werden können. Ein initialer Vergleich zwischen Dickdarm-ODMs von gesunden Kontrollspendern und UC-Patienten wiesen spenderspezifische transepitheliale Widerstände (transepithelial resistance / TER) und TJ-Protein Expressionen auf.

Zusammengefasst wurde im ersten Projekt die Hypothese gestärkt, dass TAMPs nicht nur eine Rolle innerhalb der TJ, sondern auch Einfluss auf benachbarte Zellen und weitere Kompartimente haben, wie hier gezeigt für Immunzellen. Nichtsdestotrotz müssen in weiteren Studien die Auswirkungen der veränderten Immunzellzusammensetzung und die regulatorischen Mechanismen dahinter im Detail untersucht werden. Im zweiten Projekt konnten ODMs erfolgreich in unserem Labor etabliert und in Bezug auf Barriereeigenschaften validiert werden. Die Barriereeigenschaften demonstrierten, dass ODMs die Gewebeeigenschaften und Komplexität gut widerspiegeln konnten. ODMs können daher als ein realistischeres Model als konventionelle epitheliale Zelllinien genutzt werden, um weitere Mechanismen und Angriffspunkte für Medikamente in CED zu identifizieren.

1 Introduction

1.1 Gastrointestinal tract

The gastrointestinal (GI) tract is the digestive system of our body and is build up by the stomach, the small intestine, and the large intestine. The stomach preserves and prepares the ingested food. The acidic fluid of the stomach kills pathogens and denatures proteins whereas peptidases digest carbohydrates and proteins (Speckmann, 2019). The small intestine has a muscular tube shape and can be divided into three parts: the duodenum, the jejunum, and the ileum, and plays a crucial role in digestion and absorption of nutrients (Speckmann, 2019). The large intestine also consists of three parts, the cecum, the colon and the rectum and its main function is the thickening of the stool (Speckmann, 2019).

1.1.1 Gastrointestinal epithelial architecture

The GI epithelium represents the largest epithelial surface of the body and constitutes the interface between the inner and outer world. Intact barriers are essential for the correct function of epithelial tissues and organs (Speckmann, 2019). The intestinal epithelium protects the body against loss of water and harmful environmental influences like pathogenic intruders. On the other hand, it is crucial for solute transport.

The small intestine is organised in crypts and villi, whereby the presence of villi increases the absorptive surface area (Speckmann, 2019), which in addition to the high expression of absorptive transporters in the small intestinal epithelial cells secures the proper uptake of nutrients, ions and water. Within the crypt base, intestinal stem cells (ISC) and Paneth cells (PC) are located and above a zone of transit-amplifying cells (TA cells) can be found which divide 2-5 times and finally mature into the different epithelial cell types (Figure 1) (Bjerknes and Cheng, 1981b; Bjerknes and Cheng, 1981a; Bjerknes and Cheng, 1999). Enterocytes are the most abundant cell type among the intestinal epithelial cells and absorb nutrients, ions, and water. To further increase their surface and efficiency, they possess microvilli (Speckmann, 2019). Another absorptive cell type are the microfold cells (M cells), which are located close to gut-associated lymphoid tissues (GALT) and are important for immune cell responses by sampling and presenting of antigens to the underlying immune cells. Intestinal secretory cells include next to PCs, goblet cells (GC), enteroendocrine cells (EEC) and tuft cells. PCs secret antimicrobial peptides and stem cell supporting factors; GCs produce mucus which builds a protective layer against bacteria; EEC produce hormones and tuft cells are chemosensory and therefore convey immune responses (reviewed in (Beumer and Clevers, 2021)).

The intestine has a high turnover rate of only a few days (Leblond and Stevens, 1948) and cells are shed into the intestinal lumen at the villus tip, whereas PCs are long living cells (1-2 months) and are cleared by macrophages (Bjerknes and Cheng, 1981b). In contrast to the small intestine the colon has no villi, much less absorptive transporters and no PCs, but so called deep secretory cells (DSC) which are similar to PCs with the exception that DSCs do not express WNT ligands (Figure 1) (reviewed in (Beumer and Clevers, 2021)).

1.1.2 Gastrointestinal epithelial stem cell niche

The GI tract is exposed to several factors that might be potentially harmful and damaging. To counteract these hazards the GI tract has a self-renewable capacity due to a population of adult stem cells (ASC). These crypt-based columnar (CBC) cells were first described in the 1970s by Cheng and Leblond (Cheng and Leblond, 1974). In 2007, Barker et al. identified leucin-rich repeat-containing G protein-coupled receptor 5 (LGR5) as a stem cell marker. ASCs are defined by self-renewal and multipotency, the capability to generate into the tissue specific cell lineages (Barker et al., 2007).

The surrounding stroma and the epithelium itself build up the stem cell niche. The stem cell niche maintains homeostasis and supports proliferation of stem cells.

Important stem cell factors are WNT ligands (WNT3a, R-spondin), epithelial growth factor (EGF), Notch ligands, and bone morphogenic protein (BMP) inhibitors (Figure 1) (reviewed in (Sato et al., 2009). EGF promotes stem cell proliferation and is released by PCs and stromal cells (Poulsen et al., 1986). The WNT signalling pathway is known to be essential for stem cell maintenance and Notch ligands are also crucial for stemness (VanDussen et al., 2012). The WNT ligand WNT3a is expressed by PCs and stromal cells in the bottom of the crypt and stromal cells additionally secret R-spondin which further induces the WNT pathway (Korinek et al., 1998; Pinto et al., 2003; Kuhnert et al., 2004; Kim et al., 2005). The BMP pathway on the other hand is supressed in the crypt bottom as it promotes differentiation (He et al., 2004; Kosinski et al., 2007) e.g. Noggin is a BMP inhibitor and expressed in the intestinal epithelial crypt (Haramis et al., 2004). These opposing WNT and BMP gradients are generated by specific secretion of agonists and antagonists thereby determining the stem cell zone (Figure 1). Together, these precisely balanced factors and gradients form the stem cell niche and support the self-renewing capacity of the GI.

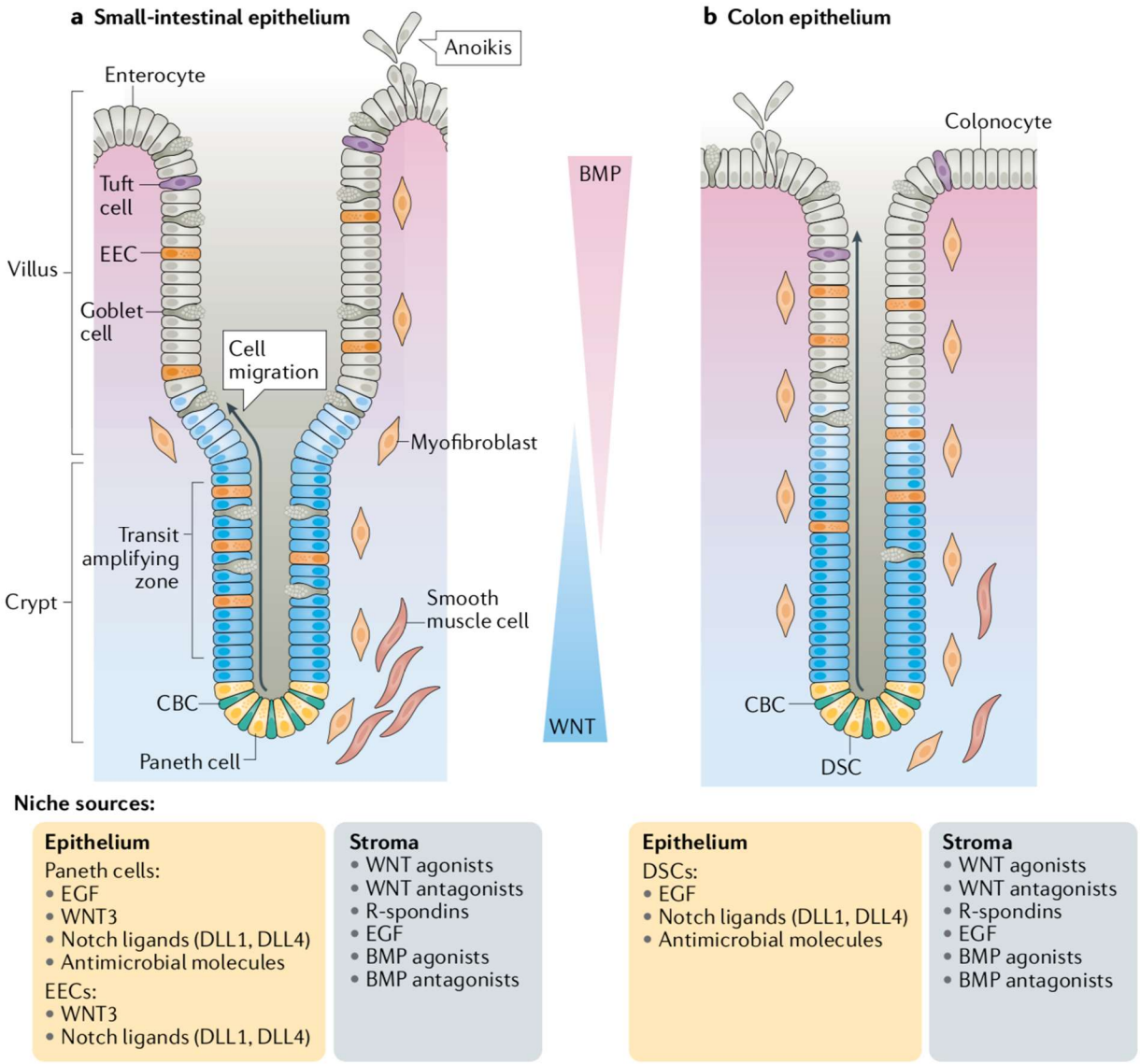

Figure 1 Gastrointestinal epithelial architecture and stem cell niche

Schematic representation of **(A)** Small-intestinal epithelium; intestinal stem cells are located in the crypt bottom and designated as crypt-base columnar cells (CBC). CBCs are surrounded by PCs, which express essential stem cell factors such as WNT3 and EGF. The daughter cells of CBCs migrate upward through the transit amplifying zone to the tip of the villus, where they undergo anoikis (programmed cell death caused by loss of attachment). During this migration process they differentiate into enterocytes, tuft cells, EECs, and M cells. The interface between differentiated cells and stem cell niche is defined by opposing gradients of WNT and BMP. These gradients are formed by the epithelial cells themselves and the surrounding mesenchymal cells such as myofibroblast and smooth muscle cells. **(B)** Colon epithelium; apart from the absence of villi, the colon epithelium has a structure similar to that of the small intestinal epithelium. Another difference is that DSCs, instead of PCs, are present in the colon. DSCs do not secret WNT. Abbreviations: crypt-base columnar cells (CBC); Paneth cells (PC), epithelial growth factor (EGF), enteroendocrine cells (EEC), microfold cells (M cells); deep secretory cells (DSC) (Beumer and Clevers, 2021)

1.1.3 Epithelial cell-cell contacts

One main function of the epithelial layer is to transport solutes and thereby it enables sufficient uptake of nutrients. Passage of ions, solutes and water can occur either via selective transporters and receptor-induced endocytosis, representing the transcellular pathway or via the paracellular pathway passing the spaces between adjacent cells.
Functionally, epithelia can be classified as leaky or tight depending on the proportion of flux or conductivity via the paracellular and the transcellular pathway. This means that in a leaky epithelium, the flux of ions through the paracellular pathway can be larger than the ion flux through the transcellular pathway and, correspondingly, vice versa in a tight epithelium.
The transepithelial resistance (TER) is inversely related to all ion permeabilities of the paracellular and transcellular pathway. By definition, in leaky epithelia the transcellular resistance (R^{trans}) is higher than the paracellular resistance (R^{para}), $R^{para} / R^{trans} < 1$. In tight epithelia the transcellular resistance is lower than the paracellular resistance ($R^{para} / R^{trans} > 1$). Although the TER does not discriminate between both, it is used to give a rough indication of whether the epithelium is leaky or tight. In most leaky epithelia the overall TER is low and in most tight epithelia the TER is high (Claude and Goodenough, 1973). In tubular shaped epithelial organs like GI tract and kidney tubules, the proximal segments are leaky while the distal parts are tight.

In any case, uncontrolled diffusion via the paracellular route must be prevented to ensure correct function of epithelial tissues and organs. This is achieved by a network of cell-cell contacts. Four groups of cell-cell contacts can be distinguished that form junctional complexes, tight junctions, adherens junctions, desmosomes, and gap junctions (Denker and Nigam, 1998; Farquhar and Palade, 1963) (Figure 2).

Communication of neighbouring cells is mediated through gap junctions (*nexus*) which form channels for small solutes up to 1 kDa. Six transmembrane proteins, called connexins, form one hemi-channel on the cell membrane. Two hemi-channels of two adjacent cells can interact, thereby allowing the exchange of small molecules (reviewed in (Kumar and Gilula, 1996)).
Adherens junctions (*Zonula adherens*, AJ) are a belt-like structure connecting two adjacent cells. They are formed by cell adhesion molecules of the cadherin family. Cadherins of adjacent cells can bind to each other and are anchored to the cell cytoskeleton by actin filaments (reviewed in (Ivanov and Naydenov, 2013)).

Desmosomes (*Macula adherens*) are located at the basal side of adherens junctions and further strengthen the connection of two neighbouring cells. Desmosomes consist – among other proteins – mainly of desmogleins and desmocollins (reviewed in (Garrod et al., 1996)).

Tight junctions (*Zonula occludens*, TJ) are a meshwork formed by transmembrane proteins located close to the apical side of the epithelium. They bring neighbouring cells in contact and by this control the paracellular diffusion, which is defined as "gate" function determining the paracellular passage of ions and small molecules. In addition, as membrane-protein complex surrounding the whole epithelial cell, they have a "fence" function, hindering the free movement of membrane compartments like membrane proteins between basolateral and apical membrane. This leads to a functional polarisation which is crucial for the proper tissue function. Basolateral and apical membranes differ molecularly and express specific transporter proteins (Diamond, 1977).

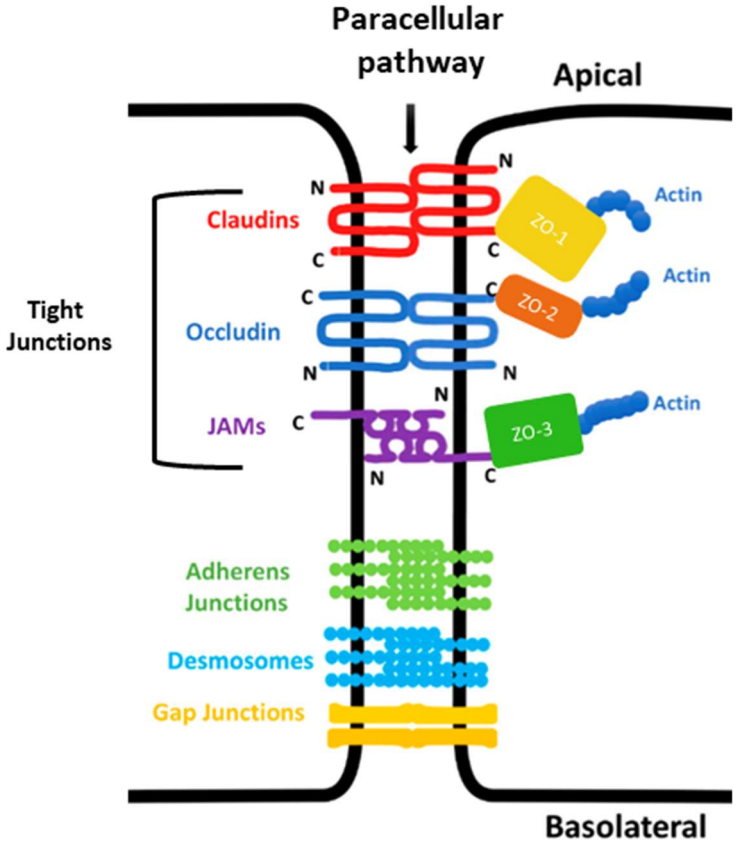

Figure 2 Junctional complex formed between two adjacent epithelial cells

The junctional complex consists of tight junctions (TJ), adherence junctions, desmosomes, and gap junctions. TJ proteins bind with their C-terminus on tight junction-associated proteins such as *Zonula occludens* (ZO)-1. ZO proteins link the TJ proteins to the cytoskeleton via actin. Modified from (Shi et al., 2018)

1.2 Tight junctions

TJ strands were discovered more than 50 years ago using freeze fracture electron microscopy (Staehelin et al., 1969). They were found to build a belt-like structure at the apical membranes of epithelial cells. TJs that form between two adjacent cells are called bicellular TJs, whereas TJs formed at the points where three or more cells meet are tricellular TJs (tTJ). tTJs form a 10 nm wide and 1 µm long tube extended to the basal side (Staehelin, 1973) and are differently constituted in comparison to bTJ.

The TJ proteins comprise four different transmembrane protein families: Claudins (Cldn[1]) (Mineta et al., 2011; Furuse et al., 1998) and the TJ-associated **M**yelin and lymphocyte **A**nd **R**elated proteins for **VE**sicle trafficking and membrane **L**ink (MARVEL) proteins (TAMP) (Ikenouchi et al., 2005; Steed et al., 2009; Furuse et al., 1993) are tetra-span proteins, while angulins (Higashi et al., 2013) and junctional adhesion molecules (JAMs) (Martin-Padura et al., 1998) are single-span proteins (Figure 3).
In addition, TJ-associated proteins like zonula occludens (ZO) and cingulin are involved in TJ formation and function. They are located intracellularly and link the TJ to the cytoskeleton via actin or myosin and therefore have regulatory functions (reviewed in (Shi et al., 2018)).

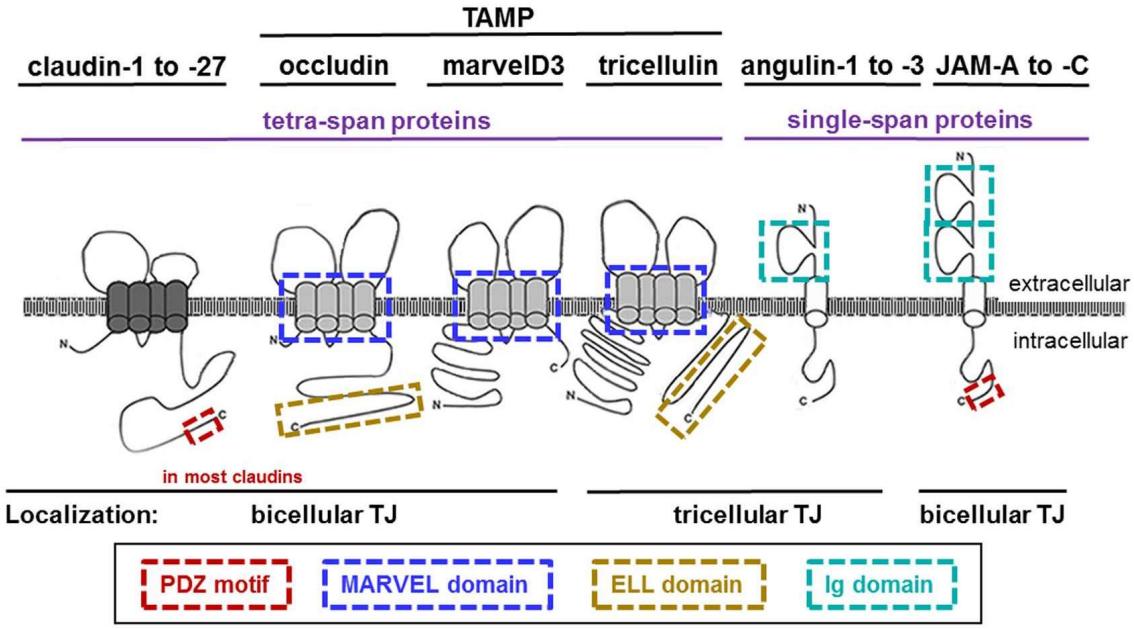

Figure 3 Tight junction protein families

Two tetra-span protein families, claudins and tight junction-associated MARVEL proteins (TAMP), and two single-span proteins families, angulins and JAMs, form together the TJ. While claudins, occludin,

[1] CLDN (claudin human)

marvelD3, and JAMs are mainly located at bicellular TJs, tricellulin and angulins are most abundant at tricellular TJs (Piontek et al., 2020)

1.2.1 JAMs (junctional adhesion molecules)

As mentioned above, JAMs are single-span proteins and their extracellular part is folded into two immunoglobulin (IG) domains. JAMs are expressed in endothelial and epithelial cells but also in leukocytes and thrombocytes (Sobocka et al., 2000; Ludwig et al., 2005). While their function for the TJ barrier is not fully understood they are known to be involved in cell-cell contacts of endothelial cells and are binding sites for viruses. Other than that, JAMs also play a role in the formation of new TJs (Ebnet et al., 2004). JAMs can be divided into two subgroups – the JAM proteins including JAM-1/A, JAM-2/B, and JAM-3/C and the second group comprising coxsackie and adenovirus receptor (CAR), CXADR-like membrane protein (CLMP), endothelial cell-selective adhesion molecule (ESAM), and JAM-like protein (JAM-4/L) (Zen et al., 2005).

1.2.2 Claudins

In mammals, 27 claudin family members are known, which are similar in sequence and structure (Mineta et al., 2011; Krause et al., 2008). Together they form the backbone of the TJ and interact with each other via their extracellular loops. Either proteins of the same cell membrane interact with each other (*cis*-interaction) or proteins of two opposing cells interact with each other (*trans*-interaction). Thereby, they define the TJ permeability properties and tissue permeability depends on the composition of the respective Cldns within the TJ. Cldns either have a barrier-forming function or a channel-forming function. Channel-forming claudins can be grouped in (1) cation and water channels, (2) cation channels, and (3) anion channels.

In the intestine, Cldn1, Cldn2, Cldn3, Cldn4, Cldn5, Cldn7, Cldn8, Cldn12, Cldn13, Cldn15, and Cldn18 are expressed. Cldn1, Cldn2, Cldn7, Cldn12, and Cldn15 are expressed throughout the whole intestine, whereas Cldn5, Cldn13, and Cldn18 are only expressed in the small intestine and Cldn3, Cldn4, Cldn7, and Cldn8 are enriched in the colon (reviewed in (Garcia-Hernandez et al., 2017)).
In the intestine, Cldn2 (Amasheh et al., 2002; Fujita et al., 2008; Rosenthal et al., 2010) and Cldn15 (Charoenphandhu et al., 2009; Tamura et al., 2011; Rosenthal et al., 2020) have cation and water channel-forming properties, and Cldn7 and Cldn12 might form cation channels (Alexandre et al., 2005; Fujita et al., 2008), while Cldn1, Cldn3, Cldn4, Cldn5, and Cldn8 are barrier-forming Cldns (Furuse et al., 2002; Amasheh et al., 2005; Amasheh et al., 2009b; Milatz et al., 2010).

The small intestine with lower expression of barrier-forming Cldns and a high expression of channel-forming Cldns is a leaky epithelium with a low TER. The colon in comparison has a lower expression of channel-forming Cldns and the expression of barrier-forming Cldns is higher, making the colon a tight epithelium with a high TER.

1.2.3 TAMPs (Tight Junction-associated Marvel Proteins)

TAMP family members are tetra-span proteins but have no sequence similarity to Cldns (Mariano et al., 2011a). The TAMPs are sharing a MARVEL domain (Raleigh et al., 2010) and this protein family includes occludin (Ocln[2]) (Furuse et al., 1993), tricellulin (Tric[3], MARVEL D2) (Ikenouchi et al., 2005), and MARVEL D3 (MD3) (Steed et al., 2009).

In 1993, occludin (Ocln) as the first TJ protein was discovered (Furuse et al., 1993). It possesses four transmembrane domains and the C-terminal elongation factor (eleven-nineteen lysine-rich leukemia) ELL domain which allows the interaction with TJ-associated proteins like ZO1 (Tsukita and Furuse, 1998). Ocln is ubiquitously expressed at bTJs; however knockout of Ocln in mice did not alter TJ morphology. Nevertheless, Ocln-deficient mice suffered from chronic inflammation and hyperplasia of the gastric epithelium, calcification in the brain and testicular atrophy (Saitou et al., 2000). These results were strengthened with the findings that in human mutations of OCLN also lead to calcification in the brain and renal dysfunction (O'Driscoll et al., 2010; LeBlanc et al., 2013). The barrier function of Ocln is not determined yet and remains rather controversial. Ocln knockout mice showed no impairment of the barrier (Saitou et al., 2000) and OCLN did not play a role in macromolecule passage (Richter et al., 2019). However, over-expression caused an increased epithelial resistance and an increase in TJ strands (McCarthy et al. 1996). Though, OCLN was found to have rather regulatory functions (Richter et al., 2019), for example in mammary Ocln regulates apical protein secretion (Zhou et al., 2020) and Ocln knockout altered differentiation in gastric epithelial cells (Saitou et al., 2000; Schulzke et al., 2005).

Ikenouchi et al. discovered tricellulin (Tric) in 2005 (Ikenouchi et al., 2005). Tric is ubiquitously expressed in epithelial cells at tTJs but can be found in small amounts also at bTJs. Four isoforms of TRIC are discussed (Riazuddin et al., 2006), TRIC-a (64 kDa), which is usually designated as TRIC, is the longest isoform with seven exons and a C-terminal ELL domain. TRIC-a (62 kDa) lacks exon three, TRIC-b (51 kDa) lacks the ELL-domain and TRIC-c (52 kDa) has an alternative spliced exon two and therefore misses two of the suggested transmembrane

[2] OCLN (Occludin human)
[3] TRIC (Tricellulin human)

domains. With the C-terminal ELL domain Tric can translocate basolaterally (Westphal et al., 2010) and binds to the lipolysis-stimulated lipoprotein receptor (LSR)/Angulin-1 (Masuda et al., 2011). Furthermore, mutations in this domain are associated with deafness (Riazuddin et al., 2006). Other functions described for Tric are an influence on TJ organization in tTJs and bTJs (Ikenouchi et al., 2005). Moreover, Tric plays an important role in the regulation of macromolecular passage. While downregulation of TRIC causes an increase, tTJ overexpression leads to a reduced macromolecular passage (Ikenouchi et al., 2005; Krug et al., 2009a).

Marvel D3 (MD3) was discovered as the third TAMP protein by Steed et al. in 2009 (Steed et al., 2009). In comparison to OCLN and TRIC, MD3 lacks the ELL domain at the C-Terminus and exists in two splice variants (v1 and v2) which differ in their MARVEL sequence (Raleigh et al., 2010). MD3 is expressed at bTJs and tTJs in several tissues including murine jejunum, hepatocytes, and renal tubules (Cording et al., 2013). While MD3-v1 was found to be more stable at tTJs, MD3-v2 was more stable at bTJs, indicating different functions of those two variances (Raleigh et al., 2010). Albeit the function of MD3 is not fully understood, it was found to have influence on cell behaviour and survival (Steed et al., 2014), to play a role in development (Vacca et al., 2016; Vacca et al., 2018) and to stabilise the TJ (Steed et al., 2009) but interestingly not being critical for TJ formation (Steed et al., 2009).

Due to the similar structure of the three TAMPs, overlapping properties can be assumed. Indeed, during functional investigations of Ocln and Tric knockouts, Ikenouchi and colleagues observed that Ocln and Tric were relocated in the respective other knockout (Ikenouchi et al., 2005; Ikenouchi et al., 2008). Moreover, MD3 was found to colocalise and interact with both, OCLN and TRIC, whereas no interaction was detected between OCLN and TRIC (Raleigh et al., 2010; Cording et al., 2013). However, Ocln expression displaces Tric from the bTJ (Ikenouchi et al., 2008). Knockdown of one of the TAMPs caused a delay in TJ assembly and did not lead to an upregulation of the other TAMP proteins (Raleigh et al., 2010). Together these findings indicate overlapping but not redundant functions of the three TAMPs.
However, the exact function of TAMPs and their interaction with each other and their environment are not completely understood and need further investigation.

1.2.4 Angulins

The name angulin originates from the latin word “angulus” meaning “corner”, indicating that angulins are located at the tTJ like Tric. Additionally, they serve as landmarks to recruit Tric to the tTJ (Masuda et al., 2011). The angulin family has three members so far – angulin-1

[lipolysis-stimulated lipoprotein receptor (LSR) / ILDR3], angulin-2 [immunoglobulin Ig-like domain-containing receptor (ILDR1)] and angulin-3 [ILDR2 / LISCH-like / C1orf32] (Higashi et al., 2013). These proteins are single-span transmembrane proteins with an extracellular Ig-domain (Masuda et al., 2011). Angulins are expressed in most epithelial tissues, angulin-1 and angulin-2 are usually complementary or in some tissues co-expressed, for example in the colon angulin-1 is expressed in the lower part of the crypt, whereas angulin-2 is expressed in the upper part. Angulin-3 is mainly expressed in epithelia covering neural tissues (Higashi et al., 2013). Although all three angulins can recruit Tric, the impact of angulin-3 on the barrier function was much lower compared to angulin-1 and -2. This suggests that recruitment of Tric is not sufficient to properly tightening the tTJ (Higashi et al., 2013). In addition to Tric, angulins are able to bind some Ocln and angulin-3 could even bind traces of MD3-v2 but not MD3-v1 (Higashi et al., 2013). Mutations in angulin-2 lead to deafness (DFNB42) (Borck et al., 2011) similar to deafness caused by mutational changes in TRIC (DFNB42) (Riazuddin et al., 2006). Recent investigations on angulin-1 revealed that it supports the vertically extended localization at tTJ of TJ proteins via its binding to ZO1. Furthermore, knockout of angulin-1 caused an increase in fluorescein flux (332 Da) and decrease in TER, which could be restored by exogenous angulin-1 expression and that angulin-1 expression corresponded with proper plasma membrane contacts at the tTJ (Sugawara et al., 2021).

1.3 Gastrointestinal organoids

In vitro investigations of the TJ barrier are often performed using immortalised cancer cell lines like CaCo-2 or the HT29/B6 cells. However, these cell lines only consist of one epithelial cell type. In contrast, organoids are 3D self-organizing structures which can contain all tissue-specific cell types. Sato et al. managed to culture the first organoids in 2009 by applying the essential stem cell niche factors like Wnt ligands, Noggin and EGF to freshly isolated ISCs (Sato et al., 2009). Organoids can derive from ASCs (Sato et al., 2009; Sato et al., 2011a) or pluripotent stem cells (PSC) (McCracken et al., 2014; McCracken et al., 2011). PSCs can either originate from embryos (embryonic stem cells, ESC) or induced pluripotent stem cells (iPSC), which are re-programmed somatic cells. With the knowledge of the specific stem cell niche factors it is possible to grow ASCs and PSCs into organoids, which reflect the crucial aspects of the tissue of origin and maintain the capacity of self-renewal and differentiation (Sato et al., 2009).

ASCs-derived GI-organoids are generated within one week and are long-lived (years), whereas it takes up to 30-60 days until PSCs form differentiated organoids and cannot be passaged several times (McCracken et al., 2011). Furthermore, the administration of niche factors and inhibitors is even more complex and sensitive than for ASCs-derived organoids.

Another difference between ASCs- and PSCs-derived organoids is that ASCs-derived organoids do not contain any mesenchymal cells and only consist of intestinal epithelial cells (IEC) after some passages, while the PSCs-derived organoids maintain a combination of mesenchymal and epithelial cells (Pompaiah and Bartfeld, 2017).

GI-organoids have a polarised apical and basolateral surface, where the apical side faces the organoid lumen and retain physiological functions of the original tissue (Blutt et al., 2018). In comparison to epithelial cancer cell lines, organoids exhibit a low occurrence of mutations (Sato et al., 2011b). Common techniques can be applied to organoids similar to cell lines and primary cells including protein analysis, microscopy, cryo-electron microscopy, single-cell RNA sequencing, mass spectroscopy, and genetic manipulations.

However, organoids have some drawbacks. One obstacle is the accessibility of the apical side of 3D organoids. To counteract this, either microinjections, inside-out organoids (Nash et al., 2021) or organoid-derived monolayers (ODMs) are used (Figure 4). ODMs polarize with the basal side down and the apical side upwards. Seeding them on a cell culture insert (e.g. transwells) enables the application to the basolateral and the apical side (Kozuka et al., 2017; VanDussen et al., 2015; Moon et al., 2014). Thereby, techniques for a more detailed investigation of the epithelial barrier such as transepithelial resistance (TER) and flux measurements or Ussing chamber experiments can be performed (Holthaus et al., 2021).

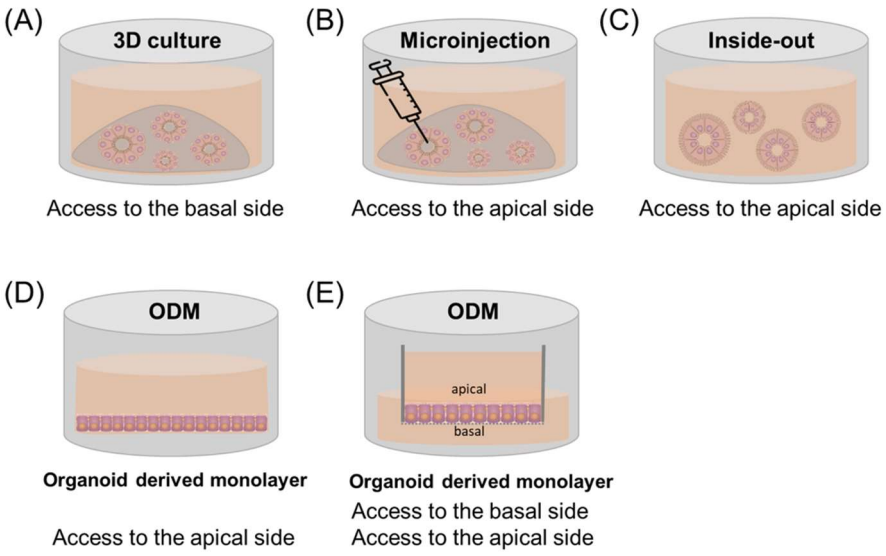

Figure 4 Ways to get access to the apical side of organoids

(A) Organoids are cultured as a 3D structure embedded in an extracellular matrix with the apical side facing the lumen of the organoid, thereby hindering apical access. Several methods are available to counteract this, including (B) microinjection, (C) inside-out organoids, and (D and E) organoid-derived monolayers (ODM). While microinjection is difficult to perform, inside-out organoids and ODMs on cell culture plates have the disadvantage of only allowing access to the apical side, not the basolateral side.

In contrast, ODMs seeded on a cell culture insert (E) allow parallel application to the basolateral and apical sides. (Created with Power Point based on (Co et al., 2019))

Another disadvantage is that several organoid culture systems are published that differ in culture conditions (e.g. different growth factors/ inhibitors) and origin (e.g. donors of different ages). This might have great influence on the experimental outcomes and requires further investigation and determination (also discussed in (Bartfeld, 2016)). Moreover, organoids only consist of epithelium or epithelium and mesenchyme but lack other cell types of the native microenvironment like immune cells, muscle cells, blood vessels or stroma cells. Therefore, they are still limited and only resemble a reduced model of an organ (Bartfeld, 2016). For solving this issue, organoids are nowadays co-cultured with other cell types e.g. immune (Nozaki et al., 2016; Noel et al., 2017) or stroma cells (Nakamura et al., 2019).
On the other hand, a pure epithelial culture can be favoured as it enables researchers to investigate the epithelium without any influences or interferences of other cell types.
However, organoids are a very advantageous model, although they certainly have some drawbacks. They close the gap between cell lines and *in vivo* studies, as they are more complex than cell lines but have properties like long-term culture, high proliferation, and the ability to be used with common techniques.
Organoids are promising models for several research topics like pathophysiology e.g. cancer and inflammatory bowel disease (IBD), infection diseases, tissue homeostasis, living biobanks, pharmacological drug screening, and personalised medicine. In the meantime the generation of organoids of different vertebrates and tissues have been established like stomach (Barker et al., 2010), small intestine (Sato et al., 2009), large intestine (Sato et al., 2011a), liver (Huch et al., 2013), lung (Rock et al., 2009), and brain (Lancaster et al., 2013).
However, other tissue components such as the immune system are also very important for proper GI function and homeostasis. Recent research combines these components to obtain models that are even closer to the *in vivo* situation than organoid cultures alone.

1.4 Gastrointestinal immunity

The immune system of the GI tract is crucial for the maintenance and homeostasis of the gut and the overall health. However, the GI immunity is very challenging as a sensible balance between tolerance and sensitivity needs to be protected. All barriers to the environment are challenged with a massive amount of commensal and pathogenic antigens. However, the intestine needs to absorb essential nutrients and protect against intruders at the same time, thereby being potentially prone for infections. Furthermore, the colonisation of the intestine

with commensals is required to ensure a sufficient nutrient uptake and therefore must be tolerated (Murphy, 2018a).

The epithelial layer is the first player that addresses this challenge by the production of mucus that shields the barrier from direct penetration of the microbiota. Secondly, the epithelial barrier serves as a physical barrier itself and TJs regulate the paracellular passage of ions and molecules as described. Additionally, the epithelial barrier acts as an immune barrier as it secretes antimicrobial peptides including lysozyme and α-defensins and the expression of pattern recognition receptors (PRR). Recognition of pathogen-associated molecular patterns (PAMP) and damage-associated molecular patterns (DAMP) by PRRs lead to the expression of pro-inflammatory cytokines and the activation of immune cells (Murphy, 2018a).

The latter are contributing to regulate the fragile homeostasis of the GI and fight against pathogens. Immune cells are found throughout the GI in the epithelium, the lamina propria (LP) or are organised in secondary lymph organs like mesentery lymph nodes (MLN) and GALT which include Peyer's patches (PP) (only in the small intestine), isolated lymphocyte follicles (ILF), tonsils and the appendix (in humans). GALTs are important for initiating the immune response and are constituted manly of B and T lymphocytes and dendritic cells. Immune effector cells are mostly located within the epithelium and the LP (Murphy, 2018a).

1.4.1 Myeloid cells

Myeloid cells include macrophages, dendritic cells (DC), and neutrophils among others. All three are involved in innate immune response and are phagocytic. Further, they induce and regulate adaptive immunity, especially macrophages and dendritic cells as antigen presenting cells (APCs) are important for adaptive immune responses.

1.4.1.1 **Neutrophils**

Neutrophils (polymorphnuclear leukocytes) are short-lived phagocytes which make up 50-70% of human and 10-25% of mouse circulating leukocytes (reviewed in (Wera et al., 2016)).

They are absent from tissues under healthy conditions and are recruited by resident macrophages, IEC or T_H17 cells upon danger signals to the site of infection. The main function of neutrophils is to kill invading microbes. Therefore, they possess several antimicrobial features. Neutrophils can produce high amounts of toxic reactive oxygen species (Murphy, 2018b), possess several intracellular granules, containing antimicrobial agents like α-defensins, and produce neutrophil extracellular traps (NET) (Brinkmann et al., 2004) upon activation. Further, neutrophils express different cytokines and chemokines to recruit other immune cells for example macrophages and thereby stimulate immune responses. Neutrophils are known to migrate through the epithelial layer to kill pathogens in the gut lumen.

Transendothelial migration of neutrophils was observed via paracellular clefts and here mainly at tricellular corners (Burns et al., 1997). Although the process of transmigration is not completely understood it is known that the leukocyte β2 integrin CD11b/CD18 and the JAM-L protein expressed by neutrophils as well as the JAM protein CAR and OCLN expressed by IECs are involved in neutrophil transepithelial migration (Zen et al., 2005). Despite their protective function, an increased accumulation of neutrophils is associated with ulcerative colitis (UC) (Bressenot et al., 2015), therefore a fast clearance of neutrophils by macrophages is important to maintain intestinal homeostasis.

1.4.1.2 Macrophages

Intestinal macrophages are located closely under the epithelial layer where they phagocyte apoptotic cells and secret intestinal epithelial growth factors e.g Wnt ligands. Therefore, they are supporting epithelial tissue remodelling. Furthermore, macrophages are involved in several processes to maintain GI homeostasis. They capture and eliminate commensals and express anti-inflammatory cytokines as e.g. Interleukin (IL)-10, transforming growth factor (TGF)-β, and IL-1β.

IL-10 and TGF-β support T regulatory cells (T_{reg}) maintenance and expansion (Hadis et al., 2011; Murai et al., 2009; Kim et al., 2018), therefore it is suggested that macrophages play a role in regulating oral tolerance. Tolerance might be further achieved by the hyposensitive PRR signalling of intestinal macrophages. IL-1β, expressed by macrophages, maintains T helper (T_H) 17 cells (Panea et al., 2015) and induces colony-stimulating factor 2 (CSF2) expression in innate lymphoid cells (ILC)3 (Mortha et al., 2014), that in turn promotes DC differentiation (Greter et al., 2012). Moreover, intestinal CX3C motif chemokine receptor 1 (CX3CR1) positive macrophages can sample luminal antigens with the formation of transepithelial dendrites (TED) (Niess et al., 2005).

$CX3CR1^{+}$ macrophages are capable of antigen transfer to cluster of differentiation (CD) 103 (syn. Integrin alpha E, ITGAE) positive cDCs via gap junctions, thus indirectly involved in priming naïve T-cells (Mazzini et al., 2014). Since mature macrophages are major histocompatibility complex class II (MHCII) high, they might present antigens to previously activated T-cells (Murphy, 2018a).

During acute infection, macrophages secrete neutrophil chemoattractants (IL-8 hu, CXCL1, 2, and 5 ms) to induce neutrophil influx to the site of infection. Conversely, recruited neutrophils are important for monocyte/macrophage recruitment and function.

Most macrophages of the LP mature from migrating blood monocytes and are high-affinity immunoglobulin (IgG) receptor FcγR1 low ($CD64^{lo}$) $Ly6C^{hi}$ $MHCII^{-}$ $CX3CR1^{int}$ in the beginning. In a first step they gain MCHII expression during maturation and then lose their Ly6C expression and finally differentiate into $CD64^{+}CX3CR1^{hi}$ $Ly6C^{-}$ $MCHII^{hi}$ resident macrophages.

This process is called the “monocyte waterfall” (Tamoutounour et al., 2012; Bain et al., 2013) (Figure 5). While resident macrophages retain their anti-inflammatory phenotype during inflammation (Bain et al., 2013; Weber et al., 2011; Kamada et al., 2008), freshly derived monocytes mature into pro- or anti-inflammatory macrophages depending on the surrounding environment.

1.4.1.3 Dendritic cells

Dendritic cells are APCs with the unique ability to prime naïve T-cells. They derive in the bone marrow and migrate into the intestinal tissue where they sample and “scan” antigens. Due to their expression of PRR, DCs can distinguish between harmful and harmless antigens and react accordingly, thereby playing an important role in regulating the immune tolerance against food and commensal antigens in the gut (reviewed in (Bernardo et al., 2018; Murphy, 2018a)). After sampling an antigen, DCs lose their antigen sampling and processing capacity and instead increase their antigen presenting capacity to naïve T-cells and migrate from the LP to the GALTs. DCs present four signals to the naïve T-cells: first an increased expression of the processed and potentially harmful antigen, second an increased expression of co-stimulating factors, third an increased expression of pro- or anti-inflammatory cytokines and fourth a tissue homing signal (reviewed in (Bernardo et al., 2018; Murphy, 2018a)). Therefore, they can regulate the type and location of immune responses.

DCs in the mouse and human intestine can be classified into plasmacytoid DCs (pDCs) and classical DCs (cCDs). cDCs can be further subdivided into four subsets: $CD103^+$ $CD11b^-$ (in humans: $CD103^+$ $SIRP\alpha^-$) and $CD103^-$ $CD11b^+$ (in humans: $CD103^-$ $SIRP\alpha^+$) $CD103^+$ $CD11b^+$ (in humans: $CD103^+$ $SIRP\alpha^+$) and $CD103^-$ CD11b expressing cDCs (reviewed in (Bernardo et al., 2018; Cerovic et al., 2014)) (Figure 5).

All cDCs can migrate to MLNs, ILFs or PPs and present soluble antigens to naïve T-cells. $CD103^+$ $CD11b^+$ are the predominant cDC subtype in the small intestine and can induce T_H1, T_H17 immune responses or T_{reg} development. In the colon, the most abundant cDC subtype is $CD103^+$ $CD11b^-$ cells. They can also induce T_H17 immune response and T_{reg} development but in contrast to $CD103^+$ $CD11b^+$ induce T_H2 instead of T_H1 immune responses (reviewed in (Bernardo et al., 2018)). $CD103^+$ $CD11b^+$ and $CD103^+$ $CD11b^-$ cDCs possess a retinaldehyde dehydrogenase 2 (RALDH2) activity in the small intestine which allows the formation of dietary vitamin A to retinoic acid (RA). RA promotes the development of immunoglobulin A (IgA) secreting B-cells (reviewed in (Bernardo et al., 2018)).

Yet, it is difficult to distinguish between DCs and macrophages, since they share several expression markers. For example, many macrophages express CD11c and MCHII, which were typical markers to identify DCs. On the other hand, the pan-macrophage marker F4/80 was

also found to be expressed in cDCs. However, the CD64 can sufficiently discriminate between DCs and macrophages (Gautier et al., 2012). While MCHII$^+$ CD11c$^+$ CD64$^-$ cells are migratory cells which depend on the cDCs specific growth factor FMS-related tyrosine kinase 3 ligand (Flt3L), MCHII$^+$ CD11c$^+$ CD64$^+$ development depends on the colony stimulating factor 1 (CSF1/M-CSF) and are non-migratory.

1.4.2 Lymphoid cells

Lymphoid cells are mainly adaptive immune cells and therefore have an antigen specific immune reaction. They include B-cells, T-cells, intraepithelial lymphocytes (IEL), and innate lymphoid cells (ILC).

1.4.2.1 B-cells

B-cell functions are antibody production, antigen presentation and cytokine generation. In GALT activated B-cells migrate from PPs/ILFs/MLNs to the LP and differentiate into plasma cells (PCs) which express high amounts of IgA (Figure 5). IgA expressing plasma cells were found to promote T_{reg} maintenance (Kim and Kim, 2014). IgA dimers are secreted into the gut lumen via transcytosis. At the apical side of the epithelium IgA protects against the binding and intrusion of microorganism on/in IECs. Furthermore, IgA can bind and neutralise large antigens like bacteria, toxins and enzymes and therefore is important for the protection of the GI tract (Murphy, 2018a).

1.4.2.2 T-cells

T-cells are divided into two main types – the MHC-I restricted CD8$^+$ cytotoxic T-cells and the MHC-II restricted CD4$^+$ T_H cells. T_H cells include T_H1, T_H2, T_H17 and T_{reg} cells. T_H1 cells eliminate intracellular pathogens and express pro-inflammatory cytokines like interferon-γ (INF-γ) and tumour necrosis factor-α (TNF-α) (Murphy, 2018c). In contrast T_H17 cells are involved in fighting extracellular parasites and fungi and express IL-17, IL-21 and IL-22 (Murphy, 2018c). Furthermore, T_H17 maintain epithelial homeostasis due to the expression of IL-22. T_H2 cells express IL-4, IL-5 and IL-13 and play a role in parasite clearance and allergic responses (Murphy, 2018c). T_{regs} are important for immune tolerance, homeostasis and prevent against abnormal immune responses T_{regs} express the transcription factor forkhead box protein P3 (FOXP3) and produce anti-inflammatory cytokines like IL-10 and TGF-β (Murphy, 2018c).

1.4.2.3 Innate lymphoid cells (ILC)

Another cell type of the lymphoid cell lineage are ILCs which accumulate in mucosal tissue, but in contrast to T-cells do not express antigen specific receptors. However, ILCs protect against infection and are important for intestinal homeostasis. ILCs are divided into natural killer (NK) cells, ILC1 (like T_H1 cells), ILC2 (like T_H2), and ILC3 (like T_H17) based on their similar cytokine expression and function with respect to T_H cells (Murphy, 2018c).

1.4.2.4 Intraepithelial lymphocytes (IEL)

IELs are restricted to the intestinal epithelium and do not circulate. They reside below TJs but above the basement membrane. Most of them express CD103, with which they can interact with E-cadherin of enterocytes (Murphy, 2018a). During migration through the epithelium, interactions with Ocln were observed (Edelblum et al., 2012). Upon activation they express the activation markers CD69 and CD44. T-cell receptor (TCR) positive and TCR negative IELs have been identified (reviewed in (Olivares-Villagomez and Van Kaer, 2018)). The population of the latter is small and knowledge is limited, but some TCR^- IELs subsets were found to resemble ILCs (Fuchs et al., 2013). TCR^+ IELs consist of natural IELs (nIELs) and induce IELs (iIELs), nIELs immediately home to the intestinal epithelium after development. In contrast, the iIELs are already antigen experienced conventional T-cells (reviewed in (Cheroutre et al., 2011)). nIELs include $TCR\alpha\beta^+$ $CD8\alpha\alpha^+$ and $TCR\gamma\delta^+$, the former ($TCR\alpha\beta^+$ $CD8\alpha\alpha^+$) share functions with T_{regs} as they are involved in tolerance and express TGF-β and IL-10 (reviewed in (Ma et al., 2021)). $TCR\gamma\delta^+$ nIELs exhibit a dual function: at the beginning of an infection they rather act cytotoxic and express several proinflammatory cytokines to fight invasive microbes (Ismail et al., 2009; Ismail et al., 2011), however at a later point of inflammation $TCR\gamma\delta^+$ nIELs limit excessive inflammation and tissue damage (Roberts et al., 1996). $TCR\gamma\delta^+$ nIELs were observed to be highly mobile migrating between epithelium and LP.

$TCR\alpha\beta^+$ $CD4^+$ IELs and $TCR\alpha\beta^+$ $CD8\alpha\beta^+$ IELs are iIELs. Similar to conventional T-cells, $TCR\alpha\beta^+$ $CD4^+$ have more T_H functions and $TCR\alpha\beta^+$ $CD8\alpha\beta^+$ are more cytotoxic. Nevertheless, both are involved in pathogen elimination and also exhibit immune regulatory functions (Murphy, 2018a).

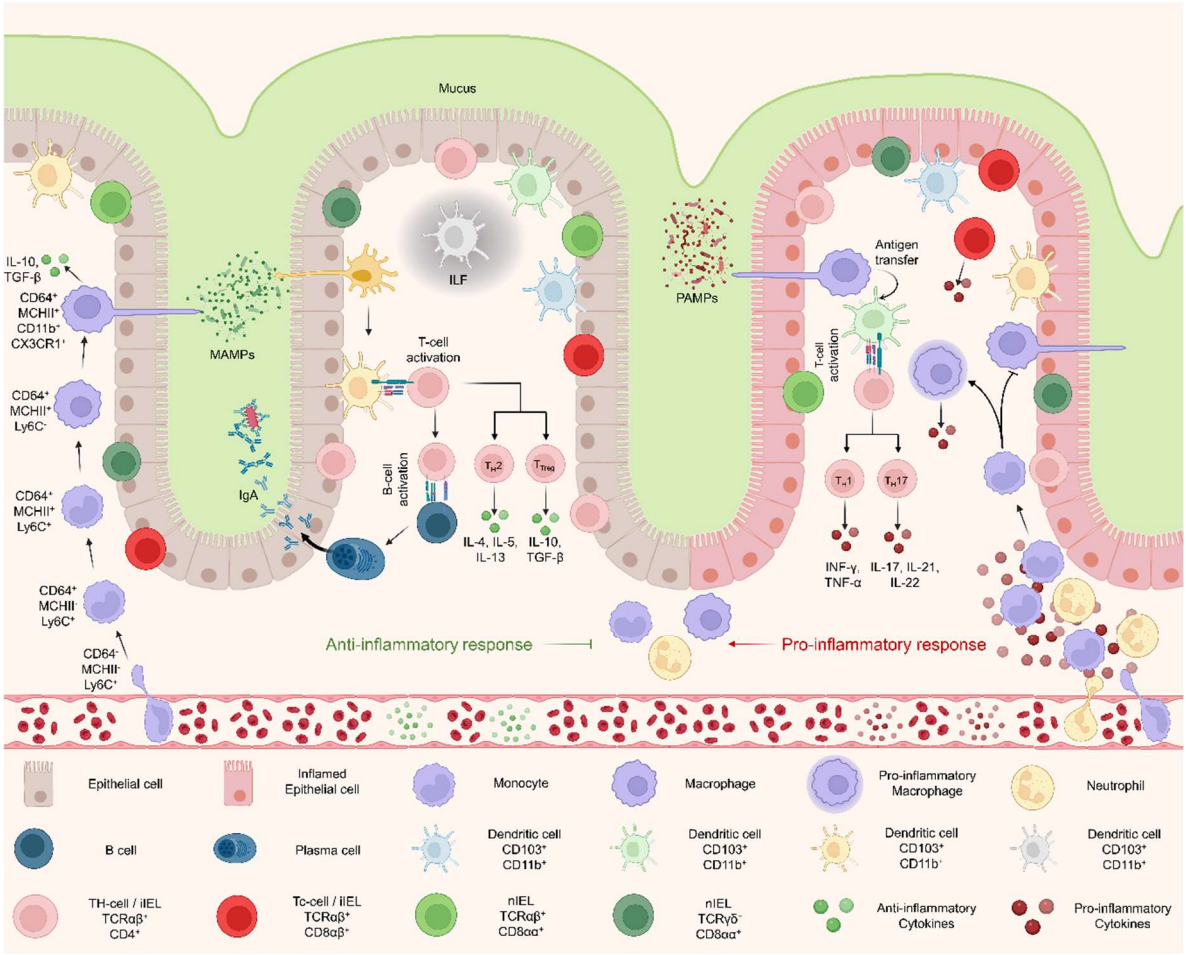

Figure 5 Gastrointestinal immunity

The mucus layer produced by epithelial cells is the first barrier that prevents the direct penetration of the microbiota. Furthermore, the epithelial cell layer itself serves as a physical barrier. In addition, innate and adaptive immune cells of the myeloid and lymphoid lineages play an important role in gastrointestinal immunity. Under healthy conditions, monocytes constitutively enter the mucosa and differentiate into gut resident macrophages, which secret anti-inflammatory cytokines under inflammatory conditions. CX3CR1-positive macrophages are able to sample luminal antigens by forming transepithelial dendrites and can transfer antigens to CD103-positive dendritic cells. During inflammation, monocytes and neutrophils are recruited to the side of inflammation and are the first cells to eliminate invaders. In an inflammatory environment, newly invaded monocytes differentiate into pro-inflammatory macrophages. Dendritic cells can differentiate between MAMPs and PAMPs and each triggering an anti- or pro- inflammatory immune response from T-cells, respectively. T-cells, in turn, can activate B-cells, which differentiate into plasma cells that can produce IgA. Natural and induced intraepithelial lymphocytes act as guardians of the gastrointestinal tract. (Created with Biorender and Power Point; based on (Cerovic et al., 2014; Popov et al., 2021)).

1.5 Inflammatory bowel disease (IBD)

In inflammatory bowel disease (IBD), the homeostasis between intestinal immunity, the epithelial layer, and the microbiota is disturbed, resulting in an overreaction of the immune system, barrier damage, and inflammation. IBD describes chronic and relapsing GI diseases, which manifest in diarrhoea, abdominal pain, intestinal bleeding, and blocking. The two major forms of IBD are Crohn's disease (CD) and ulcerative colitis (UC) (Figure 6).

CD appears in segmental inflammations and can occur in the whole digestive tract, but the terminal ileum is the most often affected segment (80% of cases). CD can be classified as ileal type, colonic type, or ileocolonic type in terms of the region affected. In contrast to CD, UC is limited to the colon, and inflammation typically starts at the rectum (proctitis) and can progress proximal to the splenic flexure (left-sided colitis) until the entire colon is affected (pancolitis, 20% of cases) (reviewed in (Neurath, 2019)). CD affects all layers of the intestine, leading to complications such as abscesses, fistulas, and strictures while in UC only the mucosa and submucosa are involved.

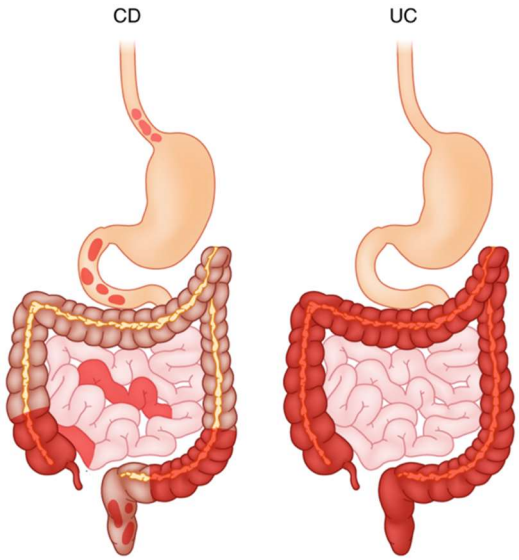

Figure 6 Crohn's disease (CD) and ulcerative colitis (UC), the two entities of inflammatory bowel disease (IBD)

CD appears in segmental inflammations and can occur in the whole digestive tract and can affect all layers of the intestine. In contrast, UC is a continuous inflammation limited to the colon and only mucosa and submucosa are involved (Neurath, 2019).

In severe but rare cases, IBD can cause death. However, the standardised mortality ratio (SMR) of CD and UC patients was similar (1.25 and 0.71, respectively) compared to the general population (Aniwan et al., 2018). IBD prevalence is increasing worldwide, initially in Western countries and today especially in developing countries (Ng et al., 2017). The onset of IBD is usually diagnosed at an age of thirty to forty years in case of UC, and twenty to thirty in

CD, but can develop at any age (Burisch and Munkholm, 2015). To date, there is no cure for IBD, and combined with its early onset in life, low mortality rate, severe symptoms, and increasing prevalence, IBD is a major burden on healthcare systems worldwide.

A disrupted homeostasis between immunity, epithelium and microbiota induces IBD. In addition, environmental factors such as smoking, diet, and medication as well as genetic predisposition are of importance in the aetiology of IBD. Meta-analysis of genome-wide associated studies (GWAS) identified 201 loci associated with IBD (Jostins et al., 2012; Liu et al., 2015). Of which 41 loci are CD-specific, 30 UC-specific and 68% (137) are shared by CD and UC, further demonstrating similar but distinct features of the two diseases. Among IBD specific associated loci, the following processes were identified: barrier function, tolerance, innate defence, T_H17/T_{reg} cells, autophagy, antigen presentation, and negative regulatory of immunity (Khor et al., 2011). This is once again pointing to the role of a disrupted epithelium and impaired immunity in the aetiology and pathogenesis of IBD.

During the last decades several alterations in intestinal immunity in IBD patients were elucidated. As a result, CD is associated with upregulated T_H1 immune responses and the expression of pro-inflammatory cytokines such as IFN-γ, TNF-α, IL-2, whereas UC is driven by a non-conventional T_H2 response and expression of TGF-β, IL-10, IL-5, and IL-13. Moreover, IBD patients have elevated IL-17α levels representing increase of T_H17 cells (Fujino et al., 2003). In addition, changes of innate immune cells were observed. Proinflammatory macrophages accumulate in the mucosa of IBD patients and produce proinflammatory cytokines such as IL-1, IL-6 and TNF-α (Bain et al., 2013; Rugtveit et al., 1997). Similar DCs lose their tolerogenic function and exhibit a more inflammatory phenotype further enhancing T_H1 and T_H17 cells (Middel et al., 2006; Mann and Li, 2014).

The epithelial barrier is also compromised, for example loss of mucus and mucus-producing goblet cells is characteristic of UC (Jass and Walsh, 2001) and cell death occurs as a natural result due to the overreaction of the immune system. Furthermore, the TJ barrier is impaired in IBD, leading to a leaky barrier. TJ structural changes were observed including reduced numbers of strands and particle-like structures with strand brakes instead of continuous and linear strands, indicating a disturbed paracellular barrier (Heller et al., 2005; Zeissig et al., 2007). Moreover, TJ protein expression is altered in IBD.
CLDN1 and CDLN2 are upregulated in UC and CD (Weber et al., 2008; Poritz et al., 2011; Prasad et al., 2005; Heller et al., 2005; Zeissig et al., 2007). CLDN12 and CLDN18 are upregulated in CD and UC, respectively (Amasheh et al., 2011; Zwiers et al., 2008). CLDN3, CLDN4, CLDN5 and CLDN8 are downregulated in CD, while CLDN3, CLDN4 and CLDN7 are

downregulated in UC (Prasad et al., 2005; Lameris et al., 2013; Zeissig et al., 2007; Oshima et al., 2008). The TAMP protein OCLN is downregulated in CD and UC (Heller et al., 2005; Zeissig et al., 2007), whereas TRIC downregulation was only observed in UC (Krug et al., 2018). Albeit, TRIC was delocalised in CD from the crypt bottom towards the surface epithelium (Krug et al., 2018), which might be due to a reduction of angulin-1 in CD patients (Hu et al., 2020).
The upregulation of CLDN2 combined with the downregulation of barrier-forming CLDNs leads to an increased flux of water and solutes from the basolateral side into the lumen, resulting in leak flux diarrhoea. Furthermore, the downregulation of TRIC opens the paracellular pathway for macromolecules (Krug et al., 2018) including antigens from food or pathogens. This might further induce inflammatory processes in the subjacent immune cells.

Until now it is not clear if an impaired TJ barrier is cause or trigger of IBD. However, it is clear that there is a high interaction between IEC and intestinal immune cells, indicated by the effects of several immune cells derived cytokines on TJ proteins. For example, TNF-α, TGF-β, IL-6 and IL-13 are linked to the upregulation of CLDN2 in IBD (Zeissig et al., 2007; Kojima et al., 2008; Suzuki et al., 2011; Heller et al., 2005). The downregulation of the barrier-forming Cldns (Cldn1, Cldn5, Cldn7) was found to be initiated by the two proinflammatory cytokines TNF-α and IFN-γ (Amasheh et al., 2009a). In addition, IL-13 leads to downregulation of TRIC in UC (Krug et al., 2018).
Immune cells can use TJs as a paracellular pathway to completely pass through the epithelium in case of neutrophils (Burns et al., 1997; Kucharzik et al., 2001) or to reach the lumen for antigen sampling in case of DCs and macrophages (Rescigno et al., 2001; Kubo et al., 2009). Some were even found to express TJ proteins (Mariano et al., 2011b; Sung et al., 2006). For example, TRIC expression was detected on cells of the monocyte/macrophage lineage in the LP (Mariano et al., 2011b).
These results highlight the close relationship between the mucosal immune system and the TJ barrier. However, knowledge of the processes behind is limited. Previous research found that immune cells influence the TJ barrier, for example, through the expression of various cytokines, but whether and how the TJ proteins might influence the underlying immune cells in the pathogenesis of IBD remains to be elucidated.

2 Aims

IBD incidences are increasing worldwide, but there is still no cure. Although some treatments are promising and can induce remission or alleviate symptoms (e.g. anti-TNF, anti-Il12/23 and corticosteroids) they do not work for all patients, and often the required treatment doses increase over time. However, all these therapies focus on the regulation/inhibition of the immune system, whereas the epithelial aspects of IBD pathogenesis seem often to be overlooked in the search for treatment targets. Even though an intact epithelium is essential for intestinal homeostasis and one aspect of the pathogenesis of IBD might be increased luminal antigen uptake due to an impaired epithelial barrier, which further promotes inflammatory processes.

The first aim of this study was to elucidate the influence of the impaired TJ barrier on the subjacent immune cells and vice versa during intestinal inflammation. As TJ proteins are potentially involved in macromolecule and thus antigen passage might be of importance, focus was laid on the three TAMPs. MD3 and Ocln are known to have more regulatory functions, whereas Tric and the tTJ were found to be directly involved in paracellular macromolecule passage and presumably in immune cell migration. Hence, TAMPs might have immune regulatory functions.

Organoids can fill the gap between traditional cell culture and animal experiments due to the greater complexity compared to cell lines and the better accessibility compared to animals. Moreover, organoids retain donor properties, which makes them a promising tool for personalised medicine. However, organoids have a major disadvantage when it comes to researching barrier properties. Their 3D structure hinders easy access to the apical side and does not allow the investigation of the barrier with common techniques. Therefore, the establishment of a 2D organoid system / ODMs is essential to enable barrier analysis. However, well-defined culture conditions are essential as they have great impact in the experimental outcome.
Thus, the second aim of this study was to establish intestinal organoids and organoid-derived monolayers (ODMs) and optimisation of standardised culturing methods in our lab.

3 Materials

3.1 Antibodies

Table 1 Antibodies

Target	Reactivity	Host		Dilution	Supplier
Angulin-1/LSR	human	rabbit	IF WB	1:200 1:1000	Atlas antibodies AB, Bromma, Sweden Cat. HPA007270
ß-Actin	chicken, dog, human, mouse, rat	mouse	WB	1:10000	Sigma-Aldrich Chemie GmbH, Traufkirchen, Germany, CAT. A5441
Claudin-1 (2H10D10)	dog, human, mouse, rat	mouse	IF	1:200	Invitrogen, Thermo Fisher Scientific GmbH, Dreireich, Germany, Cat. 374900
Claudin-1	chicken, human, rat	rabbit	WB	1:1000	Invitrogen, Thermo Fisher Scientific GmbH, Dreireich, Germany, Cat. 519000
Claudin-2 (12H12)	dog, human, mouse, rat	mouse	IF WB	1:200 1:1000	Invitrogen, Thermo Fisher Scientific GmbH, Dreireich, Germany, Cat. 325600
Claudin-2 (MH44)	dog, human, rat	rabbit	WB	1:1000	Invitrogen, Thermo Fisher Scientific GmbH, Dreireich, Germany, Cat. 516100
Claudin-3	dog, human, mouse	rabbit	IF WB	1:200 1:1000	Invitrogen, Thermo Fisher Scientific GmbH, Dreireich, Germany, Cat. 341700
Claudin-4 (3E2C1)	dog, human, mouse, rat	mouse	IF WB	1:200 1:1000	Invitrogen, Thermo Fisher Scientific GmbH, Dreireich, Germany, Cat. 329400
Claudin-7	dog, human, mouse	rabbit	IF WB	1:200 1:1000	Invitrogen, Thermo Fisher Scientific GmbH, Dreireich, Germany, Cat. 349100
Claudin-15		rabbit	IF	1:200	Invitrogen, Thermo Fisher Scientific GmbH,

Target	Reactivity	Host		Dilution	Supplier
					Dreireich, Germany, Cat. 389200
Cytokeratin 19	human, mouse	rabbit	WB	1:1000	Invitrogen, Thermo Fisher Scientific GmbH, Dreireich, Germany, Cat. PA5-32463
CD4-APC (GK1.5)	mouse	rat	FC	1:300	Biolegend GmbH, Koblenz, Germany, Cat. 100412
CD4-BV711 (GK1.5)	mouse	rat	FC	1:400	Biolegend GmbH, Koblenz, Germany, Cat. 100447
CD4-FITC (GK1.5)	mouse	rat	FC	1:200	BD Bioscience, Heidelberg, Germany, Cat. 553729
CD8a-BV785 (53-6.7)	mouse	rat	FC	1:100	Biolegend GmbH, Koblenz, Germany, Cat. 100750
CD8a-FITC (53-6.7)	mouse	rat	FC	1:100	Biolegend GmbH, Koblenz, Germany, Cat. 100706
CD8b-Alexa 700 (YTS156.7.7)	mouse	rat	FC	1:200	Biolegend GmbH, Koblenz, Germany, Cat. 126618
CD11b-APC/Cy7 (M1/70)	human, mouse	rat	FC	1:100	BD Bioscience, Heidelberg, Germany, Cat. 557657
CD11c-PerCP Cy5.5 (N418)	mouse	Armenian hamster	FC	1:200	Invitrogen, Thermo Fisher Scientific GmbH, Dreireich, Germany, Cat. 45-0114-82
CD19-FITC (1D3)	mouse	rat	FC	1:400	Biolegend GmbH, Koblenz, Germany, Cat. 152404
CD19-PE (1D3)	mouse	rat	FC	1:400	Invitrogen, Thermo Fisher Scientific GmbH, Dreireich, Germany, Cat. 12-0193-82
CD44-FITC (IM7)	human, mouse	rat	FC	1:100	Biolegend GmbH, Koblenz, Germany, Cat. 103006
CD45-APC/Cy7	mouse	rat	FC	1:200	Biolegend GmbH, Koblenz, Germany, Cat. 103116

Target	Reactivity	Host		Dilution	Supplier
CD45.2-BUV395 (104)	mouse	mouse	FC	1:100	BD Bioscience, Heidelberg, Germany, Cat. 564616
CD45-V500 (30-F11)	mouse	rat	FC	1.200	BD Bioscience, Heidelberg, Germany, Cat. 561487
CD62L-APC/Cy7 (MEL-14)	mouse	rat	FC	1:100	Biolegend GmbH, Koblenz, Germany, Cat. 104428
CD64-APC (X54-5/7.1)	mouse	mouse	FC	1:100	Biolegend GmbH, Koblenz, Germany, Cat. 139306
CD69-APC (H1.2F3)	mouse	Armenian hamster	FC	1:40	Biolegend GmbH, Koblenz, Germany, Cat. 104514
CD103-PE-CY7 (2E7)	mouse	Armenian hamster	FC	1:200	Biolegend GmbH, Koblenz, Germany, Cat. 121426
CX3CR1-BV605 (SAO11F11)	mouse	mouse	FC	1:200	Biolegend GmbH, Koblenz, Germany, Cat. 149027
FC-Block/ CD16/CD32	mouse	rat	FC	1:250	BD Bioscience, Heidelberg, Germany, Cat. 553142
Ly6C-PE (HK1.4)	mouse	rat	FC	1:400	Invitrogen, Thermo Fisher Scientific GmbH, Dreireich, Germany, Cat. 12-5932-82
Ly6G-Alexa 700 (1A8)	mouse	rat	FC	1:200	Biolegend GmbH, Koblenz, Germany, Cat. 127622
Ly6G-PE-Cy7 (RB6-8C5)	mouse	rat	FC	1:300	TONBO Biosciences, San Diego, United States, Cat. 60-5931-U025
MarvelD3		rabbit	WB	1:1000	Kind gift of Jerrold Turner, Laboratory of Mucosal Barrier Pathobiology, Brigham and Women's Hospital, Harvard Medical School, Boston, USA

Target	Reactivity	Host		Dilution	Supplier
MarvelD3	human	rabbit	IF	1:200	Proteintech Germany GmbH, Planegg-Martinsried, Germany, Cat. 25667-1-AP
MHC II-Pac. Blue (M5/114.15.2)	mouse	rat	FC	1:500	Biolegend GmbH, Koblenz, Germany Cat. 107620
Noggin	mouse	goat	WB	1:2000	R&D Systems, Bio-techne, Wiesbaden-Nordenstadt, Germany,Cat. AF719-SP
Occludin (OC-3F10)	dog, human, mouse, rat	mouse	IF WB	1:200 1:1000	Invitrogen, Thermo Fisher Scientific GmbH, Dreireich, Germany, Cat. 331500
Occludin	dog, human, rat	rabbit	WB	1:1000	Invitrogen, Thermo Fisher Scientific GmbH, Dreireich, Germany, Cat. 711500
Occludin	human, mouse, rat	rabbit	WB		Proteintech Germany GmbH, Planegg-Martinsried, Germany, Cat. 27260-1-AP
R-Spondin1	human/ mouse	mouse	WB	1:2000	R&D Systems, Bio-techne, Wiesbaden-Nordenstadt, Germany,Cat. MAB4658-SP
TCRb-Pac. Blue (H57-597)	mouse	armenian hamster	FC	1:100	Biolegend GmbH, Koblenz, Germany Cat. 109226
TCRgd-PE (GL3)	mouse	armenian hamster	FC	1:100	Biolegend GmbH, Koblenz, Germany Cat. 118108
Tricellulin (54H19L38)	human	rabbit	IF WB	1:200 1:1000	Invitrogen, Thermo Fisher Scientific GmbH, Dreireich, Germany, Cat. 700191
Tubulin-alpha	bovine, chicken, human, mouse, rat	mouse	WB	1:4000	Sigma-Aldrich Chemie GmbH, Traufkirchen, Germany, CAT. T9026

Target	Reactivity	Host		Dilution	Supplier
Vimentin (R28)	Human, mouse, rat, monkey	rabbit	WB	1:1000	Cell Signaling Technology Europe, B.V., Leiden, Netherlands, Cat. 3932
ZO1-647 (ZO1-1A12)	dog, human	mouse	IF	1:500	Invitrogen, Thermo Fisher Scientific GmbH, Dreireich, Germany, Cat. MA3-39100-A647
secondary antibody Alexa Flour 488	rabbit	goat	IF	1:500	Invitrogen, Thermo Fisher Scientific GmbH, Dreireich, Germany, Cat. A11034
secondary antibody Alexa Flour 594	mouse	goat	IF	1:500	Invitrogen, Thermo Fisher Scientific GmbH, Dreireich, Germany, Cat. A11032
secondary peroxidase-conjugated antibodies	rabbit		WB	1:10000	Jackson ImmunoResearch, Cambridge House, UK, Cat. 111-036-003
secondary peroxidase-conjugated antibodies	mouse		WB	1:10000	Jackson ImmunoResearch, Cambridge House, UK, Cat. 115-036-003

3.2 Buffers and solutions

Table 2 Buffers and solutions

Buffer/ Solution	Composition
Crypt isolation	
Coating solution	0.1% (w/v) BSA in 1x $PBS^{+/+}$
EDTA solution	2.5 mM EDTA in 1x $PBS^{+/+}$
Agarose gel electrophorese	
TRIS-Acetate-EDTA **(TAE) Buffer**	0,4 M Tris; 0,01 M EDTA
Immunofluorescence staining	
Fixing solution	2% (w/v) Paraformaldehyde

Buffer/ Solution	Composition
	in 1x $PBS^{+/+}$
Permeabilisation solution	0.2% (v/v) Triton X-100 In 1x $PBS^{+/+}$
Blocking solution	5% (w/v) BSA; 5% (v/v) Goat serum in 1x $PBS^{+/+}$
20 × TRIS – EDTA – Citrate (TEC) Buffer	41 mM Tris; 34 mM EDTA; 23 mM $Na_3C_6H_5O_7$
TBST (IF and WB)	20 mM Tris; 500 mM NaCl; 0,1% (v/v) Tween 20 in ddH_20 pH 7,3
Western Blot	
Total lysis buffer	10 mM Tris-HCl (pH 7.5); 150 mM NaCl; 0.5% (v/v) Triton X-100, 0,1% (w/v) SDS; in ddH_20 1 pill protease inhibitor per 10 ml buffer
Membrane lysis buffer	1 M Tris-HCl (pH 7.4); 1 M $MgCl_2$, 0.5 M EDTA; 0.5 M EGTA in ddH_20 1 pill protease inhibitor per 10 ml buffer
5 × Leammli buffer	500 mM DTT; 125 mM Tris/HCl (pH 6.8); 50% (v/v) Glycerol; 10% (w/v) SDS; 0.001% (w/v) Bromphenol blue in ddH_20
Separation gel	8 - 12.5% Acrylamid / Bisacrylamid (Rotiphorese Gel 30% (37.5 : 1)); 350 mM Tris buffer (pH 8.8); 0.1% (v/v) SDS, 0.1% (v/v) APS, 0.1% (v/v) TEMED in ddH_20
Stacking gel	5.1% Acrylamid / Bisacrylamid (Rotiphorese Gel 30% (37.5 : 1)); 125 mM Tris buffer (pH 6.8); 0.1% (w/v) SDS, 0.1% (v/v) APS, 0.1% (v/v) TEMED in ddH_20
10 × West buffer	1.9 M Glycin; 0.25 M Tris in ddH_20 (pH 8.1 - 8.4)
Electrophorese (EPHO) buffer	10% 10 × west buffer, 0.1% SDS in ddH_20
Transfer buffer	10% 10 × west buffer, 10% Methanol in ddH_20
WB blocking solution	1% (w/v) PVP-40; 0,05% (v/v) Tween 20 in ddH_2O
Immune cell isolation and staining	
EDTA digestion solution	5 mM EDTA; 10 mM HEPES

Buffer/ Solution	Composition
	in $HBSS^{-/-}$
Collagenase digestion solution	5% FCS; 500 µg/ml Collagenase IV; 0,025 MU/ml DNAse I; 1/100 Dispase in RPMI
100% Percoll	9 parts Percoll mixed with 1 part 10 × $PBS^{+/+}$
80% - 40% Percoll	80 - 40% 100% Percoll In $PBS^{+/+}$
T-cell stimulation solution	50 µM β-Mercaptoethanol; 20 ng/ml PMA, 1 µg/ml Ionomycin
FACS	2% FCS in $PBS^{-/-}$

3.3 Cell lines

Table 3 Cell lines

Cell line	Source	Supplier
HT-29/B6	Human colorectal adenocarcinoma	(Kreusel et al., 1991)
Caco-2	HTB-37™ Human colorectal adenocarcinoma	ATCC®
HEK-293	human embryonic kidney	AG Huber, Charité
L-WRN	CRL-3276™ Mouse Subcutaneous connective tissue; areolar and adipose	ATCC®
One Shot™ TOP10F' Chemically Competent	*E.coli*	Thermo Fisher Scientific GmbH, Dreireich, Germany

3.4 Chemicals

Table 4 Chemicals

Chemical	Supplier
1,4 Dithiothreitol (DTT)	Merck Chemicals GmbH, Darmstadt, Germany
2-Mercaptoethanol	Carl Roth GmbH, Karlsruhe, Germany
4-(2-hydroxyethyl)-1-piperazineethanesulfonic acid (HEPES)	Bio&Sell GmbH, Feucht, Germany
4', 6-diamidino-2-phenylindole (DAPI)	Roche Diagnostics GmbH, Mannheim, Germany

Chemical	Supplier
4-kDa dextran	Serva Electrophoresis GmbH, Heidelberg, Germany
4-kDa FITC-dextran (FD4)	TdB Consultancy, Uppsala, Sweden
6 × Gel loading Dye Purple	New England Biolabs GmbH, Frankfurt am Main, Germany
50 × Tris-acetate/EDTA (TAE) buffer	Serva Electrophoresis GmbH, Heidelberg, Germany
A83-1 (TGF-ß inhibitor)	Stemgent, Reprocell Europe, Glasgow, UK
Advanced Dulbecco's Modified Eagle Medium/ Nutrient Mixture F-12 (DMEM/F12)	Gibco, Thermo Fisher Scientific GmbH, Dreireich, Germany
Agarose Basic	Applichem, Darmstadt, Germany
Albumin standard	Thermo Fisher Scientific GmbH, Dreireich, Germany
Ammonium persulfate (APS)	Sigma-Aldrich Chemie GmbH, Traufkirchen, Germany
Agar	Sigma-Aldrich Chemie GmbH, Traufkirchen, Germany
B-27	Gibco, Thermo Fisher Scientific GmbH, Dreireich, Germany
BME, Type 2, Select	Cultrex, R&D Systems, Bio-techne, Wiesbaden-Nordenstadt, Germany
Bovine serum albumin (BSA) Fraction V	Biomol GmbH, Hamburg, Germany
Bovine serum albumin (BSA), heat shock fraction, protease free, fatty acid free, essentially globulin free, pH 7	Sigma-Aldrich Chemie GmbH, Traufkirchen, Germany
Brefeldin A	Sigma-Aldrich Chemie GmbH, Traufkirchen, Germany
Bromphenol blue	Sigma-Aldrich Chemie GmbH, Traufkirchen, Germany
Chloroform	Merck Chemicals GmbH, Darmstadt, Germany
Dako blocking	Dako Deutschland GmbH, Hamburg, Germany
Dimethylsulfoxid (DMSO)	Carl Roth GmbH, Karlsruhe, Germany
Dextran sulfate sodium (DSS)	TdB Consultancy, Uppsala, Sweden

Chemical	Supplier
Dulbecco's PBS with Mg^{2+}/Ca^{2+} ($PBS^{+/+}$)	Gibco, Thermo Fisher Scientific GmbH, Dreireich, Germany
Dulbecco's PBS without Mg^{2+}/Ca^{2+} ($PBS^{-/-}$)	Gibco, Thermo Fisher Scientific GmbH, Dreireich, Germany
Dulbecco's Modified Eagle Medium (DMEM) + Glutamax	Gibco, Thermo Fisher Scientific GmbH, Dreireich, Germany
Epithelial growth factor (EGF) human	Peprotech, Thermo Fisher Scientific GmbH, Dreireich, Germany
Epithelial growth factor (EGF) mouse	Peprotech, Thermo Fisher Scientific GmbH, Dreireich, Germany
Ethanol 100%	Carl Roth GmbH, Karlsruhe, Germany
Ethanol 80%	Chemsolute, TH Geyer, Renningen, Germany
Ethidium Bromide (EtBr)	Serva Electrophoresis GmbH, Heidelberg, Germany
Ethylene Diamine Tetra Acetic Acid (EDTA)	Merck Chemicals GmbH, Darmstadt, Germany
Ethylene Glycol Tetra Acetic Acid (EGTA)	Carl Roth GmbH, Karlsruhe, Germany
Fetal Bovine Serum (FBS)	Gibco, Thermo Fisher Scientific GmbH, Dreireich, Germany
Fibroblast growth factor 2	Peprotech, Thermo Fisher Scientific GmbH, Dreireich, Germany
Glucose	Carl Roth GmbH, Karlsruhe, Germany
Glutamax	Gibco, Thermo Fisher Scientific GmbH, Dreireich, Germany
Glycerol	Serva Electrophoresis GmbH, Heidelberg, Germany
Glycine	Carl Roth GmbH, Karlsruhe, Germany
Goat serum	PAN Biotech, Aidenbach, Bayern
Hanks' Balanced Salt Solution without Mg^{2+}/Ca^{2+} ($HBSS^{-/-}$)	Gibco, Thermo Fisher Scientific GmbH, Dreireich, Germany
Hygromycin B-solution	Carl Roth GmbH, Karlsruhe, Germany
Insulin-like growth factor I	Biolegend GmbH, Koblenz Germany
Ionomycin calcium salt from Streptomyces conglobatus	Sigma-Aldrich Chemie GmbH, Traufkirchen, Germany

Chemical	Supplier
Isopropanol	Chemsolute, TH Geyer, Renningen, Germany
Kanamycin sulphate	Thermo Fisher Scientific GmbH, Dreireich, Germany
LB Medium Powder	MP Biomedicals, Illkirch, France
Lipofectamine-Reagent (shRNA transfection)	Invitrogen, Thermo Fisher Scientific GmbH, Dreireich, Germany
Magnesium chloride ($MgCl_2$)	Carl Roth GmbH, Karlsruhe, Germany
Matrigel® Matrix (Basement membrane, growth factor reduced)	Corning GmbH, Kaiserslautern, Germany
Methanol	Merck Chemicals GmbH, Darmstadt, Germany
Milk powder	Carl Roth GmbH, Karlsruhe, Germany
Minimum Essential Medium (MEM) with glutamax	Corning GmbH, Kaiserslautern, Germany
Molecular weight marker HyperLadder 100 bp and 1 kb	Bioline, Luckenwalde, Germany
Nitrogen (N_2)	Gibco, Thermo Fisher Scientific GmbH, Dreireich, Germany
N-Acetylcysteine (NAC)	Sigma-Aldrich Chemie GmbH, Traufkirchen, Germany
N,N,N',N'-Tetramethylethylenediamine (TEMED)	Sigma-Aldrich Chemie GmbH, Traufkirchen, Germany
Nicotinamide (NIC)	Sigma-Aldrich Chemie GmbH, Traufkirchen, Germany
Organoid Harvesting solution	Cultrex, R&D Systems, Bio-techne, Wiesbaden-Nordenstadt, Germany
PageRuler Plus Prestained Protein Ladder	Thermo Fisher Scientific GmbH, Dreireich, Germany
Paneticin G418	PAN Biotech, Aidenbach, Bayern
Paraformaldehyde 16%	Electron microscopy sciences, Munich, Germany
Penicillin Streptomycin Solution (P/S)	Corning GmbH, Kaiserslautern, Germany
Percoll	Cytivia Europe GmbH, Freiburg, Germany

Chemical	Supplier
Phorbol 12-myristate 13-acetate (PMA)	Sigma-Aldrich Chemie GmbH, Traufkirchen, Germany
Pierce BCA-Protein Assay (Reagents A and B)	Thermo Fisher Scientific GmbH, Dreireich, Germany
Polyethyleneimine (PEI)	Serva Electrophoresis GmbH, Heidelberg, Germany
Polysorbate 20 (Tween-20)	Arcos Organics, Thermo Fisher Scientific GmbH, Dreireich, Germany
Polyvinylpyrrolidone (PVP, wt 40.000)	Sigma-Aldrich Chemie GmbH, Traufkirchen, Germany
ProTaqs MountFluor	Biocyc GmbH & Co. KG., Potsdam, Germany
Protease inhibitor cocktail tablets	Roche Diagnostics GmbH, Mannheim, Germany
Primocin	InvivoGen Europe, Toulouse, France
Puromycin (Hydrochloride)	Cayman Chemical Company,Europe, Tallinn, Estonia
RNA*later*™ Soln.	Invitrogen, Thermo Fisher Scientific GmbH, Dreireich, Germany
Roswell Park Memorial Institute (RPMI) 1640 Medium	Gibco, Thermo Fisher Scientific GmbH, Dreireich, Germany
Rotiphorese Gel 30%	Carl Roth GmbH, Karlsruhe, Germany
SB 202190 (p38 inhibitor)	Stemcell Technologies Germany GmbH, Colonge, Germany
SOC medium	Invitrogen, Thermo Fisher Scientific GmbH, Dreireich, Germany
Sodium azide (NaN_3)	Merck Chemicals GmbH, Darmstadt, Germany
Sodium chloride (NaCl)	Carl Roth GmbH, Karlsruhe, Germany
Sodium Dodecyl Sulfate (SDS)	Carl Roth GmbH, Karlsruhe, Germany
SuperSignal™ West Pico PLUS Luminol/Enhancer solution	Thermo Fisher Scientific GmbH, Dreireich, Germany
SuperSignal™ West Pico PLUS Stable peroxide solution	Thermo Fisher Scientific GmbH, Dreireich, Germany
TaqMan Universal PCR Master Mix	Applied Biosystems, Thermo Fisher Scientific GmbH, Dreireich, Germany

Chemical	Supplier
Tris	Carl Roth GmbH, Karlsruhe, Germany
Tris-HCl 0.5 M, pH 6.8	Bio-Rad Laboratories GmbH, Munich, Germany
Tris-HCl 1 M, pH 8.8	Serva Electrophoresis GmbH, Heidelberg, Germany
Tris-HCl, pH 7.5	Gibco, Thermo Fisher Scientific GmbH, Dreireich, Germany
Tris-HCL, pH 7.4	Rockland Immunochemicals, Biomol GmbH, Hamburg, Germany
Tri-sodium citrate	Carl Roth GmbH, Karlsruhe, Germany
Triton X-100	Roche Diagnostics GmbH, Mannheim, Germany
Trizol reagent	Ambion, Thermo Fisher Scientific GmbH, Dreireich, Germany
0.25% Trypsin, 2.21 mM EDTA, 1x [-] sodium bicarbonate Trypsin/EDTA	Corning GmbH, Kaiserslautern, Germany
TrypLE Express	Gibco, Thermo Fisher Scientific GmbH, Dreireich, Germany
Water for molecular biology	Millipore, Merck Chemicals GmbH, Darmstadt, Germany
Water for cell culture	Millipore, Merck Chemicals GmbH, Darmstadt, Germany
Xylene	Carl Roth GmbH, Karlsruhe, Germany
Y-27623 (Roh-K inhibitor)	Tocris, Bio-techne, Wiesbaden-Nordenstadt, Germany

3.5 Consumables

Table 5 Consumables

Consumable	Supplier
Cell culture flasks (25, 75, and 150 cm^2)	Corning GmbH, Kaiserslautern, Germany
Cell Culture Inserts PCF, 12mm diameter, 0.4 µm and 3 µm pore size)	Millicell, Millipore, Merck Chemicals GmbH, Darmstadt, Germany
Cell culture plate (6, 12, 24 wells)	Corning GmbH, Kaiserslautern, Germany

Consumable	Supplier
Cell scrapers (stirring rods)	Sarstedt AG & Co. KG, Nümbrecht, Germany
Cover glass	VWR International GmbH, Darmstadt, Germany
Eppendorf tubes (1.5 mL)	Eppendorf, Hamburg, Germany
Falcon tubes (15 and 50 ml)	Corning GmbH, Kaiserslautern, Germany
Fast optical 96-well reaction Plate with Barcode (0,1ml)	Applied Biosystems, Thermo Fisher Scientific GmbH, Dreireich, Germany
Filter paper for Western blotting (Whatman 3 mm)	GE Healthcare, Munich, Germany
Glass Pasteur pipettes	BRAND GmbH + Co, Wertheim, Germany
Luer-Lock 30 ml	Chirana GmbH & Co. KG, Gera, Germany
MACS SmartStrainers (70 µm)	Miltenyi Biotec B.V. & Co. KG, Bergisch Gladbach, Germany
Microscope slides	VWR International GmbH, Darmstadt, Germany
Microtiter plates ROTILABO U-profile 96-well	Carl Roth GmbH, Karlsruhe, Germany
PCR SingleCap 8er-SoftStrips 0.2 ml	Biozym, Hessisch Oldendorf, Germany
Pipettes (0.5 – 10 µl, 10 – 100 µl and 100 – 1000 µl)	Eppendorf, Hamburg, Germany
Pipette tips (10, 200 and 1000 µl; with and without filters)	Sarstedt AG & Co. KG, Nümbrecht, Germany
Plastic Pasteur pipettes (Pastette)	Alpha Laboratories Limited, Hamphire, United Kingdom
Polysterene round-bottom tube with cell-strainer cap 5 ml	Falcon, Corning GmbH, Kaiserslauter, Germany
PVDF transfer membrane	Thermo Fisher Scientific GmbH, Dreireich, Germany
SafeSeal reactiontube	Sarstedt AG & Co. KG, Nümbrecht, Germany
Sterican Needle 21 and 26 G	Braun GmbH, Kronberg, Germany

Consumable	Supplier
Stericup Qick Release Millipore Express PLUS 0.22 µm PES, 1L	Millipore, Merck Chemicals GmbH, Darmstadt, Germany
Surgical disposable scalpels	Braun GmbH, Kronberg, Germany
Syringe BD Discardit II 10 ml	BD, Heidelberg, Germany
Syringe BD Plastipak™ Luer 1 ml	BD, Heidelberg, Germany
Syringe Filter (25 mm^2, 0.2 µm pore size)	LABSOLUTE, Th.Geyer, Renningen, Germany
Tissue culture test plates (24 and 48 wells, polystyrene)	TPP Techno Plastic Products AG, Trasadingen, Swiss

3.6 Enzymes

Table 6 Enzymes

Enzyme	Supplier
Collagenase Type IV	Stemcell Technologies Germany GmbH, Cologne, Germany
Dispase	Corning GmbH, Kaiserslautern, Germany
DNAse I, Bovine Pancreas	Millipore, Merck Chemicals GmbH, Darmstadt, Germany

3.7 Equipment

Table 7 Equipment

Device	Version	Supplier
Aspiration pump	FB70155	Thermo Fisher Scientific GmbH, Dreireich, Germany
Autoclave	VX-150	Systec GmbH, Linden, Germany
Centrifuges	Mini Star silverline	VWR International GmbH, Darmstadt, Germany
	PerfectSpin 24R Refrigerated Microcentrifuge	PEQLAB Biotechnology GmbH, Germany
	Megafuge 16R	Heraeus, Thermo Fisher Scientific GmbH, Dreireich, Germany

Device	Version	Supplier
	Avanti J-25	Beckman, Thermo Fisher Scientific GmbH, Dreireich, Germany
CO_2 incubator	Function line	Heraeus instruments, Thermo Fisher Scientific GmbH, Dreireich, Germany
	08-38367	Binder, Tuttlingen, Germany
Confocal laser scanning microscope	LSM 780	Carl Zeiss Microscopy GmbH, Jena, Germany
Electrophoresis chamber	Mini PROTEAN Tetra Cell	R&D Systems, Bio-techne, Wiesbaden-Nordenstadt, Germany,
Flow cytometer	FACS Canto II LSR Fortessa X-20	BD, Heidelberg, Germany BD, Heidelberg, Germany
Freezer -80°C	Herafreeze, HFU T Series	Thermo Fisher Scientific GmbH, Dreireich, Germany
Freezing Container	CoolCell® LX	Corning GmbH, Kaiserslautern, Germany
Fume Hood	Secuflow	Waldner Laboreinrichtungen GmbH, Wangen, Germany
Heating block	AccuBlock™ Digital Dry Bath	Labnet International, Inc. NJ, USA
Imaging system	Fusion (FX)	Vilber Lourmat Deutschland GmbH, Eberhardzell, Germany
	Fusion FX7	Vilber Lourmat Deutschland GmbH, Eberhardzell, Germany
	Azure	Biozym, Hessisch Oldendorf, Germany
Inverted microscope	Olympus CK2	Olympus Europe SE & Co. KG, Hamburg, Germany
Lab Water System	Arium® pro UV Ultrapure Water System	Sartorius, Göttingen, Germany
Laminar airflow Workbench	MSC-ADVANTAGE	Thermo Fisher Scientific GmbH, Dreireich, Germany
Liquid nitrogen tank		Tec-lab, Königstein, Germany
Magnetic stirring	IKAMAG® REO/RCT	Janke and Kunkel GmbH, Staufen Germany
Micropipette	10, 100, 200 and 1000 µL	Eppendorf, Hamburg, Germany

Device	Version	Supplier
Microplate reader	Tecan Infinite M200 PRO (Absorbance 96 well plates)	Tecan Trading AG, Männedorf, Swiss
Nanodrop Spectrophotometer	Nanodrop 2000	Thermo Fisher Scientific GmbH, Dreireich, Germany
pH meter	HI 9017 microprocessor	Hanna Instruments, Kehl, Germany
Power supply for electrophoresis and western blotting	BioRad Power PAC 200	R&D Systems, Bio-techne, Wiesbaden-Nordenstadt, Germany,
Real-Time PCR machine	7500 Fast Real-Time PCR System	Thermo Fisher Scientific GmbH, Dreireich, Germany
Rocking platform	VWR	VWR International GmbH, Darmstadt, Germany
	WT	Biometra, Göttingen, Germany
Scale	PAS241	Thermo Fisher Scientific GmbH, Dreireich, Germany
	Sartorius	Sartorius Lab Instruments GmbH & Co. KG, Göttingen, Germany
Shaker	Ecotron	Infors AG, Bottmingen, Swiss
Tapered tissue grinder		Wheaton, DKW life sciences, Wertheim, Germany
TER measuring device	Chop-stick electrodes STX2	World Precision Instruments, Sarasota, FL, USA
	EVOM3 Epithelial Volt Ohm Meter	
Thermal cycler	PEQSTAR	PEQLAB Biotechnology GmbH, Germany
Ultrasonic Processor	UP50H	Hielscher Ultrasonics GmbH, Teltow, Germany
Vortex device	RS-VA 10	Phoenix Instrument GmbH, Garbsen, Germany
Water bath	SW21	JULABO Labortechnik GmbH, Seelbach, Germany

3.8 Kits

Table 8 Kits

Kit	Supplier
eBioscience™ FOXP3/Transcription factor Staining Buffer Set	Invitrogen, Thermo Fisher Scientific GmbH, Dreireich, Germany
High Capacity cDNA Reverse Transcription kit	Applied Biosystems, Thermo Fisher Scientific GmbH, Dreireich, Germany
NucleoSpin RNA/Protein	Macherey-Nagel, Düren, Germany
Qproteome FFPE Tissue Kit	Qiagen, Hilden, Germany
Plasmid Midi Kit	Qiagen, Hilden, Germany

3.9 Media

Table 9 Media

Medium	Composition	Supplier
SOC		Invitrogen™ Thermo Fisher Scientific Inc., Waltham, MA, US
LB medium	2.5% (w/v) LB medium powder in ddH_2O	
Caco-2 cell culture medium	15% FCS; 100 U/mL penicillin; 100 mg/mL streptomycin in MEM GlutaMAX	
HT-29/B6 cell culture medium	10% FCS; 100 U/mL penicillin; 100 mg/mL streptomycin in RPMI 1640	
HEK-293 cell culture medium	10% FCS; 100 U/mL penicillin; 100 mg/mL streptomycin in MEM	
Growth medium	10% heat inactivated (HI) FCS; in DMEM GlutaMAX	
Noggin/R – spondin1 selection medium	10% HI FCS; 1 mg/ml G418 in DMEM GlutaMAX	
L-WRN selection medium	10% HI FCS; 0.5 mg/ml G418; 0.5 mg/ml Hycromycin B in DMEM GlutaMAX	
AD++	10 mmol/L HEPES; 1 × GlutaMax in Advanced Dulbecco´s modified Eagle medium (DMEM)/ F12	

Medium	Composition Supplier
AD+++	10 mmol/L HEPES; 1 × GlutaMax; 100 U/mL penicillin; 100 mg/mL streptomycin in Advanced Dulbecco´s modified Eagle medium (DMEM)/ F12

3.9.1 Organoid and ODM media composition

Table 10 Organoid and ODM media composition

All media were based on AD++ supplemented with 100 µg/ml Primocin; 1 × B27, 1 × N2, 1 mM N – Acetylcysteine and 10 µM Y-27623 (Rho-K inhibitor) were added initially for 48h after splitting /seeding. Abbreviations: small intestine (si), colon (co) epithelial growth factor (EGF); Nicotinamide (NIC); SB 202190 (p38 inhibitor); A83-1 (TGF-ß inhibitor); insulin-like growth factor 1(IGF-1); fibroblast growth factor 2 (FGF-2)

	RN-E (mouse si)	WRN-RN-E (mouse co)	WRN-RN-NicASB (human)	WRN-RN-NicAlF (UC)	RN-ENic (differentiation)
L-WRN CM (50%)		X	X	X	
Rspo1 CM (20%)	X	X	X	X	X
Nog CM (10%)	X	X	X	X	X
EGF (50 ng/ml)	X	X	X	X	
Nic (10 mM)			X	X	X
A83-01 (500 nM)			X	X	X
SB-202190 (1 µM)			X		
IGF 100 ng/ml				X	
FGF (50 ng/ml)				X	

3.10 Plasmids

Table 11 Plasmids

Plasmid	Composition	Supplier
Mouse Noggin (Nog)	Untagged, pCMV6-Entry Vector, Kanamycin resistance, CAT. MC209047	OriGene Technologies GmbH, Herford, Germany
Mouse R-spondin homolog (Rspo1)	Untagged, pCMV6-Entry Vector, Kanamycin resistance, CAT. MC212441	OriGene Technologies GmbH, Herford, Germany

3.11 Primers & Probes

Table 12 Primers & Probes

Genes	Forward	Reverse
Primers		
ACTB	GATGTATGAAGGCTTTGGTC	TGTGCACTTTTATTGGTCTC
CCL2	CAAGATGATCCCAATGAGTAG	TTGGTGACAAAAACTACAGC
CXCL9	GAGGAACCCTAGTGATAAGG	GTTTGATCTCCGTTCTTCAG
IL-1β	GGATGATGATGATAACCTGC	CATGGAGAATATCACTTGTTGG
IL-6	AAGAAATGATGGATGCTACC	GAGTTTCTGTATCTCTCTGAAG
IL-10	CTTTAAGGGTTACTTGGGTTG	AAATGCTCCTTGATTTCTGG
IL-12β	TGCAAAGAAACATGGACTTG	GGACACTGAATACTTCTCATAG
IL-13	CTTAAGGAGCTTATTGAGGAG	CATTGCAATTGGAGATGTTG
IL-17α	ACGTTTCTCAGCAAACTTAC	CCCCTTTACACCTTCTTTTC
IL-22	ATCAGTGCTACCTGATGAAG	CATTCTTCTGGATGTTCTGG
INF-γ	CTAGCTCTGAGACAATGAAC	CTCTTTTCTTCCACATCTATGC
TGFβ1	GGATACCAACTATTGCTTCAG	TGTCCAGGCTCCAAATATAG
TagMan GE Assay	Dye	Assay ID
GAPDH	VIC (victoria; 2'-chloro-7'phenyl-1,4-dichloro-6-carboxy-flourescein)	4352339E
MUC2	FAM (Fluorescein amidite)	Mm01276696_m1 Muc2
LyZ1	FAM	Mm00657323_m1 LyZ1
CHGA	FAM	Mm00514341_m1 Chga
LGR5	FAM	Mm00438890_m1 LGR5

3.12 Software

Table 13 Software

Software	Supplier
Aida Image Analyzer v.5.1	Elysia-Raytest GmbH, Straubenhardt, Germany
Microsoft Office – Excel, Word	Microsoft Corporation, Redmond, US
FlowJo v10.8.1	Becton Dickinson, Franklin Lakes, US
GraphPad Prism v8	GraphPad Software, San Diego, US
Zen	Carl Zeiss Microscopy GmbH, Jena, Germany

4 Methods

4.1 Patient samples

The usage of human duodenum or colon biopsies from healthy controls and samples from surgery of ulcerative colitis patients was approved by the Ethics Committee of the Charité Berlin (#EA4-015-13 and #EA1-200-17). Tissue specimens were used for isolation of intestinal crypts in order to generate organoids.

4.2 Mouse models

Effects of TAMPs were studied on mice with an intestinal epithelial cell specific TAMP overexpression (TAMP-OE). Generation of B6.C-Tg(Vil-cre) tgGFP-Ocln and B6.C-Tg(Vil-cre) tgGFP-Tric was similar performed as described in Weiss et al. 2022 (Weiss et al., 2022a) for B6.C-Tg(Vil-cre)tgGFP-MD3 mice. In accordance with the German law on animal protection (Landesamt für Gesundheit und Soziales (LAGeSo), Berlin G0200/12.

4.2.1 DSS treatment

Heterozygous male mice (age 12 weeks) and their genotypical wildtype littermates were used in this study, in accordance with the German law on animal protection (LAGeSo), Berlin G0059/13.

Animal housing was standardised including a 12 h light/dark cycle; 55% ± 15% humidity, temperature of 22 - 24 °C and *ad libitum* access to standard diet and water. Experimental colitis was induced by 3% dextran sodium sulphate (DSS) in drinking water or without DSS (control mice) *ad libitum* over 6 days. Disease activity index (DAI) was determined by the

following parameters: weight loss (0 points = No weight loss or gain, 1 point = 5–10% weight loss, 2 points = 11–15% weight loss, 3 points = 16–20% weight loss, 4 points = >21% weight loss); stool consistency (0 points = normal and well formed, 2 points = soft and unformed, 4 points = watery stool); and bleeding stool score (0 points = normal colour stool, 2 points = reddish colour stool, 4 points = bloody stool). Sum of weight loss, stool consistency and bleeding scores resulted in the DAI (0-12) (Shon et al., 2015). Mice were sacrificed at day 6 and small intestine, colon and MLN removed. Colon length was measured and pieces from small intestine and colon stored in RNAlater at −80 °C for later RNA isolation. Immune cells from small intestine colon and MLN were isolated and analysed as described in 3.12.

4.3 Crypt isolation

Isolation of intestinal crypts containing PSCs is the first step to generate organoids. Crypt isolation was performed similarly as described by Bartfeld et al. 2015 (for corpus glands) (Bartfeld and Clevers, 2015) or by Holthaus et al. (Holthaus et al., 2020).

Mice were sacrificed and intestines taken. After removing feces as well as adipose and connective tissues, intestines were opened longitudinally and further rinsed with $PBS^{-/-}$. From human samples, derived from surgeries, the epithelial layer was stripped of the muscle layer using a scalpel and cleaned.

Epithelial tissues derived either from mice or humans (surgery or biopsies) were cut in small pieces and washed several times by pipetting up and down with a coated 10 ml serological pipette in a coated 50 ml Falcon tube with ice-cold $PBS^{-/-}$ until the supernatant appeared clean.

Method 1: (Bartfeld and Clevers, 2015)

Supernatants were taken and tissue pieces incubated for 5 – 10 min at room temperature in 5 ml EDTA solution, from time to time the tube was gently rocked. Next, pieces were transferred to a petri dish with as little liquid as possible before a microscope slide was placed on top to press crypts out of the tissue. A cloudy appearance around the tissue pieces indicated success. To collect crypts the Petri dish and microscope slide were rinsed with 10 ml AD^{+++} and suspension was transferred into a 15 ml Falcon tube and stored on ice until tissue pieces were settled. Supernatant containing intestinal crypts were transferred to a new Falcon tube and centrifuged by 300 × g at 4 °C for 5 min.

Method 2: (Holthaus et al., 2020; Sato et al., 2011a; Mahe et al., 2015)

Supernatant was taken and tissue pieces were incubated for 30 min on ice in 30 ml EDTA solution, from time to time the tube was gently rocked. When pieces settled, supernatant was decanted and fresh $PBS^{-/-}$ added. Tissue pieces were washed several times (5 - 8×) as

described above, but this time collecting the supernatant containing the crypts. Crypt suspension was centrifuged by 300 × g at 4 °C for 5 min.
The crypt pellet was resuspended in 50 µl extracellular matrix (BME or Matrigel) and seeded on a pre-warmed 24 well plate. To let the matrix solidify the plate was stored for 15 - 30 min at 37 °C before it was overlaid with the respective medium supplemented with 10 µM Rho-K inhibitor.

4.4 Organoid culture

Under optimal conditions, organoids can be cultured long term or even be frozen and thawed as commonly used cells. All organoids were cultured at 37 °C and 5% CO_2.

4.4.1 Organoid subculturing

Once generated, three dimensional organoids need regular media changes every two to three days and subculturing once a week to allow long term culture. During subculturing, organoids need to be broken up to release dead cells located in the lumen and to increase the organoid number. For that purpose, old medium was removed and 500 µl cold AD^{+++} added. By resuspending with a 1 ml pipette, the extracellular matrix was dissolved, and cell suspension transferred into a coated 15 ml Falcon tube. Up to six wells of one organoid line can be put together.
Small and large intestinal mouse organoids as well as human duodenum organoids were broken up by resuspending with a coated 21G needle. The used Falcon tube was filled up to 10 ml with AD^{+++} and organoid pieces were centrifuged at 300 × g for 5 min at 4 °C.
After dissolving the matrix of human colon organoids, the cell suspension was centrifuged and supernatant was discarded, before 1 ml of prewarmed TrypLE Express with 10 µM Rho-K inhibitor was added to the organoid pieces. Organoids were incubated for 5 min at 37 °C before resuspended with a coated 21G needle. To stop the reaction, the Falcon tube was filled up to 10 ml with AD^{+++} and organoid pieces were centrifuged at 300 × g for 5 min at 4 °C. The organoid pellet was resuspended in extracellular matrix (50 µl/well) and seeded on a pre-warmed 24 well plate. To let the matrix solidify the plate was stored for 15 - 30 min at 37 °C before it was overlaid with the respective medium supplemented with 10 µM Rho-K inhibitor.

4.4.2 Organoid-derived monolayer (ODM) seeding

For ODM seeding, 3D organoids were broken into pieces as described for human colon organoids. In brief, after dissolving the extracellular matrix, organoids were pelleted at 300 × g for 5 min at 4 °C and supernatant discarded. Organoids were resuspended in prewarmed TrypLE Express and incubated for 5 – 10 min at 37 °C. Using a 21G needle organoids were

broken up into single cells by resuspension. TrypLE Express was inactivated by diluting with AD^{+++} and cells were counted. Cells were centrifuged at 500 × g at 4 °C for 5 min and resuspended in differentiation medium. 0.5 – 1 × 10^6 cells per filter were seeded on matrix coated PCF filters. For coating, extracellular matrix was diluted 1:50 in ice cold Advanced DMEM/F12 and 150 µl mixture was added on each filter. Filters were incubated for at least 30 min at 37 °C and remaining Advanced DMEM/F12 was removed, before adding the cell suspension. Medium was filled up to 500 µl on the apical side and 1 ml on the basal side. Similar to normal organoid culture, medium was supplemented with 10 µM Rho-K inhibitor for the first 24 – 48 h. When ODMs reached confluence and stable TER they were used for experiments.

4.4.3 Transepithelial resistance measurements

To evaluate barrier integrity and function the transepithelial resistance (TER) of cell cultures and organoid-derived monolayers was measured, using chopstick electrodes (STX2, World Precision Instruments, Sarasota, FL, USA) and an epithelial volt ohm meter (EVOM3, World Precision Instruments, Sarasota, FL, USA). For reliable results the temperature of the culture medium should stay at 37 °C during measurements, because temperature strongly influences TER values. To achieve this, either heating plates were used or the duration of measurement outside of the incubator was kept very short**.** The shorter one of the electrode pair was placed within the filter insert (apical side) and the longer side next to the filter (basal side). Before and after each measurement the electrode was rinsed with 80% ethanol. Values were normalised by subtracting the value of the corresponding control (without cells) and multiplied by the area of the filter (0.6 cm^2) to obtain the final value in Ω*cm^2.

4.4.4 Organoid cryopreservation and thawing

For cryopreservation, the lumen of the organoids should be mostly free of dead cells and the organoids should have a healthy appearance overall. The procedure is similar to subculturing organoids. Medium was removed and 500 µl cold AD^{+++} added. By resuspending with a 1 ml pipette, the extracellular matrix was dissolved, and cell suspension transferred in a coated 15 ml Falcon tube. Up to six wells of one organoid line can be put together. Organoids were carefully resuspended with a coated 21G needle to further dissolve the extracellular matrix and to enable the release of dead cells from the lumen. After centrifugation at 300 × g for 5 min at 4 °C, the organoid pellet was resuspended in 500 µl organoid freezing medium per well. 500 µl organoid suspension was transferred per cryovial and placed promptly into a freezing container to freeze at a 1 °C per minute cooling rate in a -80 °C freezer. Samples were transferred to a liquid nitrogen freezer within 48 h after collecting for long term storage.

To thaw organoids, cryovials were taken out of the liquid nitrogen and defrosted quickly by either holding the tube in hand or into the water bath. Suspension was transferred into a coated 15 ml Falcon tube and added up to 10 ml with AD^{+++} to dilute the DMSO in the freezing medium. Organoids were centrifuged at 300 × g for 5 min at 4 °C. The organoid pellet was resuspended in extracellular matrix (50 µl/well) and seeded on a pre-warmed 24-well plate. To let the matrix solidify the plate was stored for 15 - 30 min at 37 °C before it was overlaid with the respective medium supplemented with 10 µM Rho-K inhibitor.

4.5 Cell culture

All cells were cultured at 37 °C and 5% CO_2 in T25 flasks (Caco-2, HT-29/B6) or T75 and T150 (HEK-293, L-WRN).

4.5.1 Cell subculture

For subculturing, medium was discarded and the cells were carefully rinsed with 5-10 ml $PBS^{-/-}$ to remove FBS residues which would inhibit trypsin. For the epithelial cell lines Caco-2 and HT-29/B6 this was followed by a pre-incubation with 3 ml of EDTA/trypsin solution for 5 min at 37 °C. To detach the cells from the culture flask 1-2 ml of EDTA/trypsin solution was added on top of the cells (Caco-2, HT-29/B6, L-WRN and HEK - 293) and incubated for 5 - 10 min at 37 °C until cells were floating. Cells were resuspended in culture medium and distributed into new flasks with fresh medium. For experiments, 4×10^5 cells were seeded on the apical side of PCF filters with a pore size of 0.4 µm (HT-29/B6) or 3.0 µm (Caco-2). HT-29/B6 were grown for around a week, while Caco-2 cells differentiated to a small intestinal cell like phenotype within three weeks (Engle et al., 1998).

4.5.2 Cell cryopreservation and thawing

For cryopreservation, cells were detached from the cell culture flask as described for subculturing. Cells were resuspended in 30 ml culture medium and centrifuged at 200 × g for 10 min at 4 °C. The cell pellet was resuspended in 12 ml of the respective culture medium containing 7.5% (v/v) DMSO and distributed into 1.5 ml/cryovial and placed promptly into a freezing container to freeze at a 1 °C per minute cooling rate in a -80 °C freezer. Samples were transferred to a liquid nitrogen freezer within 48 h after freezing for long term storage.

To thaw cells, cryovials were taken out of the liquid nitrogen and defrosted quickly by either holding the tube in hand or into a warm water bath. When the suspension started to thaw it was transferred into a new cell culture flask with pre-warmed culture medium.

4.6 Conditioned medium production

4.6.1 L-WRN-conditioned medium production

One cryovial of L-WRN cells was thawed as described above and seeded in T75 flasks with 25 ml growth medium. The next day, medium was changed to L-WRN selection medium, and selection medium was renewed every two to three days until cells reached 80% confluence, normally three to five days after seeding. At that point, cells were subcultured the first time in a ratio of one T75 flask into four T150 flasks, continuing with selection medium. When cells reached 80% confluency again, one flask was split in a ratio of 1:10 and medium was changed from selection to growth medium. Medium was changed every three to four days until cells were overconfluent.

For CM production, medium was renewed, and cells were stored in the incubator. After 24 h, CM was collected in 250 ml centrifuge tubes and centrifuged at 2000 × g for 5 min at room temperature to remove floating cells and supernatant collected in sterile bottles at 4°C. Fresh growth medium was added to the cells and this procedure was repeated four times. Collected CM medium was mixed, sterile filtered, aliquoted in 50 ml Falcon tubes and stored at -80 °C.

Each new batch was tested on organoids by comparison to the batch in usage, regarding organoids growth and appearance. Additionally, samples of WRN CM medium were given to the group of Prof. Aebischer and Dr. Klotz at the RKI, which performed the Luciferase assay for us. This luciferase assay gives information if a protein can activate the expression of a target protein, here it is used to determine how effective the CM medium can activate the expression of the target protein WNT. The higher the concentration of R-spo1 and WNT in the CM, the higher the expression of WNT and the stronger the luciferase signal.

4.6.2 Generation of Noggin- and R-Spondin1-producing HEK-293 cells

Additional to the L-WRN CM, it was necessary to have CM which only contains Noggin (Nog) or R-spondin1 (Rspo1) to be able to make differentiation medium. In contrast to L-WRN cells, cells producing Nog or Rspo1 are not commercially available. For generation one can transfect eukaryotic cells with plasmids containing Nog or Rspo1. Such plasmids were purchased from Origene.

First step was to amplify the plasmid DNA by transformation into competent TOP10F' cells. For this, cells were thawed on ice and 10 ng plasmid DNA added to one vial of cells and incubated for 30 min on ice. This was followed by heat shock at 42 °C for 30 s, 1 min on ice and the addition of 250 µl SOC medium. Cells were incubated for 1 h at 220 rpm at 37 °C, before either 10 µl, 50 µl or 100 µl of cell suspension was plated under sterile conditions on

LB agar dishes with kanamycin and stored at 37 °C over night. Cells that had ingested the plasmid with its kanamycin resistance could grow on the agar dish and the next day 4 colonies were picked using 100 µl pipette tips. Each tip was transferred into 4 ml liquid LB medium containing 0.1% kanamycin. These starter cultures were shaken at 200 rpm at 37 °C over night, cell growth was indicated by a turbid appearance. The next day 50 µl of each starter culture was transferred into 50 ml LB medium with 0.1% kanamycin and cultures were shaken at 200 rpm at 37 °C over night. To isolate the plasmid DNA, the plasmid midi from Qiagen was performed after manufacturer instructions. Correct sizes of the plasmids were confirmed by agarose gel electrophoresis and glycerol stocks were created for long time storage. For this, 150 µl cell suspension was mixed with 850 µl glycerol and stored at -80 °C.
Second step was to stable transfect HEK-293 cells; therefore HEK-293 cells were split as described above and plated into 6 well plates; 1.5 ml cell suspension and 3.5 ml medium per well.
The next day three different solutions were prepared:
1. Polyethyleneimine (PEI) solution: 3 ml 10% MEM + 120 µl PEI;
2. Noggin vector solution: 1.5 ml 10% MEM + CX ng Nog plasmid DNA;
3. R-Spondin1 vector solution: 1.5 ml 10% MEM + CX ng Rspo1 plasmid DNA.

These solutions were mixed as listed underneath:
1. Nog mix: 1.5 ml PEI solution + 1.5 ml Nog plasmid solution
2. Rspo1 mix: 1.5 ml PEI solution + 1.5 ml Rspo1 plasmid solution
and incubated for 20 min at room temperature.

In the meantime, the medium of the HEK-293 cells was renewed and finally 500 µl of Nog mix or Rspo1 mix were added dropwise to one well of cells and stored over night at 37 °C at 5% CO_2. The next day cells were replated, and medium was removed and each well washed 1 × with $PBS^{-/-}$ before 500 µl of a 1:1 trypsin/EDTA in $PBS^{-/-}$ solution was added and incubated until cells detached from the plate und cells were resuspended in 2.5 ml medium per well. Each well was split into six new wells, which were prepared with 5 ml medium and either 1. 500 µl, 2. 250 µl, 3. 150 µl, 4. 100 µl, 5. 50 µl or 6. 25 µl of cell suspension was added to one of the new wells. After 24 h, medium was changed to selection medium containing 1 mg/ml G418 to select for transfected cells. Cells were split before reaching confluence in a ratio of 1:3. To confirm the production of Nog and Rspo1 of the respective cells, some medium was collected and analysed via western blot. Positive clones were selected for further culturing and freezing, while negative clones were discarded. When producing CM, no G418 can be used, as organoids do not carry a G418 resistance. It must be ensured that the HEK-293 do not lose their capability of Nog and Rspo1 production without selection pressure. For that purpose, cells

were split after two month of culture and no G418 was added to the growth medium. When cells reached confluence medium was changed to AD^{++}. After one week, without further media changes, medium was collected and tested for Nog and Rspo1 by western blotting. Although media from all clones contained either Nog or Rspo1, clones with the strongest bands were selected for further CM production.

4.6.3 Noggin- and R-Spondin1-conditioned medium production

One cryovial of Nog or Rspo1 transfected HEK-293 cells was thawed as described above and seeded in T75 flasks with 25 ml growth medium. The next day, medium was changed to Nog and Rspo1 selection medium, and selection medium was renewed every two to three days until cells reached 80% confluence, normally three to five days after seeding. At that point cells were subcultured the first time in a ratio of one T75 flask into four T150 flasks, continuing with selection medium. When cells reached 80% confluence again, one flask was split in a ratio of 1:10 and medium was changed from selection to growth medium. Medium was changed every three to four days until cells were overconfluent.

For CM production, medium was changed to AD^{++} and cells were stored in the incubator. After seven days CM was collected in 250 ml centrifuge tubes and centrifuged at 500 × g for 5 min at room temperature, in order to remove floating cells. Supernatant was sterile filtered, aliquoted in 50 ml Falcon tubes and stored at -80 °C.

Each new batch was tested on organoids and compared to the batch in usage, regarding organoids growth and appearance. Additionally, samples of Rspo1 CM were given to the group of Prof. Aebischer and Dr. Klotz at the RKI, who performed the Luciferase assay for us.

4.7 Immunostaining

To determine TJ protein expression and localization immune fluorescence staining on ODMs and cell monolayers were performed.

ODMS and cell layers were washed with $PBS^{+/+}$, fixed with 2% PFA in PBS^{++} for 20 min, permeabilised with 0,2% Triton X-100 in PBS^{++} for 10 min, and blocked with 5% BSA 5% goat serum in PBS^{++} for 1 h at room temperature.

ODMs and cell monolayers were stained with primary antibodies over night at 4 °C, followed by incubation with secondary antibodies for 1 h at 37 °C and the staining for conjugated antibodies and nuclei staining with DAPI for another 1 h at 37 °C.

All antibodies with the respective concentrations and sources are listed in table 1. Images were obtained using a confocal laser-scanning microscope (LSM 780, Zeiss, Jena, Germany) with excitation wavelengths of 543 nm, 488 nm, and 633 nm.

4.8 RNA isolation, quantification, and cDNA synthesis

RNA from organoids, ODMs or cells was isolated using the NucleoSpin RNA/Protein kit (Macherey-Nagel, Düren, Germany). Organoids were first resuspended in $PBS^{+/+}$ to dissolve the extracellular matrix and centrifuged at 300 × g for 5 min at 4 °C, pellets were resuspended in 350 µl RP1 buffer with 3.5 µl beta-mercaptoethanol. Suspension was transferred to a 1.5 ml Eppendorf tube and vortexed vigorously. ODMs and cell monolayers were washed with $PBS^{+/+}$ and 350 µl RP1 buffer with 3.5 µl beta-mercaptoethanol added on the filter. Cells were scraped off the filter and suspension transferred to a 1.5 ml Eppendorf tube and vortexed vigorously. Suspension was applied on a NucleoSpin filter and centrifuged for 1 min at 11, 000 × g. The filter was discarded and 350 µl 70% ethanol added and mixed by vortexing. Lysate was loaded onto a NucleoSpin RNA/protein column and centrifuged for 1 min at 11,000 × g. After this step RNA and DNA was bound to the column membrane, while the flowthrough contained protein. Before centrifuging 1 min at 11,000 × g to let the membrane dry, 350 µl MDB buffer was applied. After that, 95 µl of mixture containing 10 µl reconstituted rDNase and 90 µl rDNase reaction buffer was added to the silica membrane and incubated for 10 min at room temperature. This was followed by washes with 200 µl RA2 centrifugation for 1 min at 11,000 × g, 600 µl RA3 centrifugation for 1 min at 11,000 × g and 250 µl RA3 centrifugation for 1 min at 11,000 × g. Finally, the column was transferred to a new 1.5 ml Eppendorf tube and 40 µl RNase-free H_2O added on the membrane, after 2 min of incubation RNA was eluted by centrifugation for 2 min at 11,000 × g.

RNA isolation from tissue pieces was performed using TRIzol. Samples were lysed and homogenised at room temperature using 1 ml TRIzol reagent per 100 mg tissue and a homogenizer. Suspension was transferred to a 1.5 ml Eppendorf tube and 200 µl chloroform per 1 ml TRIzol reagent added and mixed thoroughly by vortexing and incubated for 10 min on ice. Samples were centrifuged 12,000 × g for 5 min at 4 °C, thereby separating into a lower red phenol-chloroform, a milky, white and thin interphase, and a colourless watery phase. The latter, containing RNA, was carefully transferred into a new 1.5 ml Eppendorf tube. To precipitate the RNA, isopropanol was added in a ratio 1:1 and samples were stored over night at -20 °C. On the next day the precipitate was collected by centrifugation at 12,000 × g for 10 min at 4 °C, the supernatant was carefully discarded, and the pellet washed twice with 1 ml 75% ethanol and centrifuged at 12,000 × g for 10 min at 4 °C. To let the pellet dry, the tube was left open for 5 min before RNA was resolved in 40 µl 55 – 60 °C prewarmed RNase-free H_2O.

RNA quantification was performed using a Nanodrop 2000.

For cDNA synthesis, the high capacity cDNA reverse transcription kit was used. Therefore, the following master mix (MM) was prepared:

Table 14 Master mix for cDNA synthesis

	Volume for 1x reaction
10x RT Buffer	2.0 µl
25x dNTPs	0.8 µl
Random primers	2.0 µl
Transcriptase	1.0 µl
RNase free H_2O	4.2 µl
Total volume	10.0 µl

10 µl MM were added to 10 µl of a mixture of RNA+H_2O with a total RNA content of 1 µg. cDNA synthesis was performed in a thermocycler with the following settings:

Table 15 Thermocycler settings for cDNA synthesis

	Step 1	Step 2	Step 3	Step 4
temperature	25 °C	37 °C	85 °C	25 °C
time	10 min	120 min	5 min	∞

cDNA was stored at -20 °C.

4.9 Real-time quantitative polymerase chain reaction (qPCR)

The amount of cDNA can be determined by qPCR. The measured fluorescence signal correlates with the amount of cDNA. Since cDNA was transcribed from mRNA, this provides the quantity of mRNA expressed at the time of RNA isolation. The following reaction was pipetted into a MicroAmp Fast Optical 96-well reaction plate.

Table 16 Reaction mix for qPCR

	Volume for 1x reaction
FAM GE Assay (target)	1.0 µl
VIC GE Assay (housekeeping)	1.0 µl
Template	1.0 µl
2x Buffer	10.0 µl
RNase free H_2O	7.0 µl
Total volume	20.0 µl

Plates were sealed with a MicroAmp Optical Adhesive film and centrifuged 1 min at 1000 × g to avoid air bubbles and then put into a Thermocycler. For qPCR the following program was performed:

Table 17 Thermocycler settings for qPCR synthesis

	Step 1	Step 2	Step 3	Step 4
temperature	95 °C	95 °C	60 °C	25 °C
time	10 min	15-30 sec	1 min	∞
repeats	1x	40-50x	1x	

The “double delta C_t analysis” was performed using the following C_t values: Target gene control (TC), target gene experimental (TE), housekeeping gene control (HC) and housekeeping gene experimental (HE). First, TC and TE are normalised to the C_t values of the housekeeping gene (HC and HE), resulting in ΔC_tC and ΔC_tE, respectively. Second, ΔC_tC was subtracted from ΔC_tE, hence fold changes were interpreted as $2^{-\Delta\Delta CtE}$.

4.10 Protein isolation and western blotting

To determine TJ protein quantity of Caco-2, HT-29/B6 and ODMs filters, cells were washed with $PBS^{+/+}$ and 200 µl of either total or membrane lysis buffer added. Cells were scraped off the filter support and suspension transferred into a new Eppendorf tube and incubated on ice. For total protein isolation, cells were incubated for 1 h on ice and vortexed every 20 min. Samples were centrifuged at 15,000 × g for 15 min at 4 °C and supernatant containing proteins transferred to a new Eppendorf tube. For membrane protein isolation, cells were homogenised by resuspension with a needle (21 G) and a short centrifugation at 1000 × g for 5 min at 4 °C, supernatant was then centrifuged at 42,000 × g for 30 min at 4 °C and the pellet containing the membrane proteins resuspended in total lysis buffer. In the next step, protein concentration was calculated using the Pierce BCA (Bicin-choninic acid) Kit following the manufacturer's guidelines. The required volumes of protein solution, total lysis buffer and Laemmli buffer were mixed to obtain the targeted protein concentration and were boiled for 10 min at 95 °C. Proteins were separated according to protein size using a 12.5 % sodium dodecyl sulfate-polyacrylamide gel electrophoresis (SDS-PAGE) at 100 V in an SDS-PAGE chamber filled with electrophoresis buffer until the blue running front reached the bottom of the SDS-Gel. Proteins were transferred to polyvinylidene fluoride (PVDF) membrane via wet transfer. Fresh transfer buffer was prepared and stored at 4 °C and sponges were soaked. SDS-Gel was incubated for 5 min in transfer buffer. PVDF membrane was activated in methanol for 5 min. The transfer sandwich was built in a gel holder cassette as follows from the bottom (white side) to the top (black side): 1x sponge, 2x filter paper, PVDF membrane, gel, 2x filter paper, 1x sponge. While preparing the transfer sandwich, all components had to be covered in transfer buffer and air bubbles had to be avoided. Protein transfer was performed at 100 V for 1 h. After transfer, membranes were washed shortly in TBST and incubated in WB blocking solution for 1 h and incubated over night with primary antibodies. The next day, membranes were washed three times with TBST for 5-10 min and incubated for 2 h at room temperature with peroxidase-coupled secondary antibodies before another three washing steps and the detection using chemiluminescence, SuperSignal West Pico PLUS. Signals were detected using Fusion FX (Vilber Lourmat) and densitometric analysis was performed with AIDA (Elysia).

4.11 Flow cytometry

4.11.1 Immune cell isolation

Mice were sacrificed and the abdominal wall opened. First MLN which are located within the connective tissue next to the colon were taken. While rolling MLN over a pre wetted paper tissue, the MLNs are separated from the connective tissue and were stored in 10% RPMI on

ice. The small intestine and the colon were taken and colon length measured. After removing feces as well as adipose, connective, and muscle tissue, intestines were opened longitudinally and further rinsed with $PBS^{+/+}$. PP were removed from the small intestine using forceps. Three small tissue pieces from each small intestine and colon were collected in RNAlater for RNA isolation. Tissue pieces were transferred into a 50 ml Falcon tube with 10 ml $PBS^{+/+}$. Falcon tubes were shaken by hand and $PBS^{+/+}$ replaced by 10 ml $PBS^{-/-}$ and shaken again. This was followed by two times incubation in pre-warmed 5 ml EDTA digestion solution for 20 min at 37 °C and 200 rpm, vortexing for 20 – 30 sec and collection of the suspension over a 70 µm cell strainer into a Falcon tube with 10 ml 10% RPMI. This first fraction was stored on ice and contains next to epithelial cells, IELs and other immune cells, which are in close contact to the epithelial layer (epithelial fraction). For the isolation of lamina propria mononuclear lymphocytes (LPMC) tissues were washed in $PBS^{+/+}$ to inactivate EDTA and cut in small pieces using scissors. This was followed by three times incubation in pre-warmed 5 ml collagenase digestion solution for 20 min at 37 °C and 200 rpm, vortexing for 20 - 30 sec and collection of the suspension over a 70 µm cell strainer into a Falcon tube with 10 ml 10% RPMI. This second fraction was stored on ice (LP fraction). Epithelial and LP fractions were then pelleted at 400 × g for 10 min at room temperature and pellets dissolved in 10 ml 40% Percoll solution and stacked carefully on 5 ml 70% or 80% Percoll solution, respectively. Percoll gradients were centrifuged at 1200 × g for 25 min at RT with Acceleration: 1 and Deceleration: 0. Afterwards, immune cells appeared like a white ring between the two different Percoll solutions. This interphase was carefully taken using a plastic Pasteur pipette and transferred into a new 15 ml Falcon tube. Tubes were toped up with 10% RPMI medium and centrifuged at 400 × g for 10 min at 4 °C with Acceleration: 9 and Deceleration: 6. Supernatants were discarded, and pellets dissolved in a total volume of 2 ml in 10% RPMI and stored on ice until further processing.

4.11.2 Tissue cryopreservation

For cryopreservation, intestines were taken and cleaned as described above and cut in 0.5 cm pieces. Approximately 2 cm tissue were transferred into one cryovial prepared with 1 ml tissue cryopreservation medium (10% (v/v) DMSO in FBS 90%) and placed promptly into a freezing container to freeze at a 1 °C per min cooling rate in a -80 °C freezer. Samples were transferred to a liquid nitrogen freezer within 48 h after collecting.

4.11.3 T-cell stimulation

Cells of the second fraction of the immune cell isolation were plated into a 96 well plate and incubated for 2 h at 37°C and 5% CO2 within 250 µl T-cell stimulation or control solution. Then 1 µg/ml Brefeldin A was added to let cytokines accumulate within the cells for another 2 h.

4.11.4 Extra- and intercellular staining and acquisition

Isolated cells were counted before washing with $PBS^{-/-}$ at 400 × g for 7 min at 4 °C and transferred into a 96 well plate and washed again with $PBS^{-/-}$. Cells were then incubated in 50 µl live/dead staining solution (1:1000) for 10 min at 4 °C. Staining was stopped by adding 200 µl FACS solution and centrifugation. This was followed by FC-blocking with 100 µl of a 1:250 dilution of FC-blocking in FACS solution for 20 min on ice. FC-blocking solution was washed off with 150 µl FACS solution and centrifugation. Afterwards, extracellular surface staining was performed adding 50 µl of the respective antibody mix in FACS solution and an incubation for 30 min on ice, before a final washing step or intracellular staining.

For intracellular staining, the eBioscience™ FOXP3/Transcription factor Staining Buffer Set was used. Here, 50 µl of a 1:4 dilution of Fix/Perm diluent were added to each well and incubated for 45 min at 4 °C. For washing, 200 µl Perm buffer were added on top and centrifuged and supernatant discarded. This was followed by the incubation in 50 µl intracellular antibody mix in perm buffer for 25 min at room temperature and a last washing step with FACS solution. FACS samples were acquired by a BD FACSCanto II or BD LSRFortessa 20x device from BD and analysed using the FlowJo software 10.6.2.

4.11.5 Transcriptomic analysis

Quantitative expression of solute carrier (SLCs) transporter was compared between Caco-2, tissue, ODMs and organoids. The following data sets from Gene Expression Omnibus (GEO) were used: GSE164334 (He et al., 2021), GSE156453 (Takayama et al., 2021), GSE127938 (Kayisoglu et al., 2021), GSE167286 (Gu et al., 2022), GSE163706 (Sugimoto et al., 2021), and GSE160695 (Yamashita et al., 2021); and a data set from Ma'ayeh et al. (Ma'ayeh et al., 2018) and one from Holthaus et al. (Holthaus et al., 2021). Data were quantitatively evaluated, only considering expressed or not expressed, since they were obtained by different methods RNAseq and DNA microarray. Normalisation was performed by the respective authors or according to manufacturer`s guidelines (Yamashita et al., 2021). Results were visualised using Prism 9.1 software (GraphPad).

4.12 Statistical analysis

Prism 9.1 software (GraphPad) was used for analysis. If not stated otherwise, data are expressed as mean values ± standard error of the mean (SEM). *n* indicates the number of single measurements. Outliers were identified by Grubb's test α= 0.01 and removed from the data set. Statistical analysis was performed using Student's t-test for comparison between two groups or one-way ANOVA with Dunnett correction for multiple comparison for comparing more than two groups. $p<0.05$ was considered significant (*$p<0.05$, **$p<0.01$, ***$p<0.0001$).

5 Results

5.1 TAMP-OE influences subjacent immune cells

All three TAMPs are altered in UC and therefore might play a role in the pathogenesis (Heller et al., 2005; Krug et al., 2018; Weiss et al., 2022a; Zeissig et al., 2007). We showed that mice with an intestinal epithelial cell-specific overexpression of either MD3 (Weiss et al., 2022a), Ocln or Tric (unpublished data) suffered less from DSS-induced colitis indicated by a lower disease activity index (DAI) compared to wt mice. This could be partially explained by stabilising effects of the barrier, but other mechanisms might be involved, resulting in the ameliorating effect of DSS colitis, as for example for MD3-OE we did not find direct effects on the barrier (Weiss et al., 2022a). Therefore, changes in immune cell composition of MLNs, small intestine, and colon using flow cytometry and expression of pro- and anti-inflammatory markers in the colon tissue using qPCR were investigated, during DSS-induced colitis and control conditions. TAMP-OE mice developed normally and displayed no phenotypic differences. Only male mice were used for this study, because female and male mice differ in weight and, more importantly, it was observed that colitis manifests differently (Alex et al., 2009; DeVoss and Diehl, 2014). Moreover, TJ proteins in the gut were found to be influenced by the female hormone cycle (Zhou et al., 2017).

5.1.1 Cryopreservation of intestinal tissue led to reduced number of viable cells but preserved immune cell composition

To investigate changes in intestinal immune cell composition due to TAMP-OE, a cryopreservation method was tested, that allows collection of tissue and the collective isolation and analysis of immune cells at a later time. Some intestinal tissue samples were frozen in 10% DMSO in FBS and stored in liquid nitrogen. These samples were quickly thawed and immune cells isolated in parallel to fresh intestinal tissue samples and analysed using flow cytometry as visualised in Figure 7. Firstly, cell debris was excluded (Figure 7 A Gate1), then

single cells were selected and finally gated on viable CD45⁺ immune cells. As demonstrated in Figure 7 A, this population appeared to be smaller in the frozen samples compared to fresh samples. This observation was confirmed by statistical analysis (Figure 7 B). Immune isolation from fresh samples yielded to more viable CD45⁺ cells (20.50 ± 3.31% of single cells) than from frozen samples (6.71 ± 0.73%).

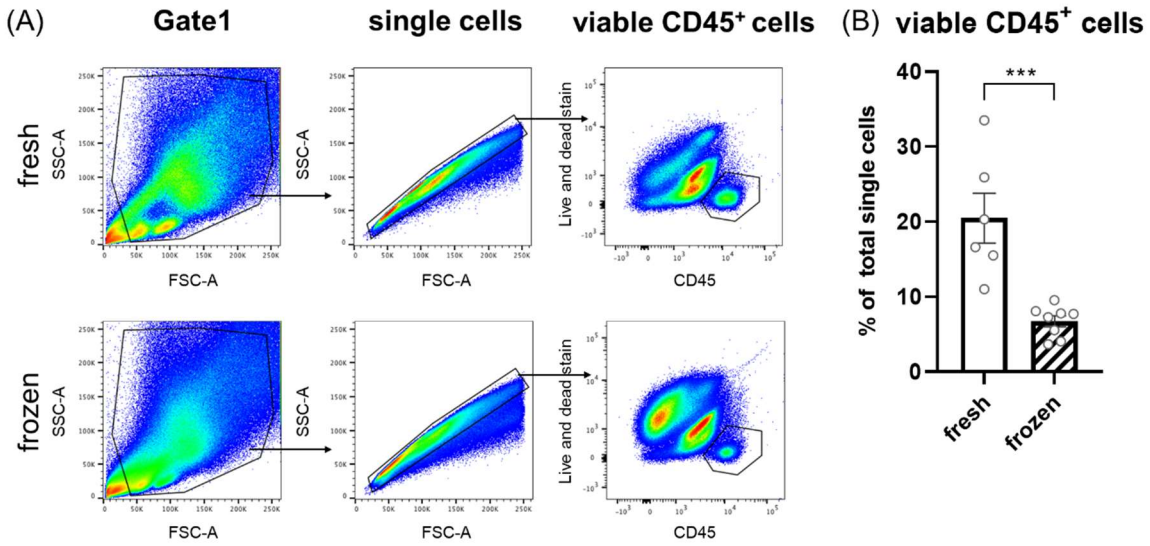

Figure 7 Cryopreservation leads to reduced number of viable CD45⁺ cells

(A) Gating strategy for lamina propria (LP) immune cells isolated from fresh and frozen samples of mouse intestines. Firstly, cell debris was excluded (Gate1), then single cells were selected and finally gated on viable CD45⁺ immune cells. **(B)** Comparison of occurrences of viable CD45⁺ cells in percentage of single cells. In fresh samples 20.50 ± 3.31% of single cells were viable CD45⁺ cells, while this occurrence was lower in frozen samples with 6.71 ± 0.73% of viable CD45⁺ cells. ($n \geq 5$; data shown as mean ± SEM; outliers identified by Grubb's test α= 0.01 and removed; *p<0.05, **p<0.01, ***p<0.001)

Comparison of viable CD45⁺ cells showed no changes in percentage (%) for CD4⁺ cells 11.50 ± 2.60% and 12.80 ± 3.41%; CD8⁺ cells 25.60 ± 7.10% and 23.10 ± 3.51%; CD19⁺ cells 45.90 ± 7.96% and 46.30 ± 6.40%; CD11c⁺ cells 5.07 ± 0.98% and 3.20 ± 0.68% and Ly6G⁺ cells 1.82 ± 0.04% and 3.37 ± 0.77% of fresh and frozen samples, respectively (Figure 8). However, the number of CD11b⁺ cells was reduced from 9.49 ± 2.1% in fresh samples to 4.61 ± 0.63% in frozen samples (Figure 8).

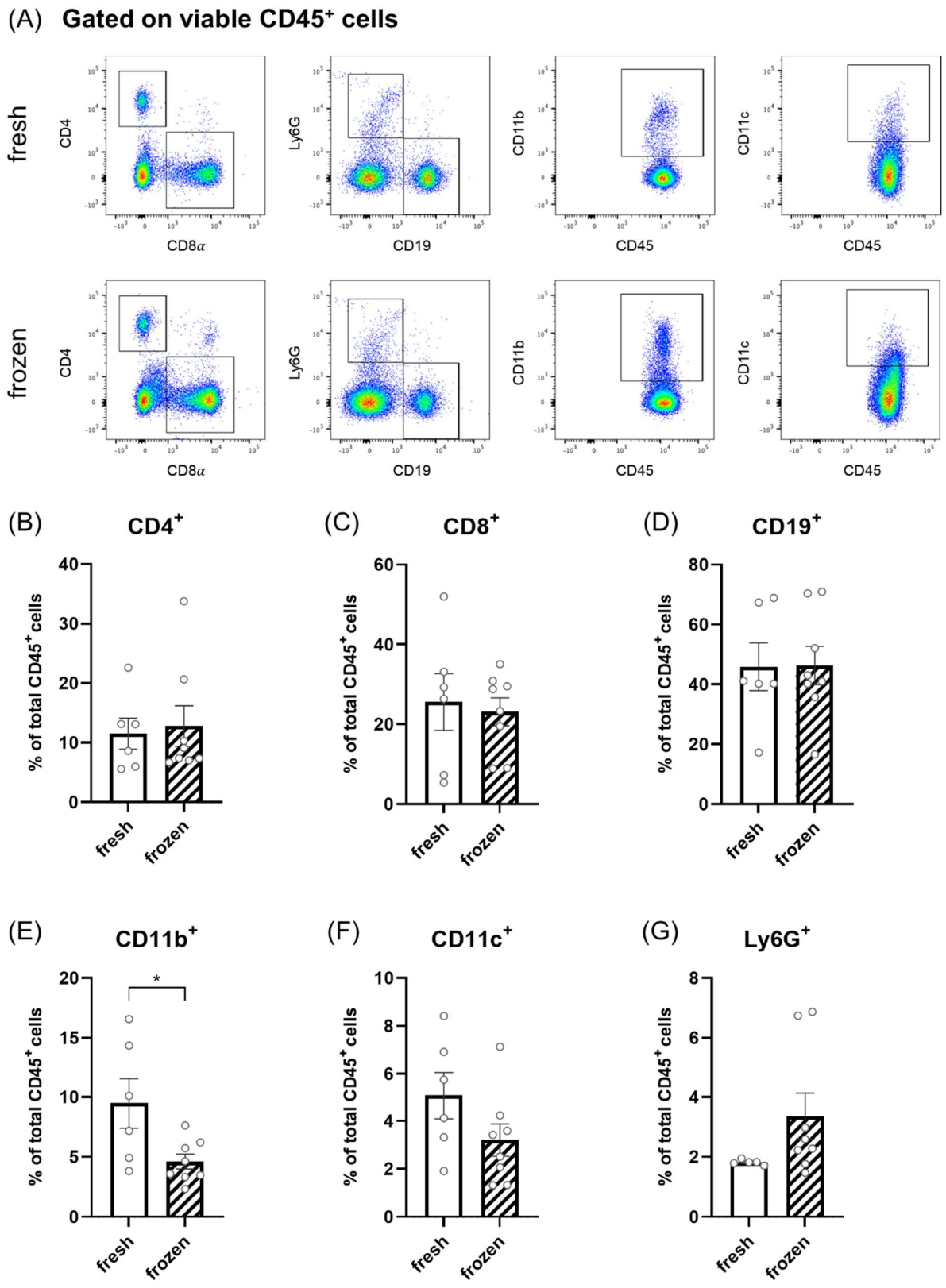

Figure 8 Cryopreservation leads to reduced number of CD11b⁺ cells.

(A) Gating strategy on viable CD45⁺ cells of LP immune cells isolated from fresh and frozen samples of mouse intestines. **(B-G)** Comparison of occurrences in percentage of viable CD45⁺ cells. **(B)** for CD4⁺

cells 11.50 ± 2,60% and 12.80 ± 3.41%; **(C)** $CD8^+$ cells 25.60 ± 7.10% and 23.10 ± 3.51%; **(D)** $CD19^+$ cells 45.90 ± 7.96% and 46.30 ± 6.40%; **(E)** $CD11b^+$ cells 9.49 ± 2.1% and 4.61 ± 0.63%; **(F)** $CD11c^+$ cells 5.07 ± 0.98% and 3.20 ± 0.68% and **(G)** $Ly6G^+$ cells 1.82 ± 0.04% and 3.37 ± 0.77%; of fresh and frozen samples, respectively. ($n \geq 5$; data shown as mean ± SEM; outliers identified by Grubb's test α= 0.01 and removed; *p<0.05, **p<0.01, ***p<0.001)

Although the flow cytometry data showed that most of the analysed immune cell populations were preserved after freezing, this method was not used for further experiments as the yield of viable $CD45^+$ cells of the mouse colon was already low in fresh samples and was further reduced by cryopreservation. In addition, the proportions of $CD11b^+$ cells were different between fresh and frozen samples.

5.1.2 MD3-OE does not affect $CD4^+$ T-cell subsets

In a preliminary experiment, changes in $CD4^+$ T-cell subsets between MD3-OE and wt mice were investigated. Especially MD3-OE might lead to changes as MD3 are known to influence proliferation of surrounding cells (Steed et al., 2014) and thereby it might be the TAMP with the most influence on other cell populations. The different subsets of $CD4^+$ cells have distinct functions, for example T_H1 cells protect against intracellular microbes and T_H2 cells against parasites. Therefore, changes in these immune cell subsets would indirectly indicate major changes in the microbiota. For $CD4^+$ T-cell subsets investigation, isolated immune cells were stimulated with Ionomycin and Phorbol 12-myristate 13-acetate (PMA) and an intracellular staining kit was used to stain for subset specific intracellular markers (Figure 9 A). T_H1 cells were defined as $INF\text{-}\gamma^+$ and $TNF\alpha^{+/-}$ cells. T_H2 as $INF\text{-}\gamma^-$ and $TNF\alpha^+$ cells, T_H17 as $IL\text{-}17\alpha^+$ cells and T_{reg} as $FoxP3^+$ cells (Mousset, 2019). Successful activation and intracellular staining of wt $CD4^+$ T-cell subsets is shown in Figure 9 B. No changes in occurrence of the four different subsets were detected between wt and MD3-OE mice [T_H1 cells (11.20 ± 1.44% and 10.50 ± 1.89%); T_H2 cells (12.67 ± 2.28% and 7.36 ± 1.23%), T_H17 cells (2.74 ± 0.53% and 4.28 ± 1.36%); T_{reg} cells (13.60 ± 1.03% and 13.10 ± 1.77%), respectively; Figure 9 C-F]. $CD4^+$ T-cell subsets were not altered in MD3-OE mice, thus indicating that there are no major changes in gut microbiota due to the MD3-OE.

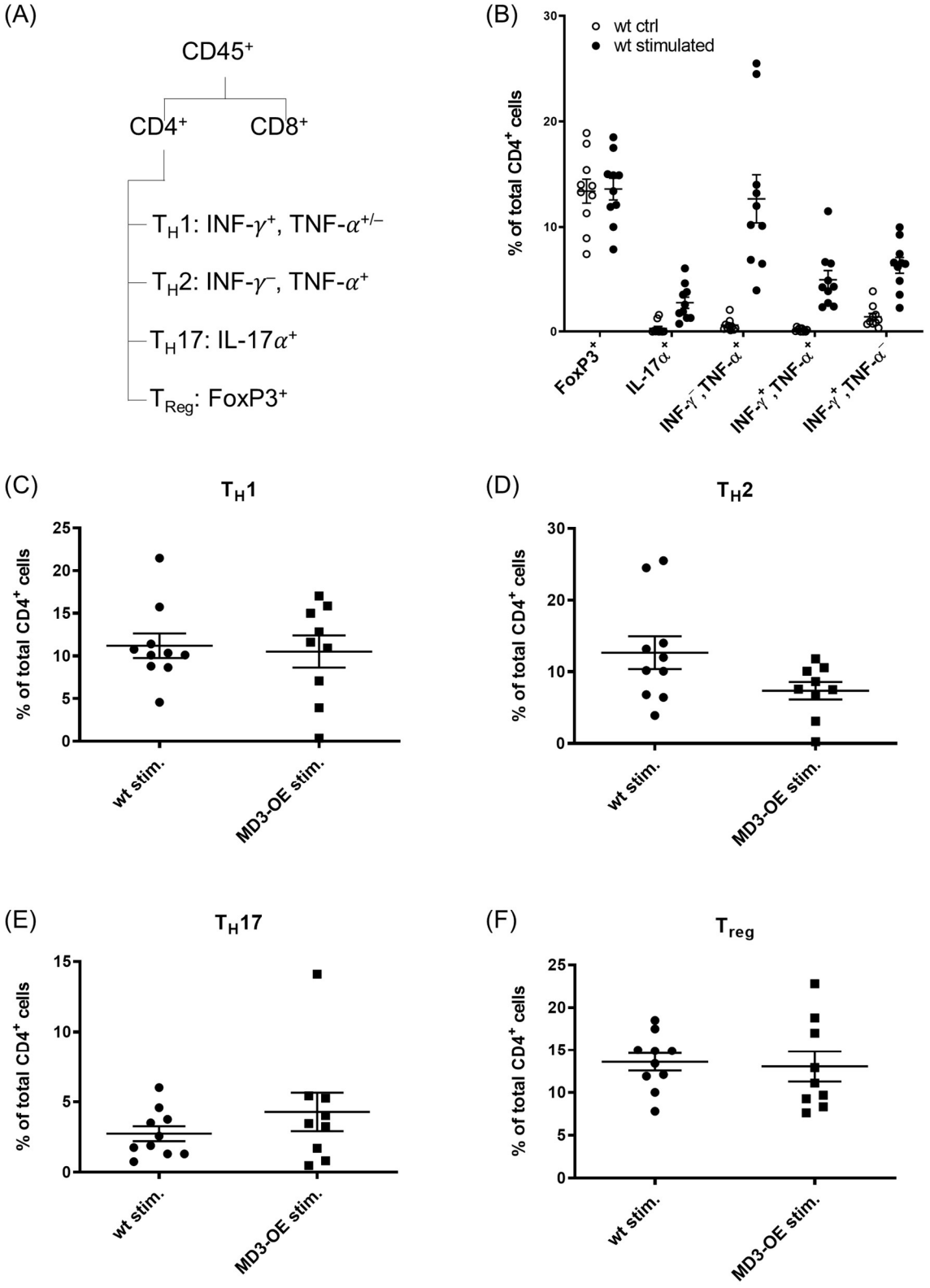

Figure 9 MD3-OE does not affect CD4⁺ T-cell subsets.

LP immune cells were isolated from wt and MD3-OE mice and cultured for 4 h with PMA and Ionomycin to induce cytokine expression. Brefeldin A was added to inhibit cytokine release and immune cells were stained using an intracellular staining kit. Cells were acquired with a FACS Canto II and analysed using

FlowJo software. Viable CD45$^+$ cells were distinguished by the expression of either CD8α or CD4. CD4$^+$ cells were further subdivided by the detected cytokine expression. T_H1 cells were defined as INF-γ$^+$ and TNFα$^{+/-}$ cells. T_H2 as INF-γ$^-$ and TNFα$^+$ cells, T_H17 as IL-17α$^+$ cells and T_{reg} as FoxP3$^+$ cells. **(A)** Scheme of the gating strategy to identify CD4$^+$ T-cell subsets. **(B)** Comparison of wt ctrl and wt stimulated immune cells. **(C-F)** No changes in occurrence of the four different subsets were detected between wt and MD3-OE. **(C)** T_H1 cells:11.20 ± 1.44% and 10.50 ± 1.89%; **(D)** T_H2 cells: 12.67 ± 2.28% and 7.36 ± 1.23%; **(E)** T_H17 cells: 2.74 ± 0.53% and 4.28 ± 1.36%; and **(F)** T_{reg} cells: 13.6 ± 1.03% and 13.1 ± 1.77%. ($n \geq 9$; data shown as mean ± SEM; outliers were identified by Grubb's test α= 0.01 and removed; *p<0.05, **p<0.01, ***p<0.001)

5.1.3 Transcriptional analysis of cytokine expression in wt and TAMP-OE mice during DSS colitis

To get a first hint about the inflammation status, colon mRNA was isolated from 2-4 mice of each group and was compared regarding the expression of cytokines involved in IBD. The DAIs for these mice showed that at day 5 all TAMP-OE DSS mice had a lower DAI than wt mice (wt DSS 5.25 ± 1.03 DAI, MD3-OE DSS 2.50 ± 0.96 DAI, Ocln-OE DSS 3.75 ± 1.32 DAI and Tric-OE DSS 2.67 ± 1.20 DAI; Figure 10A). At day 6 DAI of Ocln-OE DSS mice was lower than that from wt DSS mice (3.50 ± 0.50 DAI and 5.75 ± 1.49 DAI, respectively; Figure 10A).
No significant tests were performed for the qPCR results due to low sample number and large variances (Figure 10 B-J). Therefore, these results can only give an indication. This said, an increased expression of the tested cytokines was detected in all mice treated with DSS. Expression of Interleukin- (IL-) 1β was similar in Tric-OE DSS mice (131 Fold change (FC)) and was higher in Ocln-OE DSS (306 FC) and the highest in MD3-OE DSS (996 FC) compared to wt DSS mice (164 FC) (Figure 10 B). In Tric-OE DSS mice (298 FC) the expression of IL-6 was slightly higher than in wt DSS mice (139 FC), while IL-6 expression was higher in Ocln-OE DSS mice (740 FC) and the highest in MD3-OE DSS (1344 FC). (Figure 10 C). No difference in IL-10 expression between wt DSS (7.77 FC) and TAMP-OE DSS mice (MD3-OE DSS 11.1 FC; Ocln-OE DSS 9.3 FC; Tric-OE DSS 5.1 FC) was observed (Figure 10 D). Ocln-OE DSS mice (161 FC) expressed more IL-12β than wt DSS mice (31.8 FC) and in Tric-OE DSS mice (86.6 FC) IL-12β expression was also higher, but not as much as for Ocln-OE DSS mice (Figure 10 E). IL-17α was expressed higher in TAMP-OE DSS mice than in wt DSS mice (6.4 FC), expression was the lowest in Tric-OE DSS mice (47.1 FC) and the highest in Ocln-OE DSS mice (172 FC) (Figure 10 F).
The chemokines CC-(two N-terminal cysteines adjacent) ligand 2 (CCL2) and CXC (two N-terminal cysteines separated by a single amino acid) ligand 9 (CXCL9) tended to be expressed higher in MD3-OE DSS (78 FC and 680 FC, respectively) and Ocln-OE DSS (214 FC and 476 FC, respectively) mice than in wt DSS mice (20.1 FC and 60.1 FC, respectively), whereas Tric-

OE DSS (23.6 FC and 72.0 FC, respectively) mice had a similar fold change (FC) to wt DSS mice (Figure 10 G and H). Expression of interferon-γ (INF-y) was similar in wt DSS (34.1 FC), Ocln-OE DSS (44.6 FC) and Tric-OE DSS mice (38.6 FC) but higher in MD3-OE DSS mice (332 FC) (Figure 10 I). Wt DSS (3.6 FC) and TAMP-OE DSS mice (MD3-OE DSS 4.1 FC; Ocln-OE DSS 5.1 FC; Tric-OE DSS 1.6 FC) had a similar FC for transforming growth factor beta (TGF-β) (Figure 10 J).

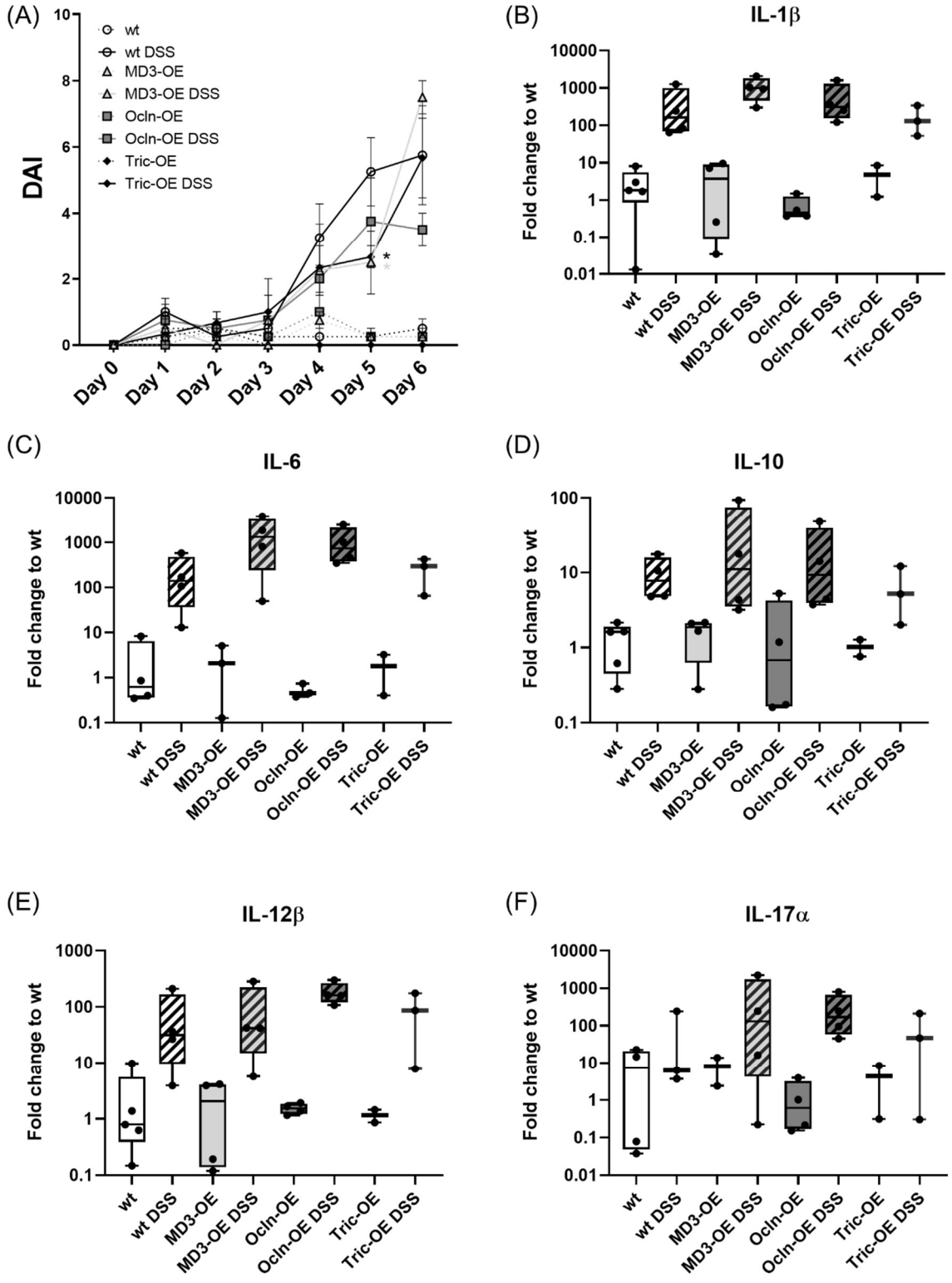
(A)
DAI
wt
wt DSS
MD3-OE
MD3-OE DSS
Ocln-OE
Ocln-OE DSS
Tric-OE
Tric-OE DSS
Day 0
Day 1
Day 2
Day 3
Day 4
Day 5
Day 6
(B)
IL-1β
Fold change to wt
(C)
IL-6
Fold change to wt
(D)
IL-10
Fold change to wt
(E)
IL-12β
Fold change to wt
(F)
IL-17α
Fold change to wt

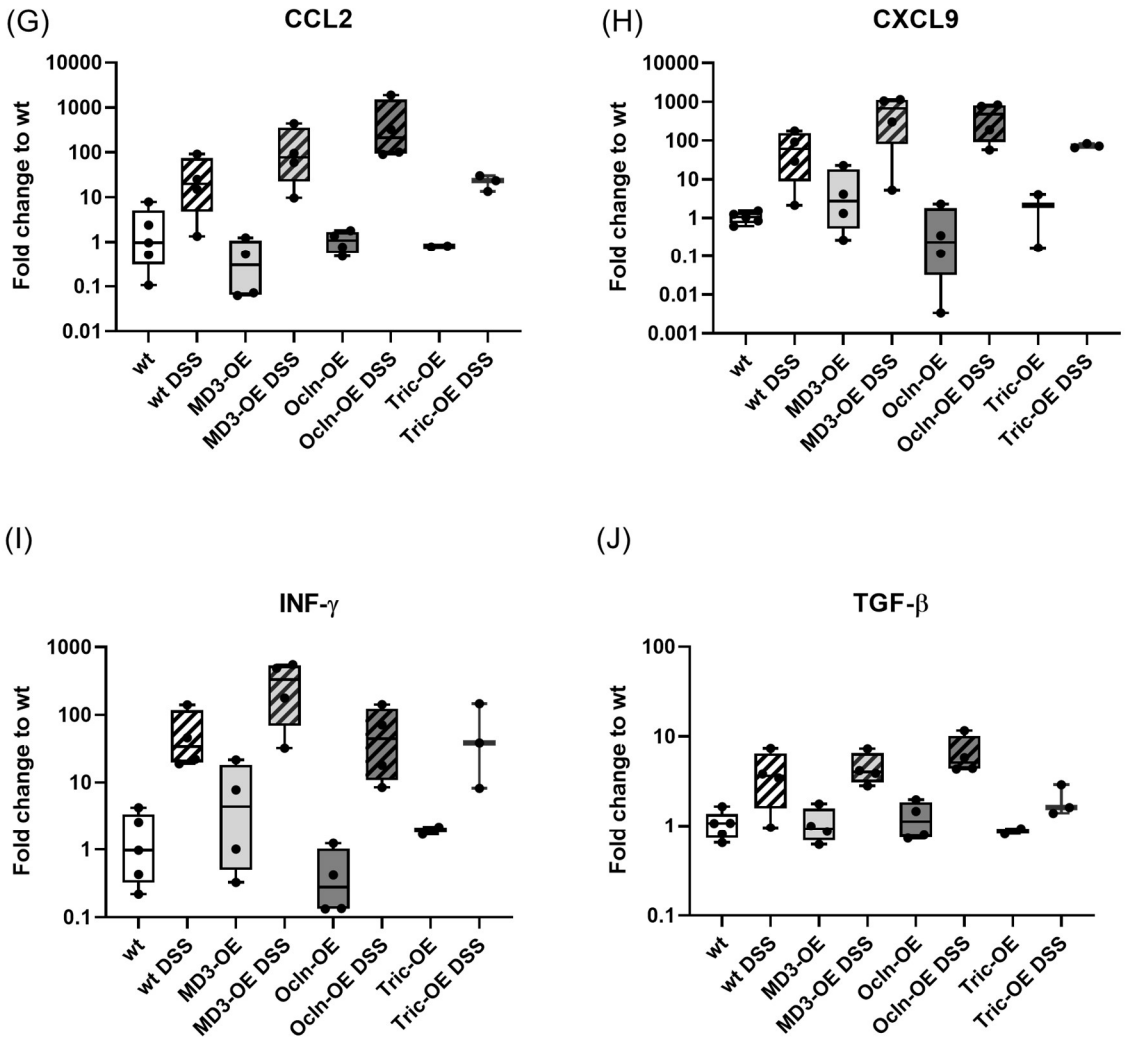

Figure 10 Transcriptional analysis of cytokine expression in wt and TAMP-OE mice during DSS colitis

mRNA was isolated from colon tissue of wt and TAMP-OE mice at day 6 of DSS treatment and analysed by qPCR for the expression of different cytokines. **(A)** Disease activity index (DAI) of wildtype (wt) and intestinal TAMP-overexpressing mice (MD3-OE; Ocln-OE; Tric-OE), that were used for RNA isolation and qPCR to detect expression of cytokines involved in IBD. (*n* ≥2; data shown as mean ± SEM; two-way ANOVA against wt DSS; *p<0.05, **p<0.01, ***p<0.001,) **B)** Expression of IL-1β was higher in MD3-OE DSS than wt DSS mice, but similar in Ocln-OE DSS and Tric-OE DSS mice. **(C)** Expression of IL-6 was slightly higher in Tric-OE DSS than wt DSS mice, higher expressed in Ocln-OE DSS mice and the highest in MD3-OE DSS mice. **(D)** Expression of IL-10 was similar in wt DSS and TAMP-OE DSS mice. **(E)** Expression of IL-12β was higher in Ocln-OE DSS than wt DSS mice. **(F)** Expression of IL-17α was higher in TAMP-OE DSS mice than in wt DSS mice, although Tric-OE DSS mice had the lowest and Ocln-OE DSS mice the highest expression. **(G)** Chemokine CC- (two N-terminal cysteines adjacent) ligand 2 (CCL2) was expressed higher in MD3-OE DSS and Ocln-OE DSS mice than in wt DSS mice. **(H)** Chemokine CXC (two N-terminal cysteines separated by a single amino acid) ligand 9 (CXCL9) was

expressed higher in MD3-OE DSS and Ocln-OE DSS mice than in wt DSS mice. **(I)** Expression of Interferon-γ (INF- γ) was similar in wt DSS, Ocln-OE DSS and Tric-OE DSS mice but higher in MD3-OE DSS mice **(J)** Expression of transforming growth factor-β (TGF-β) was similar in wt and TAMP-OE mice. (*n* ≥ 2; data shown as boxes from 25th percentile to 75th percentile with the horizontal line presenting the median; the whiskers represent the maximum and minimum values, without outlier; outliers identified by Grubb´s test α= 0.01 and removed)

5.1.4 Changes in immune cell composition due to TAMP-OE

Finally, wt and TAMP-OE mice were compared during DSS-induced colitis. Prior experiments showed a reduced (DAI) in TAMP-OE mice during DSS-induced colitis. Albeit in these experiments DAI was similar between wt and TAMP-OE mice at day 6 (Figure 11). However, DAI was lower for MD3-OE DSS and Tric-OE DSS mice at day 5 of DSS treatment (Figure 11).

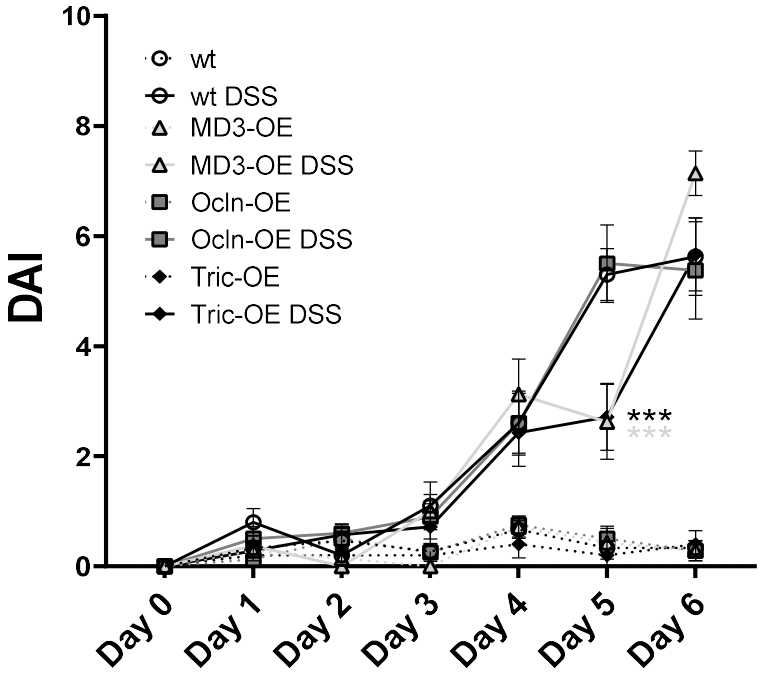

Figure 11 Disease activity index in DSS-induced colitis

Disease activity index (DAI) of wildtype (wt) and intestinal TAMP-overexpressing mice (MD3-OE; Ocln-OE; Tric-OE) during DSS-induced colitis. Similar DAI in TAMP-OE and wt mice at day 6 of DSS treatment. However, MD3-OE and Tric-OE mice had lower DAI than wt mice at day 5 of DSS treatment (*n* ≥ 6; data shown as mean ± SEM; two-way ANOVA against wt DSS; $^{*}p<0.05$, $^{**}p<0.01$, $^{***}p<0.001$)

To investigate changes in immune cell composition in the intestine of wt and TAMP-OE mice two flow cytometry panels were established. The first panel focuses on IELs which are located closely to the epithelial cells and therefore are most likely influenced by TJ changes. The gating strategy for the first panel is illustrated in Figure 12.

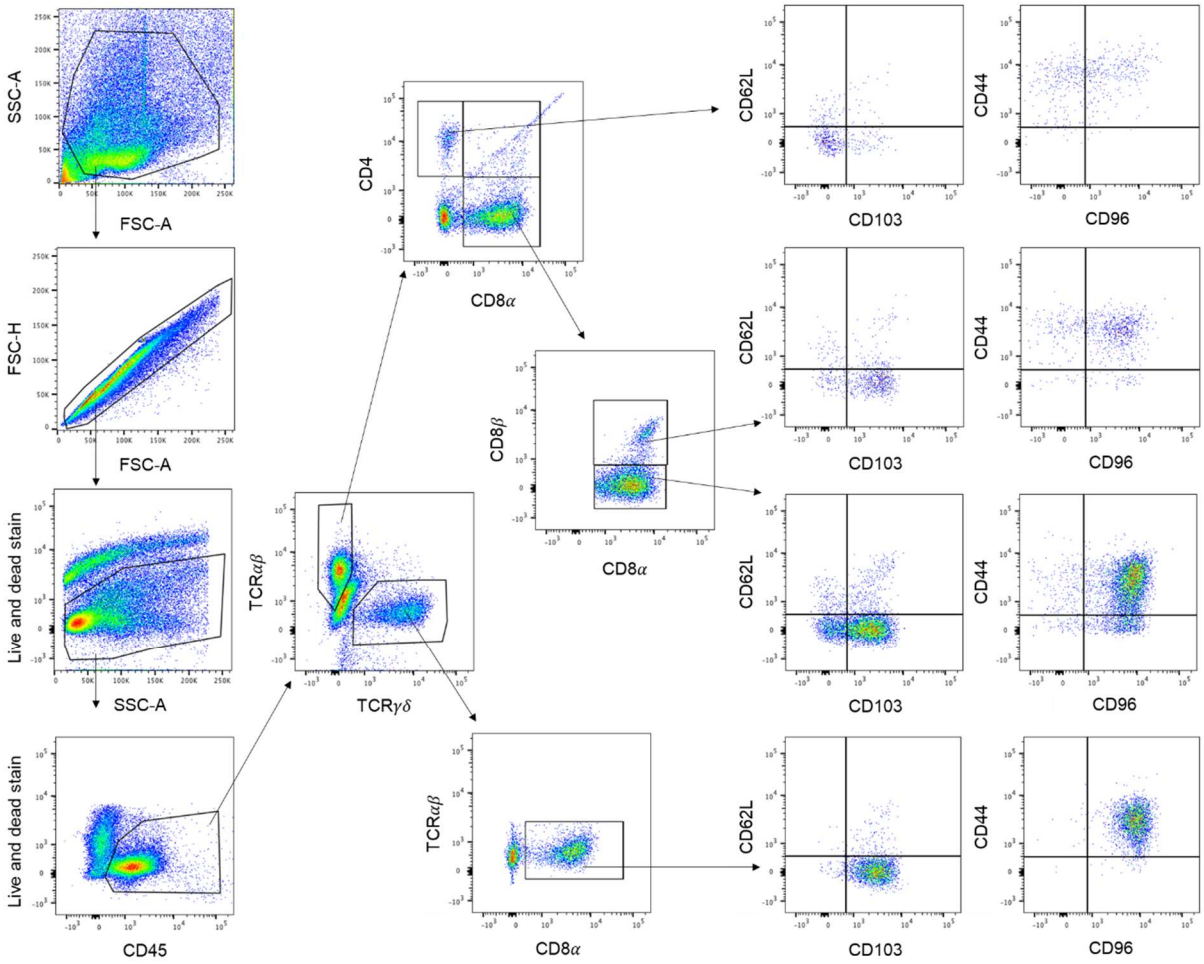

Figure 12 Intraepithelial lymphocyte gating strategy.

Gating strategy for intraepithelial lymphocytes using the FlowJo software. First cell debris was excluded and gated on single cells. Then viable and CD45$^+$ cells were identified. Those were further divided due to the expression of TCRαβ or TCRγδ. TCRαβ$^+$ cells are further distinguished by CD4 and CD8α expression. TCRαβ$^+$ CD8α$^+$ cells are then distinct by the expression of CD8αα homodimer or CD8αβ heterodimer. In addition, the populations of TCRγδ$^+$ CD8αα$^+$ cells were determined. Finally, nIELs (TCRγδ$^+$ CD8αα$^+$ and TCRαβ$^+$ CD8αα$^+$) as well as the iIELs; (TCRαβ$^+$ CD4$^+$ and TCRαβ$^+$ CD8αα$^+$) were analysed for their expression of the typical IEL integrin CD103 and the MLN homing marker CD62L. Furthermore, the expression of the activation markers CD44 and CD69 by IELs were determined.

To isolate immune cells from the mouse intestine, two digestions were performed. EDTA was used in the first digestion to disrupt the epithelial layer. This epithelial fraction contained besides epithelial cells also immune cells that were closely located to the epithelium like IELs.

The occurrence of iIELs subsets, TCRαβ⁺ CD4⁺ and TCRαβ⁺ CD8αβ⁺, were not altered due to TAMP-OE or DSS treatment with the exception that TCRαβ⁺ CD8αβ⁺ cells were reduced in wt DSS mice (5.34 ± 0.91%) compared to wt mice (2.05 ± 0.21%) (Figure 13 A and B). In contrast, TCRαβ⁺ CD8αα⁺ nIELs were reduced in Ocln-OE DSS and Tric-OE DSS mice compared to control conditions. Wt DSS and MD3-OE DSS mice also tended to have less TCRαβ⁺ CD8αα⁺ nIELs, but changes were not significant (Figure 13 C). Untreated Tric-OE mice had a higher occurrence of TCRαβ⁺ CD8αα⁺ nIELs than wt mice. TCRγδ⁺ CD8αα⁺ nIELs were reduced in TAMP-OE mice upon DSS treatment but there was no reduction in wt mice (Figure 13 D). TCRγδ⁺ CD8αα⁺ nIELs were increased in MD3-OE mice compared to wt mice, whereas upon DSS treatment Tric-OE mice had a lower occurrence of TCRγδ⁺ CD8αα⁺ nIELs than wt DSS mice.

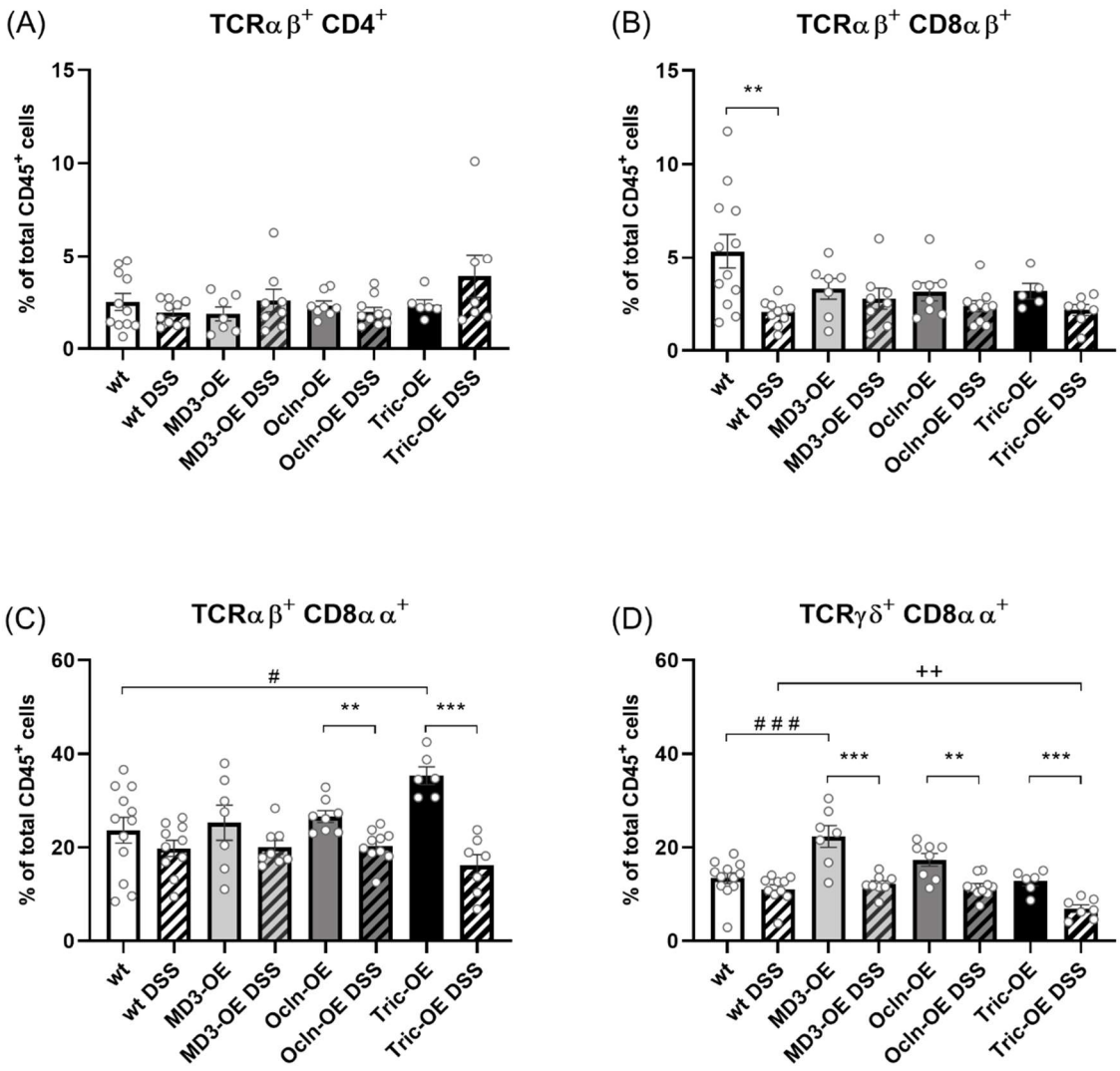

Figure 13 Occurrences for intraepithelial lymphocyte subsets (epithelial fraction)

At day 6 of DSS treatment, colon tissue of wt and TAMP-OE mice was digested with EDTA to isolate immune cells. The epithelial fraction was stained for the IEL panel, acquired by an LSR Fortessa 20x device and analysed with FlowJo software as illustrated in Figure 12. **(A)** Occurrence of TCRαβ⁺ CD4⁺

iIELs was not altered due to TAMP-OE or DSS treatment. **(B)** Occurrence of TCRαβ$^+$ CD8αβ$^+$ iIELs was reduced in wt DSS mice compared to wt mice. **(C)** Occurrence of TCRαβ$^+$ CD8αα$^+$ nIELs was reduced in wt DSS and TAMP-OE DSS mice compared to control conditions, this was significant for Ocln-OE and Tric-OE mice. Furthermore Tric-OE mice had a higher occurrence compared to wt mice. **(D)** Occurrence of TCRγδ$^+$ CD8αα$^+$ nIELs was reduced in TAMP-OE DSS mice compared to control conditions. Occurrence was higher in MD3-OE mice compared to wt mice and lower in Tric-OE DSS mice than wt DSS mice. ($n \geq 6$; data shown as mean ± SEM; outliers were identified by Grubb's test α= 0.01 and removed; student's T-test *p<0.05, **p<0.01, ***p<0.001; One-way ANOVA compared to wt $^{\#}$p<0.05, $^{\#\#}$p<0.01, $^{\#\#\#}$p<0.001; One-way ANOVA compared to wt DSS $^{+}$p<0.05, $^{++}$p<0.01, $^{+++}$p<0.001)

Only around 20% of TCRαβ$^+$ CD4$^+$ iIELs expressed the IEL typical integrin CD103 and were negative for the MLN homing marker CD62L (Figure 14 A). 40-60% of TCRαβ$^+$ CD4$^+$ iIELs expressed the activation markers CD44 and CD69 (Figure 14 B). No alterations due to TAMP-OE or DSS treatment were observed in TCRαβ$^+$ CD4$^+$ iIELs for those markers. From the population of TCRαβ$^+$ CD8αβ$^+$ iIELs 60-70% were CD103$^+$ and CD62L$^-$ with the exception in Tric-OE DSS mice only 47.20 ± 4.95% were CD103$^+$ and CD62L$^-$ and thereby significant less than in wt DSS (64.90 ± 2.18%) and Tric-OE control mice (68.00 ± 3.53%) (Figure 14 C). 60-70% TCRαβ$^+$ CD8αβ$^+$ iIELs were CD44$^+$ and CD69$^+$ (Figure 14 D).

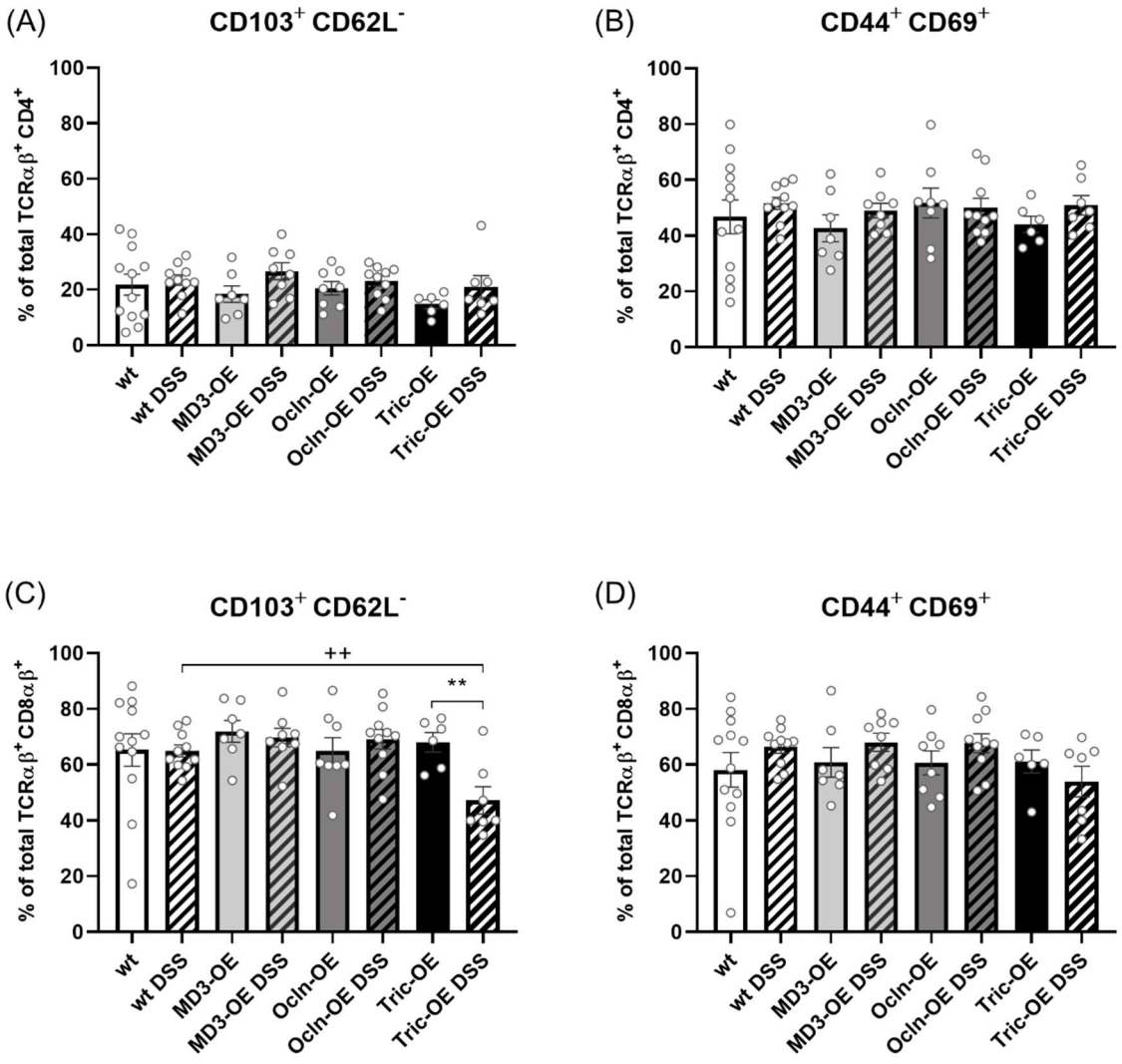

Figure 14 Occurrences of CD103⁺CD62L⁻ cells and CD44⁺ CD69⁺ cells among induced intraepithelial lymphocytes (epithelial fraction)

At day 6 of DSS treatment, colon tissue of wt and TAMP-OE mice was digested with EDTA to isolate immune cells. The epithelial fraction was stained for the IEL panel, acquired by LSR Fortessa 20x device and analysed with FlowJo software as illustrated in Figure 12. **(A and B)** Occurrences among TCRαβ⁺ CD4⁺ iIELs. No alterations in occurrence for CD103⁺CD62L⁻ cells and CD44⁺ CD69⁺ cells due to TAMP-OE or DSS treatment. **(C and D)** Occurrences among TCRαβ⁺ CD8αβ⁺ iIELs. **(C)** Tric-OE DSS mice had a lower occurrence of CD103⁺CD62L⁻ cells compared to wt DSS and Tric-OE mice. **(D)** No alteration in occurrence of CD44⁺ CD69⁺ cells due to TAMP-OE or DSS treatment were detected. ($n \geq 6$; data shown as mean ± SEM; outliers were identified by Grubb's test α= 0.01 and removed; student's T-test *p<0.05, **p<0.01, ***p<0.001; One-way ANOVA compared to wt $^{\#}$p<0.05, $^{\#\#}$p<0.01, $^{\#\#\#}$p<0.001; One-way ANOVA compared to wt DSS $^{+}$p<0.05, $^{++}$p<0.01, $^{+++}$p<0.001)

When treated with DSS more TCRαβ$^+$ CD8αα$^+$ nIELs tended to be CD103$^+$, which was significant for Ocln-OE mice (Ocln-OE 75.60 ± 2.22%; Ocln-OE DSS 82.00 ± 1,70%; Figure 15 A). This was also the case in TCRγδ$^+$ CD8αα$^+$ nIELs (Ocln-OE 92.5 ± 1.37%; Ocln-OE DSS 96.10 ± 0.65%; Figure 15 C). Less TCRαβ$^+$ CD8αα$^+$ nIELs were CD103$^+$ in Tric-OE DSS mice compared to wt DSS mice (60.10 ± 3.61% and 78.80 ± 1.55%, respectively Figure 15 A). In TCRαβ$^+$ CD8αα$^+$ nIELs an increase of CD44$^+$ CD69$^+$ cells was detected in MD3-OE and Ocln-OE mice after DSS treatment and the amount of TCRαβ$^+$ CD8αα$^+$ CD44$^+$ CD69$^+$ cells was higher in MD3-OE DSS than wt DSS mice (wt DSS 82.90 ± 0.90%; MD3-OE 81.20 ± 2.70%; MD3-OE DSS 87.70 ± 1.42%; Ocln-OE 82.10 ± 0.72%; Ocln-OE DSS 86.70 ± 0.62%; Figure 15 B). Almost all TCRγδ$^+$ CD8αα$^+$ nIELs were CD44$^+$ CD69$^+$ and this was neither influenced by DSS treatment nor by TAMP-OE (Figure 15 D).

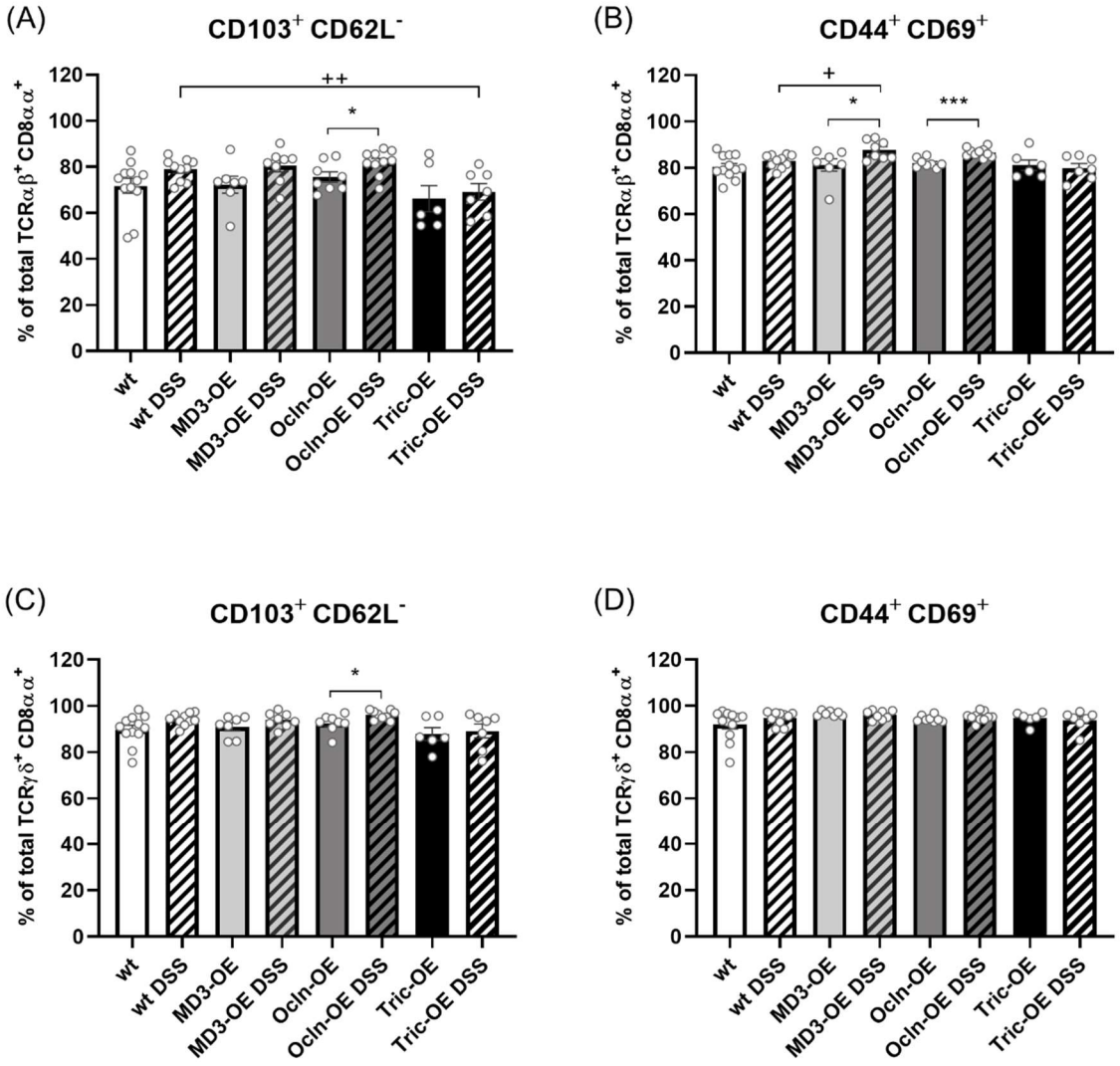

Figure 15 Occurrences of CD103$^+$CD62L$^-$ cells and CD44$^+$ CD69$^+$ cells among natural intraepithelial lymphocytes (epithelial fraction)

At day 6 of DSS treatment, colon tissue of wt and TAMP-OE mice was digested with EDTA to isolate immune cells. The epithelial fraction was stained for the IEL panel, acquired by LSR Fortessa 20x device and analysed with FlowJo software as illustrated in Figure 12. **(A and B)** Occurrences among TCRαβ$^+$ CD8αα$^+$ nIELs. (A) Occurrences of CD103$^+$CD62L$^-$ cells were significantly increased in Ocln-OE DSS compared to Ocln-OE mice and was lower in Tric-OE DSS mice compared to wt DSS mice. (B) Occurrences of CD44$^+$ CD69$^+$ cells were increased in MD3-OE and Ocln-OE mice during DSS-induced colitis compared to control conditions and was higher in MD3-OE DSS mice than wt DSS mice. **(C and D)** Occurrences among TCRγδ$^+$ CD8αα$^+$ nIELs. **(C)** Occurrences of CD103$^+$CD62L$^-$ cells were iincreased in Ocln-OE DSS mice compared Ocln-OE mice. **(D)** No alteration in occurrence for CD44$^+$ CD69$^+$ cells due to TAMP-OE or DSS treatment were detected. ($n \geq 6$; data shown as mean ± SEM; outliers were identified by Grubb's test α= 0.01 and removed; student's T-test *p<0.05, **p<0.01, ***p<0.001; One-way ANOVA compared to wt $^{\#}$p<0.05, $^{\#\#}$p<0.01, $^{\#\#\#}$p<0.001; One-way ANOVA compared to wt DSS $^{+}$p<0.05, $^{++}$p<0.01, $^{+++}$p<0.001)

LP immune cells were isolated during the second digestion with collagenase, DNase and Dispase. Although IELs should have been more prominent in the epithelial fraction, the LP fraction was stained and analysed with the IEL panel. Results confirmed that the occurrence of the nIELs subsets TCRαβ$^+$ CD8αα$^+$ (epithelial fraction 16.20-35.30%; LP fraction 0.83-1.34%) and TCRγδ$^+$ CD8αα$^+$ (epithelial fraction 6.91-22.40%; LP fraction 0.08-0.27%) were lower compared to the epithelial fraction after EDTA digestion. In contrast, the occurrence of TCRαβ$^+$ CD4$^+$ iIELs was higher in the LP fraction than the epithelial fraction (1.87-3.91% and 6.28-10.10%, respectively; Figure 13 and 16). The amount of TCRαβ$^+$ CD4$^+$ iIELs was reduced upon DSS treatment compared to control condition in wt, MD3-OE and Tric-OE mice, this tendency was also seen in Ocln-OE, however it was not significant (Figure 16 A). No alterations were observed in TCRαβ$^+$ CD8αβ$^+$ cells (Figure 16 B). Occurrence of TCRαβ$^+$ CD8αα$^+$ nIELs was increased in MD3-OE mice during DSS but not in wt, Ocln-OE and Tric-OE mice. In wt and Ocln-OE mice TCRγδ$^+$ CD8αα$^+$ nIELs were increased upon DSS treatment. No changes between wt and TAMP-OE mice during control or after DSS treatment were detected (Figure 16 C and D).

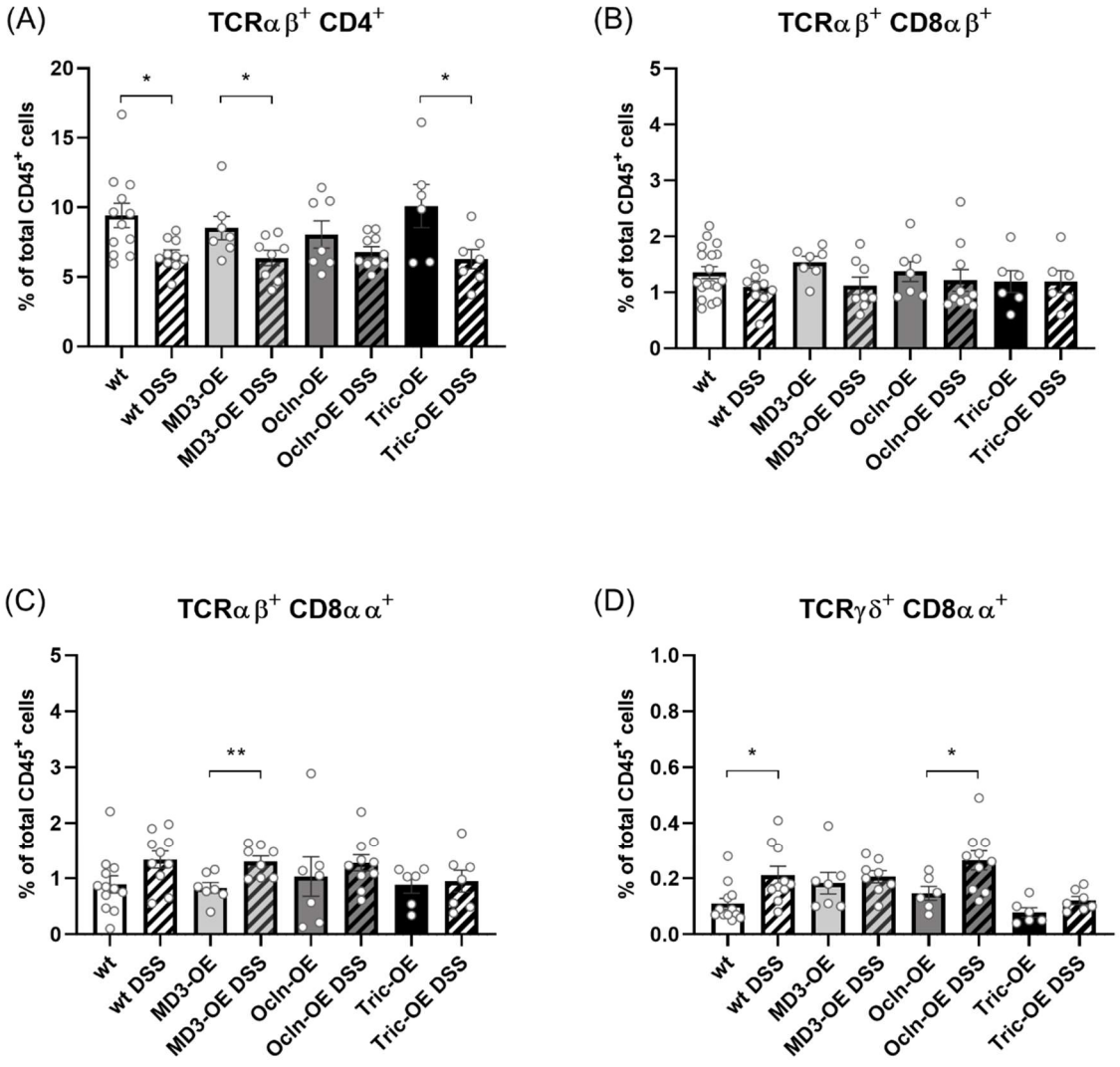

Figure 16 Occurrences for intraepithelial lymphocyte subsets (LP fraction)

At day 6 of DSS treatment, colon tissue of wt and TAMP-OE mice was digested first with EDTA and then with Collagenase, Dispase and DNase to isolate immune cells from the lamina propria (LP). This LP fraction was stained for the IEL panel, acquired by LSR Fortessa 20x device and analysed with FlowJo software as illustrated in Figure 12. **(A)** Occurrence of TCRαβ$^+$ CD4$^+$ iIELs was decreased during DSS-induced colitis, however this decrease was not significant in Ocln-OE mice. **(B)** Occurrence of TCRαβ$^+$ CD8αβ$^+$ iIELs was not altered due to TAMP-OE or DSS treatment. **(C)** Occurrence of TCRαβ$^+$ CD8αα$^+$ nIELs was increased during DSS-induced colitis, this increase was significant for MD3-OE mice. **(D)** Occurrence of TCRγδ$^+$ CD8αα$^+$ nIELs was increased during DSS-induced colitis in wt and Ocln-OE mice. ($n \geq 6$; data shown as mean ± SEM; outliers were identified by Grubb's test α= 0.01 and removed; student's T-test *p<0.05, **p<0.01, ***p<0.001; One-way ANOVA compared to wt $^{\#}$p<0.05, $^{\#\#}$p<0.01, $^{\#\#\#}$p<0.001; One-way ANOVA compared to wt DSS $^{+}$p<0.05, $^{++}$p<0.01, $^{+++}$p<0.001)

No significant changes in the occurrence of TCRαβ$^+$ CD4$^+$ CD103$^+$ CD62L$^-$ iIELs were observed (Figure 17 A). Less TCRαβ$^+$ CD4$^+$ iIELs were CD44$^+$ CD69$^+$ after DSS treatment in MD3-OE mice (MD3-OE 71.40 ± 1.47% and MD3-OE DSS 56.00 ± 2.50%; Figure 17 B). DSS-induced colitis led to a reduction of TCRαβ$^+$ CD8αβ$^+$ CD103$^+$ CD62L$^-$ iIELs in wt (ctrl 39.70 ± 2.41% and DSS 32.10 ± 2.16%) and MD3-OE mice (ctrl 44.00 ± 2.53% and DSS 36.00 ± 2.31%), no change was observed in Tric-OE mice (ctrl 34.40 ± 3.23% and DSS 29.80 ± 1.46%), in contrast there was an increase in Ocln-OE DSS mice (ctrl 36.40 ± 2.31% and DSS 46.1 ± 3.79%) (Figure 17 C). Therefore, Ocln-OE DSS mice had a higher occurrence of TCRαβ$^+$ CD8αβ$^+$ CD103$^+$ CD62L$^-$ iIELs than wt DSS mice. Less TCRαβ$^+$ CD8αβ$^+$ iELs were CD44$^+$ CD69$^+$ in Tric-OE DSS mice than wt DSS mice (41.60 ± 4.42% and 53.40 ± 2.84%, respectively; Figure 17 D). After DSS treatment, a lower occurrence of TCRαβ$^+$ CD8αβ$^+$ iELs expressed CD44$^+$ CD69$^+$ in MD3-OE mice (ctrl 59.80 ± 2.52% and DSS 50.60 ± 2.47%), whereas more cells expressed CD44$^+$ CD69$^+$ after DSS treatment in Ocln-OE mice (ctrl 49.60 ± 3.67% and DSS 61.00 ± 2.95%) (Figure 17 D).

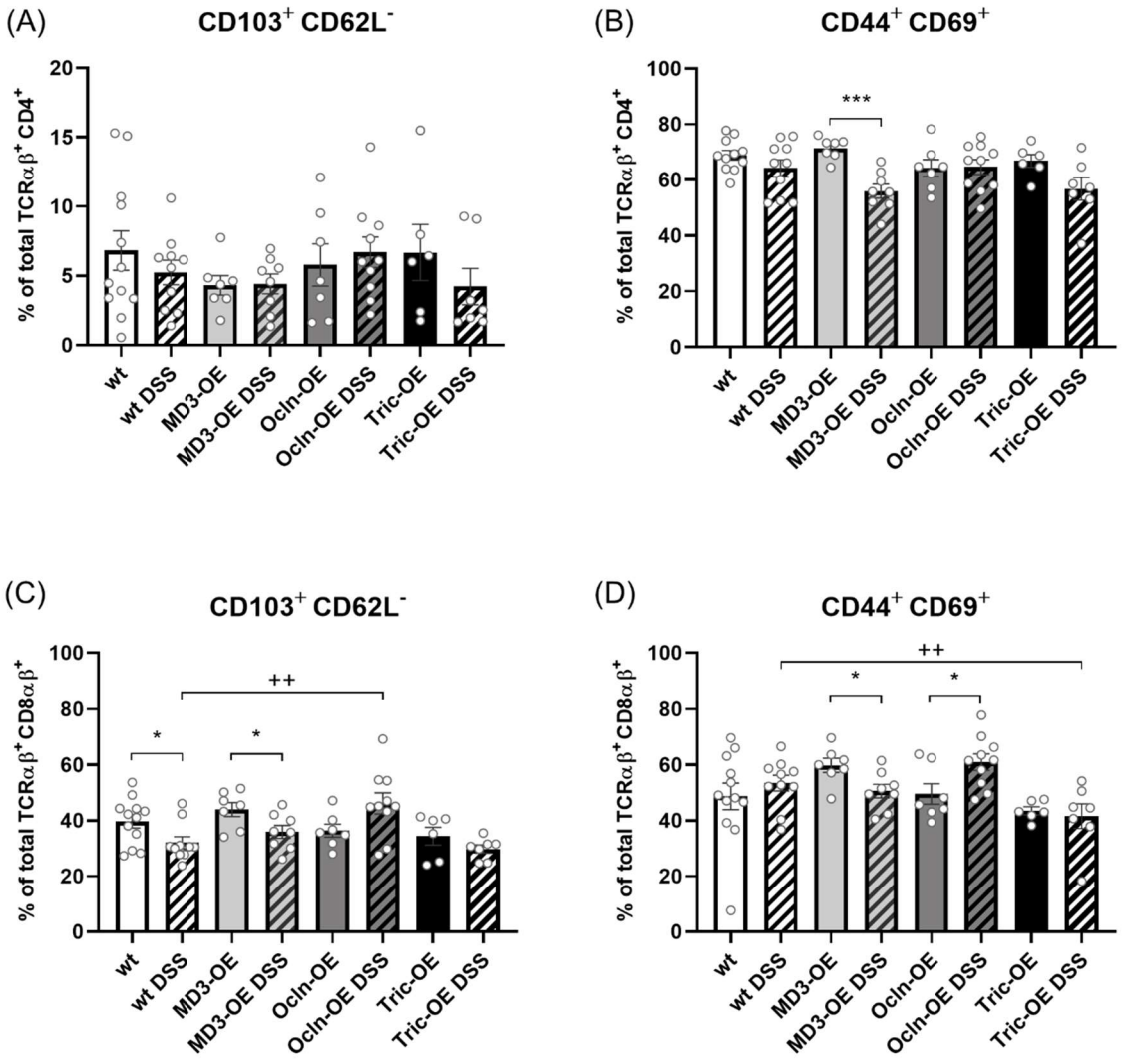

Figure 17 Occurrences of CD103⁺CD62L⁻ cells and CD44⁺ CD69⁺ cells among induced intraepithelial lymphocytes (LP fraction)

At day 6 of DSS treatment, colon tissue of wt and TAMP-OE mice was digested first with EDTA and then with Collagenase, Dispase and DNase to isolate immune cells from the lamina propria (LP). This LP fraction was stained for the IEL panel, acquired by LSR Fortessa 20x device and analysed with FlowJo software as illustrated in Figure 12. **(A and B)** Occurrences among TCRαβ⁺ CD4⁺ iIELs. **(A)** No alterations in occurrence of CD103⁺CD62L⁻ cells due to TAMP-OE or DSS treatment were detected. **(B)** Occurrences of CD44⁺ CD69⁺ cells were reduced during DSS-induced colitis in MD3-OE mice **(C and D)** Occurrences among TCRαβ⁺ CD8αβ⁺ iIELs. **(C)** Occurrences for CD103⁺CD62L⁻ cells were reduced in wt and MD3-OE during DSS-induced colitis but increased in Ocln-OE mice. Thus, occurrence of CD103⁺CD62L⁻ cells was higher in Ocln-OE DSS mice than wt DSS mice **(D)** Occurrence of CD44⁺ CD69⁺ cells was reduced in MD3-OE mice during DSS-induced colitis, but increased in Ocln-OE mice. Occurrence of CD44⁺ CD69⁺ cells was lower in Tric-OE DSS mice than wt DSS mice. ($n \geq 6$; data shown as mean ± SEM; outliers were identified by Grubb´s test α= 0.01 and removed; student's T-test *p<0.05,

**p<0.01, ***p<0.001; One-way ANOVA compared to wt #p<0.05, ##p<0.01, ###p<0.001; One-way ANOVA compared to wt DSS +p<0.05, ++p<0.01, +++p<0.001)

The occurrence of CD103$^+$ CD62L$^-$ nIELs tended to be increased during DSS-induced colitis, which was significant in wt, MD3-OE and Ocln-OE mice for TCRαβ$^+$ CD8αα$^+$ nIELs and in wt for TCRγδ$^+$ CD8αα$^+$ nIELs (Figure 18 A and C). No changes due to DSS treatment or TAMP-OE were detected for the occurrence of TCRαβ$^+$ CD8αα$^+$ CD44$^+$ CD69$^+$ nIELs (Figure 18 B). In Ocln-OE mice the occurrence of TCRγδ$^+$ CD8αα$^+$ CD44$^+$ CD69$^+$ nIELs was increased upon DSS treatment, which was not the case in wt, MD3-OE or Tric-OE mice (Figure 18 D)

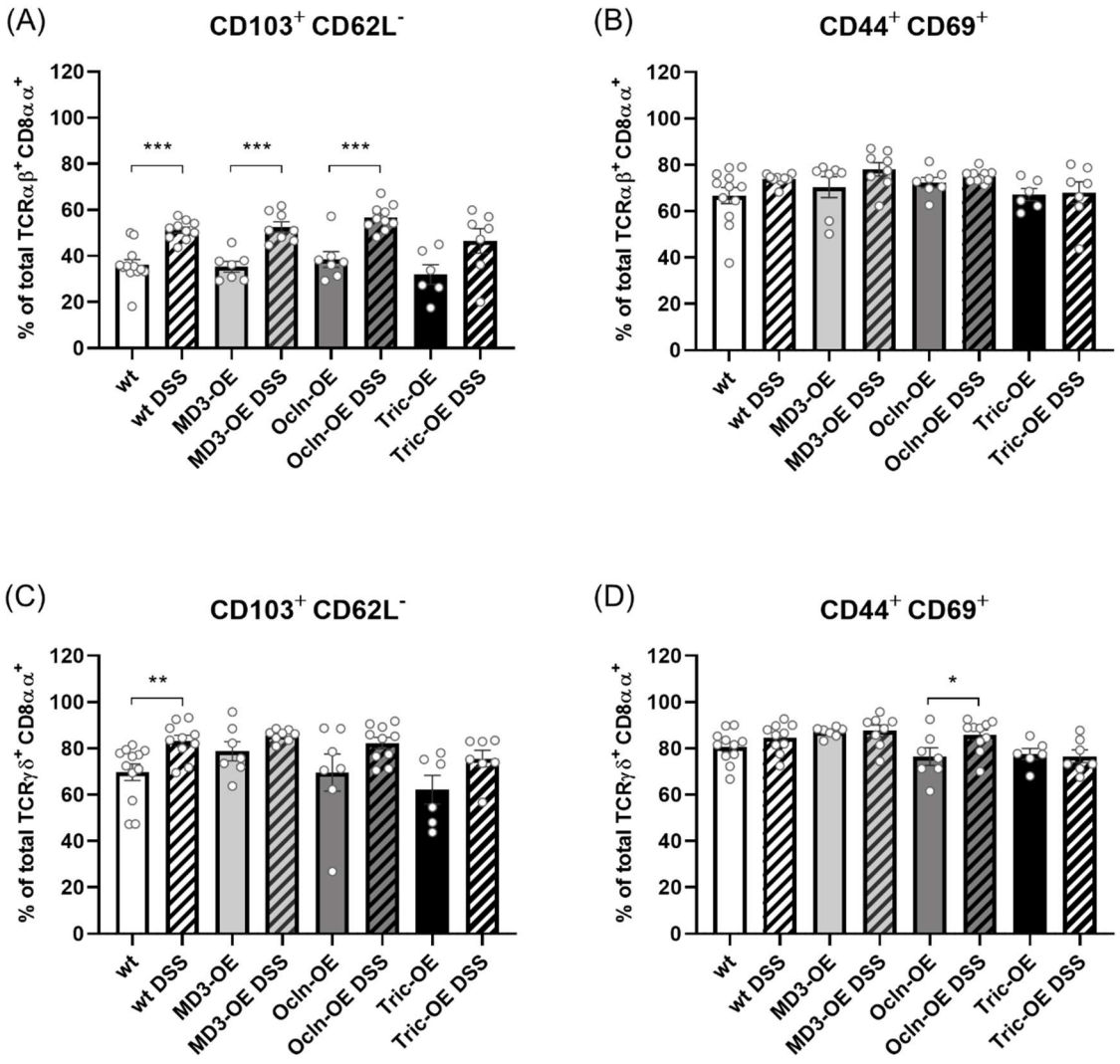

Figure 18 Occurrences of CD103$^+$CD62L$^-$ cells and CD44$^+$ CD69$^+$ cells among natural intraepithelial lymphocytes (LP fraction)

At day 6 of DSS treatment, colon tissue of wt and TAMP-OE mice was digested first with EDTA and then with Collagenase, Dispase and DNase to isolate immune cells from the lamina propria (LP). This

LP fraction was stained for the IEL panel, acquired by LSR Fortessa 20x device and analysed with FlowJo software as illustrated in Figure 12. **(A and B)** Occurrences among TCRαβ$^+$ CD8αα$^+$ nIELs. **(A)** Occurrences of CD103$^+$CD62L$^-$ cells were increased during DSS-induced colitis, this increase was not significant in Tric-OE mice. **(B)** No alterations in occurrence of CD44$^+$ CD69$^+$ cells due to TAMP-OE or DSS treatment were detected. **(C and D)** Occurrences among TCRγδ$^+$ CD8αα$^+$ nIELs. **(C)** Occurrences of CD103$^+$CD62L$^-$ cells were increased in wt DSS mice compared wt mice. **(D)** Occurrences of CD44$^+$ CD69$^+$ cells were increased during DSS-induced colitis in Ocln-OE mice. ($n \geq 6$; data shown as mean ± SEM; outliers were identified by Grubb's test α= 0.01 and removed; student's T-test *p<0.05,**p<0.01, ***p<0.001; One-way ANOVA compared to wt $^{\#}$p<0.05, $^{\#\#}$p<0.01, $^{\#\#\#}$p<0.001; One-way ANOVA compared to wt DSS $^{+}$p<0.05,$^{++}$p<0.01, $^{+++}$p<0.001)

A second flow cytometry panel focuses on myeloid cells, as those cells are the first to encounter pathogens and were found to express tight junction proteins (Mariano et al., 2011b). To recognize changes in other cell types this panel also gates for major immune cell subtypes like CD4$^+$ and CD8$^+$ T-cells, neutrophils, and B-cells. The gating strategy for the myeloid panel is illustrated in Figure 19.

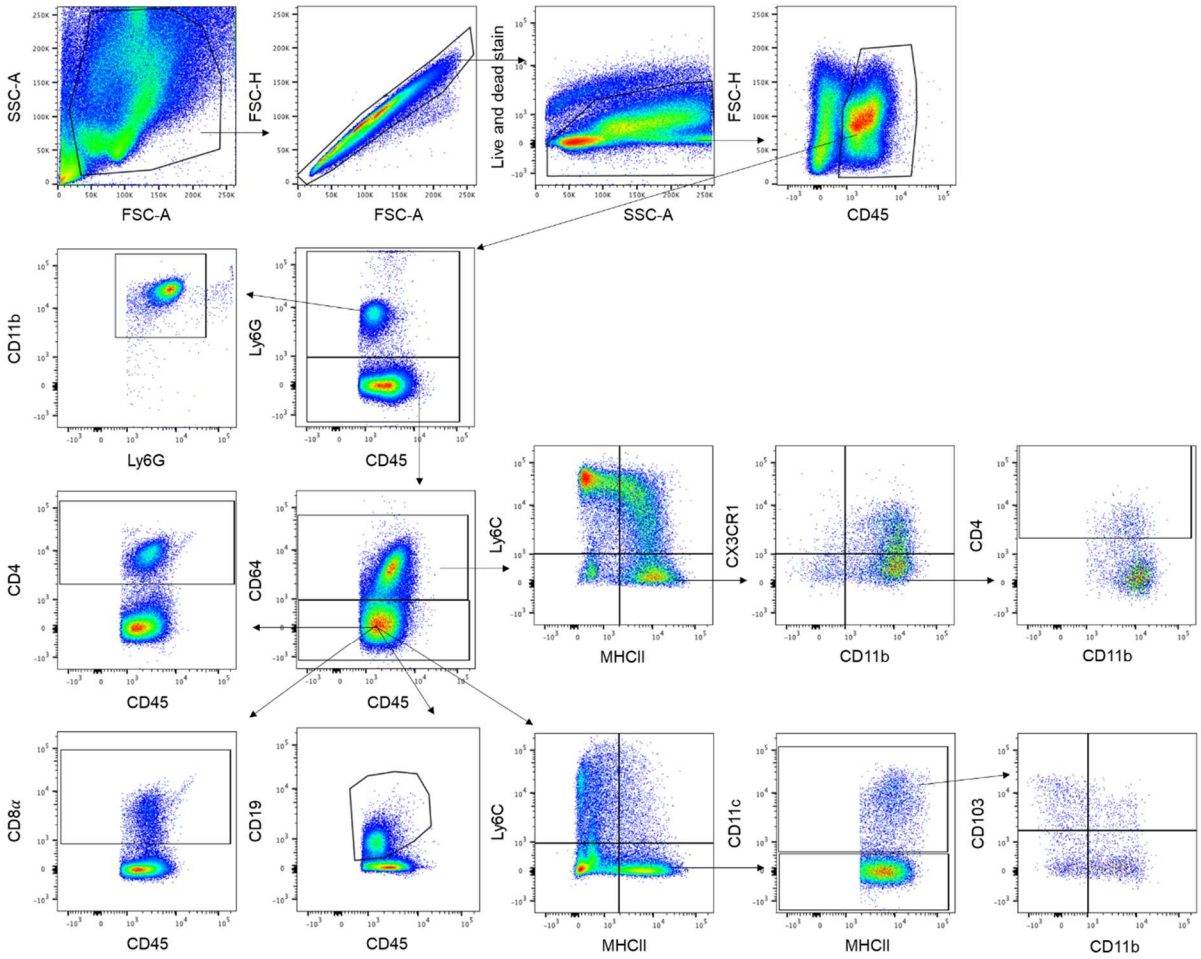

Figure 19 Myeloid cell gating strategy

Gating strategy for myeloid cells using the FlowJo software. First, cell debris was excluded and gated on single cells. Then viable and $CD45^+$ cells were identified. Those were further divided into $Ly6G^+$ neutrophils or $Ly6G^-$ cells. Neutrophils were analysed for CD11b expression. $Ly6G^-$ cells were divided into $CD64^+$ and $CD64^-$ cells. $CD64^-$ cells were analysed for CD4 expression (CD4 T-cells), CD8α expression (CD8α T-cells), CD19 expression (B-cells) and Ly6C and MHCII expression. $Ly6C^+$ $MHCII^-$ were defined as blood monocytes. $Ly6C^-$ $MCHII^+$ $CD11c^+$ cells were identified as dendritic cells (DCs). DCs were divided by the expression of CD103 and CD11b. $CD64^+$ were distinguished by the expression of Ly6C and MCHII. $Ly6C^+$ $MCHII^-$ were defined as monocytes, $Ly6C^+$ $MCHII^+$ as maturing monocytes and $Ly6C^-$ $MCHII^+$ as macrophages. Macrophages were further divided into $CD11b^+$ macrophages or resident macrophages ($CD11b^+$ $CX3CR1^+$). Resident macrophages were analysed for CD4 expression.

Both fractions were stained and analysed with the myeloid panel. Results of the epithelial fraction showed an increase of $Ly6G^+$, $Ly6G^+$ $CD11b^+$ and $CD64^+$ cells in wt and TAMP-OE mice upon DSS treatment. However, no changes due to TAMP-OE were determined (Figure 20 A-C). Blood monocytes, which were defined as $CD45^+$ $Ly6G^-$ $CD64^-$ $Ly6C^+$ $MCHII^+$ cells, also tended to be increased during DSS-induced colitis, though it was only significant in wt mice (wt 3.87 ± 0.61% and wt DSS 6.55 ± 0.87%; Figure 20 D). A higher occurrence of blood monocytes was detected in Tric-OE mice than in wt mice (3.87 ± 0.61% and 6.42 ± 0.84%; respectively).

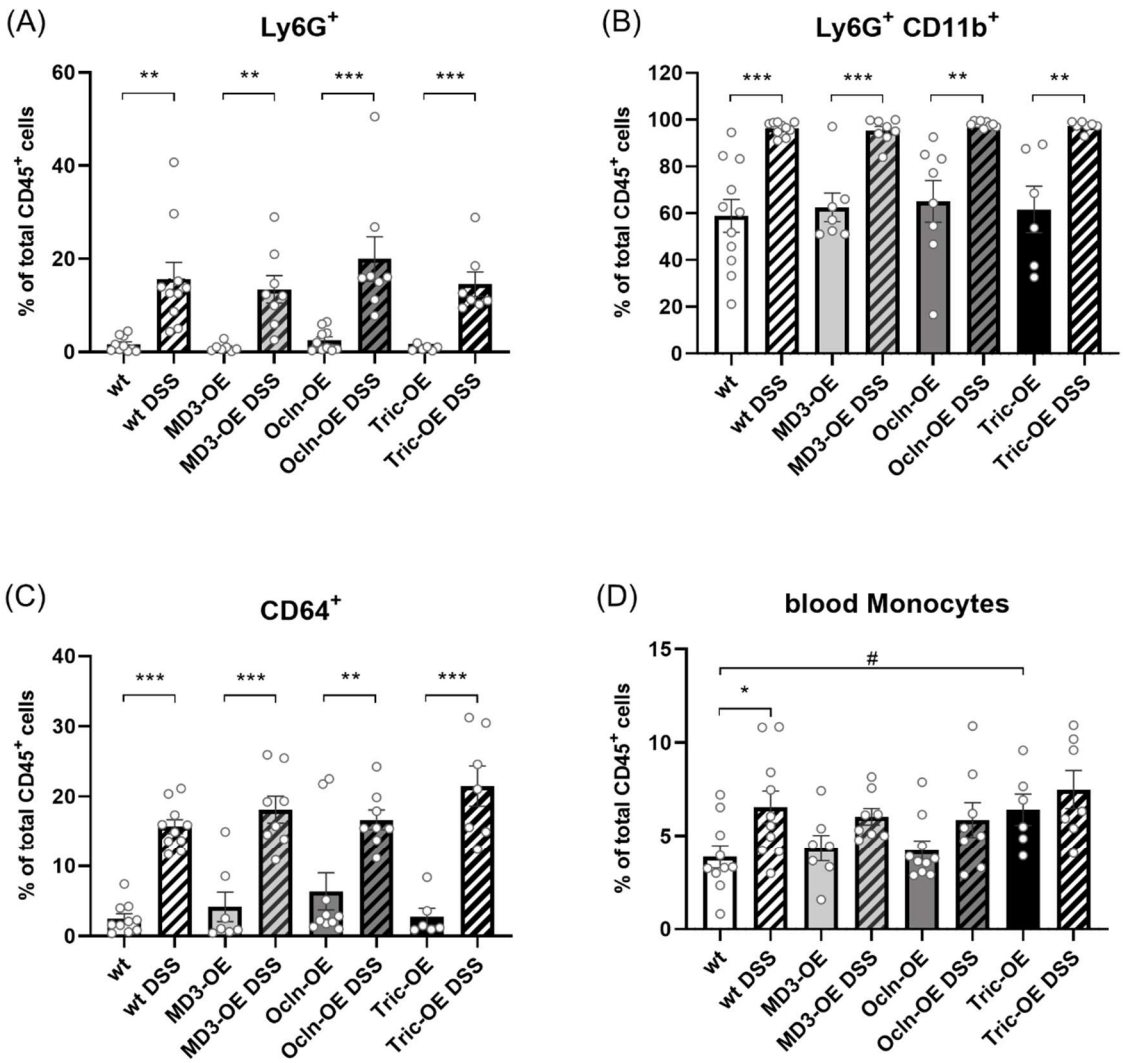

Figure 20 Occurrence of neutrophils, CD64⁺ cells and blood monocytes among viable CD45⁺ cells for (epithelial fraction)

At day 6 of DSS treatment, colon tissue of wt and TAMP-OE mice was digested with EDTA to isolate immune cells. The epithelial fraction was stained for the myeloid panel, acquired by LSR Fortessa 20x device and analysed with FlowJo software as illustrated in Figure 19. **(A)** Occurrences of Ly6G⁺ neutrophils were increased during DSS-induced colitis. **(B)** Occurrences of Ly6G⁺ CD11b⁺ neutrophils were increased during DSS-induced colitis. **(C)** Occurrence of CD64⁺ (Ly6G⁻) cells was increased during DSS-induced colitis. **(D)** Occurrence of blood monocytes (Ly6G⁻ CD64⁻ Ly6C⁺ MCHII⁻) was increased during DSS-induced colitis in wt mice and was higher in Tric-OE mice than wt mice. ($n \geq 6$; data shown as mean ± SEM; outliers were identified by Grubb's test α= 0.01 and removed; student's T-test *p<0.05,**p<0.01, ***p<0.001; One-way ANOVA compared to wt $^{\#}$p<0.05, $^{\#\#}$p<0.01, $^{\#\#\#}$p<0.001; One-way ANOVA compared to wt DSS $^{+}$p<0.05, $^{++}$p<0.01, $^{+++}$p<0.001)

No changes due to DSS treatment or TAMP-OE appeared in DCs (Figure 21 A). CD4⁺ T-cells were reduced in Ocln-OE DSS mice compared to Ocln-OE mice (4.54 ± 0.63% and 15.4 ± 3.73%, respectively Figure 21 B). The occurrence of CD8⁺ T-cells had the tendency to be reduced in DSS-induced colitis, this reduction was significant in Ocln-OE and Tric-OE mice (Ocln-OE 51.50 ± 3.17%, Ocln-OE DSS 30.80 ± 2.60%, Tric-OE 49.90 ± 1.65%, Tric-OE DSS 27.50 ± 3.27%; Figure 21 C). The occurrence of CD19⁺ B-cells was higher in MD3-OE DSS mice than in wt DSS mice (20.60 ± 4.59% and 6.89 ± 2.11%, respectively; Figure 21 D). Here the population of CD64 and DCs were not further distinguished, because cell numbers were too low to draw meaningful conclusions.

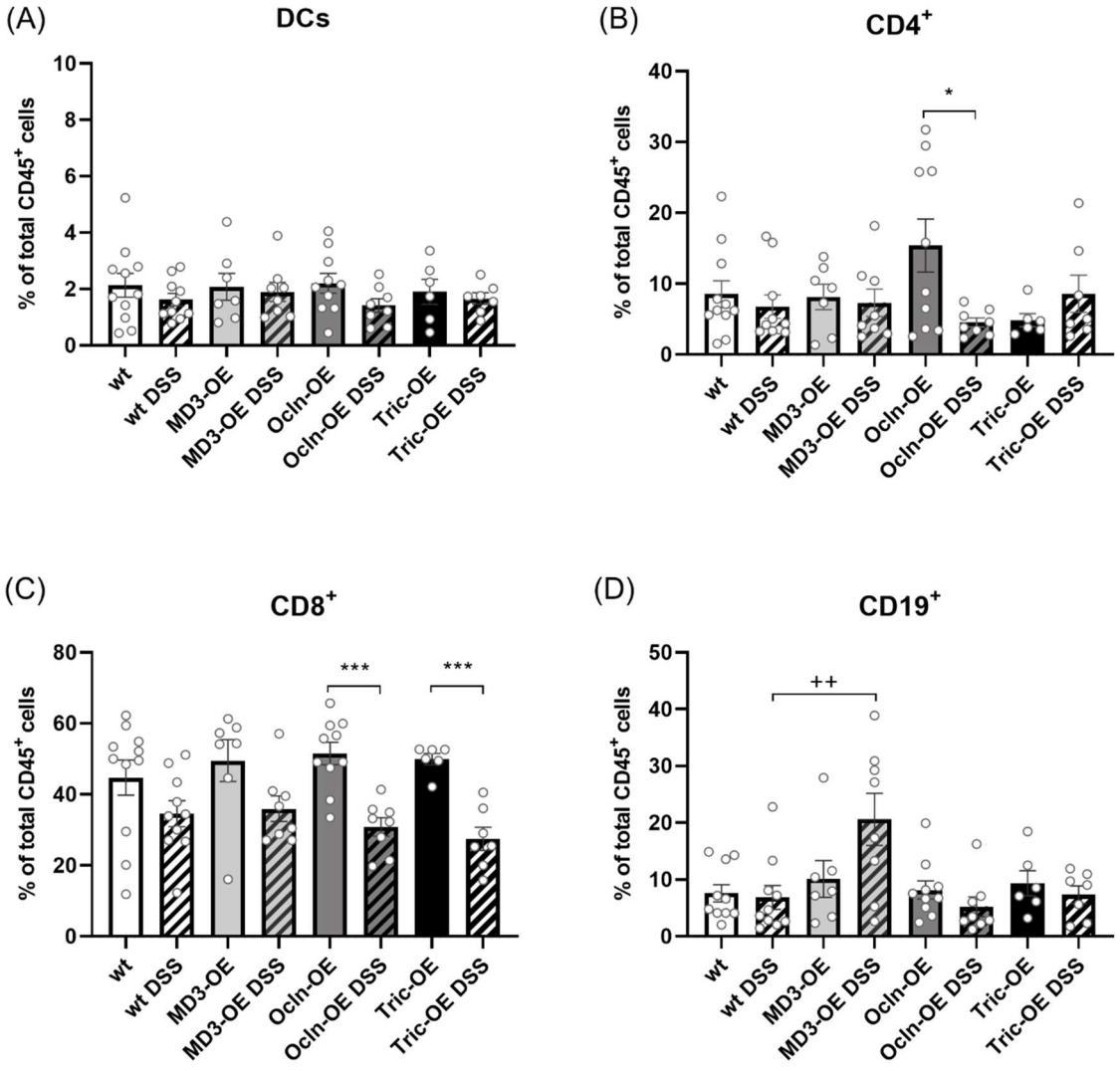

Figure 21 Occurrence of dendritic cells, CD4⁺ and CD8⁺ T-cells and B-cells among viable CD45⁺ cells (epithelial fraction)

At day 6 of DSS treatment, colon tissue of wt and TAMP-OE mice was digested with EDTA to isolate immune cells. The epithelial fraction was stained for the myeloid panel, acquired by LSR Fortessa 20x

device and analysed with FlowJo software as illustrated in Figure 19. **(A)** Occurrence of dendritic cells (DCs, Ly6G$^-$ CD64$^-$ Ly6C$^-$ MCHII$^+$ CD11c$^+$) was not altered due to TAMP-OE or DSS treatment. **(B)** Occurrence of CD4$^+$ T-cells (Ly6G$^-$ CD64$^-$ CD4$^+$) was lower in Ocln-OE DSS than Ocln-OE mice. **(C)** Occurrence of CD8α$^+$ T-cells (Ly6G$^-$ CD64$^-$ CD8α$^+$) was decreased during DSS-induced colitis, this decrease was significant in Ocln-OE and Tric-OE mice. **(D)** Occurrence of CD19$^+$ B-cells (Ly6G$^-$ CD64$^-$ CD19$^+$) was higher in MD3-OE DSS than wt DSS mice. ($n \geq 6$; data shown as mean ± SEM; outliers were identified by Grubb's test α= 0.01 and removed; student's T-test *p<0.05, **p<0.01, ***p<0.001; One-way ANOVA compared to wt $^{\#}$p<0.05, $^{\#\#}$p<0.01, $^{\#\#\#}$p<0.001; One-way ANOVA compared to wt DSS $^{+}$p<0.05, $^{++}$p<0.01, $^{+++}$p<0.001)

In the LP fraction, after collagenase digestion, the occurrences for Ly6G$^+$, Ly6G$^+$ CD11b$^+$ and CD64$^+$ cells increased in DSS-induced colitis, in contrast it decreased for blood monocytes. No changes due to TAMP-OE were detected (Figure 22).

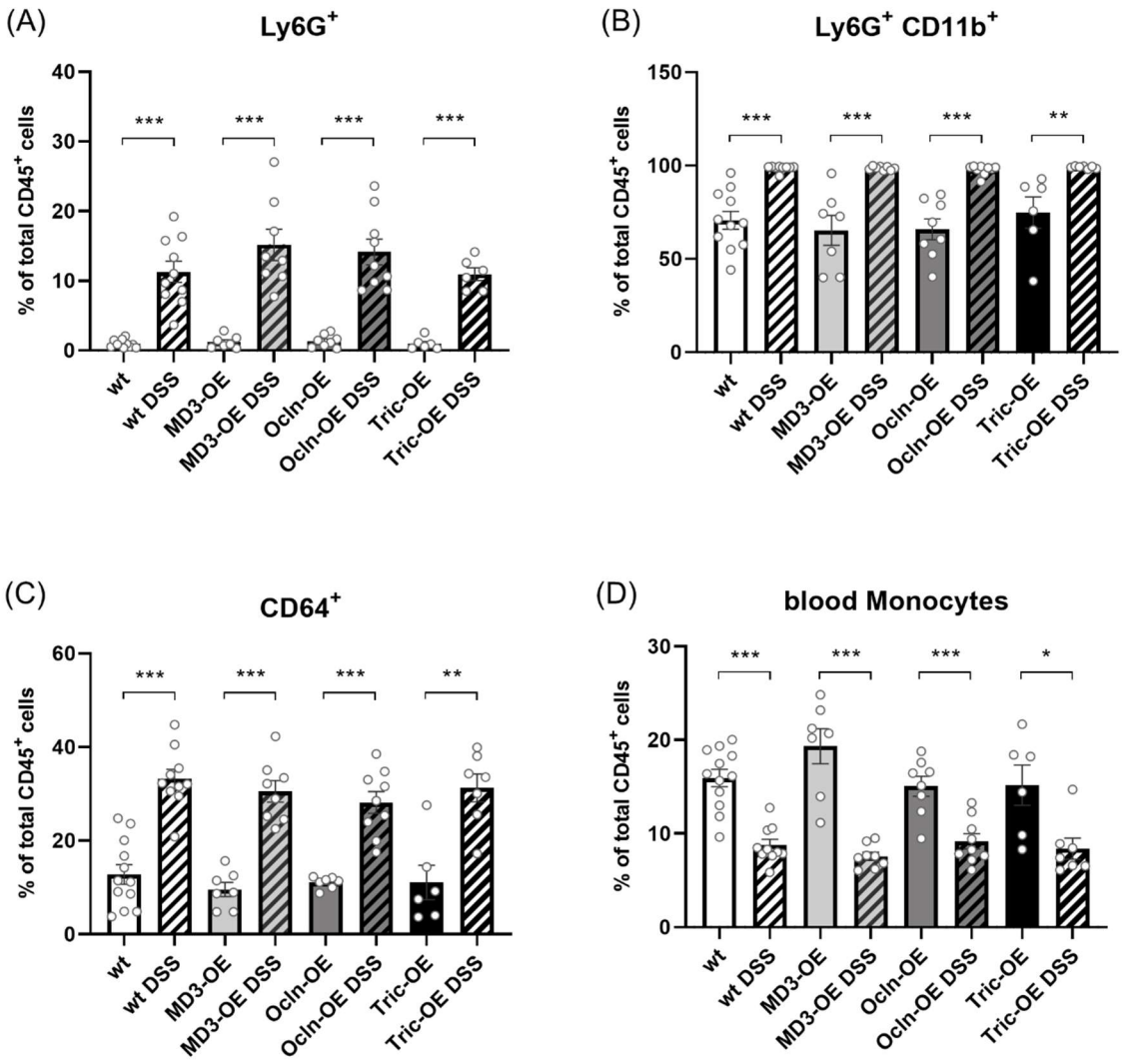

Figure 22 Occurrence of neutrophils, CD64$^+$ cells and blood monocytes among viable CD45$^+$ cells (LP fraction)

At day 6 of DSS treatment, colon tissue of wt and TAMP-OE mice was digested first with EDTA and then with Collagenase, Dispase and DNase to isolate immune cells from the lamina propria (LP). This LP fraction was stained for the myeloid panel, acquired by LSR Fortessa 20x device and analysed with FlowJo software as illustrated in Figure 19. **(A)** Occurrences of Ly6G$^+$ neutrophils were increased during DSS-induced colitis **(B)** Occurrences of Ly6G$^+$ CD11b$^+$ neutrophils were increased during DSS-induced colitis. **(C)** Occurrences of CD64$^+$ (Ly6G$^-$) cells were increased during DSS-induced colitis. **(D)** Occurrences of blood monocytes (Ly6G$^-$ CD64$^-$ Ly6C$^+$ MCHII$^-$) were increased during DSS-induced colitis. ($n \geq 6$; data shown as mean ± SEM; outliers were identified by Grubb's test α= 0.01 and removed; student's T-test *p<0.05, **p<0.01, ***p<0.001; One-way ANOVA compared to wt $^{\#}$p<0.05, $^{\#\#}$p<0.01, $^{\#\#\#}$p<0.001; One-way ANOVA compared to wt DSS $^{+}$p<0.05, $^{++}$p<0.01, $^{+++}$p<0.001)

DCs were reduced in DSS-induced colitis, this reduction was not significant in Tric-OE mice (Figure 23 A). CD4$^+$ T-cells were reduced after DSS treatment, although this was less pronounced and not significant in MD3-OE mice (Figure 23 B). No changes due to DSS treatment or TAMP-OE were observed for the occurrence of CD8$^+$ T-cells (Figure 23 C). The occurrence of CD19$^+$ B-cells was reduced during DSS-induced colitis in wt, Ocln-OE and Tric-OE mice (Figure 23 D). In MD3-OE mice however, DSS treatment led to an increased occurrence of CD19$^+$ B-cells. Furthermore, the occurrence of CD19$^+$ B-cells was lower under control conditions in MD3-OE mice than wt mice (7.08 ± 0.74% and 23.2 ± 4.19%, respectively), whereas after DSS treatment it was higher in MD3-OE DSS mice than wt DSS mice (25.50 ± 5.06% and 12.40 ± 1.50%, respectively).

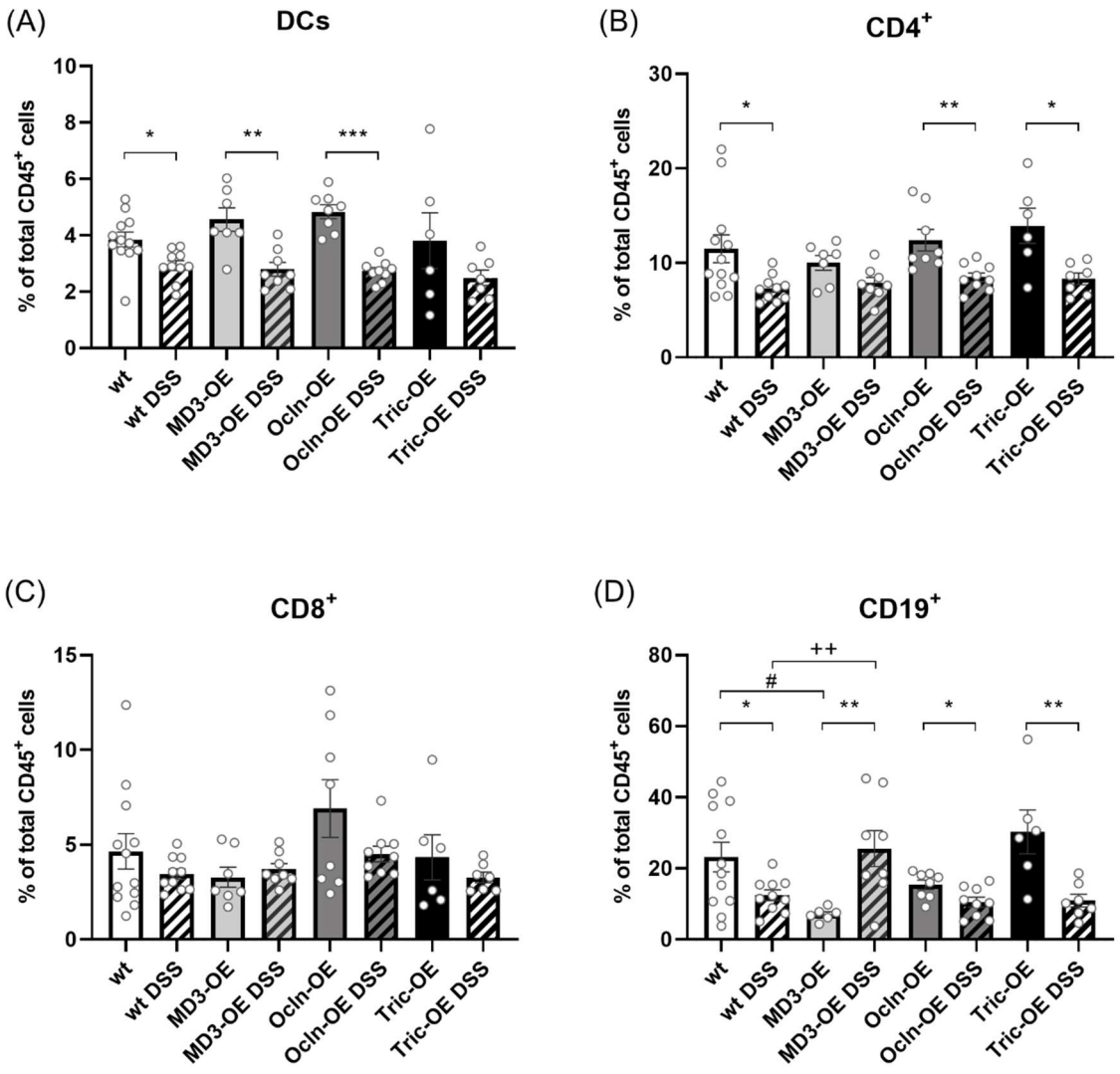

Figure 23 Occurrence of dendritic cells, CD4⁺ and CD8⁺ T-cells and B-cells among viable CD45⁺ cells (LP fraction)

At day 6 of DSS treatment, colon tissue of wt and TAMP-OE mice was digested first with EDTA and then with Collagenase, Dispase and DNase to isolate immune cells from the lamina propria (LP). This LP fraction was stained for the myeloid panel, acquired by LSR Fortessa 20x device and analysed with FlowJo software as illustrated in Figure 19. **(A)** Occurrences of dendritic cells (DCs, Ly6G⁻ CD64⁻ Ly6C⁻ MCHII⁺ CD11c⁺) were decreased during DSS-induced colitis, this decrease was not significant in Tric-OE mice. **(B)** Occurrences of CD4⁺ T-cells (Ly6G⁻ CD64⁻ CD4⁺) were decreased during DSS-induced colitis, this decrease was not significant in MD3-OE mice. **(C)** Occurrence of CD8α⁺ T-cells (Ly6G⁻ CD64⁻ CD8α⁺) was not altered due to TAMP-OE or DSS treatment. **(D)** Occurrences of CD19⁺ B-cells (Ly6G⁻ CD64⁻ CD19⁺) were decreased during DSS-induced colitis with the one exception, in MD3-OE mice. In MD3-OE mice the number of B-cells increased during DSS-induced colitis. Occurrence of B-cells was lower in MD3-OE mice than wt mice and higher in MD3-OE DSS than wt DSS mice. ($n \geq 6$;

data shown as mean ± SEM; outliers were identified by Grubb's test α= 0.01 and removed; student's T-test *p<0.05, **p<0.01, ***p<0.001; One-way ANOVA compared to wt $^{\#}$p<0.05, $^{\#\#}$p<0.01, $^{\#\#\#}$p<0.001; One-way ANOVA compared to wt DSS $^{+}$p<0.05, $^{++}$p<0.01, $^{+++}$p<0.001)

On one side the occurrence of monocytes (Figure 24 A) and maturing monocytes (Figure 24 B) is elevated, while on the other side it is decreased for macrophages (Figure 24 C) during DSS-induced colitis. Within the macrophage population less cells were CX3CR1^{+} CD11b^{+} (resident macrophages; Figure 24 E), while more cells only expressed CD11b after DSS treatment (Figure 24 D). Furthermore, less resident macrophages expressed CD4 upon DSS treatment (Figure 24 F). In Tric-OE DSS mice the occurrence of maturing monocytes was higher than in wt DSS mice (46.70 ± 2.98% and 33.40 ± 3.12%, respectively; Figure 24 B). Resident macrophages tended to be increased in Ocln-OE DSS mice than in wt DSS mice, although this increase was not significant (58.00 ± 2.27% and 50.70 ± 3.31%, respectively; Figure 24 E). However, a higher occurrence of resident macrophages CD4^{+} was seen in Ocln-OE DSS mice compared to wt DSS mice (4.82 ± 0.68% and 2.62 ± 0.31%, respectively; Figure 24 F).

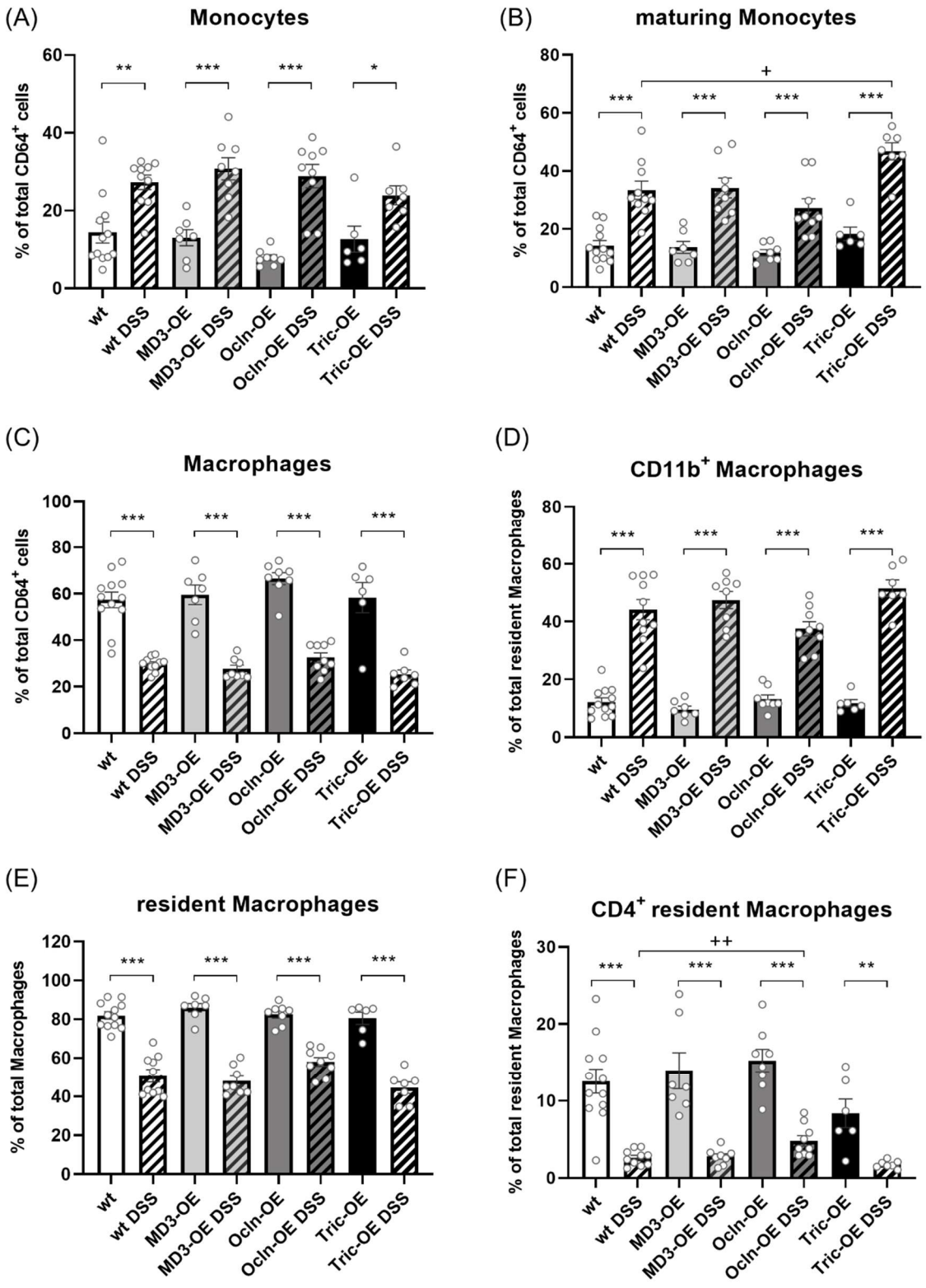

Figure 24 Occurrence of CD64⁺ cells subsets (LP fraction)

At day 6 of DSS treatment, colon tissue of wt and TAMP-OE mice was digested first with EDTA and then with Collagenase, Dispase and DNase to isolate immune cells from the lamina propria (LP). This LP fraction was stained for the myeloid panel, acquired by LSR Fortessa 20x device and analysed with

FlowJo software as illustrated in Figure 19. **(A)** Occurrences of monocytes (Ly6G$^-$ CD64$^+$ Ly6C$^+$ MCHII$^-$) were increased during DSS-induced colitis. **(B)** Occurrences of maturing monocytes (Ly6G$^-$ CD64$^+$ Ly6C$^+$ MCHII$^+$) were increased during DSS-induced colitis and was higher in Tric-OE DSS mice than wt DSS mice. **(C)** Occurrences of macrophages (Ly6G$^-$ CD64$^+$ Ly6C$^-$ MCHII$^+$) were decreased during DSS-induced colitis. **(D)** Occurrences of CD11b$^+$ macrophages (Ly6G$^-$ CD64$^+$ Ly6C$^-$ MCHII$^+$ CD11b$^+$) were decreased during DSS-induced colitis. **(E)** Occurrences of resident macrophages (Ly6G$^-$ CD64$^+$ Ly6C$^-$ MCHII$^+$ CD11b$^+$ CX3CR1$^+$) were decreased during DSS-induced colitis. However, this decrease was smaller in Ocln-OE mice. **(F)** Occurrences of CD4$^+$ resident macrophages (Ly6G$^-$ CD64$^+$ Ly6C$^-$ MCHII$^+$ CD11b$^+$ CX3CR1$^+$ CD4$^+$) were decreased during DSS-induced colitis. However, this decrease was smaller in Ocln-OE mice and occurrence was higher in Ocln-OE DSS compared to wt DSS mice. ($n \geq 6$; data shown as mean ± SEM; outliers were identified by Grubb's test α= 0.01 and removed; student's T-test *p<0.05, **p<0.01, ***p<0.001; One-way ANOVA compared to wt $^{\#}$p<0.05, $^{\#\#}$p<0.01, $^{\#\#\#}$p<0.001; One-way ANOVA compared to wt DSS $^{+}$p<0.05, $^{++}$p<0.01, $^{+++}$p<0.001)

Considering DCs subsets a reduced occurrence of CD103$^+$ CD11b$^-$ DCs was observed in MD3-OE mice during DSS induced-colitis (MD3-OE 41.70 ± 2.79%, MD3-OE DSS 30.40 ± 2.37%; Figure 25 C). Occurrence of CD103$^-$ CD11b$^+$ DCs was lower in Ocln-OE DSS mice compared to Ocln-OE mice (31.10 ± 0.60% and 37.60 ± 1.81%, respectively; Figure 25 A). CD11b$^+$ CD103$^+$ DCs were more abundant in Ocln-OE DSS mice compared to wt DSS mice (15.70 ± 1.11% and 11.5 ± 0.67%, respectively; Figure 25 B). More DCs were CD11b$^-$ CD103$^-$ in DSS-induced colitis than in control conditions. Furthermore, in Tric-OE DSS mice the occurrence was higher than in wt DSS mice (32.60 ± 2.07% and 26.10 ± 1.42%, respectively; Figure 25 D).

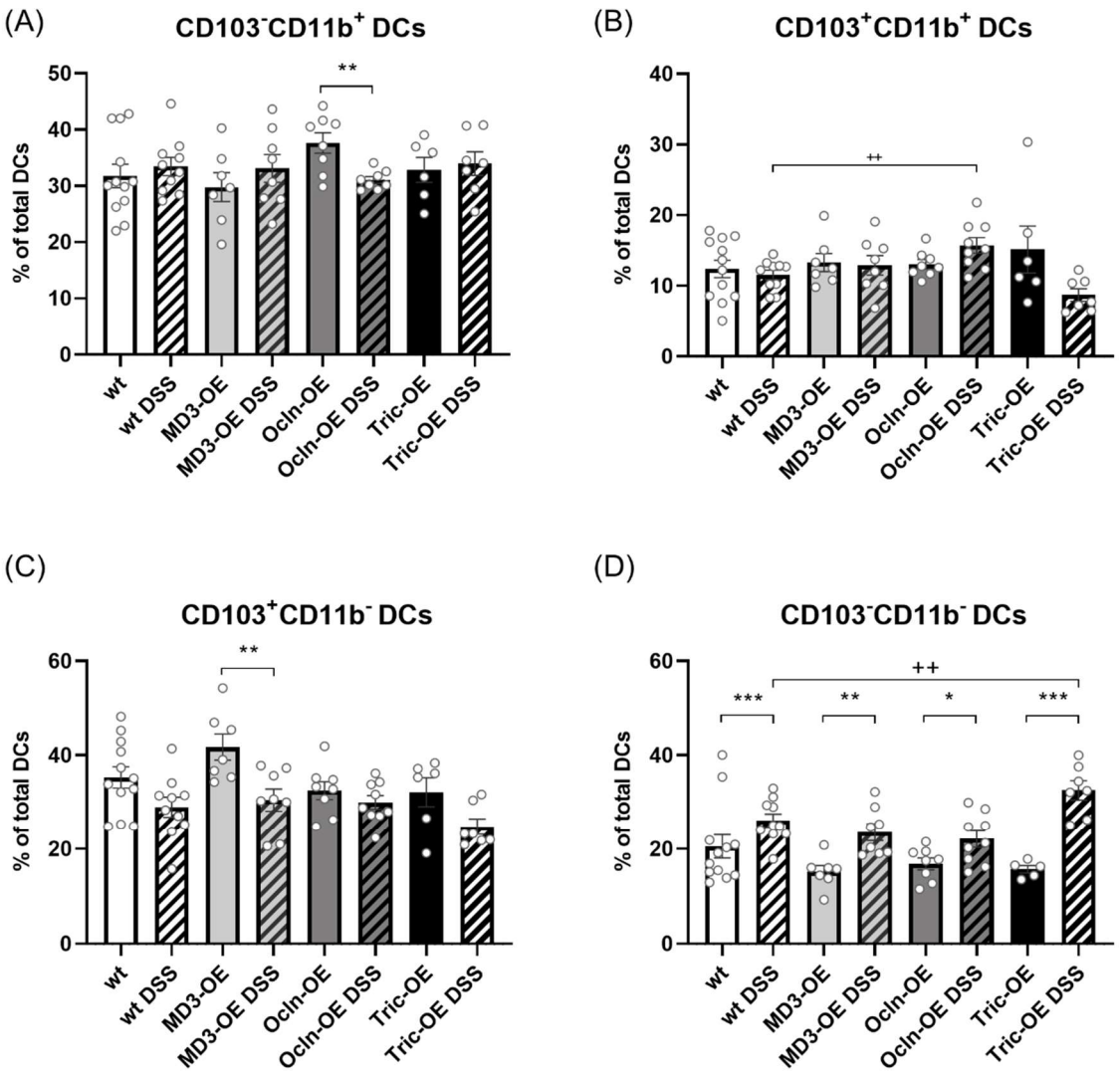

Figure 25 Occurrence of DCs subsets (LP fraction)

At day 6 of DSS treatment, colon tissue of wt and TAMP-OE mice was digested first with EDTA and then with Collagenase, Dispase and DNase to isolate immune cells from the lamina propria (LP). This LP fraction was stained for the myeloid panel, acquired by LSR Fortessa 20x device and analysed with FlowJo software as illustrated in Figure 19. **(A)** Occurrence of $CD103^{-}CD11b^{+}$ DCs was significantly decreased during DSS-induced colitis in Ocln-OE mice. **(B)** Occurrence of $CD103^{+}$ $CD11b^{+}$ DCs was higher in Ocln-OE DSS mice than wt DSS mice. **(C)** Occurrence of $CD103^{+}$ $CD11b^{-}$ DCs was significantly decreased during DSS-induced colitis in MD3-OE mice. **(D)** $CD11b^{-}$ $CD103^{-}$ DCs were increased during DSS-induced colitis and were higher in Tric-OE DSS mice than in wt DSS mice. ($n \geq 6$; data shown as mean ± SEM; outliers were identified by Grubb's test α= 0.01 and removed; student's T-test *p<0.05, **p<0.01, ***p<0.001; One-way ANOVA compared to wt $^{\#}$p<0.05, $^{\#\#}$p<0.01, $^{\#\#\#}$p<0.001; One-way ANOVA compared to wt DSS $^{+}$p<0.05, $^{++}$p<0.01, $^{+++}$p<0.001)

5.2 Gastrointestinal organoids and organoid-derived monolayers

The second main project of this thesis was the establishment and validation of intestinal organoids and organoid derived monolayers (ODMs). Human duodenal ODMs were compared to tissue samples and Caco-2 cells regarding their barrier properties. Furthermore, ODMs were used to compare TJ properties from healthy donors and UC patients.

5.2.1 Crypt isolation

Although UC manifests in the colon, mouse small intestines were used for establishing the organoid culture in the lab, because of two reasons. Duodenum organoids were known to be easier to culture in general, and mouse samples were more accessible than human samples, making them favoured for establishing and harmonising routine procedures. The first step to generate organoids was the isolation of the ASCs located in the crypts of the intestinal epithelium. For crypt isolation different methods are published. Here, the two isolation methods from Bartfeld et al. (Bartfeld and Clevers, 2015) A) and Holthaus et al. (Holthaus et al., 2020) (B) were compared. In both methods the essential step is the EDTA digestion of the tissue. While in method A the crypts are pressed out of the tissue, in B crypts are isolated by washes after EDTA digestion. Comparison of those two methods showed that pressing led to the release of whole crypts and single cells. In contrast using washes for crypt isolation the ratio of whole crypts was reduced and mainly single cells were isolated (Figure 26). Therefore, more organoids could be detected one day after isolation with method A than with B (Figure 26). Additionally, isolation of crypts was faster using method A, thus method A was used for further crypt isolation from mouse and human intestines.

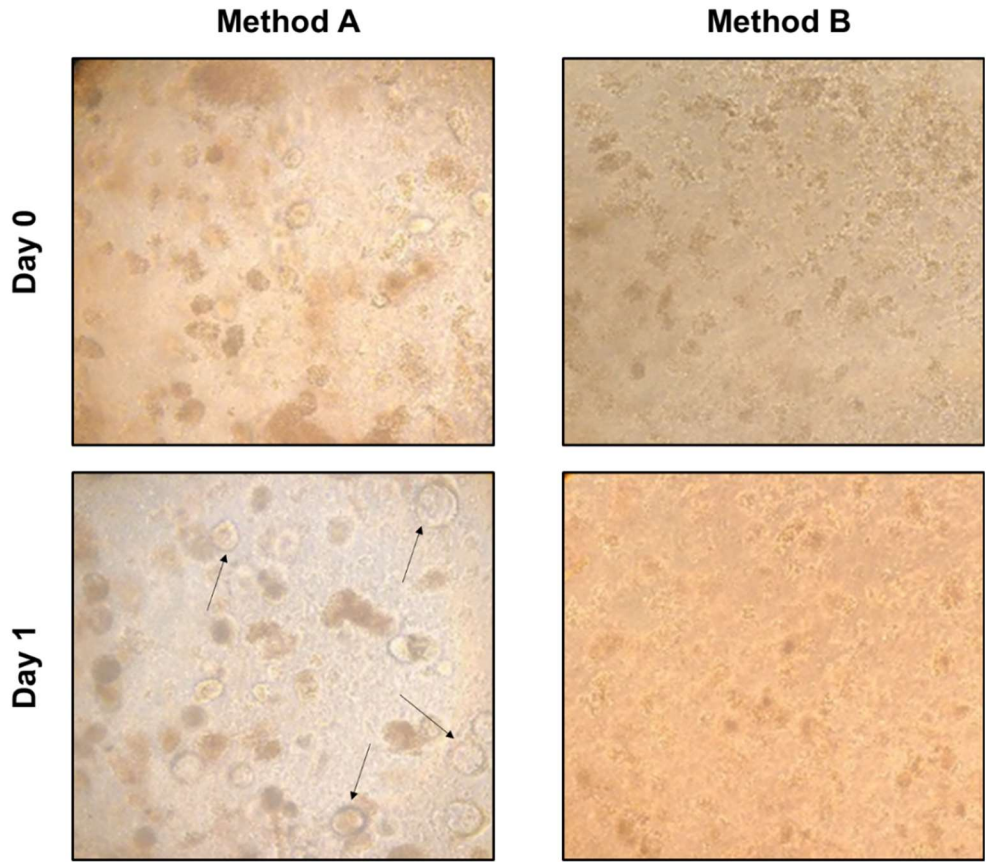

Figure 26 Comparison of methods to isolate intestinal crypts

Representative images of fresh isolated crypts (Day0) and formed organoids (Day1) using different isolation methods. Intestinal organoids can be generated from adult stem cells, which are located in the intestinal crypts. Here two methods to isolate intestinal crypts were compared. In both methods EDTA was used to digest the epithelial layer to release intestinal cells, whereas in method A crypts were released from the tissue by physical pressure, in method B crypts were released during several washes. Method A led to the release of whole crypts and single cells, while with method B mainly single cells were isolated. With method A organoids already formed one day after crypt isolation (Day1) this was not the case using method B. Some organoids are highlighted by the black arrows. (Images were taken through a 10x objective)

5.2.2 Organoid medium composition

As they may have an influence, the optimal medium conditions need to be identified for the specific research purpose. This work aimed for the ODM model to investigate TJ in the context of UC. For this, 3D organoids have been used as source of epithelial cells to seed ODMs. Thus, it is beneficial to have a more stem cell like, less differentiated 3D organoid culture, which can be easily expanded to gain enough cells for ODM seeding. Therefore, the medium composition was changed from medium containing R-spondin, noggin and EGF (RN-E) to medium containing 50% conditioned medium (CM) of L-WRN cells which secret WNT, Noggin and R-spondin plus additional R-spondin, Noggin and EGF (WRN-RN-E). Using this medium

on mouse duodenum organoids, changes in morphology were observed from small budding organoids to luminal organoids (Figure 27 A). Indicating less differentiation with the WRN-RN-E. Using qPCR, differentiation statuses of the organoids were compared by checking for specific epithelial cell markers. These results showed that organoids with RN-E medium were more differentiated than organoids with WRN-RN-E due to lower expression of the stem cell marker *Lgr5* and higher expression of markers for differentiated cells including Lysozyme *(Lyz*) for PCs, Mucin2 (*Muc2*) for GCs and chromogranin A (*Chga*) for EECs (Figure 27 B).

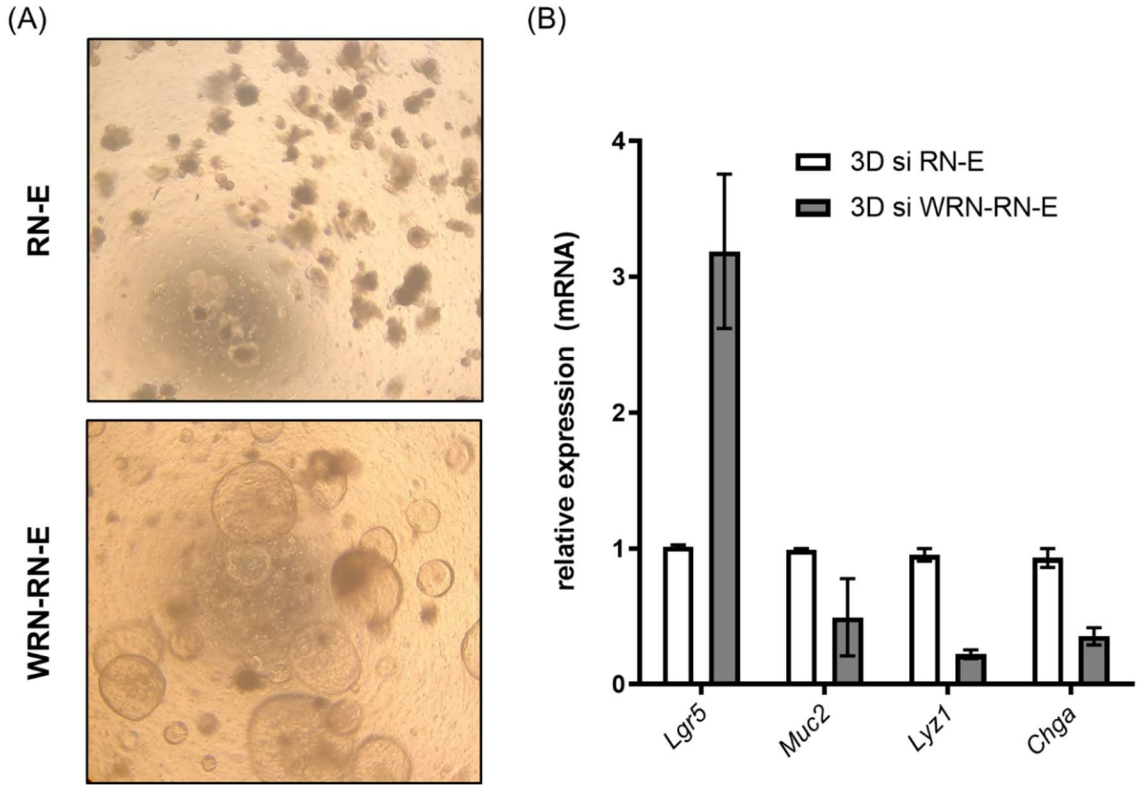

Figure 27 Organoid morphology and expression depends on medium composition

(A) Representative images of intestinal mouse organoids either cultured with RN-E medium or WRN-RN-E medium. While organoids with RN-E medium show a budding phenotype, organoids with WRN-RN-E medium have a luminal phenotype. **(B)** Transcriptional analysis revealed that the expression for the stem cell marker *Lgr5* was increased in organoids cultured with WRN-RN-E medium compared to RN-E conditions, consequently markers for goblet cells (*Muc2*), Paneth cells (*Lyz*) and enteroendocrine cells (*Chga*) were reduced, although it was not significant for *Muc2*. (*n* = 3; data shown as mean ± SEM; student's T-test *p<0.05, **p<0.01, ***p<0.001; images were taken through a 10x objective; Abbreviations W= Wnt; R= R-spondin, N= noggin; E= EGF= epithelial growth factor)

5.2.3 Establishment and validation of Human duodenal organoid-derived monolayers

Organoids have the drawback that typical electrophysiological investigations cannot be applied as in cell cultures or tissue preparations due to the closed 3D structure and the hindered

access to the apical side, which faces the lumen. In cooperation with the group of Prof Aebischer/Klotz at the RKI human duodenal ODMs were established and validated. ODMs maintain the beneficial properties of organoids and give access to the apical side and electrophysiological applications. Human duodenal organoids were cultured using WRN-RN-E with additional nicotinamide (Nic), TGF-β inhibitor (A83-01; A) and p38 inhibitor (SB 202190; SB) (WRN-RN-ENicASB) medium to promote growth and inhibit differentiation. Organoids were digested to single cells using TryplE and 0.5×10^5 cells seeded per BME/Matrigel coated PCF filter (0.6 cm^2, pore size 0.4 µm). In contrast to the 3D organoid culture ODMs should contain more differentiated cells to mimic the real tissue better.

Therefore, different published media were tested considering stable TER values and comparing transcriptional data of ODMs. The medium consistent of R-spondin, Noggin, EGF and Nic (RN-ENic) resulted in consistent TER values after 10 days and differentiation markers like *MUC2*, *LYZ* and fatty acid-binding protein 2 (*FABP2*) could be detected (Weiss et al., 2022b) and hence was used for ODM culture.

IF staining's of ODMs displayed the expression of typical duodenal CLDNs, including CLDN1, CLDN2, CLDN3, CLDN4, CLDN7 and CLDN15, and TAMPs, including OCLN and TRIC, as well as the tTJ protein angulin-1 (Figure 28). Staining's confirmed the apical membrane expression of TJ proteins and the specific localisation of Tric at tTJ.

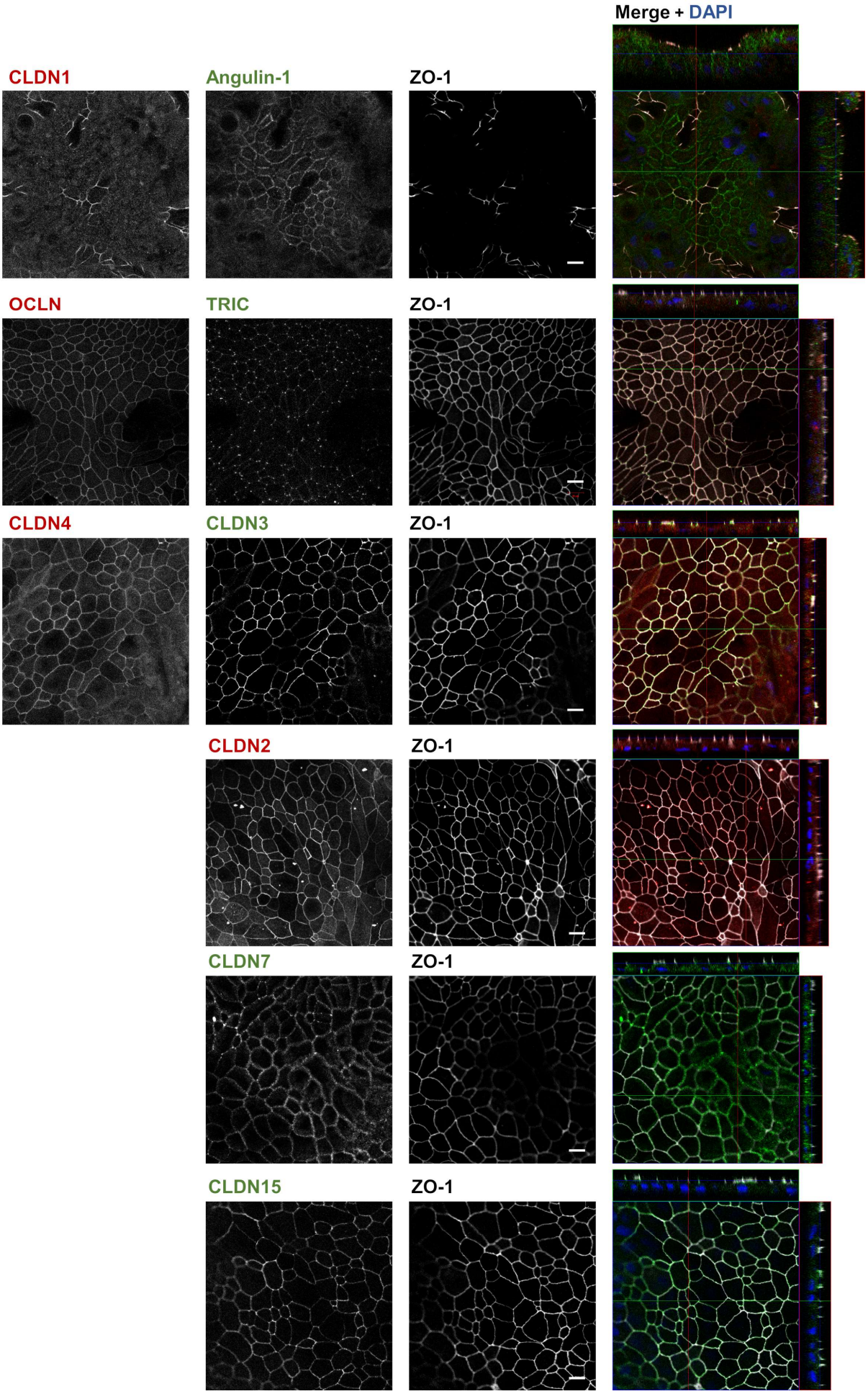
Merge + DAPI
CLDN1
Angulin-1
ZO-1
OCLN
TRIC
ZO-1
CLDN4
CLDN3
ZO-1
CLDN2
ZO-1
CLDN7
ZO-1
CLDN15
ZO-1

Figure 28 Expression and localization of TJ proteins in human duodenal ODMs

Representative immunofluorescence images of 10-day-old duodenal ODMs under RN-ENic conditions. Single panels are shown in white and signal intensities were increased for better visibility. In merge images, the counterstaining ZO-1 (white), nuclei (blue), and the detected TJ proteins (green or red) are shown. The comprehensive TJ protein expression as well as the right localisation indicates continuously expressed TJ barrier and proper polarisation of ODMs. (Bar = 10 µm, modified from (Weiss et al., 2022b))

5.2.4 ODMs TJ expression profile is more similar to human duodenal tissue compared to Caco-2 cells

Using western blot analysis, the TJ protein expression profile of ODMs and Caco-2 cells were compared to tissue samples (Figure 29). Protein was extracted from either 10-days-old ODMs, 21-day-old Caco-2 or tissue samples. Because tissue sample consist of epithelial and subepithelial tissue the epithelial cell marker cytokeratin 19 (CK19) was used for normalisation. Thereby the subepithelial protein fraction could be excluded and only the epithelial proteins were compared. Correspondingly different amounts of protein were loaded to uniform the quantity of epithelial protein. CLDN7 (22 kDa) was expressed lower in all three organoid lines and Caco-2 cells compared to tissue. Whereas Caco-2 cells expressed a similar amount of CLND4 (22 kDa), all three organoids had a lower expression than the tissue. The organoid line CBF1 and CBF5 expressed CLDN3 (22 kDa) similarly, while CBF3 and Caco-2 cells had a lower expression than the tissue. Expression of CLDN1 (22 kDa) was not significantly different between Caco-2 ODMs and tissue. However the expression of CLDN2 (22-23 kDa), OCLN (65 kDa), TRIC (65 kDa) and angulin-1 (splice variants α 68 kDa and β 56 kDa (Yen et al., 1999)) was similar between tissue and all three organoids, while the expression off these TJ-proteins was increased in Caco-2 cells. Together these results showed that the expression profiles of ODMs were more like tissue than the profile of the Caco-2 cells. Beneficially, ODMs showed donor-specific TJ protein expression. The highest protein expression was observed in CBF1 and the lowest in CBF3.

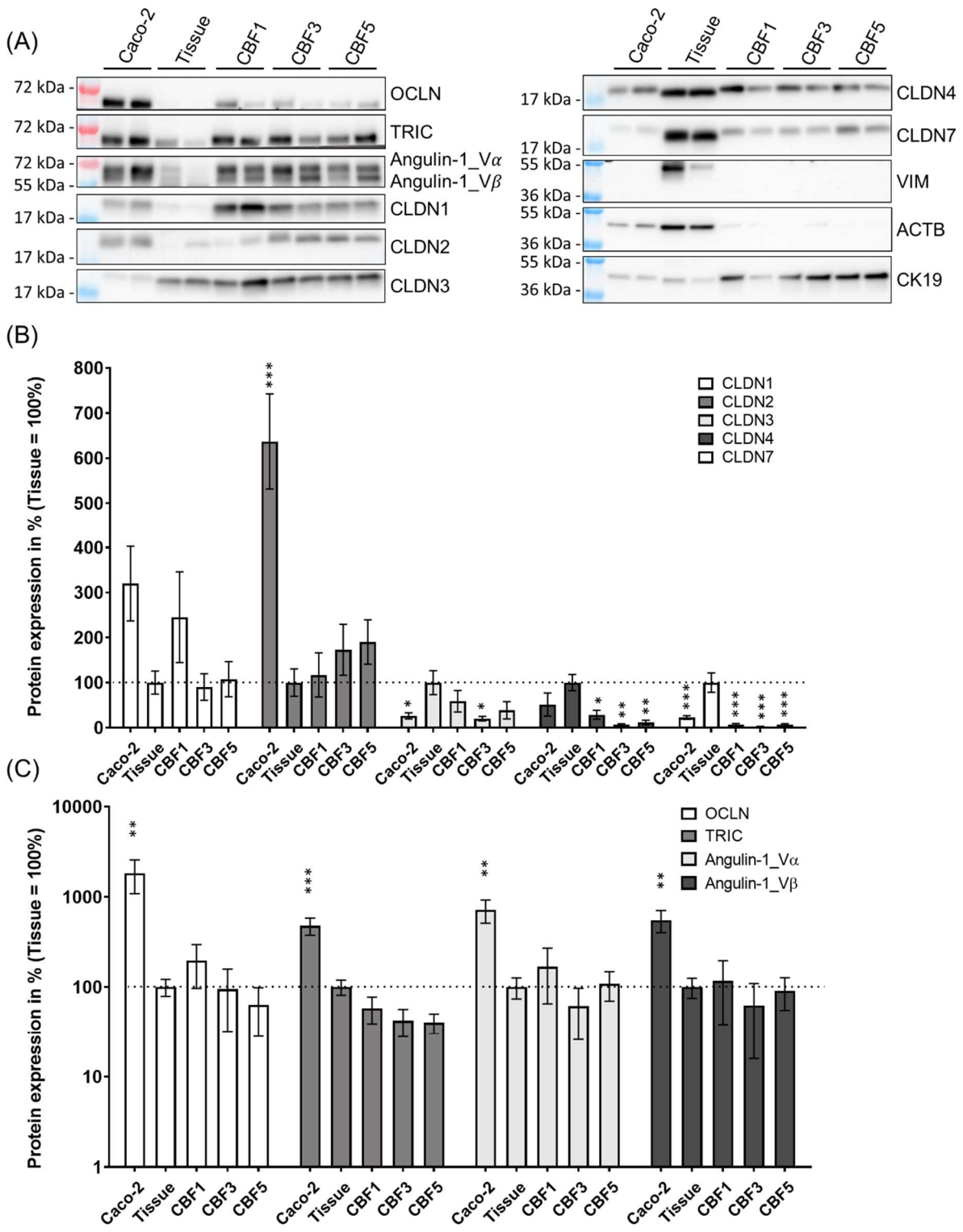

Figure 29 Comparison of TJ protein expression between duodenum tissue, ODMs and Caco-2 cells

Proteins were isolated from 10-day-old ODMs and 21-day-old Caco-2 cells. **(A)** Representative western blots of several TJ proteins, including OCLN, TRIC, Angulin-1 variant α and variant β, CLDN1, CLDN2, CLDN3, CLDN4, CLDN5, CLDN7 and the housekeeping protein ACTB, the mesenchymal marker VIM,

and the epithelial cell marker CK19. **(B)** and **(C)** Quantification of TJ proteins. CK19 was used as housekeeping gene because tissue samples did not only consist of epithelial cells but also surrounding tissue cells, which is highlighted by the expression of VIM. For quantification, densitometric intensities were normalised to CK19 an tissue mean set to 100% ($n > 4$; data shown as mean ± SEM; one-way ANOVA *p<0.05, **p<0.01, ***p<0.001; modified from (Weiss et al., 2022b))

5.2.5 Solute carrier transporter expression of ODMs is similar to the *in vivo* situation

The expression of solute carrier (SLC) transporter genes was compared between Caco-2, organoids, ODMs, and duodenal tissue samples using data available in the literature and transcriptomic data of our collaborators from the RKI (Holthaus et al., 2021) (Figure 30). 218 SLCs were expressed by all duodenal tissue samples, wherein ODMs and organoids expressed 191-214 and 188-205 of those, respectively. In one data set Caco-2 cells expressed 208-218 SLCs and therefore had a similar expression to tissue samples. However, other data could only detect the expression of 152 SLCs in Caco-2 cells (Figure 30 A). Some SLCs were not expressed in all tissue samples analysed, but were detected, for example, in three out of five tissue samples. Therefore, these SLCs were depicted separately and denoted as differentially expressed SLCs (Figure 30 B). Additional 121-126 SLCs were found to be differentially expressed in the RNAseq Data. ODMs and organoids expressed another 101-125 and 101-112 SLCs, respectively. While Caco-2 cells expressed only 71-115 of those differentially expressed SLCs. DNA microarray data detected 27 additional SLCs in Caco-2 cells, but only 20 and 21 in duodenum tissue and ODMs, respectively. Altogether these data indicated that ODMs reflect the expression of SLCs in the duodenal tissue well. Albeit a big variance within Caco-2 and ODMs pointed out that cultivation conditions may impact the expression of SLCs.

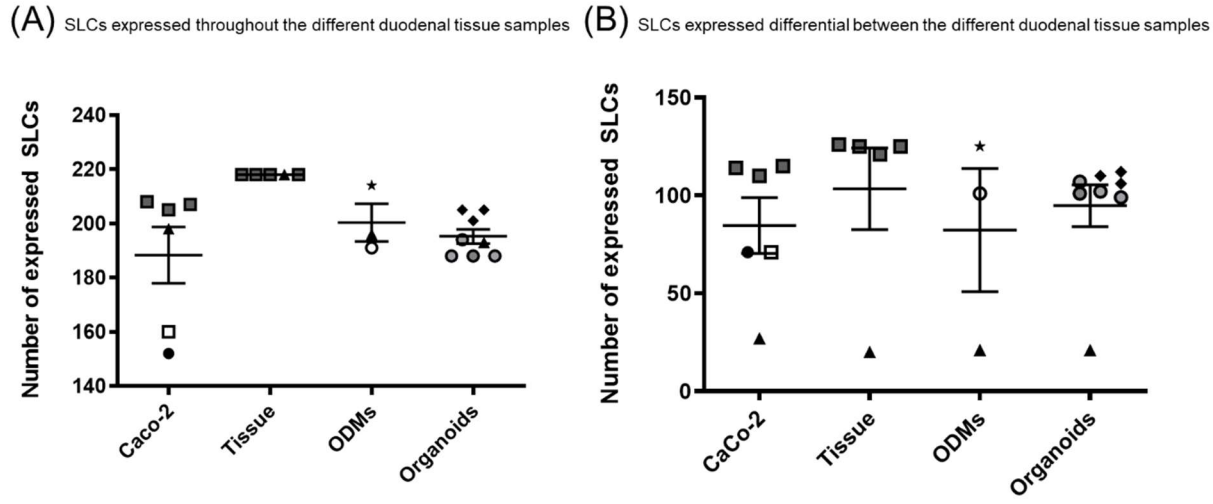

Figure 30 Comparison of transcriptomic data for SLC transporters in Caco-2 cells, duodenal tissue, organoids, and ODMs based on sequencing data in the literature

Comparison of SLC expression indicated that ODMs and organoids reflect the in vivo situation better than Caco-2 cells. **(A)** ODMs expressed 191-214 (*n* = 3) SLCs, organoids 188-205 (*n* = 8) SLCs and Caco-2 cells (*n* = 8) 152-208 SLCs of the 218 SLCs (*n* = 5), that were expressed by all tissue samples. **(B)** Differentially expressed SLCs within duodenal tissue samples (20-116; *n* = 5, ODMs (21-125; *n* = 3), organoids (21-112; *n* = 8) and Caco-2 (27-115; *n* = 6). Each symbol presents one dataset: grey square ■ = GSE156453 (Takayama et al., 2021), white square □ = Ma'ayeh et al. (Ma'ayeh et al., 2018); black circle ● = GSE164334 (He et al., 2021), black triangle ▲ = GSE160695 (Yamashita et al., 2021), white circle ○ = GSE163706 (Sugimoto et al., 2021), black square ◆ = GSE127938 (Kayisoglu et al., 2021), grey circle ● = GSE167286 (Gu et al., 2022), black star ★ = (Holthaus et al., 2021) (Values are shown as mean ± SEM) (Weiss et al., 2022b).

5.2.6 Comparison of TJ expression between healthy donor and UC patient-derived ODMs

Finally, colon ODMs of control (ctrl) donors and UC patients were established. In general, the protocol is similar to human duodenum ODMs. One difference is that during 3D expansion insulin-like growth factor 1(IGF-1) and fibroblast growth factor 2 (FGF-2) were added to the media while SB was left out (WRN-RN-ENicAIF), this composition was found to improve organoid growth (Fujii et al., 2018), which was especially important for the UC derived organoids. To maintain comparability also organoids derived from healthy controls were cultured with this medium. Another change was that ODMs were cultured for the first 48 h in the presence of Wnt (WRN-RN-ENic), before it was exchanged to RN-ENic, which is used for duodenal ODMs. To validate and compare colon ODMs derived from ctrl donors and UC patients TER values were measured and TJ protein expression and localisation determined by western blotting and immunofluorescence staining.

TER values of ODMs derived from control donor 1 (C1) were higher than those derived from ctrl donor 2 (C2). Moreover, TER values were much lower in ODMs derived from UC patients (UC1, UC2 and UC3) than controls (Figure 31 A). Although TER values between the three different UC patients were quite similar UC3 had the lowest TER values (Figure 31 B).

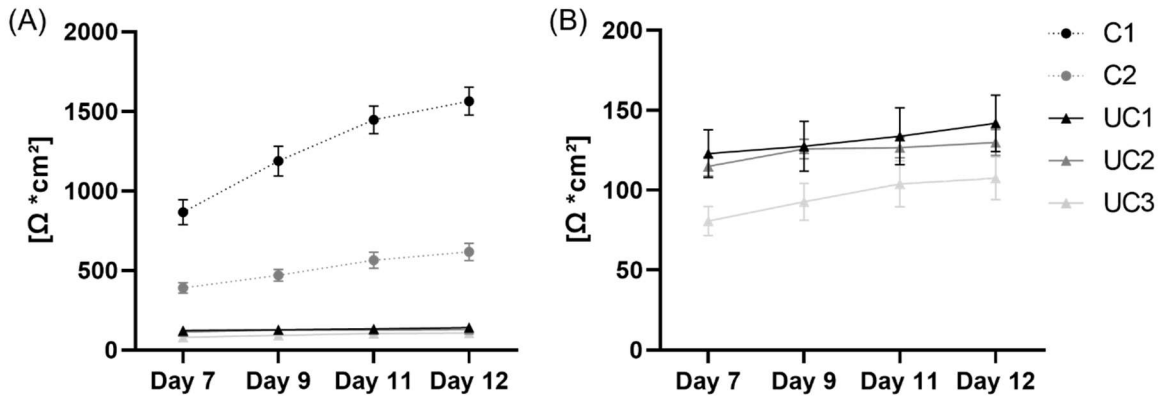

Figure 31 TER data comparing ODMs derived from ctrl donors or UC patients

TER values of ODMs from day 7 to day 12 after seeding. (A) TER values of ctrl donor and UC patients derived ODMs. (B) TER values of only the UC patient derived ODMs. TER values were much lower in UC derived ODMs than ctrl derived ODMs. (n > 15; data shown as mean ± SEM)

Immunofluorescence staining's revealed the expression of CLDN1, CLDN3 and CLDN4 and the three TAMP proteins MD3, OCLN and TRIC as well as the tTJ protein angulin-1 in ODMs derived from ctrl donors and UC patients, in Figure 32 representative IF stainings from C1 and UC2 are shown. Like in duodenal ODMs in colon ODMs the TJ proteins were located apically within the cell membranes and TRIC was expressed at tricellular corners specifically. No changes between ctrl and UC derived ODMs could be determined by immunofluorescence staining.

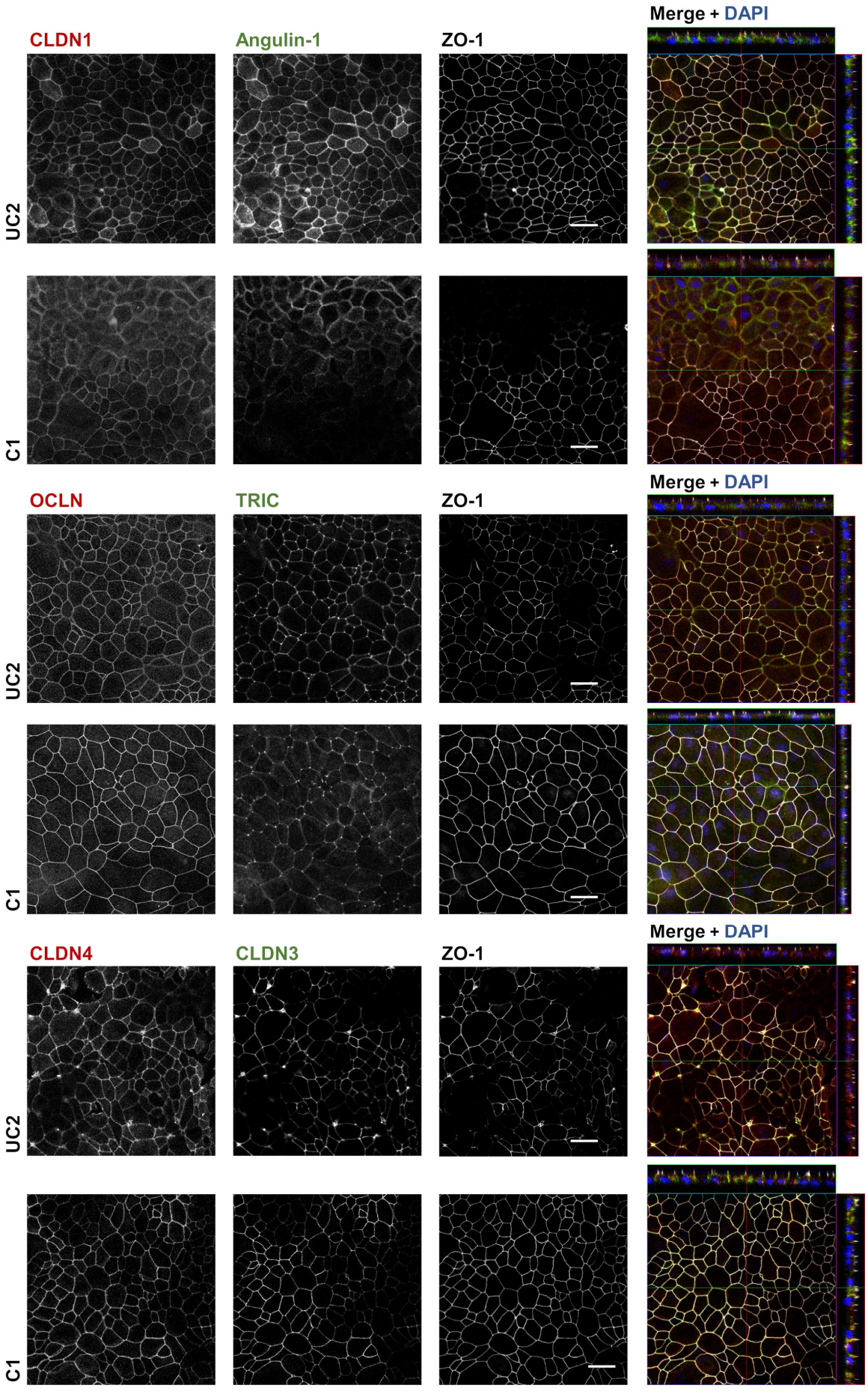
CLDN1
Angulin-1
ZO-1
Merge + DAPI
UC2
C1
OCLN
TRIC
ZO-1
Merge + DAPI
UC2
C1
CLDN4
CLDN3
ZO-1
Merge + DAPI
UC2
C1

Figure 32 Expression and localisation of TJ proteins in colon ODMs derived from ctrl donors and UC patients

Representative immunofluorescence images of 12-day-old colon ODMs derived from ctrl donor and UC patients under RN-ENic conditions. Single panels are shown in white and signal intensities were increased for better visibility. In merge images, the counterstaining ZO-1 (white), nuclei (blue), and the detected TJ proteins (green or red) are shown. In ctrl and UC patients derived ODMs comprehensive TJ protein expression as well as the right localisation indicates continuously expressed TJ barrier and proper polarization of ODMs. No differences between ctrl and UC patients derived ODMs could be elucidated by immunofluorescence imaging. (Bar = 20 µm)

To compare TJ protein expression between ctrl and UC derived ODMs protein of 12-day-old ODMs was isolated and analysed using western blotting (Figure 33). Protein concentration was normalised to β-actin (ACTB) or α-tubulin (TUBA) and values of C1 set as 100%. Although expression was rather uniform between all donors (ctrl and UC), CLDN3 expression was higher in C2 than C1 and ODMs derived from UC3 had a significant higher expression of CLDN2 and anglulin-1 than C1.

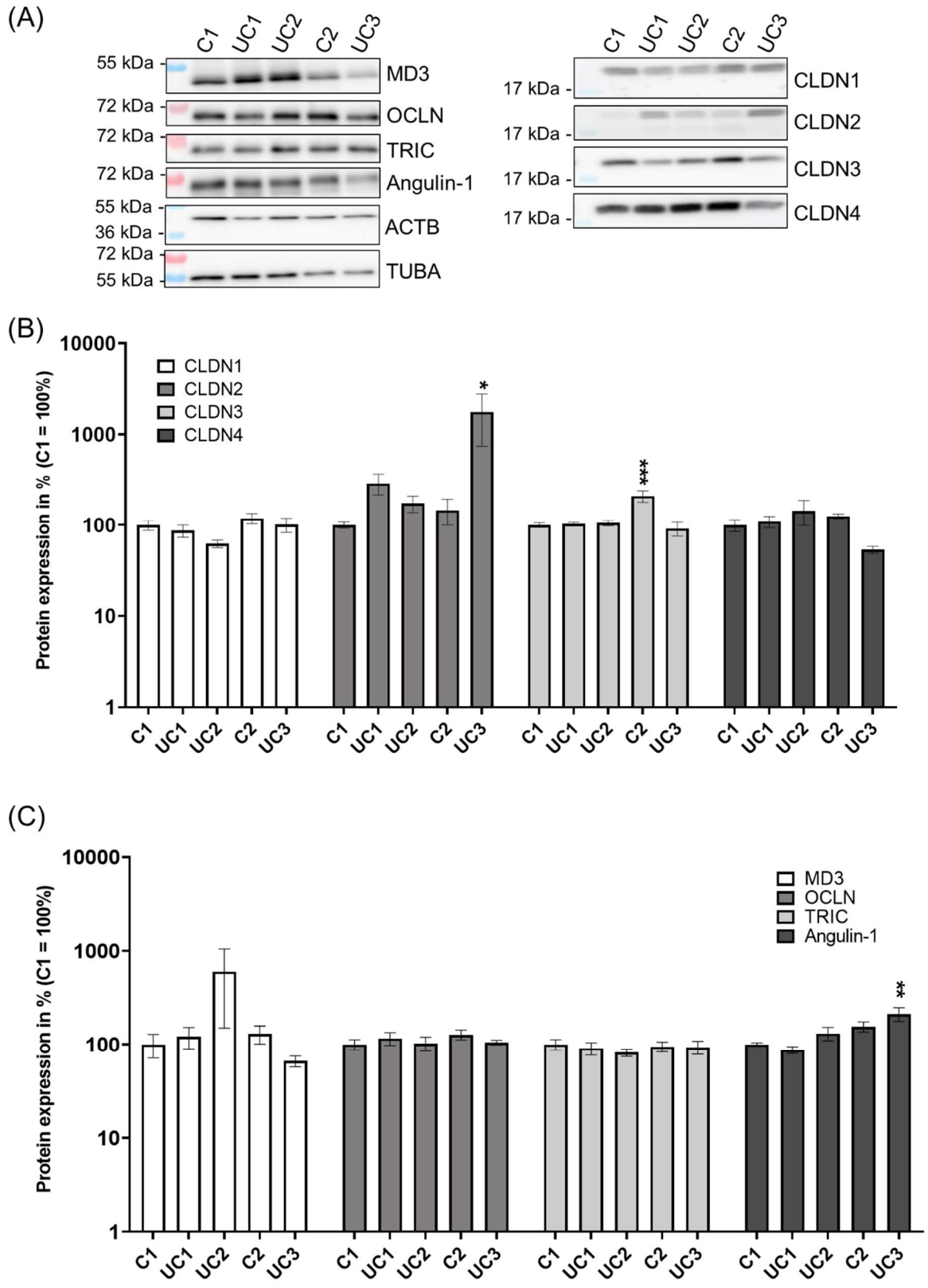

Figure 33 Comparison of TJ protein expression between ODMs derived from ctrl donors or UC patients

Proteins were isolated from 12-day-old ODMs derived from ctrl donors and UC patients. **(A)** Representative western blots of several TJ proteins, including MD3, OCLN, TRIC, Angulin-1, CLDN1,

CLDN2, CLDN3, CLDN4, and the housekeeping proteins ACTB and TUBA **(B)** and **(C)** Quantification of TJ proteins. For quantification, densitometric intensities were normalised to ACTB or TUBA and C1 mean values set to 100% (*n* = 3; data shown as mean ± SEM; one-way ANOVA *p<0.05, **p<0.01, ***p<0.001)

6 Discussion

6.1 TAMP-OE influences subjacent immune cells

6.1.1 TAMP-OE ameliorate DSS-induced colitis by partially stabilising the epithelial barrier

TAMP expression is altered in IBD. While OCLN and TRIC are downregulated in UC patients (Heller et al., 2005, Zeissig et al., 2007, Krug et al., 2018), we found MD3 to be upregulated in UC patients (Weiss et al., 2022a).

In order to clarify whether these changes in TAMP expression are promoting inflammatory processes or counteract inflammation, mice with a specific intestinal epithelial overexpression of the respective TAMPs were generated and acute colitis was induced using DSS.

All three mouse lines suffered less from DSS-induced colitis than wt mice, which was determined by lower DAIs. Detailed barrier function analysis revealed that in Ocln-OE mice as well as in Tric-OE the direct barrier properties were enhanced (unpublished data from S.M. Krug).

Functional analysis of the MD3-OE mice revealed that the typically occurring DSS-induced decrease of TER was ameliorated by MD3-OE (Weiss et al., 2022a). Using one-path impedance measurements to discriminate between epithelial and subepithelial resistance, it was elucidated that this was due to a drop of epithelial resistance in wt mice but not in MD3-OE mice. However, no changes in permeability for ions, small solutes or macromolecules were detected. Therefore, barrier stabilization effects explain only to a small extent the protective effect of MD3-OE during acute DSS-induced colitis. Thus, other mechanism must be responsible for the observed protective effect.

MD3 expression was upregulated upon IL-13 treatment via the IL13Ra1/STAT3 and -6 pathways. In accordance, MD3 expression was increased in wt mice due to DSS-induced colitis, which is known to also cause elevated levels of IL-13 (Shajib et al., 2013), supporting the finding of increased MD3 expression in UC patients. Expression levels of MD3 were increased in wt mice upon DSS-induced colitis and similar to MD3-OE mice, where expression did not further increase. IL-13 is a typical cytokine of the type 2 immunity that is known to inhibit type 1 and type 17 immune responses (Abbas et al., 1996) and promotes wound repair (Gieseck et al., 2018). MD3 was found to influence cell survival and proliferation (Steed et al.,

2014) and might thereby further support type 2 immune responses. It is of great interest if MD3 upregulation also has an influence on the intestinal immune cells located in the LP and the epithelium.

6.1.2 Cryopreservation changes occurrence of CD11b$^+$ cells

To investigate changes in the subjacent immune cells during DSS-induced colitis due to MD3-OE a tissue cryopreservation method was tested. That might allow collection of tissue and the collective isolation and analysis of immune cells at a later time (Konnikova et al., 2018). Using this method could unify the immune cell isolation and staining process, as more samples could be processed on the same day under the same conditions leading to less variation. However, it needed to be clarified if cryopreservation itself induced changes in the expression of immune cell markers and might affect immune cell types differently. This was observed for PBMC (Kadić et al., 2017; Gómez-Mora et al., 2020), while Konnikova et al. observed retention of immune cells when tissue pieces were frozen and immune cells isolated afterwards, except for granulocytes and mast cells which were reduced after cryopreservation (Konnikova et al., 2018). Results gathered for this work showed a lower yield of viable CD45$^+$ cells from frozen samples than fresh samples (Figure 7). Occurrences of CD4$^+$, CD8$^+$, CD19$^+$, CD11c$^+$ and Ly6G$^+$ cells were similar between fresh and frozen samples, indicating the retention of immune cells during the cryopreservation. Wherein a reduced occurrence of CD11b$^+$ cells was determined (Figure 8). CD11b is a marker expressed on several immune cells and is used to distinguish between subsets for example in case of DCs (Cerovic et al., 2014). Therefore, this method of cryopreservation does not seem suitable for the purpose of this study, as focus was also on DCs. However, it should be mentioned that these experiments were one of the first attempts in this laboratory to isolate LP immune cells and that the yield of viable cells could be increased by improved handling. Furthermore, this method might be considered in the case of interferences for example by a broken flow cytometer.

6.1.3 MD3-OE does not alter T_H subsets

MD3 was found to affect cell proliferation and survival and might be the TAMP that can influence surrounding cells the most (Steed et al., 2014). Therefore, a preliminary experiment was performed comparing occurrences of CD4 T_H subsets between wt and MD3-OE mice at steady state. These changes in CD4 T_H subsets could indicate major changes of the microbiota. Because the microbiota is involved in the differentiation and maturation of immune cells and thereby could influence occurrences of T_H subsets (Ivanov et al., 2009; Atarashi et al., 2011; Atarashi et al., 2013; Atarashi et al., 2015). Furthermore, T_H subsets are specialised on different kinds of microbes. While T_H1 cells eliminate intracellular pathogens, T_H17 cells

fight extracellular microbes (Abbas et al., 1996; Zhou et al., 2007). Therefore, a shift towards intracellular microbes in the microbiota might increase occurrence of T_H1 cells, for example. However, no changes of $CD4^+$ T_H -cell subsets were observed between wt and MD3-OE mice, suggesting that MD3-OE has no effect on CD4 T_H cell differentiation (Figure 9). Not even through indirect effects, such as an altered composition of the gut microbiota. T_H subsets were distinguished upon cell stimulation by their intracellular expression of INF-γ, TNF-α and IL-17-α and the transcription factor Foxp3. T_H1 cells were defined as INF-γ^+ and TNF-$\alpha^{+/-}$ cells. T_H2 as INF-γ^- and TNF-α^+ cells, T_H17 as IL-17α^+ cells and T_{reg} as $FoxP3^+$ cells (Mousset, 2019). This experimental setup could be strengthened by adding more subset specific markers to the flow cytometry panel like the transcription factor T-bet for T_H1 cells and GATA3 and the cytokines IL-4 and IL-13 for T_H2 cells (Mousset, 2019). However, more markers were not included due to the limitation of the flow cytometer (BD FACS Canto II) that can detect only up to 8 colours simultaneously. Nevertheless, these results do not indicate major changes in the composition of the microbiota as there are no changes in T_H cell subsets. However, a detailed characterisation of the microbiota by 16S rRNA sequencing would be beneficial to elaborate the influence of MD3-OE as well as Ocln-OE and Tric-OE.

6.1.4 Influence of TAMP-OE on subjacent immune cells during DSS-induced colitis

To elucidate if TAMP-OE have not only barrier stabilising effects but also indirect protective effects, TAMP-OE mice were subjected to DSS-induced colitis. Colon mRNA levels of cytokines as well as the subjacent immune cell composition was analysed. The first mRNA data clearly showed an increase of all analysed cytokines due to DSS-induced colitis like other studies (Arimura et al., 2017; Alex et al., 2009; Neudecker et al., 2017) (Figure 10).

DAIs of the respective animals indicated that in MD3-OE and Tric-OE mice symptoms were less severe at day 5 of DSS exposure, compared to wt mice, whereas at day six DAIs of MD3-OE, Tric-OE and wt mice were similar (Figure 10). In contrast, Ocln-OE mice had a lower DAI compared to wt mice, confirming prior results (unpublished data from S.M. Krug). Especially MD3-OE and Ocln-OE mice had overall higher cytokine expression compared to wt mice (Figure 10).

However, determination of the two cytokines IL-13 and IL-22 was not sufficient. IL-22 is associated with tissue homeostasis and repair; thus it would be interesting to see if there is altered expression in TAMP-OE mice. IL-13 affects the expression of TJ proteins, it increases the expression of Cldn2 and MD3, and downregulates the expression of TRIC (Weiss et al., 2022a; Krug et al., 2018; Rosen et al., 2011). It would be intriguing to find out whether, in turn, TAMP-OE affects IL-13 expression. Due to low sample numbers and large variances no

relation between DAI results and RNA data can be made. The RNA data will be further discussed together with flow cytometry data.

6.1.4.1 Flow cytometry data of control and DSS-treated mice are in line with the literature

Flow cytometry data of the IEL and the myeloid panel showed that the majority of lymphocytes in the epithelium are $CD8^+$-positive, while in the LP more lymphocytes are $CD4^+$, which is in line with the literature (Murphy, 2018a). Most of $TCR\alpha\beta^+$ $CD8\alpha\alpha^+$ cells and $TCR\gamma\delta^+$ $CD8\alpha\alpha^+$ cells are also $CD103^+CD62L^-$ and $CD44^+CD69^+$ (Figure 15 and 18) and therefore can be defined as nIELs (as reviewed in (Cheroutre et al., 2011). As suspected, occurrence of nIELs was very low in the LP fraction, confirming their close localisation to the epithelium (Figure 16). In line with prior findings, $TCR\alpha\beta^+$ $CD8\alpha\alpha^+$ cells were the most abundant IELs, $TCR\gamma\delta^+$ $CD8\alpha\alpha^+$ cells were the second most abundant and were followed by $TCR\alpha\beta^+$ $CD8\alpha\beta^+$ cells and the less abundant $TCR\alpha\beta^+$ $CD4^+$ cells ($TCR\alpha\beta^+$ $CD8\alpha\alpha^+$ < $TCR\gamma\delta^+$ $CD8\alpha\alpha^+$ << $TCR\alpha\beta^+$ $CD8\alpha\beta^+$ reduction < $TCR\alpha\beta^+$ $CD4^+$) (Suzuki, 2009) (Figure 13). Occurrence of $TCR\alpha\beta^+$ $CD8\alpha\beta^+$ cells was lower in the LP fraction than in the epithelial fraction (Figure 16 B and 13 B) and only approximately 40% of $TCR\alpha\beta^+$ $CD8\alpha\beta^+$ cells were $CD103^+CD62L^-$, indicating that those $TCR\alpha\beta^+$ $CD8\alpha\beta^+$ cells more likely depict conventional cytotoxic T_C cells (Figure 17). In the LP fraction, occurrences of $TCR\alpha\beta^+$ $CD4^+$ cells were higher than in the epithelial fraction (Figure 16 A and 13 A), but only approximately 5% were $CD103^+CD62L^-$ and therefore might be conventional T_H cells (Figure 17 A). Indeed, the occurrence of $CD4^+$ cells in the LP fraction identified with the myeloid panel was similar (Figure 23 B). However, only 20% of the $TCR\alpha\beta^+$ $CD4^+$ cells in the epithelial fraction were $CD103^+CD62L^-$ (Figure 14 A). Results of the IEL panel applied on the LP fraction will not be further discussed, because of the (expected) low occurrence of $CD103^+CD62L^-$ IELs.

DSS-induced colitis did not affect $TCR\alpha\beta^+$ $CD4^+$ iIELs, while $TCR\alpha\beta^+$ $CD8\alpha\beta^+$ iIELs, $TCR\alpha\beta^+$ $CD8\alpha\alpha^+$ nIELs and $TCR\gamma\delta^+$ $CD8\alpha\alpha^+$ nIELs tended to have lower occurrences after DSS treatment (epithelial fraction) (Figure 13). This might probably be caused by the increased occurrences of neutrophils and $CD64^+$ as a reaction to DSS treatment in both the epithelial fraction and the LP fraction (Figure 20 and 22). Upon tissue damage and/or invasion of pathogens, neutrophils and monocytes/macrophages are the first cells recruited to the side of damage/infection as part of the innate immune response (Murphy, 2018b). Therefore, the percentage of IELs ($CD8a^+$) of total $CD45^+$ viable cells was reduced upon DSS treatment. Consequently, detected $CD8a^+$ cells applying the myeloid panel showed reduced occurrences during DSS-induced colitis (Figure 21 and 23). In accordance with the literature the most abundant DC subsets in colon LP was the $CD103^+$ $CD11b^-$ DC subset and the lowest

abundance was observed for the CD103$^+$ CD11$^+$ DC subset (Denning et al., 2011) (Figure 25). Matching expectations, occurrences for monocytes and maturing monocytes increased during DSS-induced colitis and therefore a reduced occurrence of macrophages was observed (Figure 24). Taken together, these results are in agreement with the literature and thus confirmed the experimental and analytical design of this experiment.

6.1.4.2 IEL and DCs subsets are differently affected by Ocln-OE and Tric-OE

During DSS-induced colitis TCRαβ$^+$ CD8αβ$^+$ iIELs were reduced in wt mice but not in TAMP-OE mice (Figure 13 B). While occurrences were similar between wt and TAMP-OE mice upon DSS treatment, wt mice had a higher occurrence under control conditions, though not significant (Figure 13 B). iIELs are present in low numbers at birth, which increases during life as conventional T-cells migrate to the intestine upon exposure to exogenous antigens (Manzano et al., 2002; Steege et al., 1997). Therefore, a lower occurrence in TAMP-OE mice might indicate that less T-cells were exposed to exogenous antigens during their lifetime for example due to a more stable epithelial barrier. In contrast, occurrences of nIELs at steady state were similar or higher in TAMP-OE mice compared to wt mice (Figure 13 C and D). In particular MD3-OE mice had a higher occurrence of TCRγδ$^+$ CD8αα$^+$ nIELs than in wt mice, whereas TCRαβ$^+$ CD8αα$^+$ nIELs were enriched in Tric-OE mice indicating that the two TAMPs influence IELs via distinct mechanisms. CD8αα$^+$ nIELs were found to have protective function in colitis, thus they could suppress LP T-cell expansion by the production of IL-10 (Poussier et al., 2002; Hoffmann et al., 2008). Investigations on TCRαβ$^+$ CD8αα$^+$ nIELs are difficult because it is not possible to selectively deplete them. They are thought to be involved in immune cell recruitment by the expression of several cytokines (Hoffmann et al., 2008; Poussier et al., 2002). Depletion of TCRγδ$^+$ CD8αα$^+$ nIELs results in more severe diseases during TNBS and DSS-induced colitis (Tsuchiya et al., 2003; Hoffmann et al., 2001).

Occurrences for nIELs were comparable between TAMP-OE and wt mice upon DSS treatment (Figure 13 C and D). With one exception, Tric-OE DSS mice had a lower occurrence of TCRγδ$^+$ CD8αα$^+$ nIELs than wt DSS mice. Interestingly, occurrences for CD103$^+$CD62L$^-$ TCRαβ$^+$ CD8αβ$^+$ iIELs and CD103$^+$CD62L$^-$ TCRαβ$^+$ CD8αα$^+$ nIELs were lower in Tric-OE DSS mice than wt DSS mice (Figure 14 C and 15 A). Having in mind that approximately 90% of TCRγδ$^+$ CD8αα$^+$ nIELs are CD103$^+$CD62L$^-$ (Figure 15 C), these results show that during DSS-induced colitis CD103$^+$CD62L$^-$ IELs are diminished in Tric-OE mice compared to wt mice. In general occurrences of CD8a$^+$ cells were reduced upon DSS treatment in Tric-OE mice. Strikingly occurrence of CD103$^-$ CD11b$^-$ DCs was significantly higher in Tric-OE mice compared to wt mice during DSS-induced colitis (Figure 25). Function of this double negative DCs subsets is unknown so far and they are thought to derive from PP or ILFs (Cerovic et al., 2013).

Furthermore, occurrence of CD103$^-$ CD11b$^+$ was comparable to wt mice, whereas occurrences of CD103$^+$ CD11b$^-$ DCs and CD103$^+$ CD11b$^+$ DCs tended to be lower in Tric-OE mice upon DSS treatment, though not significant (Figure 25). Together these findings suggest that there are alterations in Tric-OE mice that either influence CD103 expression or affect the recruitment and/or retention of CD103$^+$ immune cells. In contrast to Tric-OE mice, Ocln-OE seems to support CD103$^+$ immune cells/CD103 expression. Occurrences of CD103$^+$ CD62L$^-$ nIELs increased in Ocln-OE mice during DSS-induced colitis (Figure 15 A and C). In addition, occurrence of TCRαβ$^+$ CD8αβ$^+$ CD103$^+$ CD62L$^-$ was higher in Ocln-OE DSS mice than wt DSS mice in the LP fraction (Figure 17 C). Furthermore, DCs subsets were regulated contrary to Tric-OE DSS mice (Figure 25). In Ocln-OE DSS mice, CD103$^-$ CD11b$^+$ DCs were diminished and CD103$^+$ CD11b$^+$ DCs elevated. Thus, CD103$^-$ CD11b$^+$ DCs might have differentiated into CD103$^+$ CD11b$^+$ DCs, this process was explored by Bain et al. 2017 (Bain et al., 2017).

6.1.4.3 Influence of CD103 expression on IELs

CD103 (integrin alpha E) forms a heterodimer with integrin beta 7 (αEβ7). The ligand for αEβ7 is E-cadherin on IECs. This interaction is important for IEL retention (Schön et al., 1999) and potentially DC retention (Siddiqui and Powrie, 2008). The influence of CD103 on IELs mobility is controversial. A reduced and slower mobility was observed for CD103-deficient IELs, which was rather caused by a defective interaction between IELs and IECs than by an intrinsic alteration of IELs (Enderle et al., 2021). Six years earlier, another study investigated the dynamic migration of TCRγδ$^+$ IELs (Edelblum et al., 2015) and in contrast to the findings of Enderle et al. 2021 observed an increased migratory speed of TCRγδ$^+$ IELs in CD103 KO mice and that TCRγδ$^+$ IELs of CD103 KO mice dwell in the epithelium for a shorter time. Loss of CD103/E-cadherin interaction could further promote the protective function of TCRγδ$^+$ IELs by increasing IEL mobility (Edelblum et al., 2015). If this is true for other IEL subsets needs to be clarified. Nevertheless, downregulation of CD103 in Tric-OE mice during DSS-induced colitis might be induced to increase IEL mobility and enhance their protective effect.

Recently a mechanism whereby CD103/E-cadherin ligation (between IELs and IECs) induces extracellular granzyme release and promotes cell shedding, was elucidated. Supporting the role of CD103 in cell shedding, villi in CD103 KO mice were larger than in wt mice (Hu et al., 2022). Thus, downregulation of CD103 in Tric-OE mice, might slow down DSS-induced cell shedding, thereby stabilising the epithelial barrier. However, interaction of CD103 in IELs with E-cadherin can promote Wnt and inhibit Notch signalling in intestinal stem cells (ISC) and TA cells. Thereby leading to an increase of GCs and PCs and a reduction of enterocytes in the small intestine (Chen et al., 2021). Both, GCs and PCs are important for the protection against commensal/pathogenic invasion. It would be interesting to compare the epithelial composition

in TAMP-OE mice and wt mice. Further investigations are required to elucidate which of these CD103 related functions are relevant for the ameliorate effect in TAMP-OE mice.

Edelblum et al. also observed that IEL migration was dependent on Ocln expression by TCRγδ$^+$ IELs and IECs (Edelblum et al., 2012). Wherein Ocln expression of TCRγδ$^+$ IELs played a greater role than the expression of IECs, both were necessary for optimal migration into the lateral intracellular space. This finding led to the assumption that TCRγδ$^+$ IELs are increased in Ocln-OE mice, but this was not the case (Figure 13). Moreover, Ocln expression was important for the effective protection against invading pathogens, which required the migration of TCRγδ$^+$ IELs into the lateral intercellular space (Edelblum et al., 2015). This might be one factor that ameliorates DSS-induced colitis in Ocln-OE mice.

Although IELs are involved in epithelial repair, oral tolerance and immune regulation (Komano et al., 1995; Boismenu and Havran, 1994; Mengel et al., 1995), they are also associated to IBD (Giacomelli et al., 1994; Kanazawa et al., 2001; Yeung et al., 2000). Thus, an antibody against β7, etrolizumab, has been tested in phase III clinical trials (Peyrin-Biroulet et al., 2022; Danese et al., 2022; Vermeire et al., 2022; Rubin et al., 2022). Etrolizumab is designed to inhibit lymphocyte homing to the intestine and to hinder IEL retention and their pro-inflammatory action on IECs. However, only two of five trails met their primary end point and reasons leading to those rather disappointing results need to be clarified.

6.1.4.4 Functions of CD103+ DCs

CD103$^+$ DCs are important for oral tolerance in the small intestine, whereas colonic tolerance can develop independent of CD103$^+$ DCs (Veenbergen et al., 2016). However, the lack of CD103$^+$ DCs negatively influenced T_{reg} activity, thus CD103$^+$ DCs are important immune regulators (Annacker et al., 2005). TGF-βR1 signalling was found to promote differentiation form CD103$^-$ CD11b$^+$ DCS to CD103$^+$ CD11b$^+$ DCs (Bain et al., 2017). Expression of TGF-β when compared to other tested cytokines were rather similar, nevertheless TGF- β expression was lower in Tric-OE DSS mice than wt mice (Figure 10 J). This observation is supported by the smaller occurrence of CD103$^+$ CD11b$^+$ DCs (Figure 25 B). Recent research found that CD103$^+$ CD11b$^+$ DCs have a pro-inflammatory mature like signature when localised in the LP but can colonise the small intestinal epithelium and gain tolerogenic properties (Rivera et al., 2022). Due to low cell number, DCs of the epithelial fraction were not further distinguished, thus it is not clear if CD103$^+$ CD11b$^+$ DCs are more abundant in the epithelium of Ocln-OE mice, too. CD103$^+$ CD11b$^-$ DCs exhibited protective effects in DSS-induced colitis, while CD103$^+$ CD11b$^+$ DCs were insufficient to do so. CD103$^+$ CD11b$^-$ DCs can express IL-12 that in turn induces INF-y secretion in lymphocytes and finally leads to the expression of anti-inflammatory cytokines (indoleamine 2,3 dioxygenase (IDO) and IL-18 -binding-protein) in epithelial cells (Muzaki et al., 2016). In addition, CD103$^+$ DCs themselves can produce IDO.

Inhibition of IDO impaired CD103$^+$ DCs to induce Foxp3 T_{reg} differentiation. IDO inhibition altered balance of T_{reg} and T_H1 and T_H17 effector cells, indicated by lower expression of Foxp3 and higher expression of IL-12 and INF-y (Matteoli et al., 2010). Indeed Ocln-OE DSS mice had the highest expression of IL-12β, which might be due to the increase of CD103$^+$ CD11b$^+$ DCs (Figure 10 E and I and 25 B).

6.1.4.5 Subsets of the monocyte/macrophage lineage are differently affected by Ocln-OE and Tric-OE

Ocln-OE and Tric-OE also influenced the monocyte/macrophage lineage and again exhibited contrasting phenotypes. Whereas in Tric-OE mice occurrences for blood monocytes (ctrl, epithelial fraction, Figure 20 D) and maturing monocytes (DSS, LP fraction, Figure 24 B) were higher compared to wt mice (ctrl and DSS, respectively), in Ocln-OE mice the occurrence of CD4$^+$ resident macrophages was higher compared to wt mice during DSS-induced colitis (Figure 24 F). A tendency for an increased occurrence of resident macrophages was noted as well in Ocln-OE DSS mice.

The higher occurrence of maturing monocytes in Tric-OE DSS mice might be explained by a later recruitment of monocytes due to a more stable macromolecular barrier, as TRIC is important for the regulation of macromolecular passage at tTJ (Krug et al., 2009a). Therefore, monocytes did not mature into macrophages at day 7 of treatment. On the other hand, it was reported that maturation of monocytes was inhibited in inflammation, which might be another reason for the increase in maturing monocytes (Bain et al., 2013). Why this inhibition was more pronounced in Tric-OE mice than in wt mice remains to be elucidated. Considering the DAIs (for all samples analysed via flow cytometry, Figure 11), a later recruitment of monocytes seems plausible, because DAIs of Tric-OE and MD3-OE mice were lower on day 5 of treatment and like those of wt mice on day 6, Ocln-OE exhibited similar DAIs to wt mice (Figure 11). Resident macrophages are closely located to the intestinal epithelial were they sample antigens and secret IL-10 and thereby maintain T_{reg} maintenance. IL-10 was expressed comparable between TAMP-OE and wt mice (Figure 10 D). Resident macrophages express CX3CR1 and CD11b, while CD11b is associated with negative regulation of TLR signalling (Bai et al., 2012; Han et al., 2010), CX3CR1 was found to be important for TED formation (Chieppa et al., 2006; Rescigno et al., 2001; Niess et al., 2005). It was observed that during TED formation the expression of Ocln on CX3CR1$^+$ cells was induced to ensure a stable TJ barrier (Rescigno et al., 2001). This interaction was not further investigated but might contribute to the increased occurrence of resident macrophages in Ocln-OE DSS mice (Figure 24 E and F). Resident macrophages can further be distinguished into three groups by the expression of T-cell membrane protein 4 (TIM-4) and CD4 (Shaw et al., 2018). Tim-4 was not included in the myeloid panel due to limited capacities of the flow cytometry panel. Since CD4

was included to the myeloid panel anyway (original to identify major changes of CD4+ T_H-cells), CD4 expression on resident macrophages was determined. As a matter of fact, occurrence of $CD4^+$ resident macrophages was higher in Ocln-OE mice (Figure 24 F). Since the expression of TIM-4 could not be determined, it was not possible to differentiate between $TIM4^+$ $CD4^+$ and TIM^- $CD4^+$ resident macrophages. Nevertheless, the group of $Tim\text{-}4^+$ $CD4^+$ resident macrophages expressed more CCL-2 but less INF-y and IL-6 compared to $Tim\text{-}4^-$ $CD4^-$ resident macrophages (Shaw et al., 2018). In accordance to this, Ocln-OE DSS mice had a high expression of CCL2 but expression of INF-y and IL-6 was not lower than in wt DSS mice (Figure 10 G and C and I). They found that $TIM\text{-}4^-$ $CD4^+$ resident macrophages are maintained independent of monocytes, and that $TIM\text{-}4^-$ $CD4^+$ had a much slower replenishment rate from monocytes compared to the $TIM\text{-}4^-$ $CD4^-$ population. Together most resident macrophages were found to be $CD4^+$. This could not be confirmed during the present study where a minor population of approximately 10% was $CD4^+$ (Figure 24 F). During DSS-induced colitis the occurrence of $CD4^+$ resident macrophages was even further reduced, maybe to DSS-induced cell death and the replenishment of macrophages maturing from monocytes, which would be according to the findings of Shaw and co-workers (Shaw et al. 2018).

6.1.4.6 Occurrence of $CD19^+$ is altered in MD3-OE mice

CD19 a typical B-cell marker was included in the myeloid panel. It turned out that MD3-OE impacted the occurrence of $CD19^+$ cells. MD3-OE DSS mice had a higher occurrence of $CD19^+$ cells in the LP fraction as well as in the epithelial fraction (Figure 23 D and 21 D). In the LP fraction of MD3-OE mice, a lower occurrence of $CD19^+$ cells was detected than in wt mice (Figure 23 D). B-cells are associated with IgA production and could ameliorate DSS-induced colitis (Wang et al., 2018; Fu et al., 2021; Melcher et al., 2022; Wang et al., 2015). Melcher et al. found that B regulatory cells which can produce IL-10 can protect from chronic DSS-induced colitis and differentiate into IgA producing plasma cells. IgA influences the gut microbiota which protects from colitis-associated colorectal cancer (Melcher et al., 2022). IL-10 was not increased in MD3-OE mice (Figure 10 D). Despite MD3 might also act as a tumour suppressor, as it can inhibit epithelial mesenchymal transition by the suppression of the NF-κB pathway (Li et al., 2021). Wang and Fu observed that $CD11b^+$ B-cells and not IL-10 expressing B-cells can ameliorate DSS-induced colitis. Wang et al. found that $CD11b^+$ B-cells in PPs recruit CXCL9 depended T_{reg} cells, which produce TGF-β and induce IgA switch in B-cells that leads to the protection against DSS-induced colitis (Wang et al., 2018; Wang et al., 2015). Fitting to those results MD3-OE DSS mice had the highest expression of CXCL9 (Figure 10 H).

6.1.4.7 Conclusion and outlook

In summary, TAMP-OE causes alterations in the composition of subjacent immune cells. MD3-OE showed an increase in the occurrence of $CD19^+$ B-cells, Tric-OE appears to depress $CD103^+$ subpopulation of both IELs and the DCs, whereas Ocln-OE supports $CD103^+$ IELs and DCs and additionally facilitates the maintenance of resident, particularly $CD4^+$ resident macrophages. Strikingly these results further support that despite their similarities MD3, Ocln and Tric have distinct functions, similar to observations considering TJ barrier properties (Raleigh et al., 2010). MD3 has influence on cell behaviour and survival (Steed et al., 2014), and thus assumptions that it might regulate neighbouring cells, including immune cells, are not so far-fetched. Ocln as discussed, was already found to interact with IELs and DCs (Edelblum et al., 2012; Rescigno et al., 2001) and TRIC expression was found on cells of the monocyte/macrophage lineage in the LP (Mariano et al., 2011b). This might be the first report that TAMPs could influence occurrences of specific immune cell populations and that these might have caused the protective effect against DSS-induced colitis.

However, it must be mentioned that DAIs tracked during this set of experiments did not differ between wt and TAMP-OE mice and could not confirm the previous results, which is a drawback of this study. Albeit this is not due to altered DAIs of the TAMP-OE mice but a lower DAI of the treated wt mice. Due to breeding difficulties and animal number restrictions, it was not always possible to treat wt and TAMP-OE mice during each experiment and mice number per single experiment was rather low. Naturally, this introduces differences in conditions and influences comparability of the results obtained, including DAIs as well as flow cytometry data. Results of DSS experiments could be further strengthened by increasing sample size number as some immune cell populations exhibited relatively large variances and higher n numbers would precise the definition of outliers. Another limitation was that the number of immune cells from the epithelial fraction was rather low and therefore did not allow an adequate differentiation of $CD64^+$ and DCs subsets. To increase the significance of the cytokine expression data, additional mRNA samples need to be analysed by qPCR. Furthermore, analysis of the microbiota would be beneficial as these might also be influenced by the alterations of TJ protein expression in TAMP-OE mice and might in turn influence the maintenance of specific immune cells. Nevertheless, this study successfully demonstrated that TAMP-OE had effects on immune cells and that these changes could cause the improvement in DSS-induced colitis observed in previous experiments.

However, studies based on these findings need to further clarify the outcomes of the observed changes and the mechanism causing them. Are these changes caused by direct interaction between TAMP and immune cell or does TAMP-OE alter epithelial expression of cytokines and other immune cell stimulators and thereby display those effects? Do these changes cause pro- or anti-inflammatory processes? Single cell RNA sequencing of isolated immune cells but also

epithelial cells could shed light on this and elucidate potential pathways and mechanisms. Further stainings could confirm the here presented results and could indicate locations of immune cells, dependent on TAMP-OE. A more detailed and focused characterisation of the affected immune cells can be performed based on the findings of this study. Identified mechanisms could then be validated using a co-culture of ODMs derived from TAMP-OE mice and the specific immune cells and this could be potentially transferred to UC patient derived ODMs and human immune cells. Therefore, ODMs of duodenum and colon were established during the second aim of the thesis. Finally, these findings might identify new therapeutic targets that could lead to a more stable TJ barrier and a more regulated immune response in IBD patients.

6.2 Gastrointestinal organoids and organoid-derived monolayers

To investigate the intestinal TJ barrier mainly epithelial tissue or cell cultures are used. Although these cell lines quite nicely reflect human intestinal permeability and transport, they are derived from carcinoma or metastases, and encumbered with mutations (Sambuy et al., 2005; Oltra-Noguera et al., 2015). In 2009, Sato et al. was able to generate so called organoids (Sato et al., 2009). Organoids are self-organizing cellular structures that can derive from ASCs and PSCs and can reflect the crucial aspects of the origin tissue (McCracken et al., 2011; Sato et al., 2009). Thus, intestinal organoids possess the different segment-specific cell types of the small or large intestine, giving them greater complexity than commonly used cell lines such as Caco-2 or T84 (Merker et al., 2016). Thus, organoids are physiologically closer to the origin tissue than common cell lines and are more accessible than *in vivo* models as discussed by Bartfeld 2016 (Bartfeld, 2016). Because organoids can be obtained from human tissue samples and animal experiments might not always resemble human diseases best, due to interspecies variations, they are often mentioned in the context of animal welfare like 3R (reduce, reuse, recycle). Indeed, organoids are beneficial for basic and translational research and findings of such studies might make some animal experiments no longer necessary. However, they should rather be seen as a bridge between traditional *in vitro* and *in vivo* models. Nevertheless, animal models are useful to determine the impact of infection, mutation or diseases to a whole organ or organism.

However, organoids are well-appreciated in gastrointestinal epithelial research and were used to solve questions in tissue homeostasis (Beumer and Clevers, 2016), infectious diseases (Schlaermann et al., 2016; Holthaus et al., 2021), cancer development (Seidlitz et al., 2019) as well as IBD (d'Aldebert et al., 2020) and barrier research (Nakamura, 2019).

6.2.1 Organoid generation and culture methods influence organoid growth and phenotype

The first attempt to start organoid culture is the isolation of the ASCs from the given tissue. Here, two published methods were tested to isolate intestinal ASCs (Bartfeld et al., 2015; Holthaus et al., 2020). The main step for both methods was the digestion of the tissue with EDTA, but they differed in the mechanic process leading to ASCs release. In our case pressing out the intestinal crypts led to a higher yield of organoid formation than isolation by vigorous pipetting and several washes (Figure 26). It is likely that isolated cells were more stressed or even dead using method B. Duration of the ASCs isolation process was much longer, when ISCs were released using vigorous pipetting. Furthermore, in our case pressing yielded to more intact crypts, while pipetting led to the dissociation of the crypts. Although Bartfeld et al. stated that disintegration of glands/crypts would not compromise the outcome, it is still reasonable to think that single cells might be more stressed as it is known that epithelial cells undergo anoikis. Anoikis is a programmed cell death that is initiated upon cell detachment from the correct extracellular matrix (Taddei et al., 2012; Grossmann et al., 2003). Therefore, the combination of more singe cells and a longer isolation process might have caused the lower yield of organoid formation.

To maintain organoid growth and self-renewal the specific stem cell niche needs to be mimicked and medium conditions can greatly impact the organoid composition, phenotype, and properties. Starting with small intestinal mouse organoids the medium composition needed is rather trivial and the main factors are R-spondin, Noggin and EGF. External Wnt is not essential for mouse small intestinal organoid survival, because PC within the organoid itself can secret Wnt. Comparing mouse small intestinal organoids growing in RN-E or WRN-RN-E (adding wnt and additional R-spondin and noggin) showed a phenotypic change from budding to cystic organoids and the downregulation of differentiation markers (*Muc2, Lyz1, Chga*) and the upregulation of *Lgr5*, concordant with previous findings (Sato et al., 2011b) (Figure 27). Since the aim of this study was to generate ODMs that derive from dissociated organoid cultures, an organoid culture with more stem cell like and highly proliferative characteristics is advantageous. Thus WRN-RN-E medium was used for organoid expansion.

6.2.2 Duodenal-derived ODMs reflect small intestinal barrier functions better than Caco-2 cells

Organoids have one major drawback for barrier research, because they are cultured in extra cellular matrix and form a closed three dimensional structure with the apical side facing the lumen and thus the access to the apical side is hindered (Sato et al., 2009; Sato et al., 2011a;

Blutt et al., 2018). To make the apical side accessible, different methods were developed including microinjection, inside out organoids (Nash et al., 2021) and the generation of ODMs (Moon et al., 2014; VanDussen et al., 2015; Kozuka et al., 2017). However, the two forms are still not feasible for techniques commonly used in barrier research. ODMs however can be utilised similarly to standard cell lines and allow measurements of TER and tracer fluxes as well as Ussing chamber experiments (Moorefield et al., 2018). In cooperation with the group of Prof Aebischer/Klotz at the RKI human duodenal ODMs were established and validated, by comparison to Caco-2 cells and duodenal tissue (Weiss et al., 2022b).

In contrast to the 3D organoid culture ODMs should differentiate into the different intestinal cell types. Therefore, a medium without WRN-CM was used and resulted in confluent monolayers with stable TER. These are essential properties for barrier investigation. Expression of differentiated epithelial cell markers was confirmed by qPCR analysis (Weiss et al., 2022b) and IF-staining's confirmed the expression and correct localisation of typical duodenal TJ proteins in ODMs (Figure 28). Thus, TRIC was detected specifically at tTJs (Ikenouchi et al., 2005) and angulin-1 staining showed its extension to the lateral membrane at tTJs and bTJs (Masuda et al., 2011). TJ protein expression was quantified using western blotting and revealed that CLDN2, OCLN, TRIC and the two angulin-1 variances were higher expressed in Caco-2 cells than duodenal tissue samples (Figure 29). CLDN7 on the other hand, was higher expressed in tissue samples than in Caco-2 and ODMs. TJ proteins are expressed differently by distinct epithelial cell types, and therefore the TJ protein expression profile can provide information about epithelial cell composition to some extent (Pearce et al., 2018). For instance, Cldn2, Ocln and Tric are expressed more prominently by stem cells and Cldn7 was found to be higher expressed on enterocytes (Pearce et al., 2018). Moreover, besides its function in TJ, Cldn7 also has a role in differentiation and stem cell self-renewal (Xing et al., 2020). Western blot results showed that ODMs have a more similar TJ expression profile to tissue samples than Caco-2 cells and this might further suggest a more similar epithelial cell composition. Although tissue samples have more differentiated enterocytes than ODMs, indicated by a higher expression of CLDN7.
ODMs showed typical duodenal TJ expression and localisation and the ability to grow as a confluent monolayer with stable TER. These properties represent the basic requirements for a functional barrier, but do not yet provide any information about the physiological function.

Hence one-path and two-path impedance spectroscopy was applied to compare the barrier function between Caco-2, ODMs and tissue. One-path impedance can determine the overall resistance of the epithelium R^t (=TER) and the subepithelial resistance (R^{sub}). Whereby the subepithelial resistance depicts the resistance of the filter membrane for Caco-2 cells and the

filter membrane plus the Matrigel coating for ODMs. With the obtained values the epithelial resistance (R^{epi}) can be calculated using $R^{epi}=R^{t}–R^{sub}$. Using the paracellular marker fluorescein and induction of opening of the paracellular cleft by addition of EGTA, two path-impedance spectroscopy can further differentiate the R^{epi} into transcellular resistance R^{trans} and paracellular resistance R^{para} (Krug et al., 2009b).

As expected Caco-2 cells had a lower R^{sub} than duodenal tissue, surprisingly the R^{sub} was comparable to duodenal tissue, which is a beneficial side effect of the Matrigel coating (Figure 34 A). R^{epi} was similar between ODMs and duodenum tissue but higher in Caco-2 cells. Two-path impedance results clarified that high R^{epi} was caused by a higher R^{trans}, as R^{para} was similar between Caco-2 cells and ODMs (Figure 34 B). This indicated that Caco-2 might fail to properly reflect transcellular barrier properties. A higher R^{trans} is to be equated with a lower transcellular ion transport in Caco-2 cells. Thus, the reduced number of expressed SLCs further strengthened these observations (Figure 30). Nevertheless, both models exhibit paracellular barrier properties comparable to duodenal tissue samples.

Additionally, the permeability for the macromolecule FITC-dextran 4kDA (FD4), a typical paracellular marker, was similar in Caco-2, ODMs and tissues (Figure 34 C). Properties of Caco-2 cells were observed to differ between laboratories, and this might include R^{trans} (Sambuy et al., 2005).

Different publications showed different SLC expression within Caco-2 and ODMs and imply that culture conditions impact the transcellular properties but may also affect paracellular properties as changes in differentiation also might influence TJ protein expression. A study that focused on the ability of ODMs to be used as a pharmacological model revealed that ODMs were more similar to adult duodenal tissue than Caco-2 cells considering apical and basolateral transporters (Yamashita et al., 2021). This is confirmed by the findings of the present research that Caco-2 cell can only be used to a limited extent for transcellular research. Although, differences are known in Caco-2 cells between laboratories they have the advantage to be less labour- and cost-intensive than organoids. However, organoids might better reflect the properties not only of the tissue of origin but also of the specific donor. Thus, one or the other model might be more suitable. For example Caco-2 cells turned out not to be a suitable model for *G. duodenalis* infection due to obstacles with co-culture attempts (Nash, 2019), which led to conflicting results (Kraft et al., 2017). ODMs on the other hand could be co-cultured with *G. duodenalis* and were successfully infected (Holthaus et al., 2021). In conclusion, duodenum ODMs reflected well both the para- and transcellular properties of human duodenum tissue and therefore can be considered as a suitable and good model for barrier research.

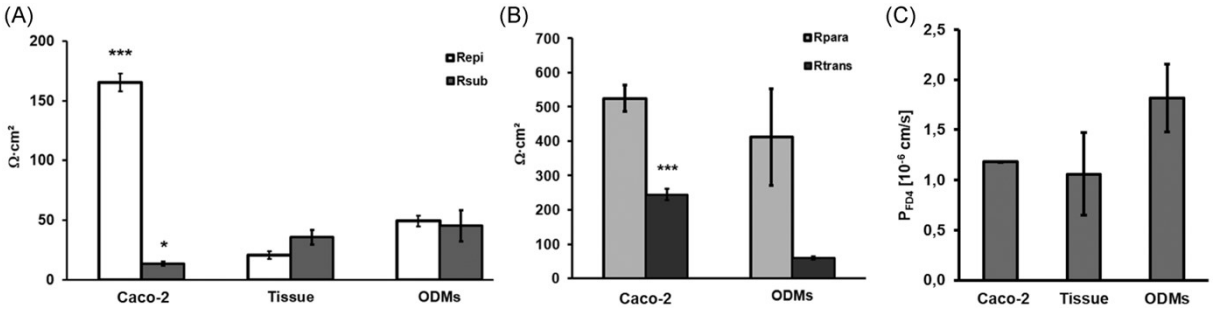

Figure 34 Comparison of barrier function of ODMs, human duodenal tissue, and Caco-2 cells

(A) One-path impedance spectroscopy revealed a higher epithelial resistance (R^{epi}), and a lower subepithelial resistance (R^{sub}), in Caco-2 than in ODMs and duodenal tissue (*n*= 5, 4, 4). (B) Two-path impedance spectroscopy revealed that a higher transcellular resistance caused the increased (R^{epi}), while paracellular resistance was similar between Caco-2 and ODMs (*n*= 5, 4, 4). (C) The permeability for the macromolecule FITC-Dextran 4 kDa (P_{FD4}) was similar between Caco-2 (1.18 ± 0.003 × 10^{-6} cm/s, *n* = 16), tissue (1.06 ± 0.41 × 10^{-6} cm/s, *n* = 5), and ODMs (1.82 ± 0.34 × 10^{-6} cm/s, *n* = 4).

6.2.3 UC-derived ODMs depict donor-specific TER values and TJ expression

Finally, initial studies were performed comparing colon ODMs of healthy controls (C) with those of UC patients (UC). IF-staining showed the expression and correct localisation of TJ proteins (Figure 32). Thus, also in colon derived ODMs TRIC was located at tTJs (Ikenouchi et al., 2005) and angulin-1 extended to the lateral membrane (Masuda et al., 2011). All three UC ODMs exhibited low TER values, although a confluent monolayer was formed, since all UC ODM filters kept the apical medium (Figure 31). Thus, these low TER values indicate an impaired epithelial barrier of those UC organoid lines. C organoid lines showed donor-specific TER values that differed greatly from each other (Figure 31 A). In a recent study, ODMs derived from three different healthy donors also exhibited donor-specific TER values that were very different, further emphasizing the ability to use organoids for personalised medicine (Ok et al., 2023).

Quantification of TJ protein expression further indicated donor-specificity for example the expression of CLDN3 was different in C2 but not for the UC ODMs compared to C1 (Figure 33). Normalising protein expression to C1 rather than the mean of C1 and C2 more strongly emphasizes the donor-specific properties and this is an important advantage of organoids/ODM culture over commonly used cell line, which was also discussed by Ok et al. (Ok et al., 2023). However, in this case of significant changes to C1, the protein expression of C2 should also be considered. In general, a higher sample size would better define what is normal and what an altered expression is and therefore patient and control samples are

collected constantly. For UC1 no significant alterations in the investigated TJ proteins were detected. Only a tendency towards a higher CLDN2 expression was noted, which is known to be upregulated in UC. However, this rather small increase in CLDN2 might not explain the lower TER values and thus either other TJ proteins are altered, or other mechanisms lead to this reduced TER values. Likewise, for UC2 no significant alterations were detected, although MD3 expression seems to be upregulated in line with a previous study of us (Weiss et al., 2022a). Further the barrier forming CDLN1 was slightly downregulated compared to C1 and C2, while there was a tendency to an upregulation of CLDN2. UC3 ODMs showed most altered TJ expression profile of the analysed UC samples. It showed a large increase In CLDN2 expression, which might be the reason for the low TER values and a tendency for downregulated CLDN4. It was reported that CLDN4 and CDLN7 are downregulated and CLDN2 is upregulated in UC patients (Oshima et al., 2008). Unfortunately, CLDN7 was not tested so far but it would be interesting to see if CLDN7 is downregulated in UC3 as well. Surprisingly an upregulation of angulin-1 was detected. Angulin-1 was found to be downregulated in CD patients and therefore can lead to the delocalization of TRIC, which leads to increased macromolecular uptake (Hu et al., 2020). In contrast no significant change of angulin-1 was detected in UC patients (Hu et al., 2021). It needs to be mentioned that angulin-1 expression was also higher in C2 than in C1, however not significantly. A higher expression of angulin-1 could imply a more stem cell like phenotype, as angulin-1 was found to be located in the crypt bottom but not in the upper part in the crypt (Higashi et al., 2013), as depicted in Figure 1 differentiated IECs are located at the upper part of the colon crypt. Here, again, the expression of CLDN7 could provide more information, as Cldn7 is associated with differentiated cells (Pearce et al., 2018). It could be speculated that in UC3 the disease progression was more driven by an impaired TJ barrier than in the donors of UC1 and UC2. Clearly, it would need much more evidence to proof this. However, these initial results could already give some insights. It would be interesting to see how closely ODMs reflect the TJ expression of tissues of the specific donors and if these changes in TJ expression are still stable after several passages, as culture conditions also impact differentiation and thus barrier functions.

6.2.4 Conclusion

Altogether during this thesis, the ODM model from mouse and human as well as from small and large intestine were established in our lab and validated for their ability in barrier research. It could be demonstrated that ODMs are a feasible model to analyse the para- as well as the transcellular properties of the intestinal epithelium and initial results on human colon ODMs

derived from control donors and UC patients indicate their ability to investigate the pathogenesis of IBD in the context of TJ barrier impairment.

7 Conclusion and outlook

In this work two topics were investigated, which differ but might be combined in future research. In the first part it was elucidated for the first time that TAMPs in addition to their barrier properties also might exhibit immune regulatory functions indicated by changes in immune cell composition in TAMP-OE mice, especially during DSS-induced colitis. The main findings were that in MD3-OE mice the occurrence of $CD19^+$ B-cells is higher compared to wt mice upon DSS treatment. Tric-OE seems to depress $CD103^+$ subpopulations of both IELs and DCs, while those were supported in Ocln-OE mice. In Ocln-OE mice a higher occurrence of resident, particularly $CD4^+$ resident macrophages were maintained. These findings emphasise even more that despite their similarities MD3, Ocln, and Tric have distinct functions, similar to observations considering TJ barrier properties (Raleigh et al., 2010).

Further studies need to clarify the outcomes of the observed changes and the mechanism causing them. Immunofluorescence stainings could elucidate the location of immune cells dependent on TAMP-OE and thereby give an indication towards direct or indirect interactions. Single cell RNA sequencing of isolated immune cells and epithelial cells might elucidate potential pathways and mechanisms that lead to the changes in immune cell composition in TAMP-OE mice. In order to confirm those mechanisms, a co-culture of the affected immune cells with ODMs derived from TAMP-OE mice could be beneficial.

In the second part of this study, the ODM model from mouse and human small and large intestine was successfully established and validated for their ability in barrier research. In a next step, findings gathered using ODMs and immune cells derived from TAMP-OE mice could be transferred and validated to ODMs and immune cells derived from UC patients and healthy controls. Initial results of human colon ODMs derived from controls and UC patients indicate their ability to investigate the pathogenesis of IBD in the context of TJ barrier impairment. Finally, this might ascertain new therapeutic targets that will help to control immune responses and TJ barrier breakdown in IBD patients.

8 References

ABBAS, A. K., MURPHY, K. M. & SHER, A. 1996. Functional diversity of helper T lymphocytes. *Nature,* 383**,** 787-93.

ALEX, P., ZACHOS, N. C., NGUYEN, T., GONZALES, L., CHEN, T. E., CONKLIN, L. S., CENTOLA, M. & LI, X. 2009. Distinct cytokine patterns identified from multiplex profiles of murine DSS and TNBS-induced colitis. *Inflamm Bowel Dis,* 15**,** 341-52.

ALEXANDRE, M. D., LU, Q. & CHEN, Y. H. 2005. Overexpression of claudin-7 decreases the paracellular Cl- conductance and increases the paracellular Na+ conductance in LLC-PK1 cells. *J Cell Sci,* 118**,** 2683-93.

AMASHEH, M., GROTJOHANN, I., AMASHEH, S., FROMM, A., SODERHOLM, J. D., ZEITZ, M., FROMM, M. & SCHULZKE, J. D. 2009a. Regulation of mucosal structure and barrier function in rat colon exposed to tumor necrosis factor alpha and interferon gamma in vitro: a novel model for studying the pathomechanisms of inflammatory bowel disease cytokines. *Scand J Gastroenterol,* 44**,** 1226-35.

AMASHEH, S., FROMM, M. & GUNZEL, D. 2011. Claudins of intestine and nephron - a correlation of molecular tight junction structure and barrier function. *Acta Physiol (Oxf),* 201**,** 133-40.

AMASHEH, S., MEIRI, N., GITTER, A. H., SCHONEBERG, T., MANKERTZ, J., SCHULZKE, J. D. & FROMM, M. 2002. Claudin-2 expression induces cation-selective channels in tight junctions of epithelial cells. *J Cell Sci,* 115**,** 4969-76.

AMASHEH, S., MILATZ, S., KRUG, S. M., MARKOV, A. G., GUNZEL, D., AMASHEH, M. & FROMM, M. 2009b. Tight junction proteins as channel formers and barrier builders. *Ann N Y Acad Sci,* 1165**,** 211-9.

AMASHEH, S., SCHMIDT, T., MAHN, M., FLORIAN, P., MANKERTZ, J., TAVALALI, S., GITTER, A. H., SCHULZKE, J. D. & FROMM, M. 2005. Contribution of claudin-5 to barrier properties in tight junctions of epithelial cells. *Cell Tissue Res,* 321**,** 89-96.

ANIWAN, S., HARMSEN, W. S., TREMAINE, W. J., KANE, S. V. & LOFTUS, E. V., JR. 2018. Overall and Cause-Specific Mortality of Inflammatory Bowel Disease in Olmsted County, Minnesota, From 1970 Through 2016. *Mayo Clin Proc,* 93**,** 1415-1422.

ANNACKER, O., COOMBES, J. L., MALMSTROM, V., UHLIG, H. H., BOURNE, T., JOHANSSON-LINDBOM, B., AGACE, W. W., PARKER, C. M. & POWRIE, F. 2005. Essential role for CD103 in the T cell-mediated regulation of experimental colitis. *J Exp Med,* 202**,** 1051-61.

ARIMURA, K., TAKAGI, H., UTO, T., FUKAYA, T., NAKAMURA, T., CHOIJOOKHUU, N., HISHIKAWA, Y., YAMASHITA, Y. & SATO, K. 2017. Crucial role of plasmacytoid dendritic cells in the development of acute colitis through the regulation of intestinal inflammation. *Mucosal Immunol,* 10**,** 957-970.

ATARASHI, K., TANOUE, T., ANDO, M., KAMADA, N., NAGANO, Y., NARUSHIMA, S., SUDA, W., IMAOKA, A., SETOYAMA, H., NAGAMORI, T., ISHIKAWA, E., SHIMA, T., HARA, T., KADO, S., JINNOHARA, T., OHNO, H., KONDO, T., TOYOOKA, K., WATANABE, E., YOKOYAMA, S., TOKORO, S., MORI, H., NOGUCHI, Y., MORITA, H., IVANOV, II, SUGIYAMA, T., NUNEZ, G., CAMP, J. G., HATTORI, M., UMESAKI, Y. & HONDA, K. 2015. Th17 Cell Induction by Adhesion of Microbes to Intestinal Epithelial Cells. *Cell,* 163**,** 367-80.

ATARASHI, K., TANOUE, T., OSHIMA, K., SUDA, W., NAGANO, Y., NISHIKAWA, H., FUKUDA, S., SAITO, T., NARUSHIMA, S., HASE, K., KIM, S., FRITZ, J. V., WILMES, P., UEHA, S., MATSUSHIMA, K., OHNO, H., OLLE, B., SAKAGUCHI, S., TANIGUCHI, T., MORITA, H., HATTORI, M. & HONDA, K. 2013. Treg induction by a rationally selected mixture of Clostridia strains from the human microbiota. *Nature,* 500**,** 232-6.

ATARASHI, K., TANOUE, T., SHIMA, T., IMAOKA, A., KUWAHARA, T., MOMOSE, Y., CHENG, G., YAMASAKI, S., SAITO, T., OHBA, Y., TANIGUCHI, T., TAKEDA, K., HORI, S., IVANOV, II, UMESAKI, Y., ITOH, K. & HONDA, K. 2011. Induction of colonic regulatory T cells by indigenous Clostridium species. *Science,* 331**,** 337-41.

BAI, Y., QIAN, C., QIAN, L., MA, F., HOU, J., CHEN, Y., WANG, Q. & CAO, X. 2012. Integrin CD11b negatively regulates TLR9-triggered dendritic cell cross-priming by upregulating microRNA-146a. *J Immunol,* 188**,** 5293-302.

BAIN, C. C., MONTGOMERY, J., SCOTT, C. L., KEL, J. M., GIRARD-MADOUX, M. J. H., MARTENS, L., ZANGERLE-MURRAY, T. F. P., OBER-BLOBAUM, J., LINDENBERGH-KORTLEVE, D., SAMSOM, J. N., HENRI, S., LAWRENCE, T., SAEYS, Y., MALISSEN, B., DALOD, M., CLAUSEN, B. E. & MOWAT, A. M. 2017. TGFbetaR signalling controls CD103(+)CD11b(+) dendritic cell development in the intestine. *Nat Commun,* 8**,** 620.

BAIN, C. C., SCOTT, C. L., URONEN-HANSSON, H., GUDJONSSON, S., JANSSON, O., GRIP, O., GUILLIAMS, M., MALISSEN, B., AGACE, W. W. & MOWAT, A. M. 2013. Resident and pro-inflammatory macrophages in the colon represent alternative context-dependent fates of the same Ly6Chi monocyte precursors. *Mucosal Immunol,* 6**,** 498-510.

BARKER, N., HUCH, M., KUJALA, P., VAN DE WETERING, M., SNIPPERT, H. J., VAN ES, J. H., SATO, T., STANGE, D. E., BEGTHEL, H., VAN DEN BORN, M., DANENBERG, E., VAN DEN BRINK, S., KORVING, J., ABO, A., PETERS, P. J., WRIGHT, N., POULSOM, R. & CLEVERS, H. 2010. Lgr5(+ve) stem cells drive self-renewal in the stomach and build long-lived gastric units in vitro. *Cell Stem Cell,* 6**,** 25-36.

BARKER, N., VAN ES, J. H., KUIPERS, J., KUJALA, P., VAN DEN BORN, M., COZIJNSEN, M., HAEGEBARTH, A., KORVING, J., BEGTHEL, H., PETERS, P. J. & CLEVERS, H. 2007. Identification of stem cells in small intestine and colon by marker gene Lgr5. *Nature,* 449**,** 1003-7.

BARTFELD, S. 2016. Modeling infectious diseases and host-microbe interactions in gastrointestinal organoids. *Dev Biol,* 420**,** 262-270.

BARTFELD, S., BAYRAM, T., VAN DE WETERING, M., HUCH, M., BEGTHEL, H., KUJALA, P., VRIES, R., PETERS, P. J. & CLEVERS, H. 2015. In vitro expansion of human gastric epithelial stem cells and their responses to bacterial infection. *Gastroenterology,* 148**,** 126-136 e6.

BARTFELD, S. & CLEVERS, H. 2015. Organoids as Model for Infectious Diseases: Culture of Human and Murine Stomach Organoids and Microinjection of Helicobacter Pylori. *J Vis Exp*.

BERNARDO, D., CHAPARRO, M. & GISBERT, J. P. 2018. Human Intestinal Dendritic Cells in Inflammatory Bowel Diseases. *Mol Nutr Food Res,* 62**,** e1700931.

BEUMER, J. & CLEVERS, H. 2016. Regulation and plasticity of intestinal stem cells during homeostasis and regeneration. *Development,* 143**,** 3639-3649.

BEUMER, J. & CLEVERS, H. 2021. Cell fate specification and differentiation in the adult mammalian intestine. *Nat Rev Mol Cell Biol,* 22**,** 39-53.

BJERKNES, M. & CHENG, H. 1981a. The stem-cell zone of the small intestinal epithelium. I. Evidence from Paneth cells in the adult mouse. *Am J Anat,* 160**,** 51-63.

BJERKNES, M. & CHENG, H. 1981b. The stem-cell zone of the small intestinal epithelium. III. Evidence from columnar, enteroendocrine, and mucous cells in the adult mouse. *Am J Anat,* 160**,** 77-91.

BJERKNES, M. & CHENG, H. 1999. Clonal analysis of mouse intestinal epithelial progenitors. *Gastroenterology,* 116**,** 7-14.

BLUTT, S. E., CRAWFORD, S. E., RAMANI, S., ZOU, W. Y. & ESTES, M. K. 2018. Engineered Human Gastrointestinal Cultures to Study the Microbiome and Infectious Diseases. *Cell Mol Gastroenterol Hepatol,* 5**,** 241-251.

BOISMENU, R. & HAVRAN, W. L. 1994. Modulation of epithelial cell growth by intraepithelial gamma delta T cells. *Science,* 266**,** 1253-5.

BORCK, G., UR REHMAN, A., LEE, K., POGODA, H. M., KAKAR, N., VON AMELN, S., GRILLET, N., HILDEBRAND, M. S., AHMED, Z. M., NURNBERG, G., ANSAR, M., BASIT, S., JAVED, Q., MORELL, R. J., NASREEN, N., SHEARER, A. E., AHMAD, A., KAHRIZI, K., SHAIKH, R. S., ALI, R. A., KHAN, S. N., GOEBEL, I., MEYER, N. C., KIMBERLING, W. J., WEBSTER, J. A., STEPHAN, D. A., SCHILLER, M. R., BAHLO,

M., NAJMABADI, H., GILLESPIE, P. G., NURNBERG, P., WOLLNIK, B., RIAZUDDIN, S., SMITH, R. J., AHMAD, W., MULLER, U., HAMMERSCHMIDT, M., FRIEDMAN, T. B., RIAZUDDIN, S., LEAL, S. M., AHMAD, J. & KUBISCH, C. 2011. Loss-of-function mutations of ILDR1 cause autosomal-recessive hearing impairment DFNB42. *Am J Hum Genet,* 88**,** 127-37.

BRESSENOT, A., SALLERON, J., BASTIEN, C., DANESE, S., BOULAGNON-ROMBI, C. & PEYRIN-BIROULET, L. 2015. Comparing histological activity indexes in UC. *Gut,* 64**,** 1412-8.

BRINKMANN, V., REICHARD, U., GOOSMANN, C., FAULER, B., UHLEMANN, Y., WEISS, D. S., WEINRAUCH, Y. & ZYCHLINSKY, A. 2004. Neutrophil extracellular traps kill bacteria. *Science,* 303**,** 1532-5.

BURISCH, J. & MUNKHOLM, P. 2015. The epidemiology of inflammatory bowel disease. *Scand J Gastroenterol,* 50**,** 942-51.

BURNS, A. R., WALKER, D. C., BROWN, E. S., THURMON, L. T., BOWDEN, R. A., KEESE, C. R., SIMON, S. I., ENTMAN, M. L. & SMITH, C. W. 1997. Neutrophil transendothelial migration is independent of tight junctions and occurs preferentially at tricellular corners. *J Immunol,* 159**,** 2893-903.

CEROVIC, V., BAIN, C. C., MOWAT, A. M. & MILLING, S. W. 2014. Intestinal macrophages and dendritic cells: what's the difference? *Trends Immunol,* 35**,** 270-7.

CEROVIC, V., HOUSTON, S. A., SCOTT, C. L., AUMEUNIER, A., YRLID, U., MOWAT, A. M. & MILLING, S. W. 2013. Intestinal CD103(-) dendritic cells migrate in lymph and prime effector T cells. *Mucosal Immunol,* 6**,** 104-13.

CHAROENPHANDHU, N., NAKKRASAE, L. I., KRAIDITH, K., TEERAPORNPUNTAKIT, J., THONGCHOTE, K., THONGON, N. & KRISHNAMRA, N. 2009. Two-step stimulation of intestinal Ca(2+) absorption during lactation by long-term prolactin exposure and suckling-induced prolactin surge. *Am J Physiol Endocrinol Metab,* 297**,** E609-19.

CHEN, S., ZHENG, Y., RAN, X., DU, H., FENG, H., YANG, L., WEN, Y., LIN, C., WANG, S., HUANG, M., YAN, Z., WU, D., WANG, H., GE, G., ZENG, A., ZENG, Y. A. & CHEN, J. 2021. Integrin alphaEbeta7(+) T cells direct intestinal stem cell fate decisions via adhesion signaling. *Cell Res,* 31**,** 1291-1307.

CHENG, H. & LEBLOND, C. P. 1974. Origin, differentiation and renewal of the four main epithelial cell types in the mouse small intestine. V. Unitarian Theory of the origin of the four epithelial cell types. *Am J Anat,* 141**,** 537-61.

CHEROUTRE, H., LAMBOLEZ, F. & MUCIDA, D. 2011. The light and dark sides of intestinal intraepithelial lymphocytes. *Nat Rev Immunol,* 11**,** 445-56.

CHIEPPA, M., RESCIGNO, M., HUANG, A. Y. & GERMAIN, R. N. 2006. Dynamic imaging of dendritic cell extension into the small bowel lumen in response to epithelial cell TLR engagement. *J Exp Med,* 203**,** 2841-52.

CLAUDE, P. & GOODENOUGH, D. A. 1973. Fracture faces of zonulae occludentes from "tight" and "leaky" epithelia. *J Cell Biol,* 58**,** 390-400.

CO, J. Y., MARGALEF-CATALA, M., LI, X., MAH, A. T., KUO, C. J., MONACK, D. M. & AMIEVA, M. R. 2019. Controlling Epithelial Polarity: A Human Enteroid Model for Host-Pathogen Interactions. *Cell Rep,* 26**,** 2509-2520 e4.

CORDING, J., BERG, J., KADING, N., BELLMANN, C., TSCHEIK, C., WESTPHAL, J. K., MILATZ, S., GUNZEL, D., WOLBURG, H., PIONTEK, J., HUBER, O. & BLASIG, I. E. 2013. In tight junctions, claudins regulate the interactions between occludin, tricellulin and marvelD3, which, inversely, modulate claudin oligomerization. *J Cell Sci,* 126**,** 554-64.

D'ALDEBERT, E., QUARANTA, M., SEBERT, M., BONNET, D., KIRZIN, S., PORTIER, G., DUFFAS, J. P., CHABOT, S., LLUEL, P., ALLART, S., FERRAND, A., ALRIC, L., RACAUD-SULTAN, C., MAS, E., DERAISON, C. & VERGNOLLE, N. 2020. Characterization of Human Colon Organoids From Inflammatory Bowel Disease Patients. *Front Cell Dev Biol,* 8**,** 363.

DANESE, S., COLOMBEL, J. F., LUKAS, M., GISBERT, J. P., D'HAENS, G., HAYEE, B., PANACCIONE, R., KIM, H. S., REINISCH, W., TYRRELL, H., OH, Y. S., TOLE, S.,

CHAI, A., CHAMBERLAIN-JAMES, K., TANG, M. T., SCHREIBER, S. & GROUP, G. S. 2022. Etrolizumab versus infliximab for the treatment of moderately to severely active ulcerative colitis (GARDENIA): a randomised, double-blind, double-dummy, phase 3 study. *Lancet Gastroenterol Hepatol,* 7**,** 118-127.

DENKER, B. M. & NIGAM, S. K. 1998. Molecular structure and assembly of the tight junction. *Am J Physiol,* 274**,** F1-9.

DENNING, T. L., NORRIS, B. A., MEDINA-CONTRERAS, O., MANICASSAMY, S., GEEM, D., MADAN, R., KARP, C. L. & PULENDRAN, B. 2011. Functional specializations of intestinal dendritic cell and macrophage subsets that control Th17 and regulatory T cell responses are dependent on the T cell/APC ratio, source of mouse strain, and regional localization. *J Immunol,* 187**,** 733-47.

DEVOSS, J. & DIEHL, L. 2014. Murine models of inflammatory bowel disease (IBD): challenges of modeling human disease. *Toxicol Pathol,* 42**,** 99-110.

DIAMOND, J. M. 1977. Twenty-first Bowditch lecture. The epithelial junction: bridge, gate, and fence. *Physiologist,* 20**,** 10-8.

EBNET, K., SUZUKI, A., OHNO, S. & VESTWEBER, D. 2004. Junctional adhesion molecules (JAMs): more molecules with dual functions? *J Cell Sci,* 117**,** 19-29.

EDELBLUM, K. L., SHEN, L., WEBER, C. R., MARCHIANDO, A. M., CLAY, B. S., WANG, Y., PRINZ, I., MALISSEN, B., SPERLING, A. I. & TURNER, J. R. 2012. Dynamic migration of gammadelta intraepithelial lymphocytes requires occludin. *Proc Natl Acad Sci U S A,* 109**,** 7097-102.

EDELBLUM, K. L., SINGH, G., ODENWALD, M. A., LINGARAJU, A., EL BISSATI, K., MCLEOD, R., SPERLING, A. I. & TURNER, J. R. 2015. gammadelta Intraepithelial Lymphocyte Migration Limits Transepithelial Pathogen Invasion and Systemic Disease in Mice. *Gastroenterology,* 148**,** 1417-26.

ENDERLE, K., DINKEL, M., SPATH, E. M., SCHMID, B., ZUNDLER, S., TRIPAL, P., NEURATH, M. F., HILDNER, K. & NEUFERT, C. 2021. Dynamic Imaging of IEL-IEC Co-Cultures Allows for Quantification of CD103-Dependent T Cell Migration. *Int J Mol Sci,* 22.

ENGLE, M. J., GOETZ, G. S. & ALPERS, D. H. 1998. Caco-2 cells express a combination of colonocyte and enterocyte phenotypes. *J Cell Physiol,* 174**,** 362-9.

FARQUHAR, M. G. & PALADE, G. E. 1963. Junctional complexes in various epithelia. *J Cell Biol,* 17**,** 375-412.

FU, Y., WANG, Z., YU, B., LIN, Y., HUANG, E., LIU, R., ZHAO, C., LU, M., XU, W., LIU, H., LIU, Y., WANG, L. & CHU, Y. 2021. Intestinal CD11b(+) B Cells Ameliorate Colitis by Secreting Immunoglobulin A. *Front Immunol,* 12**,** 697725.

FUCHS, A., VERMI, W., LEE, J. S., LONARDI, S., GILFILLAN, S., NEWBERRY, R. D., CELLA, M. & COLONNA, M. 2013. Intraepithelial type 1 innate lymphoid cells are a unique subset of IL-12- and IL-15-responsive IFN-gamma-producing cells. *Immunity,* 38**,** 769-81.

FUJII, M., MATANO, M., TOSHIMITSU, K., TAKANO, A., MIKAMI, Y., NISHIKORI, S., SUGIMOTO, S. & SATO, T. 2018. Human Intestinal Organoids Maintain Self-Renewal Capacity and Cellular Diversity in Niche-Inspired Culture Condition. *Cell Stem Cell,* 23**,** 787-793 e6.

FUJINO, S., ANDOH, A., BAMBA, S., OGAWA, A., HATA, K., ARAKI, Y., BAMBA, T. & FUJIYAMA, Y. 2003. Increased expression of interleukin 17 in inflammatory bowel disease. *Gut,* 52**,** 65-70.

FUJITA, H., SUGIMOTO, K., INATOMI, S., MAEDA, T., OSANAI, M., UCHIYAMA, Y., YAMAMOTO, Y., WADA, T., KOJIMA, T., YOKOZAKI, H., YAMASHITA, T., KATO, S., SAWADA, N. & CHIBA, H. 2008. Tight junction proteins claudin-2 and -12 are critical for vitamin D-dependent Ca2+ absorption between enterocytes. *Mol Biol Cell,* 19**,** 1912-21.

FURUSE, M., FUJITA, K., HIIRAGI, T., FUJIMOTO, K. & TSUKITA, S. 1998. Claudin-1 and -2: novel integral membrane proteins localizing at tight junctions with no sequence similarity to occludin. *J Cell Biol,* 141**,** 1539-50.

FURUSE, M., HATA, M., FURUSE, K., YOSHIDA, Y., HARATAKE, A., SUGITANI, Y., NODA, T., KUBO, A. & TSUKITA, S. 2002. Claudin-based tight junctions are crucial for the mammalian epidermal barrier: a lesson from claudin-1-deficient mice. *J Cell Biol,* 156**,** 1099-111.

FURUSE, M., HIRASE, T., ITOH, M., NAGAFUCHI, A., YONEMURA, S., TSUKITA, S. & TSUKITA, S. 1993. Occludin: a novel integral membrane protein localizing at tight junctions. *J Cell Biol,* 123**,** 1777-88.

GARCIA-HERNANDEZ, V., QUIROS, M. & NUSRAT, A. 2017. Intestinal epithelial claudins: expression and regulation in homeostasis and inflammation. *Ann N Y Acad Sci,* 1397**,** 66-79.

GARROD, D., CHIDGEY, M. & NORTH, A. 1996. Desmosomes: differentiation, development, dynamics and disease. *Curr Opin Cell Biol,* 8**,** 670-8.

GAUTIER, E. L., SHAY, T., MILLER, J., GRETER, M., JAKUBZICK, C., IVANOV, S., HELFT, J., CHOW, A., ELPEK, K. G., GORDONOV, S., MAZLOOM, A. R., MA'AYAN, A., CHUA, W. J., HANSEN, T. H., TURLEY, S. J., MERAD, M., RANDOLPH, G. J. & IMMUNOLOGICAL GENOME, C. 2012. Gene-expression profiles and transcriptional regulatory pathways that underlie the identity and diversity of mouse tissue macrophages. *Nat Immunol,* 13**,** 1118-28.

GIACOMELLI, R., PARZANESE, I., FRIERI, G., PASSACANTANDO, A., PIZZUTO, F., PIMPO, T., CIPRIANI, P., VISCIDO, A., CAPRILLI, R. & TONIETTI, G. 1994. Increase of circulating gamma/delta T lymphocytes in the peripheral blood of patients affected by active inflammatory bowel disease. *Clin Exp Immunol,* 98**,** 83-8.

GIESECK, R. L., 3RD, WILSON, M. S. & WYNN, T. A. 2018. Type 2 immunity in tissue repair and fibrosis. *Nat Rev Immunol,* 18**,** 62-76.

GÓMEZ-MORA, E., CARRILLO, J., URREA, V., RIGAU, J., ALEGRE, J., CABRERA, C., OLTRA, E., CASTRO-MARRERO, J. & BLANCO, J. 2020. Impact of Long-Term Cryopreservation on Blood Immune Cell Markers in Myalgic Encephalomyelitis/Chronic Fatigue Syndrome: Implications for Biomarker Discovery. *Frontiers in Immunology,* 11.

GRETER, M., HELFT, J., CHOW, A., HASHIMOTO, D., MORTHA, A., AGUDO-CANTERO, J., BOGUNOVIC, M., GAUTIER, E. L., MILLER, J., LEBOEUF, M., LU, G., ALOMAN, C., BROWN, B. D., POLLARD, J. W., XIONG, H., RANDOLPH, G. J., CHIPUK, J. E., FRENETTE, P. S. & MERAD, M. 2012. GM-CSF controls nonlymphoid tissue dendritic cell homeostasis but is dispensable for the differentiation of inflammatory dendritic cells. *Immunity,* 36**,** 1031-46.

GROSSMANN, J., WALTHER, K., ARTINGER, M., KIESSLING, S., STEINKAMP, M., SCHMAUTZ, W. K., STADLER, F., BATAILLE, F., SCHULTZ, M., SCHOLMERICH, J. & ROGLER, G. 2003. Progress on isolation and short-term ex-vivo culture of highly purified non-apoptotic human intestinal epithelial cells (IEC). *Eur J Cell Biol,* 82**,** 262-70.

GU, W., WANG, H., HUANG, X., KRAICZY, J., SINGH, P. N. P., NG, C., DAGDEVIREN, S., HOUGHTON, S., PELLON-CARDENAS, O., LAN, Y., NIE, Y., ZHANG, J., BANERJEE, K. K., ONUFER, E. J., WARNER, B. W., SPENCE, J., SCHERL, E., RAFII, S., LEE, R. T., VERZI, M. P., REDMOND, D., LONGMAN, R., HELIN, K., SHIVDASANI, R. A. & ZHOU, Q. 2022. SATB2 preserves colon stem cell identity and mediates ileum-colon conversion via enhancer remodeling. *Cell Stem Cell,* 29**,** 101-115 e10.

HADIS, U., WAHL, B., SCHULZ, O., HARDTKE-WOLENSKI, M., SCHIPPERS, A., WAGNER, N., MULLER, W., SPARWASSER, T., FORSTER, R. & PABST, O. 2011. Intestinal tolerance requires gut homing and expansion of FoxP3+ regulatory T cells in the lamina propria. *Immunity,* 34**,** 237-46.

HAN, C., JIN, J., XU, S., LIU, H., LI, N. & CAO, X. 2010. Integrin CD11b negatively regulates TLR-triggered inflammatory responses by activating Syk and promoting degradation of MyD88 and TRIF via Cbl-b. *Nat Immunol,* 11**,** 734-42.

HARAMIS, A. P., BEGTHEL, H., VAN DEN BORN, M., VAN ES, J., JONKHEER, S., OFFERHAUS, G. J. & CLEVERS, H. 2004. De novo crypt formation and juvenile polyposis on BMP inhibition in mouse intestine. *Science,* 303**,** 1684-6.

HE, X. C., ZHANG, J., TONG, W. G., TAWFIK, O., ROSS, J., SCOVILLE, D. H., TIAN, Q., ZENG, X., HE, X., WIEDEMANN, L. M., MISHINA, Y. & LI, L. 2004. BMP signaling inhibits intestinal stem cell self-renewal through suppression of Wnt-beta-catenin signaling. *Nat Genet,* 36**,** 1117-21.

HE, Y., YIN, X., DONG, J., YANG, Q., WU, Y. & GONG, Z. 2021. Transcriptome Analysis of Caco-2 Cells upon the Exposure of Mycotoxin Deoxynivalenol and Its Acetylated Derivatives. *Toxins (Basel),* 13.

HELLER, F., FLORIAN, P., BOJARSKI, C., RICHTER, J., CHRIST, M., HILLENBRAND, B., MANKERTZ, J., GITTER, A. H., BURGEL, N., FROMM, M., ZEITZ, M., FUSS, I., STROBER, W. & SCHULZKE, J. D. 2005. Interleukin-13 is the key effector Th2 cytokine in ulcerative colitis that affects epithelial tight junctions, apoptosis, and cell restitution. *Gastroenterology,* 129**,** 550-64.

HIGASHI, T., TOKUDA, S., KITAJIRI, S., MASUDA, S., NAKAMURA, H., ODA, Y. & FURUSE, M. 2013. Analysis of the 'angulin' proteins LSR, ILDR1 and ILDR2--tricellulin recruitment, epithelial barrier function and implication in deafness pathogenesis. *J Cell Sci,* 126**,** 966-77.

HOFFMANN, J. C., PAWLOWSKI, N. N., GROLLICH, K., LODDENKEMPER, C., ZEITZ, M. & KUHL, A. A. 2008. Gammadelta T lymphocytes: a new type of regulatory T cells suppressing murine 2,4,6-trinitrobenzene sulphonic acid (TNBS)-induced colitis. *Int J Colorectal Dis,* 23**,** 909-20.

HOFFMANN, J. C., PETERS, K., HENSCHKE, S., HERRMANN, B., PFISTER, K., WESTERMANN, J. & ZEITZ, M. 2001. Role of T lymphocytes in rat 2,4,6-trinitrobenzene sulphonic acid (TNBS) induced colitis: increased mortality after gammadelta T cell depletion and no effect of alphabeta T cell depletion. *Gut,* 48**,** 489-95.

HOLTHAUS, D., DELGADO-BETANCOURT, E., AEBISCHER, T., SEEBER, F. & KLOTZ, C. 2020. Harmonization of Protocols for Multi-Species Organoid Platforms to Study the Intestinal Biology of Toxoplasma gondii and Other Protozoan Infections. *Front Cell Infect Microbiol,* 10**,** 610368.

HOLTHAUS, D., KRAFT, M. R., KRUG, S. M., WOLF, S., MULLER, A., BETANCOURT, E. D., SCHORR, M., HOLLAND, G., KNAUF, F., SCHULZKE, J. D., AEBISCHER, T. & KLOTZ, C. 2021. Dissection of barrier dysfunction in organoid-derived human intestinal epithelia induced by Giardia duodenalis. *Gastroenterology*.

HU, J. E., BOJARSKI, C., BRANCHI, F., FROMM, M. & KRUG, S. M. 2020. Leptin Downregulates Angulin-1 in Active Crohn's Disease via STAT3. *Int J Mol Sci,* 21.

HU, J. E., WEISS, F., BOJARSKI, C., BRANCHI, F., SCHULZKE, J. D., FROMM, M. & KRUG, S. M. 2021. Expression of tricellular tight junction proteins and the paracellular macromolecule barrier are recovered in remission of ulcerative colitis. *BMC Gastroenterol,* 21**,** 141.

HU, M. D., GOLOVCHENKO, N. B., BURNS, G. L., NAIR, P. M., KELLY, T. J. T., AGOS, J., IRANI, M. Z., SOH, W. S., ZEGLINSKI, M. R., LEMENZE, A., BONDER, E. M., SANDROCK, I., PRINZ, I., GRANVILLE, D. J., KEELY, S., WATSON, A. J. M. & EDELBLUM, K. L. 2022. gammadelta Intraepithelial Lymphocytes Facilitate Pathological Epithelial Cell Shedding Via CD103-Mediated Granzyme Release. *Gastroenterology,* 162**,** 877-889 e7.

HUCH, M., DORRELL, C., BOJ, S. F., VAN ES, J. H., LI, V. S., VAN DE WETERING, M., SATO, T., HAMER, K., SASAKI, N., FINEGOLD, M. J., HAFT, A., VRIES, R. G., GROMPE, M. & CLEVERS, H. 2013. In vitro expansion of single Lgr5+ liver stem cells induced by Wnt-driven regeneration. *Nature,* 494**,** 247-50.

IKENOUCHI, J., FURUSE, M., FURUSE, K., SASAKI, H., TSUKITA, S. & TSUKITA, S. 2005. Tricellulin constitutes a novel barrier at tricellular contacts of epithelial cells. *J Cell Biol,* 171**,** 939-45.

IKENOUCHI, J., SASAKI, H., TSUKITA, S., FURUSE, M. & TSUKITA, S. 2008. Loss of occludin affects tricellular localization of tricellulin. *Mol Biol Cell,* 19**,** 4687-93.

ISMAIL, A. S., BEHRENDT, C. L. & HOOPER, L. V. 2009. Reciprocal interactions between commensal bacteria and gamma delta intraepithelial lymphocytes during mucosal injury. *J Immunol,* 182**,** 3047-54.

ISMAIL, A. S., SEVERSON, K. M., VAISHNAVA, S., BEHRENDT, C. L., YU, X., BENJAMIN, J. L., RUHN, K. A., HOU, B., DEFRANCO, A. L., YAROVINSKY, F. & HOOPER, L. V. 2011. Gammadelta intraepithelial lymphocytes are essential mediators of host-microbial homeostasis at the intestinal mucosal surface. *Proc Natl Acad Sci U S A,* 108**,** 8743-8.

IVANOV, II, ATARASHI, K., MANEL, N., BRODIE, E. L., SHIMA, T., KARAOZ, U., WEI, D., GOLDFARB, K. C., SANTEE, C. A., LYNCH, S. V., TANOUE, T., IMAOKA, A., ITOH, K., TAKEDA, K., UMESAKI, Y., HONDA, K. & LITTMAN, D. R. 2009. Induction of intestinal Th17 cells by segmented filamentous bacteria. *Cell,* 139**,** 485-98.

IVANOV, A. I. & NAYDENOV, N. G. 2013. Dynamics and regulation of epithelial adherens junctions: recent discoveries and controversies. *Int Rev Cell Mol Biol,* 303**,** 27-99.

JASS, J. R. & WALSH, M. D. 2001. Altered mucin expression in the gastrointestinal tract: a review. *J Cell Mol Med,* 5**,** 327-51.

JOSTINS, L., RIPKE, S., WEERSMA, R. K., DUERR, R. H., MCGOVERN, D. P., HUI, K. Y., LEE, J. C., SCHUMM, L. P., SHARMA, Y., ANDERSON, C. A., ESSERS, J., MITROVIC, M., NING, K., CLEYNEN, I., THEATRE, E., SPAIN, S. L., RAYCHAUDHURI, S., GOYETTE, P., WEI, Z., ABRAHAM, C., ACHKAR, J. P., AHMAD, T., AMININEJAD, L., ANANTHAKRISHNAN, A. N., ANDERSEN, V., ANDREWS, J. M., BAIDOO, L., BALSCHUN, T., BAMPTON, P. A., BITTON, A., BOUCHER, G., BRAND, S., BUNING, C., COHAIN, A., CICHON, S., D'AMATO, M., DE JONG, D., DEVANEY, K. L., DUBINSKY, M., EDWARDS, C., ELLINGHAUS, D., FERGUSON, L. R., FRANCHIMONT, D., FRANSEN, K., GEARRY, R., GEORGES, M., GIEGER, C., GLAS, J., HARITUNIANS, T., HART, A., HAWKEY, C., HEDL, M., HU, X., KARLSEN, T. H., KUPCINSKAS, L., KUGATHASAN, S., LATIANO, A., LAUKENS, D., LAWRANCE, I. C., LEES, C. W., LOUIS, E., MAHY, G., MANSFIELD, J., MORGAN, A. R., MOWAT, C., NEWMAN, W., PALMIERI, O., PONSIOEN, C. Y., POTOCNIK, U., PRESCOTT, N. J., REGUEIRO, M., ROTTER, J. I., RUSSELL, R. K., SANDERSON, J. D., SANS, M., SATSANGI, J., SCHREIBER, S., SIMMS, L. A., SVENTORAITYTE, J., TARGAN, S. R., TAYLOR, K. D., TREMELLING, M., VERSPAGET, H. W., DE VOS, M., WIJMENGA, C., WILSON, D. C., WINKELMANN, J., XAVIER, R. J., ZEISSIG, S., ZHANG, B., ZHANG, C. K., ZHAO, H., INTERNATIONAL, I. B. D. G. C., SILVERBERG, M. S., ANNESE, V., HAKONARSON, H., BRANT, S. R., RADFORD-SMITH, G., MATHEW, C. G., RIOUX, J. D., et al. 2012. Host-microbe interactions have shaped the genetic architecture of inflammatory bowel disease. *Nature,* 491**,** 119-24.

KADIĆ, E., MONIZ, R. J., HUO, Y., CHI, A. & KARIV, I. 2017. Effect of cryopreservation on delineation of immune cell subpopulations in tumor specimens as determined by multiparametric single cell mass cytometry analysis. *BMC Immunology,* 18.

KAMADA, N., HISAMATSU, T., OKAMOTO, S., CHINEN, H., KOBAYASHI, T., SATO, T., SAKURABA, A., KITAZUME, M. T., SUGITA, A., KOGANEI, K., AKAGAWA, K. S. & HIBI, T. 2008. Unique CD14 intestinal macrophages contribute to the pathogenesis of Crohn disease via IL-23/IFN-gamma axis. *J Clin Invest,* 118**,** 2269-80.

KANAZAWA, H., ISHIGURO, Y., MUNAKATA, A. & MORITA, T. 2001. Multiple accumulation of Vdelta2+ gammadelta T-cell clonotypes in intestinal mucosa from patients with Crohn's disease. *Dig Dis Sci,* 46**,** 410-6.

KAYISOGLU, O., WEISS, F., NIKLAS, C., PIEROTTI, I., POMPAIAH, M., WALLASCHEK, N., GERMER, C. T., WIEGERING, A. & BARTFELD, S. 2021. Location-specific cell identity rather than exposure to GI microbiota defines many innate immune signalling cascades in the gut epithelium. *Gut,* 70**,** 687-697.

KHOR, B., GARDET, A. & XAVIER, R. J. 2011. Genetics and pathogenesis of inflammatory bowel disease. *Nature,* 474**,** 307-17.

KIM, K. A., KAKITANI, M., ZHAO, J., OSHIMA, T., TANG, T., BINNERTS, M., LIU, Y., BOYLE, B., PARK, E., EMTAGE, P., FUNK, W. D. & TOMIZUKA, K. 2005. Mitogenic influence of human R-spondin1 on the intestinal epithelium. *Science,* 309**,** 1256-9.

KIM, M., GALAN, C., HILL, A. A., WU, W. J., FEHLNER-PEACH, H., SONG, H. W., SCHADY, D., BETTINI, M. L., SIMPSON, K. W., LONGMAN, R. S., LITTMAN, D. R. & DIEHL, G. E. 2018. Critical Role for the Microbiota in CX(3)CR1(+) Intestinal Mononuclear Phagocyte Regulation of Intestinal T Cell Responses. *Immunity,* 49**,** 151-163 e5.

KIM, M. S. & KIM, T. S. 2014. IgA+ plasma cells in murine intestinal lamina propria as a positive regulator of Treg differentiation. *J Leukoc Biol,* 95**,** 461-9.

KOJIMA, T., TAKANO, K., YAMAMOTO, T., MURATA, M., SON, S., IMAMURA, M., YAMAGUCHI, H., OSANAI, M., CHIBA, H., HIMI, T. & SAWADA, N. 2008. Transforming growth factor-beta induces epithelial to mesenchymal transition by down-regulation of claudin-1 expression and the fence function in adult rat hepatocytes. *Liver Int,* 28**,** 534-45.

KOMANO, H., FUJIURA, Y., KAWAGUCHI, M., MATSUMOTO, S., HASHIMOTO, Y., OBANA, S., MOMBAERTS, P., TONEGAWA, S., YAMAMOTO, H., ITOHARA, S. & ET AL. 1995. Homeostatic regulation of intestinal epithelia by intraepithelial gamma delta T cells. *Proc Natl Acad Sci U S A,* 92**,** 6147-51.

KONNIKOVA, L., BOSCHETTI, G., RAHMAN, A., MITSIALIS, V., LORD, J., RICHMOND, C., TOMOV, V. T., GORDON, W., JELINSKY, S., CANAVAN, J., LISS, A., WALL, S., FIELD, M., ZHOU, F., GOLDSMITH, J. D., BEWTRA, M., BREAULT, D. T., MERAD, M. & SNAPPER, S. B. 2018. High-dimensional immune phenotyping and transcriptional analyses reveal robust recovery of viable human immune and epithelial cells from frozen gastrointestinal tissue. *Mucosal Immunol,* 11**,** 1684-1693.

KORINEK, V., BARKER, N., MOERER, P., VAN DONSELAAR, E., HULS, G., PETERS, P. J. & CLEVERS, H. 1998. Depletion of epithelial stem-cell compartments in the small intestine of mice lacking Tcf-4. *Nat Genet,* 19**,** 379-83.

KOSINSKI, C., LI, V. S., CHAN, A. S., ZHANG, J., HO, C., TSUI, W. Y., CHAN, T. L., MIFFLIN, R. C., POWELL, D. W., YUEN, S. T., LEUNG, S. Y. & CHEN, X. 2007. Gene expression patterns of human colon tops and basal crypts and BMP antagonists as intestinal stem cell niche factors. *Proc Natl Acad Sci U S A,* 104**,** 15418-23.

KOZUKA, K., HE, Y., KOO-MCCOY, S., KUMARASWAMY, P., NIE, B., SHAW, K., CHAN, P., LEADBETTER, M., HE, L., LEWIS, J. G., ZHONG, Z., CHARMOT, D., BALAA, M., KING, A. J., CALDWELL, J. S. & SIEGEL, M. 2017. Development and Characterization of a Human and Mouse Intestinal Epithelial Cell Monolayer Platform. *Stem Cell Reports,* 9**,** 1976-1990.

KRAFT, M. R., KLOTZ, C., BUCKER, R., SCHULZKE, J. D. & AEBISCHER, T. 2017. Giardia's Epithelial Cell Interaction In Vitro: Mimicking Asymptomatic Infection? *Front Cell Infect Microbiol,* 7**,** 421.

KRAUSE, G., WINKLER, L., MUELLER, S. L., HASELOFF, R. F., PIONTEK, J. & BLASIG, I. E. 2008. Structure and function of claudins. *Biochim Biophys Acta,* 1778**,** 631-45.

KREUSEL, K. M., FROMM, M., SCHULZKE, J. D. & HEGEL, U. 1991. Cl- secretion in epithelial monolayers of mucus-forming human colon cells (HT-29/B6). *Am J Physiol,* 261**,** C574-82.

KRUG, S. M., AMASHEH, S., RICHTER, J. F., MILATZ, S., GUNZEL, D., WESTPHAL, J. K., HUBER, O., SCHULZKE, J. D. & FROMM, M. 2009a. Tricellulin forms a barrier to macromolecules in tricellular tight junctions without affecting ion permeability. *Mol Biol Cell,* 20**,** 3713-24.

KRUG, S. M., BOJARSKI, C., FROMM, A., LEE, I. M., DAMES, P., RICHTER, J. F., TURNER, J. R., FROMM, M. & SCHULZKE, J. D. 2018. Tricellulin is regulated via interleukin-13-receptor alpha2, affects macromolecule uptake, and is decreased in ulcerative colitis. *Mucosal Immunol,* 11**,** 345-356.

KRUG, S. M., FROMM, M. & GUNZEL, D. 2009b. Two-path impedance spectroscopy for measuring paracellular and transcellular epithelial resistance. *Biophys J,* 97**,** 2202-11.

KUBO, A., NAGAO, K., YOKOUCHI, M., SASAKI, H. & AMAGAI, M. 2009. External antigen uptake by Langerhans cells with reorganization of epidermal tight junction barriers. *J Exp Med,* 206**,** 2937-46.

KUCHARZIK, T., WALSH, S. V., CHEN, J., PARKOS, C. A. & NUSRAT, A. 2001. Neutrophil transmigration in inflammatory bowel disease is associated with differential expression of epithelial intercellular junction proteins. *Am J Pathol,* 159**,** 2001-9.

KUHNERT, F., DAVIS, C. R., WANG, H. T., CHU, P., LEE, M., YUAN, J., NUSSE, R. & KUO, C. J. 2004. Essential requirement for Wnt signaling in proliferation of adult small intestine and colon revealed by adenoviral expression of Dickkopf-1. *Proc Natl Acad Sci U S A,* 101**,** 266-71.

KUMAR, N. M. & GILULA, N. B. 1996. The gap junction communication channel. *Cell,* 84**,** 381-8.

LAMERIS, A. L., HUYBERS, S., KAUKINEN, K., MAKELA, T. H., BINDELS, R. J., HOENDEROP, J. G. & NEVALAINEN, P. I. 2013. Expression profiling of claudins in the human gastrointestinal tract in health and during inflammatory bowel disease. *Scand J Gastroenterol,* 48**,** 58-69.

LANCASTER, M. A., RENNER, M., MARTIN, C. A., WENZEL, D., BICKNELL, L. S., HURLES, M. E., HOMFRAY, T., PENNINGER, J. M., JACKSON, A. P. & KNOBLICH, J. A. 2013. Cerebral organoids model human brain development and microcephaly. *Nature,* 501**,** 373-9.

LEBLANC, M. A., PENNEY, L. S., GASTON, D., SHI, Y., ABERG, E., NIGHTINGALE, M., JIANG, H., GILLETT, R. M., FAHIMINIYA, S., MACGILLIVRAY, C., WOOD, E. P., ACOTT, P. D., KHAN, M. N., SAMUELS, M. E., MAJEWSKI, J., ORR, A., MCMASTER, C. R. & BEDARD, K. 2013. A novel rearrangement of occludin causes brain calcification and renal dysfunction. *Hum Genet,* 132**,** 1223-34.

LEBLOND, C. P. & STEVENS, C. E. 1948. The constant renewal of the intestinal epithelium in the albino rat. *Anat Rec,* 100**,** 357-77.

LI, Y., LI, T., ZHOU, D., WEI, J., LI, Z., LI, X., JIA, S., OUYANG, Q., QI, S., CHEN, Z., ZHANG, B., YU, J., JIA, J., XU, A. & HUANG, J. 2021. Role of tight junction-associated MARVEL protein marvelD3 in migration and epithelial-mesenchymal transition of hepatocellular carcinoma. *Cell Adh Migr,* 15**,** 249-260.

LIU, J. Z., VAN SOMMEREN, S., HUANG, H., NG, S. C., ALBERTS, R., TAKAHASHI, A., RIPKE, S., LEE, J. C., JOSTINS, L., SHAH, T., ABEDIAN, S., CHEON, J. H., CHO, J., DAYANI, N. E., FRANKE, L., FUYUNO, Y., HART, A., JUYAL, R. C., JUYAL, G., KIM, W. H., MORRIS, A. P., POUSTCHI, H., NEWMAN, W. G., MIDHA, V., ORCHARD, T. R., VAHEDI, H., SOOD, A., SUNG, J. Y., MALEKZADEH, R., WESTRA, H. J., YAMAZAKI, K., YANG, S. K., INTERNATIONAL MULTIPLE SCLEROSIS GENETICS, C., INTERNATIONAL, I. B. D. G. C., BARRETT, J. C., ALIZADEH, B. Z., PARKES, M., BK, T., DALY, M. J., KUBO, M., ANDERSON, C. A. & WEERSMA, R. K. 2015. Association analyses identify 38 susceptibility loci for inflammatory bowel disease and highlight shared genetic risk across populations. *Nat Genet,* 47**,** 979-986.

LUDWIG, R. J., ZOLLNER, T. M., SANTOSO, S., HARDT, K., GILLE, J., BAATZ, H., JOHANN, P. S., PFEFFER, J., RADEKE, H. H., SCHON, M. P., KAUFMANN, R., BOEHNCKE, W. H. & PODDA, M. 2005. Junctional adhesion molecules (JAM)-B and -C contribute to leukocyte extravasation to the skin and mediate cutaneous inflammation. *J Invest Dermatol,* 125**,** 969-76.

MA, H., QIU, Y. & YANG, H. 2021. Intestinal intraepithelial lymphocytes: Maintainers of intestinal immune tolerance and regulators of intestinal immunity. *J Leukoc Biol,* 109**,** 339-347.

MA'AYEH, S. Y., KNORR, L., SKOLD, K., GARNHAM, A., ANSELL, B. R. E., JEX, A. R. & SVARD, S. G. 2018. Responses of the Differentiated Intestinal Epithelial Cell Line Caco-2 to Infection With the Giardia intestinalis GS Isolate. *Front Cell Infect Microbiol,* 8**,** 244.

MAHE, M. M., SUNDARAM, N., WATSON, C. L., SHROYER, N. F. & HELMRATH, M. A. 2015. Establishment of human epithelial enteroids and colonoids from whole tissue and biopsy. *J Vis Exp*.

MANN, E. R. & LI, X. 2014. Intestinal antigen-presenting cells in mucosal immune homeostasis: crosstalk between dendritic cells, macrophages and B-cells. *World J Gastroenterol,* 20**,** 9653-64.

MANZANO, M., ABADIA-MOLINA, A. C., GARCIA-OLIVARES, E., GIL, A. & RUEDA, R. 2002. Absolute counts and distribution of lymphocyte subsets in small intestine of BALB/c mice change during weaning. *J Nutr,* 132**,** 2757-62.

MARIANO, C., SASAKI, H., BRITES, D. & BRITO, M. A. 2011a. A look at tricellulin and its role in tight junction formation and maintenance. *Eur J Cell Biol,* 90**,** 787-96.

MARIANO, C., SILVA, S. L., PEREIRA, P., FERNANDES, A., BRITES, D. & BRITO, M. A. 2011b. Evidence of tricellulin expression by immune cells, particularly microglia. *Biochem Biophys Res Commun,* 409**,** 799-802.

MARTIN-PADURA, I., LOSTAGLIO, S., SCHNEEMANN, M., WILLIAMS, L., ROMANO, M., FRUSCELLA, P., PANZERI, C., STOPPACCIARO, A., RUCO, L., VILLA, A., SIMMONS, D. & DEJANA, E. 1998. Junctional adhesion molecule, a novel member of the immunoglobulin superfamily that distributes at intercellular junctions and modulates monocyte transmigration. *J Cell Biol,* 142**,** 117-27.

MASUDA, S., ODA, Y., SASAKI, H., IKENOUCHI, J., HIGASHI, T., AKASHI, M., NISHI, E. & FURUSE, M. 2011. LSR defines cell corners for tricellular tight junction formation in epithelial cells. *J Cell Sci,* 124**,** 548-55.

MATTEOLI, G., MAZZINI, E., ILIEV, I. D., MILETI, E., FALLARINO, F., PUCCETTI, P., CHIEPPA, M. & RESCIGNO, M. 2010. Gut CD103+ dendritic cells express indoleamine 2,3-dioxygenase which influences T regulatory/T effector cell balance and oral tolerance induction. *Gut,* 59**,** 595-604.

MAZZINI, E., MASSIMILIANO, L., PENNA, G. & RESCIGNO, M. 2014. Oral tolerance can be established via gap junction transfer of fed antigens from CX3CR1(+) macrophages to CD103(+) dendritic cells. *Immunity,* 40**,** 248-61.

MCCRACKEN, K. W., CATA, E. M., CRAWFORD, C. M., SINAGOGA, K. L., SCHUMACHER, M., ROCKICH, B. E., TSAI, Y. H., MAYHEW, C. N., SPENCE, J. R., ZAVROS, Y. & WELLS, J. M. 2014. Modelling human development and disease in pluripotent stem-cell-derived gastric organoids. *Nature,* 516**,** 400-4.

MCCRACKEN, K. W., HOWELL, J. C., WELLS, J. M. & SPENCE, J. R. 2011. Generating human intestinal tissue from pluripotent stem cells in vitro. *Nat Protoc,* 6**,** 1920-8.

MELCHER, C., YU, J., DUONG, V. H. H., WESTPHAL, K., HELMI SIASI FARIMANY, N., SHAVERSKYI, A., ZHAO, B., STROWIG, T., GLAGE, S., BRAND, K., CHAN, A. C., FOGER, N. & LEE, K. H. 2022. B cell-mediated regulatory mechanisms control tumor-promoting intestinal inflammation. *Cell Rep,* 40**,** 111051.

MENGEL, J., CARDILLO, F., AROEIRA, L. S., WILLIAMS, O., RUSSO, M. & VAZ, N. M. 1995. Anti-gamma delta T cell antibody blocks the induction and maintenance of oral tolerance to ovalbumin in mice. *Immunol Lett,* 48**,** 97-102.

MERKER, S. R., WEITZ, J. & STANGE, D. E. 2016. Gastrointestinal organoids: How they gut it out. *Dev Biol,* 420**,** 239-250.

MIDDEL, P., RADDATZ, D., GUNAWAN, B., HALLER, F. & RADZUN, H. J. 2006. Increased number of mature dendritic cells in Crohn's disease: evidence for a chemokine mediated retention mechanism. *Gut,* 55**,** 220-7.

MILATZ, S., KRUG, S. M., ROSENTHAL, R., GUNZEL, D., MULLER, D., SCHULZKE, J. D., AMASHEH, S. & FROMM, M. 2010. Claudin-3 acts as a sealing component of the tight junction for ions of either charge and uncharged solutes. *Biochim Biophys Acta,* 1798**,** 2048-57.

MINETA, K., YAMAMOTO, Y., YAMAZAKI, Y., TANAKA, H., TADA, Y., SAITO, K., TAMURA, A., IGARASHI, M., ENDO, T., TAKEUCHI, K. & TSUKITA, S. 2011. Predicted expansion of the claudin multigene family. *FEBS Lett,* 585**,** 606-12.

MOON, C., VANDUSSEN, K. L., MIYOSHI, H. & STAPPENBECK, T. S. 2014. Development of a primary mouse intestinal epithelial cell monolayer culture system to evaluate factors that modulate IgA transcytosis. *Mucosal Immunol,* 7**,** 818-28.

MOOREFIELD, E. C., BLUE, R. E., QUINNEY, N. L., GENTZSCH, M. & DING, S. 2018. Generation of renewable mouse intestinal epithelial cell monolayers and organoids for functional analyses. *BMC Cell Biol,* 19**,** 15.

MORTHA, A., CHUDNOVSKIY, A., HASHIMOTO, D., BOGUNOVIC, M., SPENCER, S. P., BELKAID, Y. & MERAD, M. 2014. Microbiota-dependent crosstalk between macrophages and ILC3 promotes intestinal homeostasis. *Science,* 343**,** 1249288.

MOUSSET, W. H., ROB WOESTENENK, FRANK PREIJERS, HARRY DOLSTRA, ANNIEK B. VAN DER WAART 2019. Comprehensive Phenotyping of T Cells Using Flow Cytometry. *Journal of Quantitative Cell Science,* 95**,** 647-654.

MURAI, M., TUROVSKAYA, O., KIM, G., MADAN, R., KARP, C. L., CHEROUTRE, H. & KRONENBERG, M. 2009. Interleukin 10 acts on regulatory T cells to maintain expression of the transcription factor Foxp3 and suppressive function in mice with colitis. *Nat Immunol,* 10**,** 1178-84.

MURPHY, K. W., C. 2018a. Das mucosale Immunsystem. *Janeway immunologie.* Springer Spekrum.

MURPHY, K. W., C. 2018b. Die induzierten Reaktionen der angeborenen Immunität. *Janeway immunologie.* Springer Spektrum.

MURPHY, K. W., C. 2018c. Die T-Zell vermittelte Immunität. *Janeway Immunologie.* Springer Spektrum.

MUZAKI, A. R., TETLAK, P., SHENG, J., LOH, S. C., SETIAGANI, Y. A., POIDINGER, M., ZOLEZZI, F., KARJALAINEN, K. & RUEDL, C. 2016. Intestinal CD103(+)CD11b(-) dendritic cells restrain colitis via IFN-gamma-induced anti-inflammatory response in epithelial cells. *Mucosal Immunol,* 9**,** 336-51.

NAKAMURA, H., SUGANO, M., MIYASHITA, T., HASHIMOTO, H., OCHIAI, A., SUZUKI, K., TSUBOI, M. & ISHII, G. 2019. Organoid culture containing cancer cells and stromal cells reveals that podoplanin-positive cancer-associated fibroblasts enhance proliferation of lung cancer cells. *Lung Cancer,* 134**,** 100-107.

NAKAMURA, T. 2019. Recent progress in organoid culture to model intestinal epithelial barrier functions. *Int Immunol,* 31**,** 13-21.

NASH, T. E. 2019. Long-Term Culture of Giardia lamblia in Cell Culture Medium Requires Intimate Association with Viable Mammalian Cells. *Infect Immun,* 87.

NASH, T. J., MORRIS, K. M., MABBOTT, N. A. & VERVELDE, L. 2021. Inside-out chicken enteroids with leukocyte component as a model to study host-pathogen interactions. *Commun Biol,* 4**,** 377.

NEUDECKER, V., HANEKLAUS, M., JENSEN, O., KHAILOVA, L., MASTERSON, J. C., TYE, H., BIETTE, K., JEDLICKA, P., BRODSKY, K. S., GERICH, M. E., MACK, M., ROBERTSON, A. A. B., COOPER, M. A., FURUTA, G. T., DINARELLO, C. A., O'NEILL, L. A., ELTZSCHIG, H. K., MASTERS, S. L. & MCNAMEE, E. N. 2017. Myeloid-derived miR-223 regulates intestinal inflammation via repression of the NLRP3 inflammasome. *J Exp Med,* 214**,** 1737-1752.

NEURATH, M. F. 2019. Targeting immune cell circuits and trafficking in inflammatory bowel disease. *Nat Immunol,* 20**,** 970-979.

NG, S. C., SHI, H. Y., HAMIDI, N., UNDERWOOD, F. E., TANG, W., BENCHIMOL, E. I., PANACCIONE, R., GHOSH, S., WU, J. C. Y., CHAN, F. K. L., SUNG, J. J. Y. & KAPLAN, G. G. 2017. Worldwide incidence and prevalence of inflammatory bowel disease in the 21st century: a systematic review of population-based studies. *Lancet,* 390**,** 2769-2778.

NIESS, J. H., BRAND, S., GU, X., LANDSMAN, L., JUNG, S., MCCORMICK, B. A., VYAS, J. M., BOES, M., PLOEGH, H. L., FOX, J. G., LITTMAN, D. R. & REINECKER, H. C. 2005. CX3CR1-mediated dendritic cell access to the intestinal lumen and bacterial clearance. *Science,* 307**,** 254-8.

NOEL, G., BAETZ, N. W., STAAB, J. F., DONOWITZ, M., KOVBASNJUK, O., PASETTI, M. F. & ZACHOS, N. C. 2017. Erratum: A primary human macrophage-enteroid co-culture model to investigate mucosal gut physiology and host-pathogen interactions. *Sci Rep,* 7**,** 46790.

NOZAKI, K., MOCHIZUKI, W., MATSUMOTO, Y., MATSUMOTO, T., FUKUDA, M., MIZUTANI, T., WATANABE, M. & NAKAMURA, T. 2016. Co-culture with intestinal epithelial organoids allows efficient expansion and motility analysis of intraepithelial lymphocytes. *J Gastroenterol,* 51**,** 206-13.

O'DRISCOLL, M. C., DALY, S. B., URQUHART, J. E., BLACK, G. C., PILZ, D. T., BROCKMANN, K., MCENTAGART, M., ABDEL-SALAM, G., ZAKI, M., WOLF, N. I., LADDA, R. L., SELL, S., D'ARRIGO, S., SQUIER, W., DOBYNS, W. B., LIVINGSTON, J. H. & CROW, Y. J. 2010. Recessive mutations in the gene encoding the tight junction protein occludin cause band-like calcification with simplified gyration and polymicrogyria. *Am J Hum Genet,* 87**,** 354-64.

OK, M. T., LIU, J., BLITON, R. J., HINESLEY, C. M., SAN PEDRO, E. E. T., BREAU, K. A., GOMEZ-MARTINEZ, I., BURCLAFF, J. & MAGNESS, S. T. 2023. A leaky human colon model reveals uncoupled apical/basal cytotoxicity in early Clostridioides difficile toxin exposure. *Am J Physiol Gastrointest Liver Physiol*.

OLIVARES-VILLAGOMEZ, D. & VAN KAER, L. 2018. Intestinal Intraepithelial Lymphocytes: Sentinels of the Mucosal Barrier. *Trends Immunol,* 39**,** 264-275.

OLTRA-NOGUERA, D., MANGAS-SANJUAN, V., CENTELLES-SANGUESA, A., GONZALEZ-GARCIA, I., SANCHEZ-CASTANO, G., GONZALEZ-ALVAREZ, M., CASABO, V. G., MERINO, V., GONZALEZ-ALVAREZ, I. & BERMEJO, M. 2015. Variability of permeability estimation from different protocols of subculture and transport experiments in cell monolayers. *J Pharmacol Toxicol Methods,* 71**,** 21-32.

OSHIMA, T., MIWA, H. & JOH, T. 2008. Changes in the expression of claudins in active ulcerative colitis. *J Gastroenterol Hepatol,* 23 Suppl 2**,** S146-50.

PANEA, C., FARKAS, A. M., GOTO, Y., ABDOLLAHI-ROODSAZ, S., LEE, C., KOSCSO, B., GOWDA, K., HOHL, T. M., BOGUNOVIC, M. & IVANOV, II 2015. Intestinal Monocyte-Derived Macrophages Control Commensal-Specific Th17 Responses. *Cell Rep,* 12**,** 1314-24.

PEARCE, S. C., AL-JAWADI, A., KISHIDA, K., YU, S., HU, M., FRITZKY, L. F., EDELBLUM, K. L., GAO, N. & FERRARIS, R. P. 2018. Marked differences in tight junction composition and macromolecular permeability among different intestinal cell types. *BMC Biol,* 16**,** 19.

PEYRIN-BIROULET, L., HART, A., BOSSUYT, P., LONG, M., ALLEZ, M., JUILLERAT, P., ARMUZZI, A., LOFTUS, E. V., JR., OSTAD-SAFFARI, E., SCALORI, A., OH, Y. S., TOLE, S., CHAI, A., PULLEY, J., LACEY, S., SANDBORN, W. J. & GROUP, H. S. 2022. Etrolizumab as induction and maintenance therapy for ulcerative colitis in patients previously treated with tumour necrosis factor inhibitors (HICKORY): a phase 3, randomised, controlled trial. *Lancet Gastroenterol Hepatol,* 7**,** 128-140.

PINTO, D., GREGORIEFF, A., BEGTHEL, H. & CLEVERS, H. 2003. Canonical Wnt signals are essential for homeostasis of the intestinal epithelium. *Genes Dev,* 17**,** 1709-13.

PIONTEK, J., KRUG, S. M., PROTZE, J., KRAUSE, G. & FROMM, M. 2020. Molecular architecture and assembly of the tight junction backbone. *Biochim Biophys Acta Biomembr,* 1862**,** 183279.

POMPAIAH, M. & BARTFELD, S. 2017. Gastric Organoids: An Emerging Model System to Study Helicobacter pylori Pathogenesis. *Curr Top Microbiol Immunol,* 400**,** 149-168.

POPOV, J., CAPUTI, V., NANDEESHA, N., RODRIGUEZ, D. A. & PAI, N. 2021. Microbiota-Immune Interactions in Ulcerative Colitis and Colitis Associated Cancer and Emerging Microbiota-Based Therapies. *Int J Mol Sci,* 22.

PORITZ, L. S., HARRIS, L. R., 3RD, KELLY, A. A. & KOLTUN, W. A. 2011. Increase in the tight junction protein claudin-1 in intestinal inflammation. *Dig Dis Sci,* 56**,** 2802-9.

POULSEN, S. S., NEXO, E., OLSEN, P. S., HESS, J. & KIRKEGAARD, P. 1986. Immunohistochemical localization of epidermal growth factor in rat and man. *Histochemistry,* 85**,** 389-94.

POUSSIER, P., NING, T., BANERJEE, D. & JULIUS, M. 2002. A unique subset of self-specific intraintestinal T cells maintains gut integrity. *J Exp Med,* 195**,** 1491-7.

PRASAD, S., MINGRINO, R., KAUKINEN, K., HAYES, K. L., POWELL, R. M., MACDONALD, T. T. & COLLINS, J. E. 2005. Inflammatory processes have differential effects on claudins 2, 3 and 4 in colonic epithelial cells. *Lab Invest,* 85**,** 1139-62.

RALEIGH, D. R., MARCHIANDO, A. M., ZHANG, Y., SHEN, L., SASAKI, H., WANG, Y., LONG, M. & TURNER, J. R. 2010. Tight junction-associated MARVEL proteins marveld3, tricellulin, and occludin have distinct but overlapping functions. *Mol Biol Cell,* 21**,** 1200-13.

RESCIGNO, M., URBANO, M., VALZASINA, B., FRANCOLINI, M., ROTTA, G., BONASIO, R., GRANUCCI, F., KRAEHENBUHL, J. P. & RICCIARDI-CASTAGNOLI, P. 2001. Dendritic cells express tight junction proteins and penetrate gut epithelial monolayers to sample bacteria. *Nat Immunol,* 2**,** 361-7.

RIAZUDDIN, S., AHMED, Z. M., FANNING, A. S., LAGZIEL, A., KITAJIRI, S., RAMZAN, K., KHAN, S. N., CHATTARAJ, P., FRIEDMAN, P. L., ANDERSON, J. M., BELYANTSEVA, I. A., FORGE, A., RIAZUDDIN, S. & FRIEDMAN, T. B. 2006. Tricellulin is a tight-junction protein necessary for hearing. *Am J Hum Genet,* 79**,** 1040-51.

RICHTER, J. F., HILDNER, M., SCHMAUDER, R., TURNER, J. R., SCHUMANN, M. & REICHE, J. 2019. Occludin knockdown is not sufficient to induce transepithelial macromolecule passage. *Tissue Barriers,* 7**,** 1612661.

RIVERA, C. A., RANDRIAN, V., RICHER, W., GERBER-FERDER, Y., DELGADO, M. G., CHIKINA, A. S., FREDE, A., SORINI, C., MAURIN, M., KAMMOUN-CHAARI, H., PARIGI, S. M., GOUDOT, C., CABEZA-CABRERIZO, M., BAULANDE, S., LAMEIRAS, S., GUERMONPREZ, P., REIS E SOUSA, C., LECUIT, M., MOREAU, H. D., HELFT, J., VIGNJEVIC, D. M., VILLABLANCA, E. J. & LENNON-DUMENIL, A. M. 2022. Epithelial colonization by gut dendritic cells promotes their functional diversification. *Immunity,* 55**,** 129-144 e8.

ROBERTS, S. J., SMITH, A. L., WEST, A. B., WEN, L., FINDLY, R. C., OWEN, M. J. & HAYDAY, A. C. 1996. T-cell alpha beta + and gamma delta + deficient mice display abnormal but distinct phenotypes toward a natural, widespread infection of the intestinal epithelium. *Proc Natl Acad Sci U S A,* 93**,** 11774-9.

ROCK, J. R., ONAITIS, M. W., RAWLINS, E. L., LU, Y., CLARK, C. P., XUE, Y., RANDELL, S. H. & HOGAN, B. L. 2009. Basal cells as stem cells of the mouse trachea and human airway epithelium. *Proc Natl Acad Sci U S A,* 106**,** 12771-5.

ROSEN, M. J., FREY, M. R., WASHINGTON, M. K., CHATURVEDI, R., KUHNHEIN, L. A., MATTA, P., REVETTA, F. L., WILSON, K. T. & POLK, D. B. 2011. STAT6 activation in ulcerative colitis: a new target for prevention of IL-13-induced colon epithelial cell dysfunction. *Inflamm Bowel Dis,* 17**,** 2224-34.

ROSENTHAL, R., GUNZEL, D., PIONTEK, J., KRUG, S. M., AYALA-TORRES, C., HEMPEL, C., THEUNE, D. & FROMM, M. 2020. Claudin-15 forms a water channel through the tight junction with distinct function compared to claudin-2. *Acta Physiol (Oxf),* 228**,** e13334.

ROSENTHAL, R., MILATZ, S., KRUG, S. M., OELRICH, B., SCHULZKE, J. D., AMASHEH, S., GUNZEL, D. & FROMM, M. 2010. Claudin-2, a component of the tight junction, forms a paracellular water channel. *J Cell Sci,* 123**,** 1913-21.

RUBIN, D. T., DOTAN, I., DUVALL, A., BOUHNIK, Y., RADFORD-SMITH, G., HIGGINS, P. D. R., MISHKIN, D. S., ARRISI, P., SCALORI, A., OH, Y. S., TOLE, S., CHAI, A., CHAMBERLAIN-JAMES, K., LACEY, S., MCBRIDE, J., PANES, J. & GROUP, H. S. 2022. Etrolizumab versus adalimumab or placebo as induction therapy for moderately to severely active ulcerative colitis (HIBISCUS): two phase 3 randomised, controlled trials. *Lancet Gastroenterol Hepatol,* 7**,** 17-27.

RUGTVEIT, J., NILSEN, E. M., BAKKA, A., CARLSEN, H., BRANDTZAEG, P. & SCOTT, H. 1997. Cytokine profiles differ in newly recruited and resident subsets of mucosal macrophages from inflammatory bowel disease. *Gastroenterology,* 112**,** 1493-505.

SAITOU, M., FURUSE, M., SASAKI, H., SCHULZKE, J. D., FROMM, M., TAKANO, H., NODA, T. & TSUKITA, S. 2000. Complex phenotype of mice lacking occludin, a component of tight junction strands. *Mol Biol Cell,* 11**,** 4131-42.

SAMBUY, Y., DE ANGELIS, I., RANALDI, G., SCARINO, M. L., STAMMATI, A. & ZUCCO, F. 2005. The Caco-2 cell line as a model of the intestinal barrier: influence of cell and culture-related factors on Caco-2 cell functional characteristics. *Cell Biol Toxicol,* 21**,** 1-26.

SATO, T., STANGE, D. E., FERRANTE, M., VRIES, R. G., VAN ES, J. H., VAN DEN BRINK, S., VAN HOUDT, W. J., PRONK, A., VAN GORP, J., SIERSEMA, P. D. & CLEVERS, H. 2011a. Long-term expansion of epithelial organoids from human colon, adenoma, adenocarcinoma, and Barrett's epithelium. *Gastroenterology,* 141**,** 1762-72.

SATO, T., VAN ES, J. H., SNIPPERT, H. J., STANGE, D. E., VRIES, R. G., VAN DEN BORN, M., BARKER, N., SHROYER, N. F., VAN DE WETERING, M. & CLEVERS, H. 2011b. Paneth cells constitute the niche for Lgr5 stem cells in intestinal crypts. *Nature,* 469**,** 415-8.

SATO, T., VRIES, R. G., SNIPPERT, H. J., VAN DE WETERING, M., BARKER, N., STANGE, D. E., VAN ES, J. H., ABO, A., KUJALA, P., PETERS, P. J. & CLEVERS, H. 2009. Single Lgr5 stem cells build crypt-villus structures in vitro without a mesenchymal niche. *Nature,* 459**,** 262-5.

SCHLAERMANN, P., TOELLE, B., BERGER, H., SCHMIDT, S. C., GLANEMANN, M., ORDEMANN, J., BARTFELD, S., MOLLENKOPF, H. J. & MEYER, T. F. 2016. A novel human gastric primary cell culture system for modelling Helicobacter pylori infection in vitro. *Gut,* 65**,** 202-13.

SCHÖN, M. P., ARYA, A., MURPHY, E. A., ADAMS, C. M., STRAUCH, U. G., AGACE, W. W., MARSAL, J., DONOHUE, J. P., HER, H., BEIER, D. R., OLSON, S., LEFRANCOIS, L., BRENNER, M. B., GRUSBY, M. J. & PARKER, C. M. 1999. Mucosal T Lymphocyte Numbers Are Selectively Reduced in Integrin αE (CD103)-Deficient Mice. *The Journal of Immunology,* 162**,** 6641-6649.

SCHULZKE, J. D., GITTER, A. H., MANKERTZ, J., SPIEGEL, S., SEIDLER, U., AMASHEH, S., SAITOU, M., TSUKITA, S. & FROMM, M. 2005. Epithelial transport and barrier function in occludin-deficient mice. *Biochim Biophys Acta,* 1669**,** 34-42.

SEIDLITZ, T., MERKER, S. R., ROTHE, A., ZAKRZEWSKI, F., VON NEUBECK, C., GRUTZMANN, K., SOMMER, U., SCHWEITZER, C., SCHOLCH, S., UHLEMANN, H., GAEBLER, A. M., WERNER, K., KRAUSE, M., BARETTON, G. B., WELSCH, T., KOO, B. K., AUST, D. E., KLINK, B., WEITZ, J. & STANGE, D. E. 2019. Human gastric cancer modelling using organoids. *Gut,* 68**,** 207-217.

SHAJIB, M. S., WANG, H., KIM, J. J., SUNJIC, I., GHIA, J. E., DENOU, E., COLLINS, M., DENBURG, J. A. & KHAN, W. I. 2013. Interleukin 13 and serotonin: linking the immune and endocrine systems in murine models of intestinal inflammation. *PLoS One,* 8**,** e72774.

SHAW, T. N., HOUSTON, S. A., WEMYSS, K., BRIDGEMAN, H. M., BARBERA, T. A., ZANGERLE-MURRAY, T., STRANGWARD, P., RIDLEY, A. J. L., WANG, P., TAMOUTOUNOUR, S., ALLEN, J. E., KONKEL, J. E. & GRAINGER, J. R. 2018. Tissue-resident macrophages in the intestine are long lived and defined by Tim-4 and CD4 expression. *J Exp Med,* 215**,** 1507-1518.

SHI, J., BARAKAT, M., CHEN, D. & CHEN, L. 2018. Bicellular Tight Junctions and Wound Healing. *Int J Mol Sci,* 19.

SHON, W. J., LEE, Y. K., SHIN, J. H., CHOI, E. Y. & SHIN, D. M. 2015. Severity of DSS-induced colitis is reduced in Ido1-deficient mice with down-regulation of TLR-MyD88-NF-kB transcriptional networks. *Sci Rep,* 5**,** 17305.

SIDDIQUI, K. R. & POWRIE, F. 2008. CD103+ GALT DCs promote Foxp3+ regulatory T cells. *Mucosal Immunol,* 1 Suppl 1**,** S34-8.

SOBOCKA, M. B., SOBOCKI, T., BANERJEE, P., WEISS, C., RUSHBROOK, J. I., NORIN, A. J., HARTWIG, J., SALIFU, M. O., MARKELL, M. S., BABINSKA, A., EHRLICH, Y. H. & KORNECKI, E. 2000. Cloning of the human platelet F11 receptor: a cell adhesion molecule member of the immunoglobulin superfamily involved in platelet aggregation. *Blood,* 95**,** 2600-9.

SPECKMANN, H., KÖHLING 2019. Magen Darm Trakt, Pankreas und Leber. *Physiologie.* München: Elsevier.

STAEHELIN, L. A. 1973. Further observations on the fine structure of freeze-cleaved tight junctions. *J Cell Sci,* 13**,** 763-86.

STAEHELIN, L. A., MUKHERJEE, T. M. & WILLIAMS, A. W. 1969. Freeze-etch appearance of the tight junctions in the epithelium of small and large intestine of mice. *Protoplasma,* 67**,** 165-84.

STEED, E., ELBEDIWY, A., VACCA, B., DUPASQUIER, S., HEMKEMEYER, S. A., SUDDASON, T., COSTA, A. C., BEAUDRY, J. B., ZIHNI, C., GALLAGHER, E., PIERREUX, C. E., BALDA, M. S. & MATTER, K. 2014. MarvelD3 couples tight junctions to the MEKK1-JNK pathway to regulate cell behavior and survival. *J Cell Biol,* 204**,** 821-38.

STEED, E., RODRIGUES, N. T., BALDA, M. S. & MATTER, K. 2009. Identification of MarvelD3 as a tight junction-associated transmembrane protein of the occludin family. *BMC Cell Biol,* 10**,** 95.

STEEGE, J. C., BUURMAN, W. A. & FORGET, P. P. 1997. The neonatal development of intraepithelial and lamina propria lymphocytes in the murine small intestine. *Dev Immunol,* 5**,** 121-8.

SUGAWARA, T., FURUSE, K., OTANI, T., WAKAYAMA, T. & FURUSE, M. 2021. Angulin-1 seals tricellular contacts independently of tricellulin and claudins. *J Cell Biol,* 220.

SUGIMOTO, S., KOBAYASHI, E., FUJII, M., OHTA, Y., ARAI, K., MATANO, M., ISHIKAWA, K., MIYAMOTO, K., TOSHIMITSU, K., TAKAHASHI, S., NANKI, K., HAKAMATA, Y., KANAI, T. & SATO, T. 2021. An organoid-based organ-repurposing approach to treat short bowel syndrome. *Nature,* 592**,** 99-104.

SUNG, S. S., FU, S. M., ROSE, C. E., JR., GASKIN, F., JU, S. T. & BEATY, S. R. 2006. A major lung CD103 (alphaE)-beta7 integrin-positive epithelial dendritic cell population expressing Langerin and tight junction proteins. *J Immunol,* 176**,** 2161-72.

SUZUKI, H. 2009. Differences in intraepithelial lymphocytes in the proximal, middle, distal parts of small intestine, cecum, and colon of mice. *Immunol Invest,* 38**,** 780-96.

SUZUKI, T., YOSHINAGA, N. & TANABE, S. 2011. Interleukin-6 (IL-6) regulates claudin-2 expression and tight junction permeability in intestinal epithelium. *J Biol Chem,* 286**,** 31263-71.

TADDEI, M. L., GIANNONI, E., FIASCHI, T. & CHIARUGI, P. 2012. Anoikis: an emerging hallmark in health and diseases. *J Pathol,* 226**,** 380-93.

TAKAYAMA, K., ITO, K., MATSUI, A., YAMASHITA, T., KAWAKAMI, K., HIRAYAMA, D., KISHIMOTO, W., NAKASE, H. & MIZUGUCHI, H. 2021. In Vivo Gene Expression Profile of Human Intestinal Epithelial Cells: From the Viewpoint of Drug Metabolism and Pharmacokinetics. *Drug Metab Dispos,* 49**,** 221-232.

TAMOUTOUNOUR, S., HENRI, S., LELOUARD, H., DE BOVIS, B., DE HAAR, C., VAN DER WOUDE, C. J., WOLTMAN, A. M., REYAL, Y., BONNET, D., SICHIEN, D., BAIN, C. C., MOWAT, A. M., REIS E SOUSA, C., POULIN, L. F., MALISSEN, B. & GUILLIAMS, M. 2012. CD64 distinguishes macrophages from dendritic cells in the gut and reveals the Th1-inducing role of mesenteric lymph node macrophages during colitis. *Eur J Immunol,* 42**,** 3150-66.

TAMURA, A., HAYASHI, H., IMASATO, M., YAMAZAKI, Y., HAGIWARA, A., WADA, M., NODA, T., WATANABE, M., SUZUKI, Y. & TSUKITA, S. 2011. Loss of claudin-15, but not claudin-2, causes Na+ deficiency and glucose malabsorption in mouse small intestine. *Gastroenterology,* 140**,** 913-23.

TSUCHIYA, T., FUKUDA, S., HAMADA, H., NAKAMURA, A., KOHAMA, Y., ISHIKAWA, H., TSUJIKAWA, K. & YAMAMOTO, H. 2003. Role of gamma delta T cells in the inflammatory response of experimental colitis mice. *J Immunol,* 171**,** 5507-13.

TSUKITA, S. & FURUSE, M. 1998. Overcoming barriers in the study of tight junction functions: from occludin to claudin. *Genes Cells,* 3**,** 569-73.

VACCA, B., SANCHEZ-HERAS, E., STEED, E., BALDA, M. S., OHNUMA, S. I., SASAI, N., MAYOR, R. & MATTER, K. 2016. MarvelD3 regulates the c-Jun N-terminal kinase pathway during eye development in Xenopus. *Biol Open,* 5**,** 1631-1641.

VACCA, B., SANCHEZ-HERAS, E., STEED, E., BUSSON, S. L., BALDA, M. S., OHNUMA, S. I., SASAI, N., MAYOR, R. & MATTER, K. 2018. Control of neural crest induction by MarvelD3-mediated attenuation of JNK signalling. *Sci Rep,* 8**,** 1204.

VANDUSSEN, K. L., CARULLI, A. J., KEELEY, T. M., PATEL, S. R., PUTHOFF, B. J., MAGNESS, S. T., TRAN, I. T., MAILLARD, I., SIEBEL, C., KOLTERUD, A., GROSSE, A. S., GUMUCIO, D. L., ERNST, S. A., TSAI, Y. H., DEMPSEY, P. J. & SAMUELSON, L. C. 2012. Notch signaling modulates proliferation and differentiation of intestinal crypt base columnar stem cells. *Development,* 139**,** 488-97.

VANDUSSEN, K. L., MARINSHAW, J. M., SHAIKH, N., MIYOSHI, H., MOON, C., TARR, P. I., CIORBA, M. A. & STAPPENBECK, T. S. 2015. Development of an enhanced human gastrointestinal epithelial culture system to facilitate patient-based assays. *Gut,* 64**,** 911-20.

VEENBERGEN, S., VAN BERKEL, L. A., DU PRE, M. F., HE, J., KARRICH, J. J., COSTES, L. M., LUK, F., SIMONS-OOSTERHUIS, Y., RAATGEEP, H. C., CEROVIC, V., CUPEDO, T., MOWAT, A. M., KELSALL, B. L. & SAMSOM, J. N. 2016. Colonic tolerance develops in the iliac lymph nodes and can be established independent of CD103(+) dendritic cells. *Mucosal Immunol,* 9**,** 894-906.

VERMEIRE, S., LAKATOS, P. L., RITTER, T., HANAUER, S., BRESSLER, B., KHANNA, R., ISAACS, K., SHAH, S., KADVA, A., TYRRELL, H., OH, Y. S., TOLE, S., CHAI, A., PULLEY, J., EDEN, C., ZHANG, W., FEAGAN, B. G. & GROUP, L. S. 2022. Etrolizumab for maintenance therapy in patients with moderately to severely active ulcerative colitis (LAUREL): a randomised, placebo-controlled, double-blind, phase 3 study. *Lancet Gastroenterol Hepatol,* 7**,** 28-37.

WANG, L., RAY, A., JIANG, X., WANG, J. Y., BASU, S., LIU, X., QIAN, T., HE, R., DITTEL, B. N. & CHU, Y. 2015. T regulatory cells and B cells cooperate to form a regulatory loop that maintains gut homeostasis and suppresses dextran sulfate sodium-induced colitis. *Mucosal Immunol,* 8**,** 1297-312.

WANG, Z., ZHANG, H., LIU, R., QIAN, T., LIU, J., HUANG, E., LU, Z., ZHAO, C., WANG, L. & CHU, Y. 2018. Peyer's patches-derived CD11b(+) B cells recruit regulatory T cells through CXCL9 in dextran sulphate sodium-induced colitis. *Immunology,* 155**,** 356-366.

WEBER, B., SAURER, L., SCHENK, M., DICKGREBER, N. & MUELLER, C. 2011. CX3CR1 defines functionally distinct intestinal mononuclear phagocyte subsets which maintain their respective functions during homeostatic and inflammatory conditions. *Eur J Immunol,* 41**,** 773-9.

WEBER, C. R., NALLE, S. C., TRETIAKOVA, M., RUBIN, D. T. & TURNER, J. R. 2008. Claudin-1 and claudin-2 expression is elevated in inflammatory bowel disease and may contribute to early neoplastic transformation. *Lab Invest,* 88**,** 1110-20.

WEISS, F., CZICHOS, C., KNOBE, L., VOGES, L., BOJARSKI, C., MICHEL, G., FROMM, M. & KRUG, S. M. 2022a. MarvelD3 Is Upregulated in Ulcerative Colitis and Has Attenuating Effects during Colitis Indirectly Stabilizing the Intestinal Barrier. *Cells,* 11.

WEISS, F., HOLTHAUS, D., KRAFT, M., KLOTZ, C., SCHNEEMANN, M., SCHULZKE, J. D. & KRUG, S. M. 2022b. Human duodenal organoid-derived monolayers serve as a suitable barrier model for duodenal tissue. *Ann N Y Acad Sci*.

WERA, O., LANCELLOTTI, P. & OURY, C. 2016. The Dual Role of Neutrophils in Inflammatory Bowel Diseases. *J Clin Med,* 5.

WESTPHAL, J. K., DORFEL, M. J., KRUG, S. M., CORDING, J. D., PIONTEK, J., BLASIG, I. E., TAUBER, R., FROMM, M. & HUBER, O. 2010. Tricellulin forms homomeric and heteromeric tight junctional complexes. *Cell Mol Life Sci,* 67**,** 2057-68.

XING, T., BENDERMAN, L. J., SABU, S., PARKER, J., YANG, J., LU, Q., DING, L. & CHEN, Y. H. 2020. Tight Junction Protein Claudin-7 Is Essential for Intestinal Epithelial Stem Cell Self-Renewal and Differentiation. *Cell Mol Gastroenterol Hepatol,* 9**,** 641-659.

YAMASHITA, T., INUI, T., YOKOTA, J., KAWAKAMI, K., MORINAGA, G., TAKATANI, M., HIRAYAMA, D., NOMOTO, R., ITO, K., CUI, Y., RUEZ, S., HARADA, K., KISHIMOTO, W., NAKASE, H. & MIZUGUCHI, H. 2021. Monolayer platform using human biopsy-derived duodenal organoids for pharmaceutical research. *Mol Ther Methods Clin Dev,* 22**,** 263-278.

YEN, F. T., MASSON, M., CLOSSAIS-BESNARD, N., ANDRE, P., GROSSET, J. M., BOUGUELERET, L., DUMAS, J. B., GUERASSIMENKO, O. & BIHAIN, B. E. 1999. Molecular cloning of a lipolysis-stimulated remnant receptor expressed in the liver. *J Biol Chem,* 274**,** 13390-8.

YEUNG, M. M., MELGAR, S., BARANOV, V., OBERG, A., DANIELSSON, A., HAMMARSTROM, S. & HAMMARSTROM, M. L. 2000. Characterisation of mucosal lymphoid aggregates in ulcerative colitis: immune cell phenotype and TcR-gammadelta expression. *Gut,* 47**,** 215-27.

ZEISSIG, S., BURGEL, N., GUNZEL, D., RICHTER, J., MANKERTZ, J., WAHNSCHAFFE, U., KROESEN, A. J., ZEITZ, M., FROMM, M. & SCHULZKE, J. D. 2007. Changes in expression and distribution of claudin 2, 5 and 8 lead to discontinuous tight junctions and barrier dysfunction in active Crohn's disease. *Gut,* 56**,** 61-72.

ZEN, K., LIU, Y., MCCALL, I. C., WU, T., LEE, W., BABBIN, B. A., NUSRAT, A. & PARKOS, C. A. 2005. Neutrophil migration across tight junctions is mediated by adhesive interactions between epithelial coxsackie and adenovirus receptor and a junctional adhesion molecule-like protein on neutrophils. *Mol Biol Cell,* 16**,** 2694-703.

ZHOU, L., IVANOV, II, SPOLSKI, R., MIN, R., SHENDEROV, K., EGAWA, T., LEVY, D. E., LEONARD, W. J. & LITTMAN, D. R. 2007. IL-6 programs T(H)-17 cell differentiation by promoting sequential engagement of the IL-21 and IL-23 pathways. *Nat Immunol,* 8**,** 967-74.

ZHOU, T., LU, Y., XU, C., WANG, R., ZHANG, L. & LU, P. 2020. Occludin protects secretory cells from ER stress by facilitating SNARE-dependent apical protein exocytosis. *Proc Natl Acad Sci U S A,* 117**,** 4758-4769.

ZHOU, Z., ZHANG, L., DING, M., LUO, Z., YUAN, S., BANSAL, M. B., GILKESON, G., LANG, R. & JIANG, W. 2017. Estrogen decreases tight junction protein ZO-1 expression in human primary gut tissues. *Clin Immunol,* 183**,** 174-180.

ZWIERS, A., FUSS, I. J., LEIJEN, S., MULDER, C. J., KRAAL, G. & BOUMA, G. 2008. Increased expression of the tight junction molecule claudin-18 A1 in both experimental colitis and ulcerative colitis. *Inflamm Bowel Dis,* 14**,** 1652-9.

9 List of abbreviations

Table 18 Abbreviations

ACTB	ß-actin
AD	Advanced Dulbecco's modified Eagle medium (DMEM)/ F12
AJ	Adherens junction
APC	Antigen-presenting cell
APS	Ammonium persulfate
ASC	Adult stem cell
BCA	Bicin-choninic acid
BMP	Bone morphogenic protein
BSA	Bovine serum albumin
bTJ	Bicellular tight junction
CAR	Coxsackie and adenovirus receptor
CBC	Crypt-based columnar cell
cCD	Classical dendritic cell
CCL	Two N-terminal cysteines adjacent ligand
CD	Cluster of differentiation
CD	Crohn’s disease
CD64	High-affinity immunoglobulin (IgG) receptor FcγR1
CHGA	Chromogranin A
CK19	Cytokeratin 19
Cldn	Claudin
CLDN	Claudin (human)
CLMP	CXADR-like membrane protein
CM	Conditioned medium
Co	Colon
CSF	Colony-stimulating factor
CX3CR1	CX3C motif chemokine receptor 1
CXCL	Chemokine (C-X-C motif) ligand (C-X-C: two N-terminal cysteines separated by a single amino acid) ligand
DAI	Disease activity index
DAMP	Damage-associated molecular pattern
DAPI	4', 6-Diamidino-2-phenylindole
DC	Dendritic cell
DMEM	Dulbecco's modified Eagle medium
DMSO	Dimethylsulfoxid

DSCs	Depp secretory cell
DSS	Dextran sulfate sodium
EDTA	Ethylene diamine tetra acetic acid
EEC	Enteroendocrine cell
EGF	Epithelial growth factor
EGTA	Ethylene glycol tetra-acetic acid
EPHO	Electrophoresis
ESAM	Endothelial cell-selective adhesion molecule
ESC	Embryonic stem cell
EtBr	Ethidium bromide
FABP	Fatty acid-binding protein
FBS	Fetal bovine serum
FC	Fold change
FD4	FITC dextran 4 kDa
FGF	Fibroblast growth factor
Flt3L	FMS-related tyrosine kinase 3 ligand
FOXP3	Forkhead-box-protein P3
GAPDH	Glycerinaldehyde-3-phosphate dehydrogenase
GC	Goblet cell
GEO	Gene expression omnibus
GI	Gastrointestinal
GWAS	Genome-wide association study
HBSS	Hanks’ balanced salt solution
HC	Housekeeping gene control
HE	Housekeeping gene experimental
IBD	Inflammatory bowel disease
IEC	Intestinal epithelial cell
IEL	Intraepithelial lymphocyte
IF	Immunofluorescence
IG	Immunoglobulin
IGF	Insulin-like growth factor
iIEL	Induced IEL
IL	Interleukin
ILC	Innate lymphoid cell
ILDR1	Immunoglobulin Ig-like domain-containing receptor 1 / angulin-2
ILDR2	Immunoglobulin Ig-like domain-containing receptor 2 / angulin-3

ILDR3	see LSR
ILF	Isolated lymphoid follicle
INF	Interferon
iPSC	Induced pluripotent stem cell
ITGAE	Integrin alpha E / CD103
JAM	Junctional adhesion molecule
JAM-L	JAM-like protein
LDR	Immunoglobulin Ig-like domain-containing receptor
LGR5	Identified leucin-rich repeat-containing G protein-coupled receptor 5
LP	Lamina propria
LPMC	Lamina propria mononuclear cell
LSR	Lipolysis-stimulated lipoprotein receptor / angulin-1
LyZ1	Lysozyme
MARVEL	Myelin and lymphocyte and related proteins for vesicle trafficking and membrane link
M cell	Microfold cell
MD3	MARVEL D3
MEM	Minimum essential medium
MHC II	Major histocompatibility complex class II
MLN	Mesentery lymph node
MUC2	Mucin2
NAC	N-Acetylcysteine
NET	Neutrophil extracellular trap
NIC	Nicotinamide / Niacinamide
nIEL	Natural IEL
NK	Natural killer
Ocln	Occludin
OCLN	Occludin (human)
ODM	Organoid-derived monolayer
OE	Overexpression
PAMP	Pathogen-associated molecular pattern
pDC	Plasmacytoid dendritic cell
PEI	Polyethyleneimine
PFA	Paraformaldehyde
PMA	Phorbol 12-myristate 13-acetate
PP	Peyer's patches

P/S	Penicillin-streptomycin solution
PSC	Pluripotent stem cell
PPR	Pattern recognition receptor
qPCR	Real-time quantitative polymerase chain reaction
RA	Retinoic acid
RALDH	Retinaldehyde dehydrogenase
R^{Para}	Paracellular resistance
RPMI	Roswell Park Memorial Institute
Rspo1	R-spondin-1
R^{Trans}	Transcellular resistance
SDS	Sodium dodecyl sulfate
SDS-PAGE	Sodium dodecyl sulfate-polyacrylamide gel electrophoresis
si	Small intestine
SLC	Solute carrier
SMR	Standardised mortality ratio
TA	Transit-amplifying
TAE	TRIS-acetate-EDTA buffer
TAMP	TJ-associated MARVEL protein
TC	Target gene control
TCR	T cell receptor
TE	Target gene experimental
TEC	TRIS-EDTA-citrate buffer
TED	Transepithelial dendrite
TEMED	N,N,N',N'-Tetramethylethylenediamine
TER	Transepithelial resistance
TGF	Transforming growth factor
T_H	T helper cell
TIM	T-cell membrane protein
TJ	Tight junction
TNF-α	Tumour necrosis factor-α
T_{reg}	T regulatory cell
Tric	Tricellulin
TRIC	Tricellulin (human)
tTJ	Tricellular tight junction
TUBA	Tubulin-alpha
UC	Ulcerative colitis

VIM	Vimentin
WB	Western blot
wt	Wild type
ZO	Zonula occludens protein

10 List of figures

11 List of tables

12 List of own publications

Kayisoglu O, **Weiss F**, Niklas C, Pierotti I, Pompaiah M, Wallaschek N, Germer CT, Wiegering A, Bartfeld S. Location-specific cell identity rather than exposure to GI microbiota defines many innate immune signalling cascades in the gut epithelium. Gut. 2021 Apr;70(4):687-697. doi: 10.1136/gutjnl-2019-319919. Epub 2020 Jun 22. PMID: 32571970; PMCID: PMC7948175.

Hu JE, **Weiß F**, Bojarski C, Branchi F, Schulzke JD, Fromm M, Krug SM. Expression of tricellular tight junction proteins and the paracellular macromolecule barrier are recovered in remission of ulcerative colitis. BMC Gastroenterol. 2021 Mar 31;21(1):141. doi: 10.1186/s12876-021-01723-7. PMID: 33789594; PMCID: PMC8010963.

Weiß F, Czichos C, Knobe L, Voges L, Bojarski C, Michel G, Fromm M, Krug SM. MarvelD3 Is Upregulated in Ulcerative Colitis and Has Attenuating Effects during Colitis Indirectly Stabilizing the Intestinal Barrier. Cells. 2022 May 4;11(9):1541. doi: 10.3390/cells11091541. PMID: 35563847; PMCID: PMC9102383.

Weiß F, Holthaus D, Kraft M, Klotz C, Schneemann M, Schulzke JD, Krug SM. Human duodenal organoid-derived monolayers serve as a suitable barrier model for duodenal tissue. Ann N Y Acad Sci. 2022 Sep;1515(1):155-167. doi: 10.1111/nyas.14804. Epub 2022 Jun 6. PMID: 35666953.